Driftwood as a tool for investigation of Holocene Pan-Arctic Sea Ice Dynamics

by

Georgia Melodie Hole
Hertford College, Oxford University

THESIS SUBMITTED IN FULFILLMENT OF
THE REQUIREMENTS FOR THE DEGREE OF
DOCTOR OF PHILOSOPHY

In

The School of Geography and the Environment

THE UNIVERSITY OF OXFORD

Trinity 2021

Acknowledgments

My appreciation goes to all those who have provided scientific, pedagogical, and personal support and guidance throughout the journey of the DPhil. It is my pleasure to acknowledge the roles of several individuals who were instrumental in the progress of my doctoral research, and who inspired me to persevere to completion.

I would like to express my gratitude to my primary supervisor, Dr Marc Macias-Fauria, whose guidance, encouragement, and support were a constant, and whose scientific knowledge and insight into the Arctic was unmatched. Thank you also for the valued assistance when there were hurdles along the way, and for keeping faith in me. I must also acknowledge my less-than-official research group OxLEL – the Oxford Long Term Ecology Lab, where I was welcomed with desk space (asbestos permitting), and meetings were often had by punt, and with whom I often felt a renewed inspiration for 'science time'.

I also have deep appreciation for Hertford College, where in the community, friendships and support I found an anchor and a belonging. The vibrant community of the Middle Common Room provided the needed refuge and rest from intense scholarship and personal difficulties, as well a rich source of passionate, exceptional people, many of whom I was lucky enough to call good friends. Thank you to all those that joined me there, and in particular: Liisa, LD, Georgie, Aidan, Alice, Josie, Steve, Alex, Hormuz, Andrew, Helen and Bear Hammond. Thank you for making enough memories to last a lifetime, and for making Hertford a home. A special thank you to the College Chaplain Rev. Mia Smith, and to Nicola Psaila, who both provided earnest counsel, were always in my corner, and who showed me the light at the end of the tunnel many a time.

I am thankful to my brother Matthew, who provided a much-needed perspective outside of the academic bubble, and who always had thoughts and advice with my best interests at heart. My grandmother Joan gave me such love and pride in myself as a scientist, and although she passed away before she could see herself thanked here, I know how happy she would have been to be included.

And finally, a thank you to Thom Rawson, for the deepest support and kindness I have ever known, and for showing me the future.

Abstract

Arctic sea ice is rapidly declining in area and volume, with impacts on local and global climatic and ecological conditions. Without knowledge of past changes, this modern trend cannot be placed within a broader context that would aid future predictions for Arctic sea ice. Driftwood forms an under-utilised proxy for reconstructing Arctic sea ice extent over the Holocene (~12,000 yrs ago to present): its transport and deposition is determined by sea ice and surface current dynamics; making it a robust proxy for sea ice reconstructions. Driftwood in the Arctic results from the falling of trees into the large rivers that drain the circum-Arctic, which upon flowing into the Arctic Ocean can then become locked up in forming sea ice. This enables the driftwood to travel across the Arctic Ocean without sinking, making it an invaluable proxy for sea ice extent by recording variations in Arctic Ocean surface currents (and therefore sea ice drift) and ice cover. Given it takes on average multiple years for driftwood to travel from origin to destination in a high Arctic beach, multi-year sea ice is required for its transport. Driftwood is abundant on many raised Arctic beaches, as it is captured on shorelines that have risen out of the sea due to the retreat of the weight of glaciers at the end of the last ice age. Analysis of the driftwood's age and provenance can be used to form a reconstruction of the driftwood transport routes through time, and therefore Arctic sea ice extent and dynamics. I present a first pan-Arctic collation of Holocene driftwood data providing a reconstruction of higher spatial and temporal resolution than other proxy-based methods. The collation of 913 driftwood samples from across the western Arctic with spatiotemporal distribution and available provenance data enabled the production of a proxy-based reconstruction of Holocene Arctic Ocean surface current and sea ice dynamics. This revealed that Holocene sea ice extent and drift is characterised by a gradual progression from millennial to centennial shifts in the relative position of the Transpolar Drift and Beaufort Gyre, which is consistent with the dynamics of the Arctic Oscillation. Building on this I present the development of novel methodological

approaches which successfully employ driftwood as a proxy for Arctic Ocean surface current and sea ice dynamics. These reveal a 500-year history of driftwood incursion to northern Svalbard, directly reflecting regional sea ice conditions and Arctic Ocean circulation. This record indicates centennial- to decadal-scale shifts in source regions for driftwood incursion to Svalbard, aligning with Late Holocene high variability and high frequency shifts in the Transpolar Drift and Beaufort Gyre strengths and associated fluctuating climate conditions. Driftwood occurrence and provenance also tracks the northward seasonal ice formation shift and migration of seasonal sea ice to the peripheral Arctic seas in the past century. A distinct decrease in driftwood incursion during the last 30 years matches the observed decline in pan-Arctic sea ice extent in recent decades. Lastly, I present the development of novel techniques to refine the provenance of driftwood through radiogenic isotopic analysis ($^{87}Sr/^{86}Sr$). The use of geochemical provenance techniques can potentially address some of the limitations of current methods, warranting further development. The results show the utilisation of $^{87}Sr/^{86}Sr$ ratios to establish provenance for Arctic driftwood has potential, with current confounding factors in contamination issues of driftwood during transport and in the scale, spatial heterogeneity and temporal variations of pan-Arctic source regions. Combination of all techniques can further define the role of atmospheric and oceanic circulation in sea ice and climatic changes throughout the Holocene. The components of the thesis describe the successful employment and further development of driftwood as a proxy for Arctic Ocean surface current and sea ice dynamics.

Format of Chapters

This thesis is submitted as a paper-based thesis, with Chapters 3, 4 and 5 as free-standing manuscripts. Chapters 3 & 4 have been published within *Journal of Geophysical Research - Oceans*, while Chapter 5 is currently under review in *Palaeogeography, Palaeoclimatology, Palaeoecology*. Each has been formatted to meet the requirements of their respective journals and are presented as published herein. This therefore also means there is some inevitable overlap in concepts introduced throughout the chapters of the thesis. The supplementary materials for each chapter are provided in the Appendices.

Funding

This thesis was funded through the Natural Environment Research Council (NERC - https://nerc.ukri.org/) award grant 1514291 as part of the Environmental Research Doctoral Training Program at the University of Oxford.

Statement of Authorship

Each paper that constitutes the main chapters of this thesis were co-authored between myself, my primary supervisor (Dr Marc Macias-Fauria), and other collaborators who assisted in data collection and interpretation. In each instance I am the first and corresponding author. Below I list the authors and author contributions for each chapter.

- **Chapter 3: Georgia M. Hole and Marc Macias-Fauria**. The study was conceived by GMH and MMF. GMH authored the paper with contributions from all co-authors. All authors contributed with literature compilation, data interpretation and the discussion of results. Driftwood sample data was collated from researchers from multiple institutions in contribution to the pan-Arctic driftwood database that formed the basis of this study (see Supporting Information Table A1 and references therein which contains all of the data used in this study).
- **Chapter 4: Georgia M. Hole, Thomas Rawson, Wesley R. Farnsworth, Anders Schomacker, Ólafur Ingólfsson, & Marc Macias-Fauria**. GMH and MMF conceived this work. GMH authored the paper with contributions from all co-authors. All authors contributed with literature compilation, data interpretation and the discussion of results. This study is based on data collected in collaboration with the University Centre in Svalbard (UNIS), with the field campaign to Sjuøyane, training and logistics provided and funded by UNIS. The 2016 fieldwork was completed with sample collection by GMH and MMF across Sjuøyane in collaboration with the field course cohort. The samples from Ringhorndalen, Wijdefjorden were collected in 2016 by MMF and from Vassfarbukta, Wijdefjorden in 2018 by WRF and S. Brynjolfsson.
- **Chapter 5: Georgia M. Hole, Danielle Sinclair & Marc Macias-Fauria.** GMH and MMF conceived this study. GMH authored the chapter with contributions from all co-

authors. Geochemical analysis was undertaken in the clean-suite labs in the Earth Sciences Department, University of Oxford, by GMH and DS. Jane Barling and Kathrin Schilling provided assistance and training with equipment and clean-suite lab protocols. Yu-Te Alan Hsieh and Philip Holdship provided training and assistance with MC-ICP-MS/ICP-MS analysis All authors contributed with literature compilation, data interpretation and the discussion of results

- **Chapters 1, 2, 6** and **7** were written by GMH with comments from MMF.

Publications

The following publications have arisen from this thesis and are presented in chapters 3, 4 and 5:

- **Hole, G. M.** & Macias-Fauria, M. (2017). Out of the woods: Driftwood insights into Holocene pan-Arctic sea ice dynamics. *Journal of Geophysical Research: Oceans*, 122(9), 7612–7629. https://doi.org/10.1002/2017JC013126.
- **Hole, G. M.,** Rawson, T., Farnsworth, W. R., Schomacker, A., Ingólfsson, Ó., & Macias-Fauria, M. (2021). A driftwood-based record of Arctic sea ice during the last 500 years from northern Svalbard reveals sea ice dynamics in the Arctic Ocean and Arctic peripheral seas. *Journal of Geophysical Research: Oceans*, e2021JC017563. https://doi.org/10.1029/2021JC017563.
- **Hole, G.M.,** Sinclair, D., Macias-Fauria, M. (2021). Dropped in the Ocean – $^{87}Sr/^{86}Sr$ as a provenance tool for ice-rafted Arctic driftwood. *Palaeogeography, Palaeoclimatology, Palaeoecology*. In review.

The following research spotlights / press releases have also arisen from this thesis, associated with Chapters 3 and 4:

- Lipuma, L. (2017, September 20). Tracking driftwood gives researchers insight into past Arctic Ocean changes. AGU Blogosphere. https://blogs.agu.org/geospace/2017/09/20/tracking-driftwood-gives-researchers-insight-into-past-arctic-ocean-changes/
- American Geophysical Union. (2021, October 19). *Ancient Driftwood Tracks 500 Years of Arctic Warming and Sea Ice* [Press release]. Retrieved from https://news.agu.org/press-release/arctic-driftwood-tracks-500-years-of-arctic-warming-and-sea-ice/

Table of Contents

List of Figures

List of Tables

1 Introduction

1.1 Arctic Sea Ice

The rapid decline in Arctic sea ice extent, age and thickness is well documented, with such changes due to cause far-reaching impacts on both localised and global climatic and ecological processes (Bhatt et al., 2014). Arctic sea ice fluctuations are strongly coupled with Arctic climate, involving the influence of a variety of mechanisms, which incorporate natural climatic forcings occurring over a wide range of timescales (geological to intra-annual) and recent changes induced by anthropogenic influence. These forcings are being reflected in the observations of a rapid decline in the extent and thickness of sea ice (Polyak et al., 2010; Maslowski et al., 2012) with a decline in sea ice volume of 75% since the 1980s (Overland et al., 2013). The greatest decline in extent and multi-year ice has been observed in late-summer at the end of the melt season (Serreze et al., 2007), which mostly consists of thick multi-year ice and is shrinking at 13.3% per decade (Serreze & Stroeve, 2015). This has contributed to the decrease in ice age, with a drop from 4+ years old ice constituting 33% of the total ice extent in the mid-1980s to 3.1% in 2016 (Tschudi et al., 2016).

The continuing decline in sea ice cover is expected to have a diverse range of consequences including a warmer, wetter Arctic, impacts on terrestrial and marine productivity, changes to global atmospheric and ocean circulation patterns, terrestrial fauna and flora population fragmentation and habitat reduction, increased marine species interaction and connectivity, and northward expansion of lower-latitude species (Overland & Wang, 2010; Screen & Simmonds, 2010, 2014; Francis & Vavrus, 2012; Post & Høye, 2013; Overland et al., 2016; Vavrus et al., 2017; Bintanja & Andry, 2017). The knowledge of the dynamics behind such changes is constantly evolving, and the importance of factors such as the Arctic Oscillation – AO; defined as the principal component of sea-level pressure north of 20º N and

regarded as the most influential mode of atmospheric circulation and climate in the Arctic (Thompson & Wallace, 1998; Comiso & Hall, 2014) – and associated changes in ocean current and sea ice dynamics remains under active research (e.g. Rigor et al., 2002; Comiso and Hall, 2014; Barnes and Screen, 2015; Ding et al., 2017). This is explored in more detail in Chapter 2.

The spatiotemporal dynamics of Arctic sea ice conditions throughout the Holocene remain largely unknown, given the sparse knowledge preceding satellite observation, and so modern trends cannot be accurately assessed within centennial and millennial timescales. With the state of the Arctic clearly being such an influential factor in the wider climatic system, further knowledge of past sea ice dynamics is needed for revealing the late Quaternary Arctic climatic state and to investigate the Arctic system's climatic, geophysicalc and biotic responses and feedbacks to increasing global average temperatures.

The extent, thickness and dynamics of Arctic sea ice are driven by a range of factors that fall broadly into two components: those of the thermal and physical dynamics of the Arctic Ocean system. Thermodynamic processes in the Arctic such as the thermohaline circulation, surface warming and advection of warm waters contribute to changes in ice extent, age and thickness. The physical dynamics of sea ice are driven by both ocean and atmospheric circulations, which influence the strength and position of the Beaufort Gyre and Transpolar Drift (Figure 3.1).

The Beaufort Gyre (BG) displays a mean annual clockwise motion in the western Arctic Ocean (Polyak et al., 2010), and this anticyclonic nature results in the recirculation and enhanced persistence of sea ice within the Arctic basin. The mean residence time for ice in the BG is *c.*5 years (Rigor et al., 2002) and so it aids in the formation and preservation of multi-year ice that can reach up to 5m thickness (de Vernal et al., 2013). The Transpolar Drift (TPD)

is a surface ocean current running more or less parallel to the Siberian coast and transporting Arctic ice and waters southwards to the North Atlantic through the Fram Strait, favouring the loss of ice. Holocene fluctuations in the extent and orientation of the TPD – which are in turn related to the extent and strength of the BG – have been proposed to vary between three overall states (Dyke et al., 1997): there are lateral shifts from a) an eastward route toward Fram Strait, with sea ice (and any driftwood entrained in it) advection to the European side of the Arctic; b) a westward route toward Greenland with sea ice advection to the Canadian Arctic Archipelago (CAA); and c) a split route with sea ice transport divided between the east and west. A driftwood-based reconstruction of these lateral shifts in the TPD shows abrupt 40-50yr timescale shifts in the TPD position over the last 8.5 ka, with stable periods on centennial to millennial scales (Dyke et al., 1997; Tremblay et al., 1997).

The interaction of physical and thermal forcings can lead to feedback mechanisms that amplify fluctuations in sea ice, including spatiotemporally variable atmospheric and oceanic heat fluxes, prevailing winds, and ocean currents (Haas & Thomas, 2017). For example, when sea ice is thinned or reduced in age by dynamic ice and atmospheric processes, a positive feedback can occur as whereby this 'preconditioned' thinned ice is more susceptible to being lost by surface warming and wind stress changes (Hutchings & Rigor, 2012). The observed sustained reduction in March and September ice extent from 1850 - 2013 (Walsh et al., 2017) includes a striking thinning of undeformed ice (Rothrock & Zhang, 2005), and acceleration of seasonal and annual ice retreat with spatially-variable sea ice distribution changes across the Arctic (Kinnard et al., 2008). To determine the uniquity of the recent trend in decreasing multi-year sea ice and sea ice thickness (Kwok & Rothrock, 2009), as well as the region's abiotic and biotic responses, a greater understanding of the role of physical and thermal forcings and their resulting global impacts is needed (Dieckmann & Hellmer, 2010; Armand et al., 2016).

The AO is a key physical driver of the position of the TPD and the balance between the strength of the BG and TPD circulation patterns. It is characterised as the variable atmospheric mass exchange between the Arctic Ocean and temperate latitudes (Rigor et al., 2002), with positive or negative polarity determined by anomalies in Sea Level Pressures (SLPs) over the polar regions and mid-latitudes (*c.* 55°–60°N) (Kwok et al., 2013). A negative polarity of the AO results in weaker winds over the Arctic and an enhanced BG, leading to reduced sea ice motion and lead formation and so enhancing the retention and growth of multiyear sea ice (Figure 3.1a). Positive AO index configurations (Figure 3.1b) are associated with stronger westerlies at subpolar latitudes and lower SLP over the Arctic, resulting in cyclonic surface winds which increase sea ice motion. This physical process renders the Arctic Ocean more susceptible to thermal forcing, such as under recent climate change, by increased heat exchange from the ocean to the atmosphere, further reducing the thickness and concentration of sea ice (Rigor et al., 2002). A positive AO also causes expansion of the TPD, with increased export of sea ice from the Arctic Ocean through the Fram Strait, further enhancing sea ice reduction (Kwok & Rothrock, 1999; Hilmer & Jung, 2000; Rigor et al., 2002).

1.2 Observation and reconstruction of past Arctic sea ice conditions

There is only fragmented and scarce data (in time and space) on sea ice extent prior to the generation of spatially explicit sea ice extent information by satellite observations in the late 1970s (Post & Høye, 2013). Since Iceland's settlement in *c.*870 AD, records were kept of sea ice incidence by Icelandic fisheries (Polyak et al., 2010), enabling the development of a sea ice index for the period A.D. 1600 – 1850 (Ogilvie & Jónsdóttir, 2000). The observational record has been extended back in time to the late 19th century by compiling various

observational data sources including ship reports, airplane surveys, compilations by naval oceanographers and analyses by national ice services (Walsh et al., 2017). In Svalbard, sea ice information since 1800 has been collected from sealers, ships and trappers wintering on the archipelago by the Norwegian Polar Institute (Vinje, 2001), while April sea ice extent (a good proxy for maximum sea ice extent) in the Nordic Seas from 1850–1998 was generated from ship data, aircraft reconnaissance flights and satellite observation data (Vinje, 2001). April sea ice in the Barents Sea region was recorded by Norwegian ice charts by sealing and hunting expeditions from 1850-1949 and 1966-2001, and intervening years measured by Soviet reconnaissance aircraft (Shapiro et al., 2003). Sea ice draft and thickness were also measured through upwards sonar data by submarine cruises throughout the Arctic from 1958 onwards (Rothrock et al., 2008). These include comparisons of draft data (the thickness of sea ice extending below the water surface) from two summer polar cruises in 1958 and 1970 (A. S. McLaren, 1989), before more extensive draft data collection as part of the Scientific Ice Expeditions (SCICEX) program (Gossett, 1996). These historical sea ice observations provide information to varying degrees of accuracy and coverage, with records from the past two millennia being the most abundant. Since the 1970s, spatially explicit sea ice extent information has been available by the development of satellite observations (Post & Høye, 2013). Using these records, Walsh et al. (2017) produced a spatially-explicit sea ice dataset since the late 19th century at fine spatiotemporal resolution, enabling a comparison between historic data sets and proxy-based reconstructions (Post & Høye, 2013). Such spatiotemporally limited historic data sets therefore offer some context for recent sea ice changes, but provide inadequate insight on trends driven by broader-scale climatic trends. Further knowledge of past sea ice dynamics is needed to understand the context of recent change and gain insight into possible future sea ice trajectories under conditions of increasing global average temperatures.

The geological record and proxy data are important sources of information for environmental and climatic conditions preceding the advent of direct observations, though they are currently limited by abundance, length and/or resolution of records (Abram et al., 2013). Much of these data for past sea ice inference derive from ocean cores, which provide a variety of both biogenic and inorganic information from tracers, marker species to microfossil assemblages (Gersonde & De Vernal, 2013). Examples of biogenic palaeontological data include dinoflagellate cysts, ostracods, diatom and benthic foraminifera assemblages (Cronin et al., 2013; De Vernal et al., 2013; Seidenkrantz, 2013). Biomarkers used include IP_{25} – a C_{25} isoprenoid lipid formed by diatoms (e.g. Abram et al., 2013; Belt and Müller, 2013; Brown et al., 2014), phytoplankton-derived brassicasterol, and PIP_{25}, an index developed combining IP_{25} and the phytoplankton markers brassicasterol and dinosterol (Müller et al., 2011), and DIP_{25} – an isoprenoid diene to IP_{25} ratio (Cabedo-Sanz et al., 2016). Inorganic biomarkers include the use of ice-rafted debris (IRD) and radiogenic isotopes for tracking ice drift and provenance (e.g. Stickley et al., 2009; Hillaire-Marcel et al., 2013; Fagel et al., 2014). Sea ice extent has also been reconstructed from ice core data, using sea salt sodium (Levine et al., 2014) and flux rates of methanesulfonic acid (MSA) (Becagli et al., 2009; Criscitiello et al., 2013) and halogens (Spolaor et al., 2013, 2016), though these do not yet supply robust reconstructions due to interpretation and calibration limitations (Abram et al., 2013). Combining ice core isotopic composition with tree ring data has been shown to yield sea ice extent variability on centennial scales (Macias-Fauria et al., 2010), improving the coarse temporal resolution obtained by ocean records due to extremely low sedimentation rates in the central Arctic Ocean.

Such data provide information on environmental and climatic conditions preceding the advent of direct observations, and relative sea level variations can provide evidence of palaeosea levels and their changes in elevation (e.g. Andrews, 1970; Farnsworth et al., 2020a; Forman et al., 2004; Van de Plassche, 1986). Raised beaches that occur in northern Eurasia are

a result of glacioisostatic adjustment (GIA) following deglaciation. Their current elevation results from the balance between eustatic sea level change, and isostatic rebound of the lithosphere following the latest deglaciation of northern Eurasian ice sheets (Forman et al., 2004). Such raised beaches in Svalbard often lack vegetation due to their low temperatures, aridity, high alkalinity and low nutrient availability (Dyke et al., 1997; Forman et al., 2004). Such harsh conditions preserve datable driftwood, whalebones and pumice as decomposition is limited (Feyling-Hanssen & Olsson, 1959; Blake Jr, 1961; Bondevik et al., 1995; Schomacker et al., 2019; Farnsworth et al., 2020b). Whalebones are commonly utilised for reconstructing relative sea-level changes. As with whalebone, mollusc shells require correction for the marine reservoir effect, but in addition often have the limitation that the elevation of their living habitat cannot be accurately determined. Therefore, driftwood is the preferred target for analysis due to its terrestrial origin (and therefore radiocarbon dating suitability) and delivery to within 1-2 m above sea level by storm or ice pressure, although it can later migrate shoreward by post-depositional slope processes (Funder et al., 2011). Driftwood can also be used as a proxy for past sea ice conditions in the Arctic.

1.3 Arctic driftwood as a proxy for sea ice

Deposits of driftwood on Arctic shorelines reveal the transport by sea ice within large-scale Arctic Ocean circulations, which enables the reconstruction of past surface-current dynamics and sea ice conditions in the Arctic (Häggblom, 1982; Dyke et al., 1997; Funder et al., 2011). The collection of driftwood and its analysis began in the late 1800s, with collections made by Arctic explorers (e.g. Agardh, 1869; Kindle, 1921). Driftwood studies have increased in number and complexity in recent years, with examination of provenance, climate reconstruction and links to anthropogenic uses of wood (Giddings, 1952; Eurola, 1971; O.

Eggertsson, 1993; Ó. Eggertsson, 1994b, 1994a; Tremblay et al., 1997; Johansen, 1998, 2001; Alix, 2005; England et al., 2008; Vare et al., 2010; Funder et al., 2011; Hellmann et al., 2017). More recently Arctic driftwood has been used as a proxy for sea ice reconstruction, with the age and source of examined driftwood combined with and compared to hypotheses on the dynamics of the Beaufort Gyre and Transpolar drift. (Häggblom, 1982; Dyke et al., 1997; England et al., 2008; Funder et al., 2011; Hellmann et al., 2013b, 2017; Nixon et al., 2016; R. A. Blanchette et al., 2016; Hole & Macias-Fauria, 2017; Dalaiden et al., 2018).

Driftwood is a highly useful proxy for reconstructing sea ice patterns not only due to its inherent link to Arctic sea ice drift routes (Funder et al., 2011), but also due to it ubiquity and abundance on many Arctic coasts; with ages that span the climatic fluctuations of the Holocene. Arctic driftwood is not local given the absence of forests at these northern latitudes. Its delivery to the shores of the high Arctic requires sea ice for long-distance transport due to its limited buoyancy once waterlogged (Häggblom, 1982), and seasonally open waters to enable wave action to deliver the driftage to the shoreline. The incurred driftwood derives from the major rivers that drain the boreal forest regions of North America and Eurasia and contribute 38% of the freshwater influx into the Arctic Basin (Serreze et al., 2006).

Due to wood's limited buoyancy, it may not seem expected for driftwood from Arctic Ocean-draining rivers to reach such quantities on shorelines on the other side of the Arctic Ocean. The low water temperature and high Arctic Ocean salinity increase the buoyancy, but it is the presence of ice that enables transport of wood that would otherwise sink within a matter of months, making ice a key factor for long-distance driftwood movement (Eurola, 1971; Häggblom, 1982; Ó. Eggertsson, 1994a; Dyke et al., 1997; Johansen, 1999). Individual species differ in buoyancy, with the average values for each species compiled from various reports by Häggblom (1982):

Table 1.1. Species buoyancy compiled by Häggblom (1982)

Tree Species	Buoyancy period
Spruce (*Picea abies* – Norway Sprice)	17 months
Pine (*Pina silvestris* – Scots pine)	10 months
Larch (*Larix sibirica* – Siberian larch)	9-10 months
Birch (*Betula sp*. – birch)	6 months
Aspen (*Populus tremula* – aspen)	10 months
Willow (*Salix sp*. - willow)	6-10 months

Individual tree characteristics also have an impact on buoyancy upon entering the rivers, with a positive correlation between volume and buoyancy for conifers (Häggblom, 1982). While these differences likely have an impact on the likelihood of the wood remaining afloat long enough to become entrained within ice, wood often enters rivers during storm events and winter ice breakup, reducing the duration that the wood is free-floating. Therefore, sea ice is still the determining factor for long-distance transport of any tree species in the Arctic Ocean.

In regions of permafrost, incursion of trees into Arctic rivers is due mainly to riverbank erosion, which peaks with storm events. During the summer, the June and July snow and glacier melt increase erosion, while during August rainfall, the warmer and higher waters lead to the peak in riverbank erosion (Ashton & Bredthauer, 1986; Mason & Beget, 1991). One of the major rivers that drain into the Arctic Ocean is the Lena in Siberia; one of the largest to flow along the permafrost region. During the spring ice-breakup, river water temperatures rise up to 18°C, with water levels up 8-10m from May-July, submerging floodplains and islands (Costard et al., 2007). By June, floodwaters reach their highest velocities of up to 100,000 m^3s^{-1} in some localities (Yang et al., 2002; Gautier et al., 2003; Liu et al., 2005). The rising temperatures and levels substantially increase the thermal and mechanical erosion (Costard et al., 2003; H. J. Walker & Hudson, 2003; Randriamazaoro et al., 2007); leading to the peak retreat and erosion of river banks of up to over 20m in a year in prone localities, while the average rate is closer to 5-10m per year (Aré, 1988; Gautier et al., 2003).

Driftwood found on modern Arctic coasts includes both natural fallen trees, felled by erosion processes and storm events, and logged wood from the rafting of timber on rivers in the boreal regions (Hellmann et al., 2013a). Logged wood has discerning features such as missing rootstock and lack of branches that can aid in separating it from fallen wood. Beached driftwood also often has a set of particular features that may inhibit anatomical classification, including erosion, decomposition by fungi, missing rings, and holes from shipworms (*Teredinidae navalis*) (Hellmann et al., 2013a). Nevertheless, examination of features in a study discussed further below found that genus (and species in some cases) differentiation was still possible through anatomical examination of macroscopic and microscopic characteristics.

The major rivers contributing freshwater to the Arctic Ocean have been surrounded by boreal forest throughout the Holocene (Ritchie & Hare, 1971; Hopkins et al., 1981; MacDonald et al., 2000). The Eurasian boreal tree limit in the early Holocene of *c.*9.5-6ka BP lay up to 200km northwards at the circumpolar coastlines, due to increased summer insolation and temperatures compared to modern conditions (MacDonald et al., 2008), before migrating to its modern limit at 60-70°N (Sokolov et al., 1977; Bigelow et al., 2003). The boreal forest reached its current composition by *c.* 6 ka BP in Canada (Tremblay et al., 1997), and by 3-4ka BP in Eurasia (MacDonald et al., 2000), with increased *Larix* between 10 – 3.5ka BP. Low numbers of *Picea* in the Asian boreal forest have been consistent throughout the Holocene (MacDonald et al., 2008). In North America, *Picea* dominates west of Hudson Bay (the boreal forest east of Hudson Bay does not contribute driftwood to the Arctic Basin beyond Hudson Bay due to the lack of large north-flowing river drainage basins). In Asia, *Larix* (and *Pinus* to a lesser extent) dominates the eastern Siberian boreal forest, with *Picea* very slowly increasing in abundance westwards – though still at minimal percentages in central Siberia – to dominate, together with *Pinus*, in westernmost Eurasia (Europe) (Sidorova et al., 2016). *Pinus* is present throughout central and western Siberia, and in some parts of the watersheds of the Mackenzie and Yukon

in North America (Hellmann et al., 2013b), though at lower abundance in the boreal forests compared to *Larix* and *Picea*. It also constitutes a small percentage of naturally felled Holocene Arctic driftwood, making *Pinus* less useful for driftwood provenance analysis based on genus alone. With this knowledge of the geographical distribution of Arctic/boreal tree species, numerous studies exploring driftwood as a proxy for sea ice have used a genus-based division of driftwood to indicate wood provenance, with *Larix* assumed to indicate a Siberian origin, and *Picea* assumed to signify a North American origin (e.g. Dyke et al., 1997; Eggertsson, 1993; Funder et al., 2011; Häggblom, 1982; Hellmann et al., 2013b; Nixon et al., 2016).

In the high-latitude boreal forest zone, climate is a common limiting factor of tree growth, leading to coherency in tree-ring growth patterns within broad climatic region/watersheds (O. Eggertsson, 1993). This coherency enables regional chronologies of mean tree-ring growth patterns to be created across the boreal forest zone (Schweingruber, 2012) and utilised for dendrochronological matching to driftwood derived from possible boreal source regions.

Dendrochronology and tree ring width (TRW) analysis allows for more spatially – and temporally – precise provenance determination. The majority of driftwood dendrochronological studies will consider only reference chronologies associated with a particular drainage basin (Eggertsson, 1993; Eggertsson & Laeyendecker, 1995) based upon consideration of Arctic surface currents. However, some recent studies have highlighted that such assumptions can be incorrect, and a far wider extent of circumpolar sites must be considered during such processes, to accurately capture the potential history of samples (Hellmann et al., 2013). Employing a dataset of recent naturally-felled driftwood material from Northern Svalbard, Chapter 4 addresses the use of dendrochronology for Arctic driftwood provenance utilising a pan-Arctic reference record, and develops new numerical approaches to account for the patchy nature of the reference chronologies.

1.4 New driftwood provenance tools

Dendro-provenancing can only cover the regions and periods for which reference chronologies exist. To achieve a more precise definition of the role of atmospheric and oceanic circulation in sea ice and climatic changes throughout the Holocene, a pan-Arctic focus incorporating a more definitive determination of driftwood provenance fluctuations is needed. This would strengthen its use as a proxy for sea ice reconstruction by enabling the dynamics of the BG and TPD to be better determined at key climatic points of the past 12,000 years. Isotopic analysis of the driftwood tissue is one future avenue, with the strontium radiogenic isotope system previously explored for provenance studies in the form of $^{87}Sr/^{86}Sr$ ratios. Lithologies can be characterised by a defined $^{87}Sr/^{86}Sr$ ratio (English et al., 2001; Reynolds et al., 2005), which is not significantly fractionated by biological processes such as incorporation into wood tissue (English et al., 2001; Dijkstra et al., 2003). These features enable a spatial link between the wood and its growth site, providing that a framework of potential source strontium signatures is established. A further novel provenance tool is that of ancient DNA (aDNA) analysis or palaeogenetics. As wood is a commonly occurring archaeological remain (Gugerli et al., 2005), a variety of studies have already shown the application of aDNA analysis for archaeological/preserved wood for uses such as wood traceability and monitoring species evolution (Speirs et al., 2009). Sequencing of genomes of plant and animal tissue has been successfully employed on time scales exceed 0.5Ma (Orlando et al., 2021) and the possibilities of aDNA are likely to increase as technologies develop further.

In the use of driftwood's biological characteristics and isotopic signatures as tracers, an important consideration is the level of degradation and contamination that the wood has undergone in its journey from boreal riverside to Arctic shoreline. The degradation of wood by microorganisms occurs in a variety of environments, (Kim & Singh, 2000), but there has been a lack of assessment of the preservation of isotopic ratios in fossil wood (Boettger et al., 2003;

Savard et al., 2012). The immersion of wood in seawater has also been found to alter its chemical signature (Yamada et al., 2014; Fermé et al., 2015; Steelandt et al., 2016). In a study examining how drifted, imported and native wood in Iceland might be differentiated through chemical methods (Mooney, 2018), electrical conductivity testing found overlap between the wood types, as well as variation within individual driftwood samples. The author highlighted the many variabilities impacting archaeological wood that introduce uncertainty, such as length of time immersed and beached, leaching out of seawater by rainwater, and the level of burial or weather exposure of the samples before collection. The study surmised that the chemical signature of archaeological wood remains may be influenced more significantly by the depositional environment than by its origin.

Tree components and species also vary in their predisposition to decay, due to the individual biological constituents. Softwoods contain sugars that are more resistant to biotic decay compared to hardwoods (Fengel, 1991), while the level of protective extractives (non-structural or secondary constituents of plants e.g. resins (Hillis, 1971)) are greater in hardwoods, but also within trees these are greater in heartwood than in sapwood (Sandak et al., 2014). Thus, heartwood is more resistant to degradation, although the extractives themselves are prone to decay. Comparing the species-specific decay of lignin (the complex organic polymers providing structure within support tissue of most plants), archaeological pinewood was found to show more degradation than oak, despite being 400 years younger (Sandak et al., 2014). Similarly in a study on waterlogged wood degradation, pine, birch and other species with lower extractives were found to be less durable than more extractive-rich species once waterlogged (Blanchette, 2000). With such differences, it has been advised for the interpretation of isotopic data in fossil tree species to only be undertaken following investigation of the impact of decay on the wood constituent's isotopic ratios (Savard et al., 2012). Arctic driftwood also has its own unique set of conditions that influence the level and

type of decay that occurs. Upon entering the boreal rivers and the ocean, sediment scouring and shipworm *(Teredinidae navalis)* tunnelling can deteriorate the wood (Eriksen et al., 2015), exacerbated by the bacterial enzymes used by shipworms to ease cellulose digestion (Distel et al., 2002a, 2002b; Betcher et al., 2012).

1.4.1 Isotope systems for provenance

An element's isotopic composition is usually expressed as a ratio of atoms; for example the variation of strontium is expressed by the $^{87}Sr/^{86}Sr$ isotope ratio, resulting from differing numbers of neutrons and therefore atomic number (Allègre, 2008). Stable isotopes have compositions that are energetically stable, with sufficient neutrons to prevent repulsion of the atom's protons, while radiogenic isotopes result from the transformation of unstable radioactive isotopes into more stable nuclei, with resulting release of radiation. This occurs over a specific 'decay constant' that denotes the number of nuclei that decay per unit time, and is a constant fraction of the number of nuclei remaining. The isotopic composition ratios of many elements therefore vary by time and location, making possible their use as tracers and dating tools. Environmental inputs during tree growth determine the concentrations and ratios of various isotopes within wood. These inputs from sources including soil, water and airborne isotopes affect the wood composition of such isotopes in a variety of ways. Depending on the mechanism of uptake and utilisation by the tree, direct correlations to the sources can be determined, or if influenced by physiological processes within the tree, integrated signals can result. This is explored further below and in Chapter 5.

Variation in the stable isotopic ratios within trees due to physiological processes is well understood, as is the sensitivity of $\delta^{13}C$ and $\delta^{18}O$ isotope ratios to variation in meteorological and environmental conditions (Brandes et al., 2006). There is, however, remaining uncertainty

on the physiological process impacts on fractionation during metabolic and transport processes after wood tissue formation. The significance and utility of stable isotopic variation also depends on whether the absolute signature from bulk wood or series variability of values within each ring is used, as yearly variability will require standardisation (similarly to tree-ring width series) to express the tree isotopic variability to a common mean and therefore reveal comparable responses to external forcings. When extracting wood components for stable isotope analysis, there is some debate on whether α-cellulose (the most stable form of cellulose, the complex natural polysaccharide providing structure in cell walls) or lignin are the best for reconstructions of climate (Savard et al., 2012). For fossil or sub-fossil wood, degradation processes further complicate this choice. In an anaerobic environment, the polysaccharides of cellulose and hemi-cellulose (polysaccharides with shorter polymer chain lengths than cellulose) degrade at a faster rate than lignin (Björdal et al., 1999; Van Bergen & Poole, 2002; Gelbrich et al., 2008; Sandak et al., 2014)**,** which can generate a decrease in the $\delta^{13}C$ signature and obscure climatic signals. However in the place of cellulose, lignin may not be as sensitive to climatic change (Loader et al., 2003). Isotope systems that are less sensitive to short-term climate, environmental and physiological factors are therefore useful sources of provenance tools, such as inorganic radiogenic isotopes that are taken up from the environment into wood tissue. The most useful radiogenic isotopes for provenance are those that derive from elements that exist in concentrations above 10ppb within the target sample (trees in this study). These include strontium, sulphur and lead (Reynolds et al., 2005), whereas neodymium is of less use due to very low (<10ppb) concentration in wood. Metal isotopes can also migrate from the tree-rings of the year they were deposited (Lepp, 1975), with trace metal mobility being found to extend across the width of the sapwood (Lukaszewskp et al., 1988; Zayed et al., 1992; Brackhage et al., 1996). Such mobility affects the ability of any isotopic time-series through the rings to be used as an environmental proxy or for cross-dating. Isotopic tools that can utilise

the bulk measurement of a sample (not individual rings) is an avenue for development, due to reduced time and cost consumption, particularly given the primary goal of provenance determination, not climate reconstruction.

The strontium radiogenic isotope system has been widely employed for provenance studies in the form of $^{87}Sr/^{86}Sr$ ratios for over 30 years, in environmental, archaeological and regulatory studies, such as food product provenance authentication (e.g. Aberg, 1995; Durante et al., 2013; Gosz & Moore, 1989; Graustein & Armstrong, 1983; Voerkelius et al., 2010). The alkali metal strontium is a component within all rocks (English et al., 2001), with relative abundance of the radiogenic isotope form (^{87}Sr) specific to certain rock types (Guinn, 1978). Therefore, lithologies can be characterized by a defined $^{87}Sr/^{86}Sr$ ratio (English et al., 2001; Reynolds et al., 2005). With an ionic radius similar to that of calcium, strontium Sr^{2+} ions can substitute for Ca^{2+} in calcium-rich minerals including calcite, plagioclase feldspar, dolomite, gypsum etc (Bentley, 2006). However, the isotope of use in provenance, Strontium-87, is derived from the radioactive decay of Rubidium-87 ($t_{1/2}$=48.8 Ga), and consequently the Sr isotopic signature of bedrock derives from the initial $^{87}Rb/^{86}Sr$ ratio and the age of the rock (English et al., 2001; Reynolds et al., 2005). Rubidium is also an alkali metal, with an ionic radius similar to potassium, enabling Rb^{1+} to substitute for K^{1+} in minerals including potassium feldspar, biotite and muscovite (Bentley, 2006). The bedrock lithology determines the Sr ratio; old metamorphic rocks contain a greater initial proportion of ^{87}Rb and therefore contains more of the decay product ^{87}Sr and a higher $^{87}Sr/^{86}Sr$ ratio (> 0.710) than other lithologies. Younger volcanic, basaltic rocks have lower initial Rb and so lower ratios (~0.702–0.704), while sedimentary rocks have intermediate values (~0.707– 0.709), resulting from the ocean Sr composition at the time of deposition (Gosz & Moore, 1989; English et al., 2001; Banner, 2004; Bentley, 2006; Rich et al., 2012). Bedrock lithology and age therefore determine the Sr ratio.

Strontium is not as prone to geological or biological fractionation due to its higher mass compared with other isotopic systems such as H, C, O, meaning that weathering products such as secondary clay minerals will retain the parental bedrock signature (Capo et al., 1998; Bentley, 2006), along with the soils above the bedrock and the plants sampling them (English et al., 2001; Dijkstra et al., 2003). Yet the Sr signature of surface waters derived from bedrock, and particularly potassic silicate rocks, has a differing isotopic signal than the bulk rock it is released from. This is due to weathering that initially favours the dissolution of mineral inclusions and cation-leaching from mineral defect sites (Blum & Erel, 2003). These waters and the surrounding soils are then more dominated by the Sr that is more rapidly released from reactive minerals such as calcite and evaporates (Blum et al., 1998; Bataille et al., 2014). The bioavailable Sr signatures of soils are often dominated by weathering processes, with alluvial soils containing the mixture of sediment and their Sr signatures from upstream inputs. A study looking at the processes affecting Sr uptake in mixed Norway spruce and Scots pine examined $^{87}Sr/^{86}Sr$ and $^{18}O/^{16}O$ variation in soils at varying depths found an increasing $^{87}Sr/^{86}Sr$ ratio with depth (Poszwa et al., 2004). The study results were also used to develop a simple flux model for the investigation of the variations in Sr cycling, soil mineral weathering and depth of Sr uptake on soil and tree $^{87}Sr/^{86}Sr$ ratios. The variation of $^{87}Sr/^{86}Sr$ ratio in bulk soils with depth correlated with the variation of soil contents and mineralogy due to chemical weathering losses over time (Olsson & Melkerud, 2000), though for spruce, a Z-shaped profile of $^{87}Sr/^{86}Sr$ meant that Sr ratios could not be immediately linked to a depth of Sr uptake. The Sr signature of soil water also originates not only from those weathering processes that form the soils, but also atmospheric dust (Graustein & Armstrong, 1983), as well as rainfall and groundwater (Poszwa et al., 2004); that can all lead to varied Sr signatures.

Atmospheric dust influences soil strontium by the effects on soil mineralogy. As strontium derives from the cation components of carbonate dust, it therefore originates from

carbonate bedrock and soil carbonate that has been entrained into the transported dust (Naiman et al., 2000). Precipitation can dissolve the carbonate and the soil/water exchangeable fraction, with carbonate then precipitated once at depth within the soil. The silicate fraction may be weathered to release Ca which if transferred to depth within soil can then precipitate as calcium carbonate. Calcium is often investigated alongside strontium due to their very similar behaviour within biological and environmental processes (Silkin & Ekimova, 2012), including their similar incorporation into tree bark. In the Siberian regions a particular important atmospheric influence may derive from radiogenic dust transported long distances from Central Asia (Bagard et al., 2013). In such permafrost regions this input may be especially significant; after it was found the weathering rates in permafrost-dominated boreal regions were found to be some of the lowest in the world, increasing the dominance of external inputs such as dust (Pokrovsky et al., 2005; Viers et al., 2013).

Proximity to rivers has been shown to also influence the dominant bioavailable strontium ratio; a study found that plants bordering streams reflected the stream-water $^{87}Sr/^{86}Sr$ ratio that itself integrates the signatures from the bedrock of the drainage area, while further from the stream the signature tended towards the local soil Sr ratio (Sillen et al., 1998). Rivers carry most terrestrial weathering products to the oceans as both suspended load and a small percentage of the strontium in solution. River water Sr concentrations globally average at 0.06 ppm and vary from about 0.006 to 0.8 ppm (Capo et al., 1998), while the $^{87}Sr/^{86}Sr$ ratio shows consistency over a range of flow rates (Bain et al., 1998). Like soils, river Sr composition is not necessarily simply a reflection of the drainage basin bedrock compositions due to variable erosion rates depending on the geology. This is particularly the case for low-elevation rivers such as those that drain into the Arctic Ocean, as the rivers have sampled the integrated signal of upstream lithologies and regional precipitation (Bentley, 2006). As such water would also be deposited on low-elevation floodplains, the $^{87}Sr/^{86}Sr$ ratio of rivers is a good predictor of the

Sr signature that is bioavailable to plants (Bentley, 2006). For trees flanking the Arctic rivers that fall to become driftwood, the Sr signature is therefore likely to be dominated by the river water Sr signature. Any measurement of pan-Arctic rivers should ideally be measured at the point in time when flow rates exceed mean annual discharge to avoid the spring thaw/freshet (Brennan et al., 2014), as the increased discharge during spring melt yield elevated dissolved organic carbon and dissolved nitrogen concentrations, and diluted major ion concentrations that are shifted from base flow toward precipitation values (Douglas et al., 2013).

The Sr that is taken up by a tree again remains unfractionated. In a study of Cypriot cedars (Rich et al., 2012), local bedrock, early heartwood of the innermost pith ring and the late heartwood $^{87}Sr/^{86}Sr$ signature were compared to enable a physiological comparison between samples. The bedrock $^{87}Sr/^{86}Sr$ ratios were substantially lower than the sampled wood, but very consistent between the two sites. Other studies such as on groundwater strontium in southeast Australia has highlighted the likely importance of rainfall $^{87}Sr/^{86}Sr$ ratios (Raiber et al., 2009), while studies demonstrated that in regions proximal to the coast, plant ratios were closely coupled to the signatures found in sea-induced rainfall and sea-spray (Kennedy et al., 1998; Vitousek et al., 1999; Whipkey et al., 2000; J. A. Evans et al., 2009). In Scotland, precipitation $^{87}Sr/^{86}Sr$ values were found to be consistent across sites ~300km apart and closely matched ocean water $^{87}Sr/^{86}Sr$ values (Bain & Bacon, 1994). Therefore, the higher ratio in wood in Cyprus likely reflected the same marine influence (Rich et al., 2012). The Sr signature of trees is also dependant on rooting depth and the residence time of the soil water (Reynolds et al., 2005).

For riparian trees flanking Arctic rivers that become driftwood, the Sr signature of the tree while living is likely to be dominated by the river water Sr signature. The main contributions of Sr in river systems are weathering of the local bedrock and rainfall and runoff water, therefore, the Sr isotopic composition of rivers varies geographically (depending on the

bedrock inputs and precipitation of the river watershed). Consideration must also be given to possible contamination once the tree has fallen and entered the river and eventually reached the ocean; overprinting the source signature by biological and physicochemical processes from interaction with river water, ocean water, and sea salt aerosols (Hajj et al., 2017). The Sr concentration of seawater is about 8 ppm, in river water it is about 50 ppb (Van Ham-Meert et al., 2020)., with contributions both from weathering and from volcanic inputs to the total Sr in sea water, leading to variation in seawater $^{87}Sr/^{86}Sr$ signatures over geological time. The modern $^{87}Sr/^{86}Sr$ signature of seawater is 0.7092 and geographically homogeneous (Van Ham-Meert et al., 2020). Due to constant erosion and ocean circulation processes, the $^{87}Sr/^{86}Sr$ signature of seawater reflects the globally averaged signal of eroded continental bedrock. This signature is also homogeneous due a residence time of Sr of millions of years; greater than the millennial turnover time of the oceans (Bentley, 2006).

Exogenous/contaminant sources of strontium within samples can be tested for through comparison of Sr concentrations with $^{87}Sr/^{86}Sr$ ratios, and of living with architectural wood (Reynolds et al., 2005). A differing concentration was taken to indicate contamination, with the contamination showing an isotopic ratio biased towards a contamination source signature. Mixing models can be used to elucidate the extent of differing strontium sources as inputs and therefore endmembers for the signature found within bedrock, soil and wood. Different contributing reservoirs can be plotted on a mixing line, with $^{87}Sr/^{86}Sr$ ratios plotted against 1/Sr (e.g. Montgomery et al., 2007). 1/Sr is used in place of Sr to form a straight line between end-members, as the differing levels of contribution from each reservoir gives a curve for a ratio vs. Sr plot. The proportional contributions of differing bio-available Sr can then be calculated (Bentley, 2006). As an example, for a mixing model that includes dust, the total dust Sr is composed of the water-soluble snowmelt, acid soluble dust leach, and insoluble dust grains fractions (O. L. Miller et al., 2014). The bioavailable components are the water and acid soluble

fractions, which can then be combined to calculate the total dust endmember of the mixing model. Investigations into the isotopic impact of waterlogging found that waterlogging significantly contributes to the overall Sr content in wood and hence there is a large proportion of exogenous Sr in waterlogged wood (Steelandt et al., 2016; Hajj et al., 2017). In the 2016 study by Steelandt et al., wood samples were placed in the Hudson River, and a 3-fold increase in the bulk Sr concentration after just one week in the river was observed. Archaeological wood placed in seawater for 3 months (Hajj et al., 2017) resulted in a 10-fold increase in Sr concentration. Such experiments confirm that waterlogging significantly contributes to the overall Sr content in wood, and that waterlogged wood contains a large proportion of exogenous Sr, which must be taken into consideration when considering cleaning and analytical approaches.

With these complexities in mind, the features of Sr enable the local geological and sediment isotopic signature of the target materials to be linked to the source providing that a framework of potential source strontium signatures can be established. Either the framework is established through extensive sampling of potential sources such as bedrock and water sources (e.g. Frei & Frei, 2011; Maurer et al., 2012; Rich et al., 2012), or the baseline can be described through developing a model (e.g. Bataille et al., 2012, 2020; Beard & Johnson, 2000; Brennan et al., 2014). For baseline establishment, the method of geochemical map-building requires reference databases of $^{87}Sr/^{86}Sr$ that can be assembled through several methods. If a region has been covered by geological mapping, then through an extrapolated map of assumed $^{87}Sr/^{86}Sr$, values can be derived from the lithologies and ages of the local bedrock, or from measured bedrock extracted from the locality (Laffoon et al., 2012). Bio-available strontium is not necessarily primarily driven by the local lithology, while achieving sufficient coverage for sampling is costly and inevitably incapable of covering the entire target region (Brennan et al., 2014), particularly for a global (or pan-Arctic) scope. For high-latitude rivers, there is also

temporal variation on Sr signatures on an intra-annual scale (Douglas et al., 2013; Keller et al., 2010), due to permafrost causing a seasonal variation in the contributing sources of strontium to groundwater. An example is the Chena River basin in Alaska (Douglas et al., 2013), which samples an area underlain by discontinuous permafrost. In winter, with soil profiles frozen and a shallow active layer, the river $^{87}Sr/^{86}Sr$ values reflect the low $^{87}Sr/^{86}Sr$ signature of subsurface carbonate rocks. In spring the thawed active layer is sampled by the groundwater, increasing the $^{87}Sr/^{86}Sr$ signature due to the carbonate-depleted soils. Such seasonal variation in groundwater interaction paths is also shown in Siberian rivers. A significant hurdle when determining a viable circum-Arctic map of $^{87}Sr/^{86}Sr$ for provenance (or indeed for any location), as revealed in these studies, is that the local variations in $^{87}Sr/^{86}Sr$ can exceed the variation in major regional lithological trends. Hoogewerff et al. (2019) note that locally there is often a significant statistical correlation between bedrock and soil and/or plant $^{87}Sr/^{86}Sr$, but that the slope of such correlation is often <1 in a plot of $^{87}Sr/^{86}Sr$ bedrock on the X-axis versus $^{87}Sr/^{86}Sr$ soil or plant (Baroni et al., 2011; Goitom Asfaha et al., 2011). This indicates an influence of contamination on the lithological signal, such as surface deposits, sea spray, airborne dust and land use.

The diversity of contributors of bioavailable Sr means that for wood provenance studies it has been suggested that focusing on sampling trees from the study localities instead of the geology may yield better results (Laffoon et al., 2012; Rich et al., 2015). Yet due to variation in $^{87}Sr/^{86}Sr$ values through time, including anthropogenic change from pollution and fertiliser use (Borg & Banner, 1996; Kamenov et al., 2011; Laffoon et al., 2012), sampling modern trees and vegetation may not reflect exactly the values throughout the Holocene. Anthropogenic sources of strontium from industrial and agricultural inputs have an isotope ratio lower than that of the present-day seawater (Böhlke & Horan, 2000; Négrel et al., 2004; Jiang, 2011), therefore meaning that for living wood from the boreal riversides, lower isotopic ratios than

expected may indicate the influence of such anthropogenic strontium. A decreasing strontium ratio trend was observed in North American red spruce from 1870 to 1960 (Bullen & Bailey, 2005), and this was explained with a hypothesis of a shallowing of the depth of element take-up. Expansion and growth of the fine roots of the shallow forest floor were observed, and $^{87}Sr/^{86}Sr$ and Sr/Ba ratios where analysed within spruce tissues and soil fractions. The expansion was explained as a possible result of acid deposition and response by roots to Ca depletion and aluminium toxicity. This shifted the region of uptake from shallow, high $^{87}Sr/^{86}Sr$ soils to the uppermost/organic soil horizons with lower isotopic ratios. Observed $^{87}Sr/^{86}Sr$ decreases in the periods of 1870-1890 have also been suggested as linking to the contemporaneous increased in sulphur emission from the increase of industrialisation in the late 19th century (Drouet et al., 2005). The mobility of strontium within tree rings up to 50 years after assimilation observed however, means that the effects might not be a result of a response to the gradual acid deposition from 1870-1890, but instead a more rapid change at 1920, lessening the likelihood of the sulphur emission's main role (Drouet et al., 2005). Preceding the industrial revolution, bicarbonate (HCO_{3-}) or organic anions dominated, before fossil fuel combustion lead to the replacement of the dominant carbonic acid by sulphuric acid (Tomlinson, 2003)**.** This leads to increased transfer of cations from exchangeable sites to the soil solution, eventually reaching a new equilibrium of Sr weathering, leaching and uptake and a stabilisation of Sr ratios after 1920 (Drouet et al., 2005). The characteristics of the strontium system and the potential use of radiogenic $^{87}Sr/^{86}Sr$ as a provenance tool for driftwood are therefore further explored in detail in Chapter 5.

1.4.2 Genetic methods for provenance

Given the limitations to existing methods, a further novel provenance tool warranting exploration is that of ancient DNA (aDNA) analysis or palaeogenetics. Microanatomical analysis of driftwood can only glean taxonomy to genus level, and therefore aDNA analysis provides the possibility of further techniques to refine the wood's taxonomic identification. The examined aDNA could then be compared with existing palaeoecological and phylogeographic data on boreal tree species distribution during the Holocene; therefore providing a possible determination of provenance. This could be further refined in combination with dating to provide a time window for palaeoecological and phylogeographic data. The extraction of ancient DNA requires preservation of sufficiently unique sequences of DNA, which is known to be problematic for fossil and subfossil wood due to the speed of DNA degradation leading to fragmentation and modification of the recoverable DNA (Lindahl, 1993; Pääbo et al., 2004). Specifically, in the case of Arctic driftwood, the long duration of exposure to ocean waters and subaerially on shorelines means DNA-degrading temperature fluctuations of up to tens of degrees. However, the cold and dry conditions of the Arctic and alkaline soils act as preserving factors and limiting any microbial action on the wood (Dyke et al., 1997). Despite the DNA-compromising factors, with improvements in technology sequencing of genomes of plant and animal tissue has been successfully employed on time scales exceeding 0.5Ma (Orlando et al., 2021), with the oldest successful genome sequenced from horse bone tissue preserved in permafrost for 560,000–780,000 years (Orlando et al., 2013). Chloroplast DNA from the oak timber of a waterlogged 16th century shipwreck, the Mary Rose, has also been successfully extracted and amplified (Speirs et al., 2009). Recent progress has also been made through high throughput (HTS) DNA sequencing of archaeological and subfossil wood up to 9,800 years old (S. Wagner et al., 2018). That successful extraction supplies evidence in support of the feasibility of extraction of DNA from marine waterlogged archaeological wood,

and therefore indicates that the same may be possible for the extraction of driftwood aDNA for species and provenance analysis. The characteristics of ancient DNA analysis and attempted extraction from sub-Arctic driftwood is outlined in Appendix D.

1.5 Specific Aims and Hypotheses

The exploration and development of driftwood as a tool for proxy-based Arctic sea ice reconstructions consist of three main aims:

1. The use of a pan-Arctic driftwood collection, with radiocarbon and genus data, newly assembled as part of this DPhil, to investigate the following hypotheses:
    i. Pan-Arctic driftwood data can provide insight into centennial and millennial variation in the predominant Arctic surface currents (the Beaufort Gyre and Transpolar drift), throughout the Holocene, with associated impacts on sea ice extent and dynamics.
    ii. These changes are linked to large-scale modes of climatic variability such as the Arctic Oscillation.
    iii. There is an interplay of surface currents driven by atmospheric circulation *vs.* thermal forcing on the sea ice extent during the Holocene, and this can aid in placing the current observed 20th and 21st century Arctic sea ice trends within this much larger framework.

    Collated radiocarbon and genus data from Holocene driftwood across the Arctic can test these hypotheses via revealing the spatiotemporal trends in distribution, age and genus-based provenance of driftwood throughout the Holocene, which are determined by sea ice and surface current dynamics. The resulting reconstruction, of higher spatiotemporal resolution than other proxy data sources, is then used to infer the role of atmospheric and oceanic circulation in controlling the patterns of sea ice conditions and dynamics (and consequently driftwood deposition). For this a pan-Arctic perspective of driftwood fluctuations is important, as local trends are influenced by local conditions,

coastal geomorphology and smaller scale coastal currents. This is outlined further in Chapter 3.

2. The development and validation of the novel use of dendro-provenancing at a pan-Arctic scale to increase the spatio-temporal resolution of driftwood-based sea ice reconstructions.
3. The exploration of further novel techniques to refine the provenance of driftwood through radiogenic isotopic analysis ($^{87}Sr/^{86}Sr$) and ancient DNA (aDNA). Provenance by genus is limited by spatially coarse resolution, while provenance by dendrochronology is reliant on existing boreal forest reference chronologies. The use of geochemical and genetic techniques addresses the limitations of these current methods, and if successful, will achieve a clearer definition of the role of atmospheric and oceanic circulation in sea ice and climatic changes throughout the Holocene at a clearer spatial and temporal resolution.

To fulfil these aims, the use of driftwood as a novel proxy enables investigation into the dynamics of Arctic sea ice throughout the Holocene at centennial to decadal timescales. The work within this thesis has explored a suite of techniques including dendrochronology, radiocarbon dating, micro-anatomical analyses and novel methods such as radiogenic isotope analysis ($^{87}Sr/^{86}Sr$) and ancient DNA extraction, in collaboration with a network of researchers.

1.6 Outline of Chapters

Chapters 1 and **2** describe the overarching aims of the thesis and methods employed. **Chapter 1** outlines the current state of the research field, and introduces the concepts and areas of research that form a cohesive contribution to the exploration and development of driftwood as a tool for proxy-based Arctic sea ice reconstructions. **Chapter 2** outlines the processes of dendrochronological, anatomical analysis, geochemical laboratory methods for strontium extraction and analysis, and the reasoning behind method selections. **Chapter 3**, examining the spatiotemporal distribution of driftwood from the collated database of previously published data, is published in *Journal of Geophysical Research: Oceans*, under the title *"Out of the woods: Driftwood insights into Holocene pan-Arctic sea ice dynamics"* – Hole, G.M., & Macias-Fauria, M. - https://doi.org/10.1002/2017JC013126. The analysis of 913 driftwood samples from across the western Arctic with available provenance data has enabled the production of a high-resolution proxy-based reconstruction of Holocene Arctic Ocean surface current and sea ice dynamics. Although regionally-bounded, driftwood-based sea ice reconstruction studies suggest spatiotemporally complex past Arctic sea ice extent and movement, a large-scale compilation of Holocene Arctic driftwood had not previously been developed. The results from this paper have brought new insights into the variable climatic and environmental conditions that have impacted the Arctic throughout the past 12,000 years, and provide a dataset of higher spatial and temporal resolution than other sea ice proxy-based methods in the Arctic. This has enabled the detection of the pattern of change at different frequencies through the Holocene. This article was highlighted by the editor upon submission and featured in the AGU blog (https://agupubs.onlinelibrary.wiley.com/hub/article/10.1002/2017JC013126/editor-highlight/), subsequently gaining media impact. The results of this study have also been presented through oral and poster presentations at national and international conferences.

Chapters 4 and **5** examine the validation of driftwood as a proxy for reconstruction with the development of novel provenance techniques. **Chapter 4**, consisting of the second research paper, presents a 500-year history of driftwood incursion to northern Svalbard, directly reflecting regional sea ice conditions and Arctic Ocean circulation. The paper is published in *Journal of Geophysical Research: Oceans*, under the title "*A driftwood-based record of Arctic sea ice during the last 500 years from northern Svalbard reveals sea ice dynamics in the Arctic Ocean and Arctic peripheral seas.*" - Hole, G. M., Rawson, T., Farnsworth, W. R., Schomacker, A., Ingólfsson, Ó., Macias-Fauria, M. (2021). - https://doi.org/10.1029/2021JC017563. Provenance and age determinations by dendrochronology and wood anatomy provide insights into dynamic Arctic Ocean currents and climatic conditions through time at a finer spatial resolution than by genus alone. The study also considers alternate mathematical approaches to selecting more probable origin sites, by weighting scores via reference chronology span and visualising results through spatiotemporal density plots, as opposed to more basic ranking systems. The resulting record indicates centennial- to decadal-scale shifts in source regions for driftwood incursion to Svalbard, aligning with Late Holocene high variability and high frequency shifts in the Transpolar Drift and Beaufort Gyre strengths and associated fluctuating climate conditions. The new methodological approach successfully employs driftwood as a proxy for Arctic Ocean surface current and sea ice dynamics. This article was also picked by AGU as being of potential media interest, with a subsequent press release (https://news.agu.org/press-release/arctic-driftwood-tracks-500-years-of-arctic-warming-and-sea-ice/) and media impact.

Chapter 5 presents the development of novel techniques to refine the provenance of driftwood through radiogenic isotopic analysis ($^{87}Sr/^{86}Sr$), and is currently submitted to *Palaeogeography, Palaeoclimatology, Palaeoecology*, under the title "*Dropped in the Ocean*

– *$^{87}Sr/^{86}Sr$ as a provenance tool for ice-rafted Arctic driftwood*." - Hole, G.M., Sinclair, D., & Macias-Fauria, M. Methods for the extraction, isolation and purification of strontium from driftwood through microwave digestion, extraction chromatography and MC-ICP-MS analysis were successfully developed. The use of geochemical techniques addresses the limitations of existing methods, and can define of the role of atmospheric and oceanic circulation in sea ice and climatic changes throughout the Holocene at a finer spatial and temporal resolution than currently possible. The utilisation of $^{87}Sr/^{86}Sr$ ratios to establish provenance for Arctic driftwood was determined to hold potential, with confounding factors in the potential overprinting of the source signature by biological and physicochemical processes from interaction with river and ocean water, and in the scale and heterogeneity and temporal variations of pan-Arctic source regions. Increased sample populations and source samples for calibration to enable validation are recommended for this work to be built upon in combination with previously developed provenance tools and reconstructions. The chapter provides a first step in a multi-proxy reconstruction of Holocene driftwood incursion onto northern Svalbard shorelines.

In **Chapter 6**, the resulting findings of the three manuscript chapters are brought together in a discussion of their overarching contribution to increasing insights into Holocene Arctic sea ice changes. Finally, proposed future trajectories and considerations are discussed, concluding in **Chapter 7**. Within the appendices, supplementary materials, detailed procedural information, and data tables are included where not included in the main thesis chapters. This includes, in **Appendix D**, details of the exploration of palaeogenetic techniques to refine the provenance of driftwood via attempted extraction of ancient DNA from driftwood tissue. Though not successful, there remain avenues for future investigation.

1.7 Significance and Scope

The reconstructed Holocene sea ice dynamics serve as the basis for future proxy-model comparison of climate and sea ice-conditions, as well as a framework for testing hypotheses on the coupling between sea ice and arctic biota. Benefits beyond the DPhil project arise from this gathering of new and re-analysed pan-Arctic driftwood data, in contribution to efforts around the boreal region to construct long-term millennial tree-ring chronologies that serve as proxies for past climatic reconstructions. The driftwood-based sea ice chronology can also be validated and combined with a suite of other sea ice proxies, such as deep ocean cores, other proxy measures of Arctic sea ice, and modelling, with some of these already underway and utilising the data produced from this thesis (Dalaiden et al., 2018; Farnsworth et al., 2020a), discussed further in the thesis conclusions. These cover a variety of geographical areas and timespans and so provide opportunities for comparison and integration of the data produced. Chapters 3 & 4 also gained media interest with further dispersal of the research by American Geophysical Union (AGU) through a research highlight and press release respectively, as detailed in the Outline of Chapters. By increasing the understanding of the Arctic system and dynamics, the feedback links between biotic and abiotic processes in the light of current environmental change can be better addressed, therefore aiding to plan and manage this highly sensitive region. Given the increasing importance of Arctic climate change on a global scale, and the well documented recent rapid decline in Arctic sea ice extent, age and thickness, increasing the understanding of Arctic sea ice fluctuations is relevant to current and future UK and international climate research. This scientific field is constantly evolving and remains under active research, while methodological developments, such as those presented in Chapter 4, highlight dendro-provenancing as the current best-available tool to improve spatiotemporal determination of driftwood and a method that warrants being used in tandem with geochemical and genetic methods to further define the role of atmospheric and oceanic circulation in sea ice

and climatic changes throughout the late Holocene. This gives added benefit to the research outcomes and new datasets arisen from the work of this thesis.

2 Research Approach and Methodology

In order to address the research questions and expected outputs of the project, the research approach has included collation and analysis of existing data, primary sample collection, and development of a range of methodologies for the anatomical, dendrochronological, genetic and geochemical analysis of driftwood samples. Established wood anatomical and dendrochronological methods are being utilised, while the testing and development of new analytical methods of ancient DNA extraction, and radiogenic $^{87}Sr/^{86}Sr$ isotopic analysis of driftwood are significant outputs of the thesis.

2.1 Collation of Existing Driftwood Data

A first pan-Arctic collation of Holocene driftwood data was undertaken in order to generate a reconstruction of sea ice and surface current dynamics. As detailed in **Chapter 3**, (and **Appendix A**) data from 913 driftwood samples previously collected throughout the western Arctic coastline and covering the Holocene were collated from a range of previous studies (Figure 2.1). These were used to produce a spatiotemporal dataset of deposited driftwood identified at the genus level, where available. The radiocarbon ages (^{14}C yr BP), where given in the literature, were calibrated with the IntCal13 calibration curve using the program OxCal v4.2 (Bronk Ramsey, 2009) and are presented in median calibrated radiocarbon years before present (cal. yr BP) and are directly comparable to calendar years BP for samples dated by other methods. The low errors associated with radiocarbon dating of wood material allow for the high temporal resolution of analysis compared to other proxy methods in the Arctic such as ice-rafted debris and ocean sediment core data (outlined further in Chapters 3 and 4) . The 913 driftwood samples from across the Arctic coastline provides a dataset of higher

spatial and temporal resolution than other sea ice proxy-based methods in the Arctic, with preservation of driftwood in substantial volumes from the early Holocene indicating a low likelihood of preservation issues in the interpretation of distribution patterns.

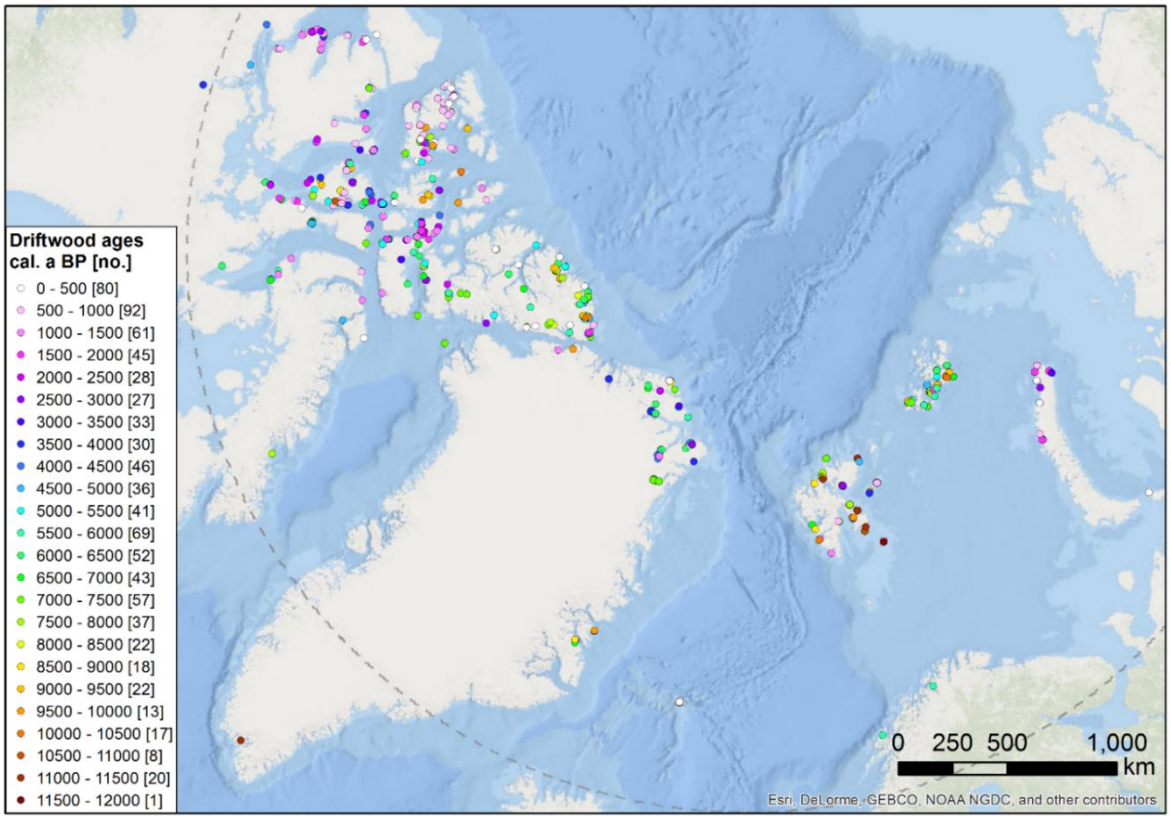

Figure 2.1. Geographical distribution of the driftwood data collated in the analysis conducted in Chapter 3 (Hole & Macias-Fauria, 2017). The colours represent the calibrated driftwood ages B.P, separated into 500 year intervals for visual clarity, calibrated with the IntCal13 calibration curve using the program OxCal v4.2 (Bronk Ramsey, 2009). The resulting age range represents the 95% confidence interval ± 2 sigma, and the median value was used for the purpose of the map. Square bracketed figures denote the number of samples from within each interval. For list of data and sources see Appendix A1.

2.2 Sample Collection

Initially, a few test samples of driftwood from the island of Jan Mayen in the Arctic Ocean and Nordkapp in northern Norway were prepared for dendrochronology, DNA extraction, microanatomy and isotopic analysis in order to begin methodology testing, followed by the sourcing and collection of samples through both fieldwork and visiting Arctic driftwood researchers' collections. As explored further in **Chapter 4** (and **Appendix B**), one region

targeted for Arctic driftwood collection is the Svalbard archipelago (Figure 2.2). The shorelines of Svalbard are rich in raised beaches that preserve stranded driftwood. It is located at the proposed north-western part of the Late Weichselian Svalbard-Barents Sea Ice Sheet (SBSIS), with abundant preserved raised beach sequences reflecting the pattern and rate of relative sea

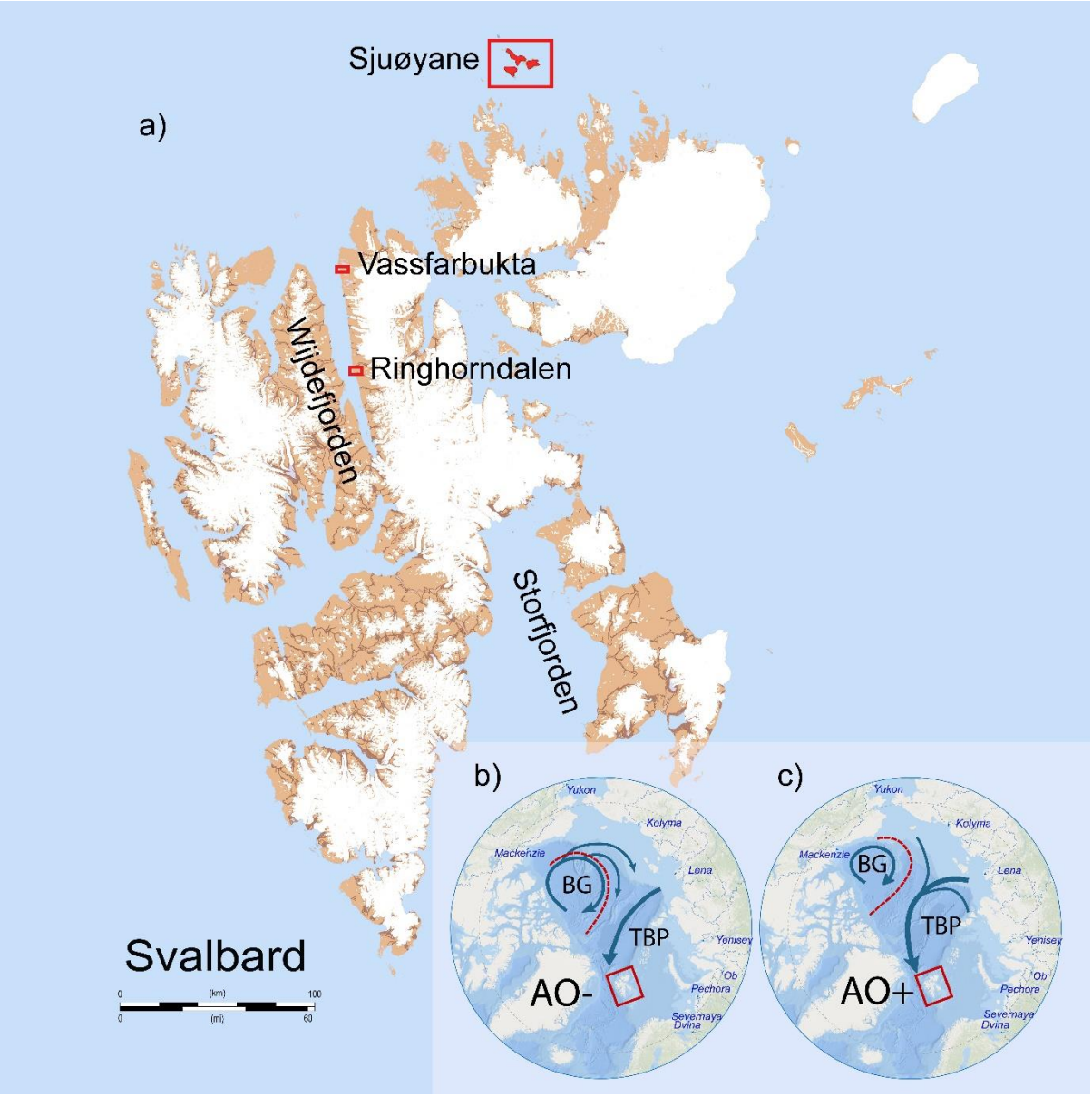

Figure 2.2. a) Driftwood sampling locations of Sjuøyane, Ringhorndalen, and Vassfarbukta. Insert panel: Two modes of the Arctic Oscillation Index (AO), showing wintertime surface circulation patterns of Beaufort Gyre (BG) and Transpolar Drift (TBP). Map figure modified from Norwegian Polar Institute (2014). (b) Low index, negative AO polarity with a strengthened Beaufort Gyre and recirculation of sea ice. (c) High index, positive AO polarity with a weakened BG. The red dashed lines encircle the region of ice recirculation in the BG by the mean sea ice motion field (circulations compiled and modified from Rigor et al. (2002)).

level changes on Svalbard in response to the deglaciation of the SBSIS (Forman et al. 2004; Ingólfsson & Landvik, 2013). Relative sea-level changes signalled by raised marine landforms around Svalbard were first recognised in the 19th century by Scandinavian geologists (de Geer, 1919; Nordenskiöld, 1866), before the first radiocarbon dating of strandlines in the 1950s and 60s (Feyling-Hanssen, 1955; Blake Jr, 1961a). Uplift patterns following the retreat of ice sheets were first recognised by Schytt et al. (1968), and were confirmed by the production of relative sea level curves and the resulting ice load reconstructions they enable (Forman, 1990; Landvik et al., 1998; Forman et al., 2004). This has led to a good understanding of the extent of the last SBSIS and subsequent deglaciation, established by multiple data collections from the Svalbard archipelago (Ingólfsson & Landvik, 2013). Relative sea-level changes has been used to constrain models of the SBSIS dynamics and thickness (e.g. Patton et al., 2017). In eastern Svalbard, Late Weichselian and Holocene raised beaches occur at 60 to 130 m above high tide (a.h.t.) covering the range of marine limit shorelines with greater postglacial rebound, whereas more marginal areas to the north and west show beaches at 65 m a.h.t. or lower (Forman, 1990; Forman et al., 1997a). On Phippsøya, the largest island of Sjuøyane, a lower marine limit of 22 m a.h.t. was identified (Forman & Ingólfsson, 2000), contrasting to adjacent Nordaustlandet where the limit occurs at 60 to 100 m a.h.t. (Salvigsen and Nydal, 1981; Schomacker et al., 2019). Such differences indicate varied glacioisostatic adjustment (GIA) related to former ice seet extent and timin, with less loading in the marginal areas of the former ice sheet and greater loading towards the former ice divides (the thickest parts of ice sheets). The SVALHOLA database, a compilation of Holocene geochronology for Svalbard and the surrounding waters (Farnsworth et al., 2020a) indicates that residual SBSIS ice still covered parts of Svalbard by 12.0 ka BP, with subsequent ice loss and marginal retreat extending through the Early Holocene.

In the summer of 2016, fieldwork was undertaken in northern Svalbard in collaboration with Prof Ólafur Ingolfsson at the University Centre in Svalbard (UNIS) as part of the postgraduate course "AG-848 - Arctic Late Quaternary Glacial and Marine Environmental History". Field sampling was undertaken of 95 driftwood samples of varying Holocene ages from three localities (outlined further in **Chapter 4**): Sjuøyane, an archipelago north of Nordaustlandet, and two localities within Wijdefjorden, northern Spitsbergen. Driftwood samples sourced from the shoreline of Vassfarbukta, Wijdefjorden in northern Spitsbergen, were received from Wesley Farnsworth from UNIS, with samples from Ringhorndalen collected by Marc Macias-Fauria supported by NERC IRF grant: NE/L011859/1. The samples were collected from regions of driftwood incursion on the modern shorelines of raised beach sequences, with a small number from raised palaeo-shorelines. Therefore, the majority are recent samples from within the past ~500 years (estimated from collection site location and geomorphology, with features evidencing the local isostatic readjustment and relative sea level change patterns outlined further in Chapter 4).

2.3 Macro- and microanatomical analysis

Utilising the macroscopic differences between tree genus and species provides an initial discrimination of the wood's possible source regions. For differentiating the species of wood, the macroscopic characteristics (by the naked eye or with a magnifier of 5-20x) of the various components of the wood can be utilised, as tree species differ in the presence and morphology of features within the wood structure. Macroscopic classification can distinguish *Pinus* from other coniferous genera (*Larix, Picea* and *Abies*) and between some deciduous genera (Hellmann et al., 2013a; Schweingruber, 2007). Following this, microscopic analyses of thin sections of stained radial, tangential and longitudinal sections can enable the separation of some

Pinus species as well as the genera *Larix*, *Picea*, *Abies*, *Salix*, *Populus*, and *Betula*. Genus or species information then acts as a provenance tool thanks to their distributions in the Eurasian and North American boreal forests. Earlywood to latewood transition is abrupt for European Larch *(Larix decidua Mill.)*, silver Fir (*Abies alba Mill)*, and Scots Pine (*Pinus silvestris L.*) while more gradual for Norway Spruce *(Picea abies Karsten)*. The variation in the various cell types aids in distinguishing between wood species, although it is not always possible to determine *Larix* from *Picea*. Resin canals, bordered by 8 to 12 or more thick-walled epithelial cells, are present in all but fir, unless in rare traumatic tangential rows where resin ducts form in response to damage, while pine shows large resin canals with thin-walled epithelial cells (Schoch et al., 2004). Microscopic analysis of radial cuts also aids species differentiation. Softwood cells are dominated by axial tracheids (elongated fluid-conducting xylem cells), which comprise over 90% of the wood cells. Their radial diameter is dependent on growth

rates, the growing season when growing (earlywood tracheids are larger than latewood tracheids) and environmental conditions (Jane, 2013).

Thin sections were created from samples to identify the genus via microanatomical examination (Figure 2.1). Initially, thin sections were created for 7 sub-Arctic test samples from Nordkapp, northern Norway, before the developed methods were used to process samples collected from northern Svalbard. Samples were cut into prepared ~1cm^3 pieces and soaked overnight in water ready for processing with a Lab-Microtome (Gärtner et al., 2015). Slices were made to a thickness of ~18-20µm using a blade angle of 11º. Sections were then stained to further highlight anatomical features, in well-ventilated laboratory conditions and safe storage and handling of the cleaning and staining chemicals. Radial, tangential and longitudinal

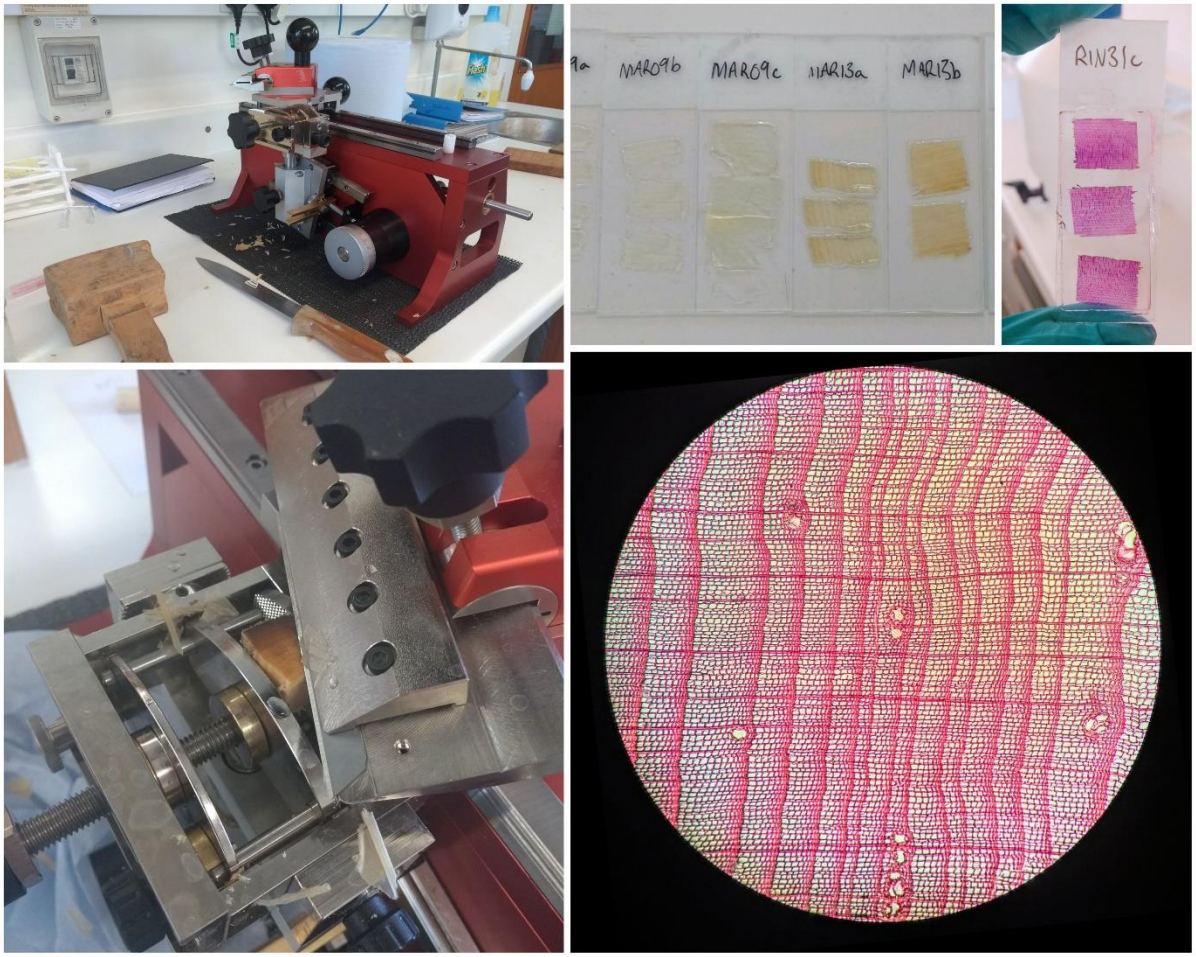

Figure 2.3. Stages of sample preparation for microanatomical analysis via microtome cutting and staining of thin sections, with *Picea* section exhibiting gradual transition from thin-walled earlywood to thick-walled latewood tracheids, and thick-walled epithelial cells within resin canals.

sections were created. Thin sections were immersed in glycerol to maintain moisture before staining. When ready, the glycerol was washed off with water, with stain added for ~5 minutes. The section was subsequently flushed with 75% alcohol to remove water and excess stain. This was then followed by flushing with 96% ethanol, following methodology adapted from Schweingruber (2007). To check that all water has been removed, a drop of xylol was added: if this becomes milky in contact with the section, then further washing with alcohol if needed. Once all water was removed, a drop of viscous Canada balsam was added and then a cover slip was added on top and pressed to remove any trapped air. The finished thin section was then placed in an oven at 60ºC for 12 hours, with magnets to weight each section to keep the sections enclosed between the slide and cover slip. To prevent sticking from any leaked Canada balsam, a heat resistant plastic sheet was placed between the magnet, thin section and base tray. Then the section was left to cool for 12 hours with weights remaining.

2.4 Dendrochronology

Driftwood samples were assessed for viable tree ring series that are not dominated by individual growth anomalies, and with sufficient tree ring preservation for measurement and analysis. These were then sanded using drill-mounted sanding bands, and annual ring widths of each sample measured to 1/1000 mm accuracy using LINTAB tree-ring measurement table and TSAP-Win Professional version 0.89 (Rinn, 2011) (Figure 2.4). At least two radii per driftwood disc were measured and combined through a bi-weight robust estimate of the mean to form one chronology per sample. Climatic low-frequency variance may be present within the series, but resolvability of this depends on the length of the tree-ring sample series and the detrending methods used (Cook et al., 1995). Therefore, signals on a timescale exceeding the individual sample series lengths will be lost with any detrending method. The upper limit of

low-frequency climatic variance than can be resolved can be identified through the median segment length of series within a detrended series chronology (Esper et al., 2003). Determining the possible causes driving low-frequency variability in any dendro-chronological times series depends largely on observation of the location of the sampled tree, since this variability can be dominated by abiotic variables as well as by stand dynamics if the tree grows or has grown in close proximity to other trees. Since this is impossible to determine with driftwood material sampled thousands of kilometres from the site where the tree grew, removal of low-frequency variability was deemed to be the best option.

Tree ring series were standardised to remove non-climatic trends such as growth and competition effects, with tree-ring widths decreasing with age as the stem circumference

Figure 2.4. Preparation steps for driftwood samples for tree ring width analysis with LINTAB tree-ring measurement table and TSAP-Win Professional version 0.89 (Rinn, 2011) for dendrochronological crossdating.

increases, while neighboring trees may impact an individual tree's growth rate. This was done using a two-part trend elimination (Cook & Peters, 1997), resulting in high-frequency time-series. The growth trend was removed through the application of a negative exponential curve or regression line, followed by de-trending through a 5-year moving-average curve to remove further possible local variance. The residuals of such curve-fitting exercises were then taken.

Samples with sufficient measured time series were cross-dated both visually by comparison of ring-width marker ring lists and by use of the chronology-building statistics of TSAP-Win software through a variety of parameters to assess correlation between samples (Figure 2.5). Multiple scoring metrics have been utilised in assessing between-TRW time series similarity. A t-statistic is commonly employed to compare a sample set against a reference chronology, however to ensure the data are bi-variate normal the TRW are standardised by converting to a percentage of the mean of the five ring widths of which it is the centre value. This is then normalised by taking the natural log of percentage figures (Baillie & Pilcher, 1973). This de-trended value is referred to as TVBP, however the measure lacks descriptive power in the absence of extreme ring-differences between chronologies. For cases with less extreme ring-differences, the Gleichläufigkeit (Glk) parameter (or concordance coefficient) is also employed, which instead assesses similarity of sample slope intervals (Eckstein & Bauch, 1969; Schweingruber, 2012). To capture the strengths of both metrics, we consider the Cross-Date Index (CDI) within our study, provided by the TSAP-Win package (Rinn, 2011). CDI gives the quality of agreement between sample series by combining the Gleichläufigkeit

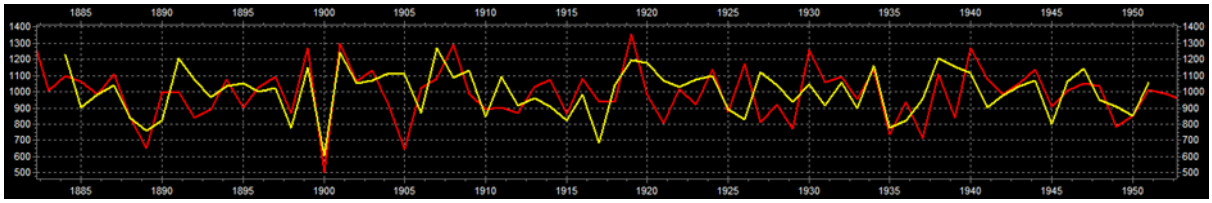

Figure 2.5. Example of tree ring series resulting from measurement with Lignovision and visual comparison to reference chronology of a possible crossdate match.

measure of overall accordance of two series with the t-value measure of the correlation significance:

$$CDI = \frac{\left(G - 50 + \left(50 \times \sqrt{\frac{overlap}{\max overlap}}\right)\right) \times T}{10}$$

G is the Glk and T is the t-value, hence the CDI measure captures the magnitude of both measures. Therefore, the combined CDI gives a date index of possible series (Rinn, 2011). Significant correlation was set to Glk >60%, TBP>3.0 and a CDI≥10 (Rinn, 2011). The cross-dating of series within the chronologies was examined using the COFECHA-style (R. L. Holmes, 1983) Cross-Date Check feature of TSAP-Win. Any series or segments of series that did not surpass sufficient cross-date parameters were removed. Series were combined to floating chronologies when possible.

Reference chronologies from the circum-Arctic boreal forest zone were sourced from the *International Tree Ring Data Bank* (ITRDB, http://www.ncdc.noaa.gov/data-access/paleoclimatology-data/datasets/tree-ring) (Grissino-Mayer & Fritts, 1997). Individual, dated TRW measurement series used to form locality reference chronologies were downloaded before undergoing the same two-stage detrending process as driftwood samples. These dated series were then formed into chronologies via the TSAP-Win™ chronology building tool with the resulting chronology database covering the last 500 years (Figure 4.3). Driftwood samples were the compared to this chronology database to provide possible age and source data for sample-chronology crossdate matches.

As explored in **Chapter 4**, given that this research considers a pan-boreal scope in potential source regions and therefore a large uneven spatial and temporal distribution of reference chronologies, there is a risk of over-representing the geographic regions and time-periods that are better constrained by the reference chronology dataset. Therefore, a sample

may be more likely to match to a period/region for which there are more reference chronologies available this. To address these limitations, a new metric is computed and utilised in **Chapter 4** – "Weighted Score" - to help inform on of the most likely match within our results for each sample.

2.5 Development of Novel Techniques for the Analysis of Driftwood

2.5.1 Strontium ($^{87}Sr/^{86}Sr$)

The use of a suite of analytical techniques minimises the risk to project outcomes from the failure of any one technique in driftwood analysis: dendrochronology, wood anatomy, and radiogenic isotopes have all shown success to varying degrees, including the first use of radiogenic isotopic analysis ($^{87}Sr/^{86}Sr$) for driftwood. Methods for the extraction, isolation and purification of strontium from driftwood through cleaning, microwave digestion, extraction chromatography and MC-ICP-MS (Multicollector-Inductively Coupled Plasma Mass Spectrometer) analysis have been developed and successfully employed in **Chapter 5** (Figure 2.6). The geochemical analysis was undertaken in the clean-suite labs in the Earth Sciences Department, University of Oxford. Initially, method testing for strontium concentration and $^{87}Sr/^{86}Sr$ ratio analysis was conducted on 7 test samples of driftwood. Initial manual extraction chromatography used shrink-Teflon elution columns and Triskem Sr resin. Isotopic analyses were then performed on the Nu Plasma Multi-collector Inductively Coupled Plasma Mass Spectrometer (MC-ICP-MS). Strontium $^{87}Sr/^{86}Sr$ signatures and concentrations, with consistent replication of the data, were retrieved with values in the expected range for wood material.

Subsequently, a subset of the Arctic driftwood samples collected from northern Svalbard were analysed utilising and refining these developed protocols, with updated Sr extraction methods of automated chromatographic purification using the prepFAST-MC™ system (Elemental Scientific (ESI), Omaha, NE, USA), on an ESI Sr/Ca-1000 column (ESI part no. CF-MC-SrCa-1000) including supplied Sr-Ca ion exchange resin. Further details are available in **Chapter 5** and **Appendix C**. Further samples from the northern Svalbard collection were prepared for analysis, but disruption to the study workflow, including due to the COVID-19 pandemic, prevented MC-ICP-MS analysis of these samples and therefore limited the quantity of data for final analysis.

Figure 2.6. Subsample extraction of wood shavings, geochemical column-chemistry for strontium extraction and analysis via MC-ICP-MS.

2.5.2 Ancient DNA

Microanatomical analysis of driftwood can only glean taxonomy to genus level; requiring further techniques to refine the wood's taxonomic identification, and therefore enhance – i.e., geographically constrain – determination of provenance. One method tested was of ancient DNA (aDNA) from the wood tissue. As wood is a commonly occurring archaeological remain (Gugerli et al., 2005), a variety of studies have already shown the application of ancient DNA analysis for archaeological/preserved wood for uses such as wood traceability and monitoring species evolution (Speirs et al., 2009). The extraction of ancient DNA requires preservation of sufficiently unique sequences of DNA, which is known to be problematic for fossil and subfossil wood due to the speed of DNA degradation leading to fragmentation and modification of the recoverable DNA (Lindahl, 1993; Pääbo et al., 2004). Specifically, in the case of Arctic driftwood, the long duration of exposure to ocean waters and subaerially exposed on shorelines means DNA-degrading temperature fluctuations of up to tens of degrees. However, the cold and dry conditions of the Arctic and alkaline soils act as preserving factors and limiting any microbial action on the wood (Dyke et al., 1997). Recent progress has also been made through methodological developments, with successful extractions supporting the feasibility of extraction of DNA from marine waterlogged archaeological wood, and thus also potential extraction of and utilisation of driftwood aDNA for species and provenance analysis.

The attempted method of ancient DNA extraction, in collaboration with Dr James Haile and the Palaeobarn research team, RLAHA, University of Oxford, led by Prof Greger Larson, was unfortunately not successful, with details further outlined in **Appendix D**. The PCR recipe trialled was adapted from a protocol utilised by the Gilbert group at the centre for GeoGenetics, Copenhagen for most of their plant tissue (e.g. Wales et al., 2014), optimized for maize cobs. A primer was chosen for primer pairs that amplify <200 base pairs; specifically trnL (g/h)

primers (Taberlet et al., 2007) for its robust amplification and therefore applicability to degraded DNA, but in this case the resulting strength of the amplicons were insufficient for sequencing.

Chapter 3 Linking Statement

Chapter 3 begins the exploration and development of driftwood as a tool for proxy-based Arctic sea ice reconstructions by addressing the first of the three main aims of the Specific Aims and Hypotheses. The new collation and analysis of 913 driftwood samples from across the western Arctic with available with radiocarbon and genus data is used to investigate the following hypotheses:

i. Pan-Arctic driftwood records can provide insight into centennial and millennial variation in the predominant Arctic surface currents (the Beaufort Gyre and Transpolar drift), throughout the Holocene, with associated impacts on sea ice extent and dynamics.

ii. These changes are linked to large-scale modes of climatic variability such as the Arctic Oscillation.

iii. There is an interplay of surface currents driven by atmospheric circulation vs. thermal forcing on the sea ice extent during the Holocene, and this can aid in placing the current observed 20th and 21st century Arctic sea ice trends within this much larger framework.

Spatiotemporal trends in distribution, radiocarbon-dated age and genus-based driftwood provenance throughout the Holocene reveal the concurrent sea ice and surface current dynamics. The resulting high-resolution reconstruction is then used to infer the role of atmospheric and oceanic circulation in controlling the patterns of sea ice conditions and dynamics. A pan-Arctic perspective is important as local trends are influenced by local conditions, coastal geomorphology and smaller scale coastal currents. Regarding hypothesis iii, the chapter results also indicate that a more definitive provenance of driftwood could further delineate the contribution of thermal and local dynamic forcing driving the driftwood patterns in the Holocene.

3 Out of the woods – driftwood insights into Holocene pan-Arctic sea ice dynamics[1]

Georgia M. Hole[1] & Marc Macias-Fauria[1]

[1]School of Geography and the Environment, University of Oxford, Oxford, OX1 3QY, UK.

Key Points

- Arctic driftwood transport and deposition is determined by sea ice and surface current dynamics; making it a robust proxy for Holocene sea ice reconstructions.
- The first pan-Arctic collation of Holocene driftwood data provides a reconstruction of higher spatial and temporal resolution than other proxy-based methods.
- Holocene sea ice extent and drift is characterised by a gradual progression from millennial to centennial shifts in the relative position of the Transpolar Drift and Beaufort Gyre, which is consistent with the dynamics of the Arctic Oscillation.

3.1 Abstract

The collation of 913 driftwood samples from across the western Arctic, with spatiotemporal distribution and available provenance data, enabled the production of a high-resolution proxy-based reconstruction of Holocene Arctic Ocean surface current and sea ice dynamics. Regionally bounded, driftwood-based sea ice reconstructions studies suggest spatiotemporally complex past Arctic sea ice extent and movement; however, a large-scale compilation of Holocene Arctic driftwood has not previously been developed. Sparse driftwood in the early Holocene (≥8.2 cal ka B.P.) deglacial period was followed by increased driftwood deposition

[1] Published as: Hole, G. M., & Macias-Fauria, M. (2017). Out of the woods: Driftwood insights into Holocene pan-Arctic sea ice dynamics. *Journal of Geophysical Research: Oceans*, 122(9), 7612–7629. https://doi.org/10.1002/2017JC013126

in the warmer mid-Holocene (8.2–4.2 cal ka B.P.); characterized by an enhanced Transpolar Drift (TPD) ~7 cal ka B.P., leading to sea ice loss through the Fram Strait. Driftwood incursion peaks show spatial E-W progression from the Eurasian Archipelagos to Greenland and the Canadian Arctic Archipelago, suggesting a progressive shift in the orientation of the TPD on centennial-millennial time scales and intermediate phases in the Arctic Oscillation. Late Holocene cooling (≤4.2 cal ka B.P.) is indicated by increased influx of probably North American *Picea* via a strengthened Beaufort Gyre (BG) which enhanced sea ice recirculation, starting in the western Arctic and progressing eastward. In recent millennia (<2 cal ka B.P.), a more variable driftwood record alternates between BG and TPD dominance on centennial time scales. To further constrain a spatiotemporal reconstruction of variations in Holocene ocean current and sea ice dynamics, a more definitive determination of driftwood provenance is recommended to build upon the current framework, such as through radiogenic isotope tracing and aDNA analysis.

3.2 Introduction

The rapid decline in Arctic sea ice extent, age and thickness is well documented, with such changes due to cause far-reaching impacts on both localised and global climatic and ecological processes (Bhatt et al., 2014). Arctic sea ice fluctuations are strongly coupled with Arctic climate, involving the influence of a variety of mechanisms, which incorporate natural climatic forcings occurring over a wide range of timescales (geological to intra-annual) and recent changes induced by anthropogenic influence. These forcings are being reflected in the observations of a rapid decline in the extent and thickness of sea ice (Polyak et al., 2010; Maslowski et al., 2012) with a decline in sea ice volume of 75% since the 1980s (Overland et al., 2013). The greatest decline in extent and concentration has been observed in late-summer

at the end of the melt season (Serreze et al., 2007), which mostly consists of thick multi-year ice and is shrinking at 13.3% per decade (Serreze & Stroeve, 2015). This has contributed to the decrease in ice age, with a drop from 4+ years old ice constituting 33% of the total ice extent in the mid-1980s to 3.1% in 2016 (Tschudi et al., 2016). The continuing decline in sea ice cover is expected to have a diverse range of consequences including a warmer, wetter Arctic, impacts on terrestrial and marine productivity, changes to global atmospheric and ocean circulation patterns, terrestrial fauna and flora population fragmentation and habitat reduction, increased marine species interaction and connectivity, and northward expansion of lower-latitude species (Overland & Wang, 2010; Screen & Simmonds, 2010, 2014; Francis & Vavrus, 2012; Post & Høye, 2013; Overland et al., 2016; Vavrus et al., 2017; Bintanja & Andry, 2017). The knowledge of the dynamics behind such changes is constantly evolving, and the importance of factors such as the Arctic Oscillation – AO; defined as the principal component of Northern Hemisphere sea-level pressure and regarded as the most influential mode of atmospheric circulation and climate in the Arctic (Thompson & Wallace, 1998; Comiso & Hall, 2014) – and associated changes in ocean current and sea ice dynamics remains under active research (e.g. Rigor et al., 2002; Comiso and Hall, 2014; Barnes and Screen, 2015; Ding et al., 2017). An increasing appreciation of the impact of atmospheric circulation on sea ice is also revealing the importance of teleconnections from lower-latitude components of the climate such as tropical Pacific sea surface temperatures (SSTs) (Ding et al., 2017).

The spatiotemporal dynamics of Arctic sea ice conditions throughout the Holocene remain largely unknown, given the sparse knowledge preceding satellite observation, and so modern trends cannot be accurately assessed within centennial and millennial timescales. With the state of the Arctic clearly being such an influential factor in the wider climatic system, further knowledge of past sea ice dynamics is needed for revealing the late Quaternary Arctic

climatic state and to investigate the Arctic system's climatic and biotic responses and feedbacks to increasing global average temperatures.

3.2.1 The Arctic sea ice system

The extent, thickness and dynamics of Arctic sea ice are driven by a range of factors that fall broadly into two components: those of the thermal and physical dynamics of the Arctic Ocean system. Thermodynamic processes in the Arctic such as the thermohaline circulation, surface warming and advection of warm waters contribute to changes in ice extent, age, and thickness. The physical dynamics of sea ice are driven by both ocean and atmospheric circulations, which influence the strength and position of the Beaufort Gyre and Transpolar Drift (Figure 3.1).

The Beaufort Gyre (BG) displays a mean annual clockwise motion in the western Arctic Ocean (Polyak et al., 2010), and this anticyclonic nature results in the recirculation and enhanced persistence of sea ice within the Arctic basin. The mean residence time for ice in the BG is ~5 years (Rigor et al., 2002) and so it aids in the formation and preservation of multi-year ice that can reach up to 5m thickness (de Vernal et al., 2013). The Transpolar Drift (TPD) is a surface ocean current running more or less parallel to the Siberian coast and transporting Arctic ice and waters southwards to the North Atlantic through the Fram Strait, favouring the loss of ice. Holocene fluctuations in the extent and orientation of the TPD have been proposed to vary between three overall states (Dyke et al., 1997): there are lateral shifts from a) an eastward route toward Fram Strait, with sea ice (and any driftwood entrained in it) advection to the European side of the Arctic; b) a westward route toward Greenland with sea ice advection to the Canadian Arctic Archipelago (CAA); and c) a split route with sea ice transport divided between the east and west. A driftwood-based reconstruction and modelling of these lateral shifts in the TPD shows abrupt 40-50 year timescale shifts in the TPD position over the last 8.5

ka, with stable periods on centennial to millennial scales (Dyke et al., 1997; Tremblay et al., 1997).

The interaction of physical and thermal forcings can lead to feedback mechanisms that amplify fluctuations in sea ice. For example, when sea ice is thinned or reduced in age by dynamic ice and atmospheric processes, a positive feedback can occur as whereby this 'preconditioned' thinned ice is more susceptible to being lost by surface warming and wind stress changes (Hutchings & Rigor, 2012). To determine the uniquity and cause of the recent trend in decreasing multi-year sea ice and sea ice thickness (Kwok & Rothrock, 2009), a greater understanding of the role of physical and thermal forcings is needed.

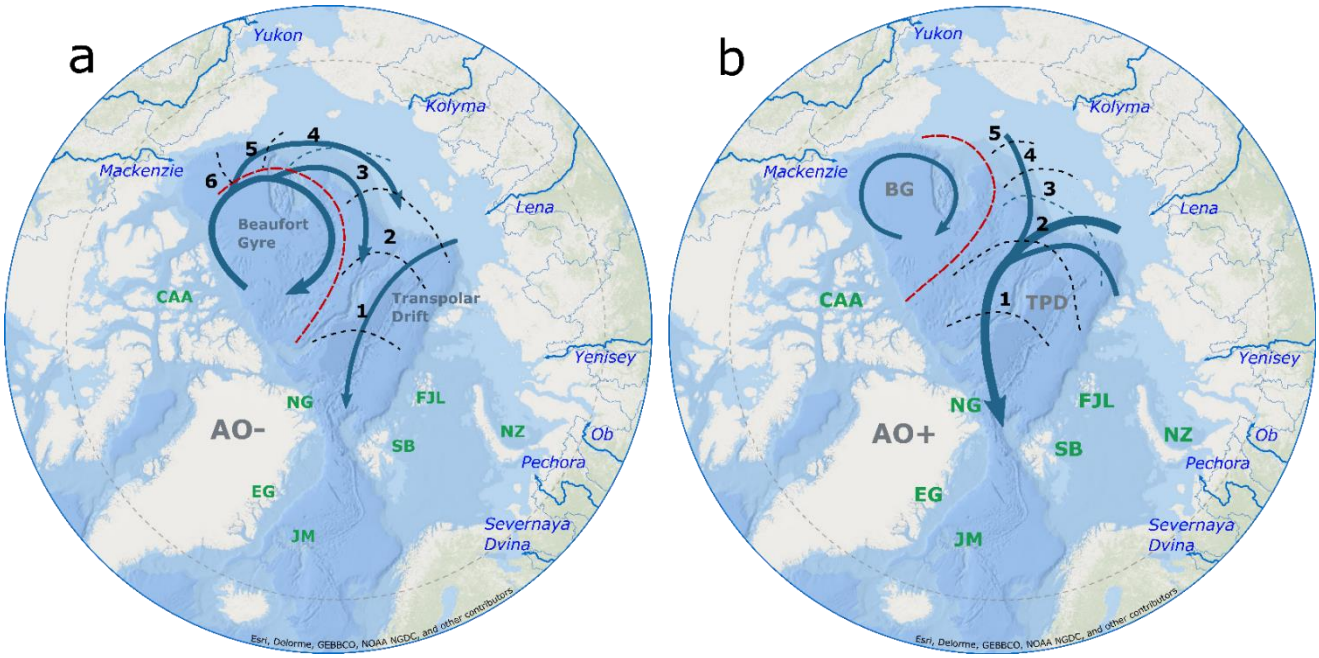

Figure 3.1. Two modes of the Arctic Oscillation, showing wintertime surface circulation patterns, and the resulting influence on ice residence times. a) Low index, negative AO polarity with a strengthened Beaufort Gyre and recirculation of sea ice b) High index, positive AO polarity with a weakened BG. Numbered isochrones show the average time in years for ice at various locations to be exported through the Fram Strait under low-index and high-index conditions. The red dashed lines encircle the region of ice recirculation in the BG by the mean sea ice motion field (Rigor et al., 2002). Over continents, light blue lines show watersheds with named major rivers (shown as bold blue lines) that export driftwood into the Arctic Ocean. Sample regions; CAA = Canadian Arctic Archipelago, EG = East Greenland, JM = Jan Mayen, NG = North Greenland Ages, FJL = Franz Josef Land. NZ = Novaya Zemlya. SB = Svalbard (circulations compiled and modified from Rigor et al., 2002).

The AO is a key physical driver of the position of the TPD and the balance between the strength of the BG and TPD circulation patterns. It is characterised as the variable atmospheric mass exchange between the Arctic Ocean and temperate latitudes (Rigor et al., 2002), with positive or negative polarity determined by anomalies in Sea Level Pressures (SLPs) over the polar regions and mid-latitudes (~ 55°–60°N) (Kwok et al., 2013). A negative polarity of the AO results in weaker surface winds over the Arctic and an enhanced BG, leading to reduced sea ice motion and lead formation and so enhancing the retention and growth of multiyear sea ice (Figure 3.1a). Positive AO index configurations (Figure 3.1b) are associated with stronger westerlies at subpolar latitudes and lower SLP over the Arctic, resulting in cyclonic surface winds, which increase sea ice motion. This physical process renders the Arctic Ocean more susceptible to thermal forcing, such as under current climate change, by increased heat exchange from the ocean to the atmosphere, further reducing the thickness and concentration of sea ice (Rigor et al., 2002). A positive AO also causes expansion of the TPD, with increased export of sea ice from the Arctic Ocean through the Fram Strait, further enhancing sea ice reduction.

However, the AO index has reached near-neutrality over the past decade, while the Arctic has warmed and sea ice decline has accelerated (Comiso & Hall, 2014; Mauritsen, 2016). Analysis of 1979-2012 data showed very poor correlation of winter AO indices with sea ice extent, for both perennial and young sea ice (Parkinson & Comiso, 2013). Similarly, the relationship between Arctic sea ice and the North Atlantic Oscillation (NAO) – a measure of the contrast in SLPs between the Subtropical (Azores) High and the Subpolar Low (Maslanik et al., 1996), has also been found to break down over the past two decades, indicating that recent sea ice decline under increased thermal forcing does not correlate to a single index of atmospheric circulation variability (Deser & Teng, 2008). Hence, other factors, such as short-term but radical shifts in atmospheric circulation patterns, and increased interactions between

the Arctic climate and sub-Arctic, have been suggested as important drivers of the Arctic climate system's recent changes (X. Zhang et al., 2008; Overland et al., 2011; Ding et al., 2017). As the Arctic continues to warm under increased thermal forcing (Mauritsen, 2016) such uncertainties on the contribution of dynamic processes to Arctic sea ice decline indicate the importance of efforts to increase knowledge of the influential patterns and drivers.

3.2.2 Sea ice observation and reconstructions

There is only fragmented and scarce data (in time and space) on sea ice extent prior to the generation of spatially explicit sea ice extent information by satellite observations in the late 1970s (Post & Høye, 2013). Since Iceland's settlement in circa 870 A.D., records were kept of sea ice incidence by Icelandic fisheries (Polyak et al., 2010), enabling the development of a sea ice index for the period A.D. 1600 – 1850 (Ogilvie & Jónsdóttir, 2000). In Svalbard, sea ice information since 1800 has been collected from sealers, ships and trappers wintering on the archipelago by the Norwegian Polar Institute (Vinje, 2001), while April sea ice extent (a good proxy for maximum sea ice extent) in the Nordic Seas from 1850–1998 was generated from ship data, aircraft reconnaissance flights and satellite observation data (Vinje, 2001). April sea ice in the Barents Sea region was recorded by Norwegian ice charts by sealing and hunting expeditions from 1850 to 1949 and 1966 to 2001, and intervening years measured by Soviet reconnaissance aircraft (Shapiro et al., 2003). Sea ice draft and thickness was also measured through upwards sonar data by submarine cruises throughout the Arctic from 1958 onwards (Rothrock et al., 2008). These include comparison of drift data from two summer polar cruises in 1958 and 1970 (A. S. McLaren, 1989), before more extensive draft data collection as part of the Scientific Ice Expeditions (SCICEX) program (Gossett, 1996). Such

spatiotemporally limited historic data sets offer some context for recent sea ice changes but provide inadequate insight on trends driven by broader-scale climatic trends.

The geological record and proxy data are important sources of information for environmental and climatic conditions preceding the advent of direct observations, though they are currently limited by abundance, length and/or resolution of records (Abram et al., 2013). Much of this data for past sea ice inference derives from ocean cores, which provide a variety of both biogenic and inorganic information from tracers, marker species to microfossil assemblages (Gersonde and de Vernal, 2013). Examples of biogenic palaeontological data include dinoflagellate cysts, ostracods, diatom and benthic foraminifera assemblages (Cronin et al., 2013; De Vernal et al., 2013; Seidenkrantz, 2013). Biomarkers used include IP_{25} – a C_{25} isoprenoid lipid formed by diatoms (e.g. Abram et al., 2013; Belt and Müller, 2013; Brown et al., 2014), phytoplankton-derived brassicasterol, and PIP_{25}, an index developed combining IP_{25} and the phytoplankton markers brassicasterol and dinosterol (Müller et al., 2011), and DIP_{25} – an isoprenoid diene to IP_{25} ratio (Cabedo-Sanz et al., 2016). Inorganic biomarkers include the use of ice-rafted debris (IRD) and radiogenic isotopes for tracking ice drift and provenance (e.g. Stickley et al., 2009; Hillaire-Marcel et al., 2013; Fagel et al., 2014). Sea ice extent has also been reconstructed from ice core data, using sea salt sodium (Levine et al., 2014) and flux rates of methanesulfonic acid (MSA) (Becagli et al., 2009; Criscitiello et al., 2013) and halogens (Spolaor et al., 2013, 2016), though these do not yet supply robust reconstructions due to interpretation and calibration limitations (Abram et al., 2013). Combining ice core isotopic composition with tree-ring data has been shown to yield sea ice extent variability on centennial scales (Macias-Fauria et al., 2010), improving the coarse temporal resolution obtained by ocean records due to extremely low sedimentation rates in the central Arctic Ocean.

3.2.3 Driftwood

The transport and deposition of Arctic driftwood is determined by sea ice and surface current dynamics; making it a proxy for sea ice reconstructions in the Arctic (Häggblom, 1982; Dyke et al., 1997; Funder et al., 2011). Driftwood found on the shores of Arctic islands and continental land masses is released into the Arctic Ocean at the mouths of the large rivers that drain the boreal forest regions of North America and Eurasia (see Figure 3.1). These major rivers are responsible for 10% of the total flow from the world's rivers (Nicholls et al., 2016), and contribute 38% of the freshwater influx into the Arctic Basin (Serreze et al., 2006). The boreal forest has covered the large driftwood-producing river drainage basins of North America and Eurasia throughout the Holocene (Ritchie & Hare, 1971; Hopkins et al., 1981; MacDonald et al., 2000) . The Eurasian boreal tree limit in the early Holocene of ~9.5-6ka BP lay up to 200km northwards at the circumpolar coastlines, due to increased summer insolation and temperatures compared to modern conditions (MacDonald et al., 2008), before migrating to its modern limit at 60-70°N (Sokolov et al., 1977; Bigelow et al., 2003). The boreal forest reached its current composition by ~6 ka BP in Canada (Tremblay et al., 1997), and by 3-4ka BP in Eurasia (MacDonald et al., 2000), with increased *Larix* between 10 and 3.5ka BP. Low numbers of *Picea* and *Pinus* in the Eurasian boreal forest have been consistent throughout the Holocene (MacDonald et al., 2008). In North America, *Picea* dominates west of Hudson Bay (the boreal forest east of Hudson Bay does not contribute driftwood to the Arctic Basin beyond Hudson Bay due to the lack of large northward river drainage basins). In Eurasia, *Larix* (and *Pinus* to a lesser extent) dominates the eastern Siberian boreal forest, with *Picea* very slowly increasing in abundance westwards – though still at minimal percentages in central Siberia. *Pinus* is present in central and western Siberia, in addition to within portions of the watersheds of the Mackenzie and Yukon in North America, though at lower abundance in the boreal forests

compared to *Larix* and *Picea*. It also therefore constitutes a small percentage of naturally felled Holocene Arctic driftwood, making *Pinus* less useful for driftwood provenance analysis

The low water temperature of the Arctic Ocean increases buoyancy, which differs between individual species and the size and condition of the driftwood upon entering the ocean. Buoyancy times range from 6 to 17 months (Häggblom, 1982), whereas drifting across the Arctic Ocean takes on the order of multiple years, meaning that for driftwood to reach the high-Arctic coastlines, multi-year pack-ice must be present, and driftwood must be assimilated into forming sea ice soon after entering the Arctic Ocean (Funder et al., 2011; Häggblom, 1982). The TPD provides a direct route between the outlets of driftwood from the Siberian boreal forests and the landmasses proximal to the Fram Strait such as Franz Josef Land, Svalbard, Iceland and the north-eastern coastline of Greenland. The path for wood originating from North America is more indirect: the majority of this wood is first transported by the BG before being transported to a beach or exported through the Fram Strait (Funder et al., 2011), lengthening its journey time to over 5 years (Rigor et al., 2002) (see Figure 3.1).

Sampling Holocene subfossil driftwood relies on its incursion onto raised beach terraces that result from the Arctic region's postglacial emergence following the retreat of past land ice loads through the Holocene. Raised beaches are abundant across formerly – and currently in many cases – glaciated regions of North America, Greenland, and Western Eurasia. Such raised beaches often lack vegetation to their low temperatures, coarse grain size, aridity, high alkalinity and low nutrient availability (Dyke et al., 1997). Such harsh conditions preserve datable driftwood, whalebones and pumice as decomposition is limited. However, on the northern shorelines of Beringia (Eastern Siberia, Alaska, and Yukon), early to mid-Holocene driftwood is missing due to the lack of glacioisostatic uplift and sea level rise in the region, which submerged most old shorelines (Dyke & Savelle, 2001; England & Furze, 2008).

Arctic driftwood-based sea ice reconstructions to date have been predominantly based on data from specific regions (e.g. Dyke et al., 1997; England et al., 2008; Funder et al., 2011; Nixon et al., 2016). In order to infer the role of atmospheric and oceanic circulation in controlling the patterns of sea ice conditions and dynamics – and consequently driftwood deposition, a pan-Arctic perspective of driftwood fluctuations is important, as local trends are influenced by local conditions, coastal geomorphology and smaller scale coastal currents. Less driftwood is recorded in Greenland than in the CAA or Svalbard (Briner et al., 2016), particularly lacking in regions prone to perennial landfast sea ice such as observed on Greenland's central northern coastline (Kelly & Bennike, 1992), contrasting to North-eastern Greenland, where summer open waters allow driftwood deposition (Bennike, 1987). Raised beach landforms as signals of littoral processes provide indications of past sea ice conditions, as driftwood incursion onto shorelines requires ice-free coastlines (Häggblom, 1982), which result in raised beach terraces, but sufficient multi-year ice for driftwood transport across the Arctic Ocean. Hence lack of driftwood can indicate lack of sea ice, or extensive landfast ice depending on the presence or lack of coexistent raised beaches.

Previous studies exploring driftwood as a proxy for sea ice have used a genus-based division of driftwood to indicate wood provenance, with *Larix* and *Picea* signifying the Siberian and North American boreal forests, respectively (e.g. Dyke et al., 1997; Eggertsson, 1993; Funder et al., 2011; Häggblom, 1982; Hellmann et al., 2013; Nixon et al., 2016). Although this broad demarcation has shown to be a useful tool, the complexity of the species distribution (e.g. Hellmann et al., 2016), and the presence of *Larix* and *Picea* in both continents suggest that a refinement in such methods could be achieved through increasing the taxonomic precision of driftwood identification.

3.3 Materials and methods

Data from 913 driftwood samples previously collected throughout the western Arctic coastline and covering the Holocene was collated from a range of previous studies (Preston et al., 1955; Broecker & Olson, 1959; Crary, 1960; Nydal, 1960; Blake Jr, 1970, 1972, 1974, 1975, 1984, 1986, 1987, 1989, 1993, 1961a, 1961b; Marthinussen, 1962; Washburn, 1962; Grosswald, 1963; Trautman, 1963; Henoch, 1964; Ives et al., 1964; Dibner, 1965; Knuth, 1967; Hattersley-Smith et al., 1969; Hoppe et al., 1969; Mielke & Long, 1969; Birkenmajer & Olsson, 1970; Webber et al., 1970; Weidick, 1972, 1975, 1977; Lowdon & Blake Jr, 1973, 1978, 1979; Kovaleva, 1974; R. B. Taylor, 1975; England, 1976a, 1976b, 1978, 1983, 1985, 1990; Hillaire-Marcel, 1976; O. Salvigsen, 1978, 1984; P. McLaren & Barnett, 1978; Schledermann, 1978; Dyke, 1979, 1984, 1993, 1998; O. Salvigsen & Nydal, 1981; B. O. Salvigsen & Osterholm, 1982; Häggblom, 1982; Allard & Tremblay, 1983; Stewart & England, 1983; Bednarski, 1984; Landvik & Salvigsen, 1987; D. J. A. Evans, 1988; Lemmen, 1988; Dyke et al., 1989, 1991, 1996, 2011; Dyke & Morris, 1990; Forman, 1990; J. A. Evans, 1990; Hodgson et al., 1991; McNeely & McCuaig, 1991; O. Salvigsen & Mangerud, 1991; O. Salvigsen et al., 1991; D. J. A. Evans & England, 1992; Glazovskiy et al., 1992; Hodgson, 1992; Sharpe, 1992; Zale & Brydsten, 1993; Näslund et al., 1994; Bondevik et al., 1995; Weihe, 1996; Forman et al., 1996, 1997b, 1999b, 1999a; Hjort, 1997; Johansen, 1998; Lubinski, 1998; Lubinski et al., 1999; Ó Cofaigh, 1999; Dyke & Savelle, 2000, 2001, 2003; Forman & Ingólfsson, 2000; Zeeberg et al., 2001b; Bennike & Weidick, 2001; Landvik et al., 2001; Atkinson & England, 2004; Bennike, 2004; McNeely, 2005, 2006; England & Furze, 2008; England et al., 2008; B. Wagner et al., 2010; Funder et al., 2011; Nixon et al., 2014, 2016; St-Hilaire-Gravel et al., 2015) (also see Supporting Information table A1). These were used to produce a spatiotemporal dataset of deposited driftwood identified at the genus level, where available. The radiocarbon ages (^{14}C year BP), where given in the literature, were

calibrated with the IntCal13 calibration curve using the program OxCal v4.2 (Bronk Ramsey, 2009) and are presented in median calibrated radiocarbon years before present (cal. year BP) and are directly comparable to calendar years BP for samples dated by other methods. The resulting age range represents the 95% confidence interval ± 2 sigma, with sample ages collated into 250-year intervals for analysis (see table A1). The low errors associated with radiocarbon dating of wood material allow for the high temporal resolution of analysis compared to other proxy methods in the Arctic.

In order to segregate source regions for the provenance of driftwood, a variety of analyses can be used. Utilising the macroscopic differences between tree species can provide an initial discrimination of the wood's possible source regions. The macroscopic classification has distinguished *Pinus* from other coniferous genera (*Larix, Picea* and *Abies*) and some deciduous genera (Hellmann et al., 2013a; Schweingruber, 2007). Following this, microscopic analyses can enable the separation of some *Pinus* species as well as the genera *Larix, Picea, Abies, Salix, Populus*, and *Betula*. If fungi infestation is present in *Picea* and *Larix*, this can complicate their differentiation due to their similar structure and the rich diversity of fungi that can be present (Blanchette et al., 2016; Hellmann et al., 2013a). As methods and level of identification inevitably varied between the many previous studies that constitute the dataset, the taxonomic data was classified into the genera *Larix, Picea, Pinus, Populus, Salix* and *Tsuga*, with the last three combined into an 'other' category due to their small proportion of the total dataset and weaker link to dominant boreal forest species of *Larix, Picea, Pinus* and *Abies* (Hellmann et al., 2013b). Samples without taxonomic identification were classed as *unknown*. Where radiocarbon dating and sample collection location data were available, this was used to produce a map of the existing available data showing its spatial distribution over the Arctic.

3.4 Results

The samples' locations range from the CAA to the archipelagos north of western Siberia (Figure 3.2). Ocean circulation and sea ice patterns of the Arctic favour deposition in these areas, the spatial patterns of data availability coinciding with heavily glaciated regions rich in raised beaches and thus prone to old driftwood preservation, with the exception of Severnaya Zemlya off the Taymyr coastline. Although driftwood does occur throughout the circumpolar region, much of the driftwood deposited on eastern Siberia, Alaska, and Hudson Bay coastlines is from local sources and so not linked to large-scale sea ice patterns; as such, it is not a suitable

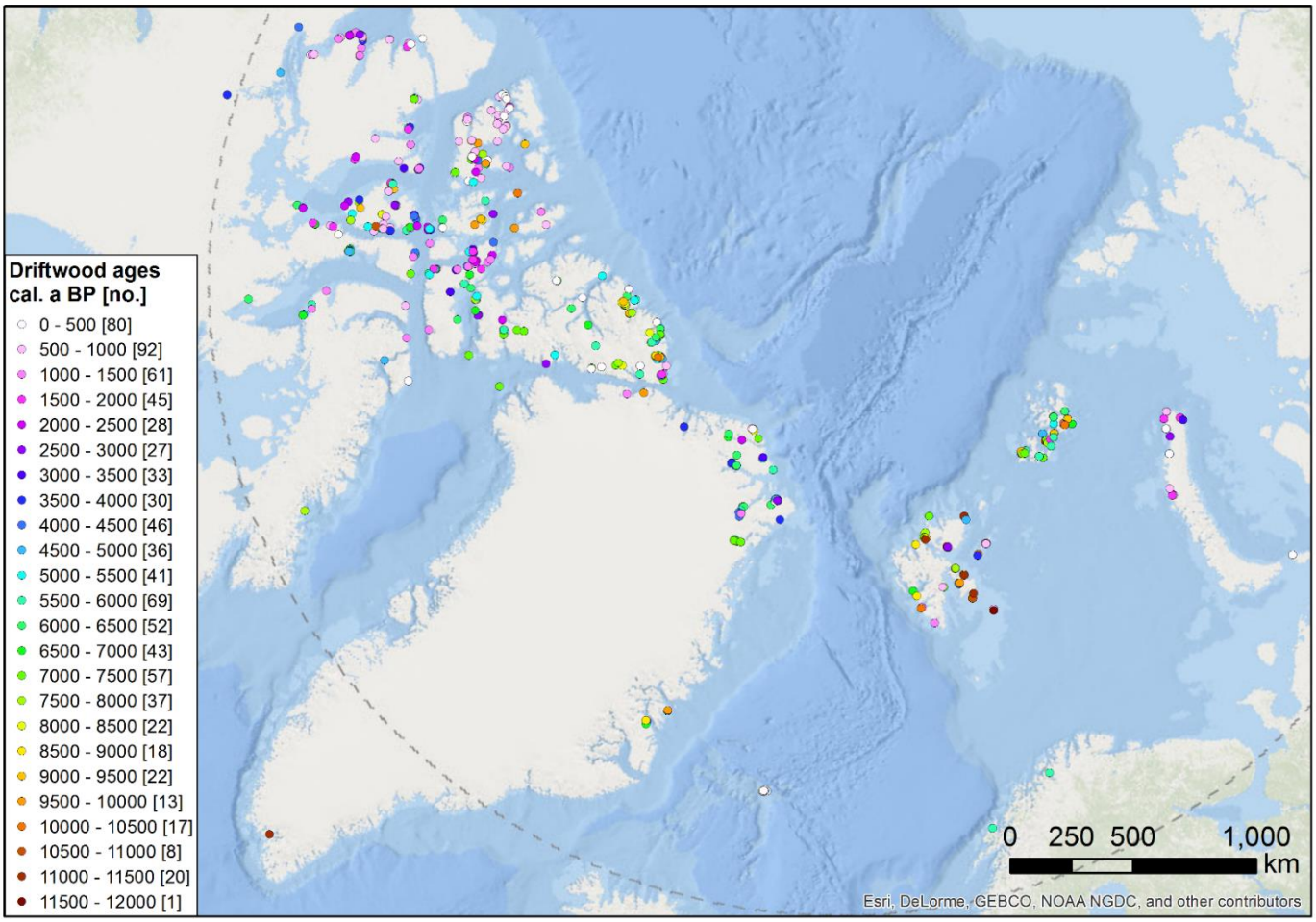

Figure 3.2. Geographical distribution of the driftwood data collated in the current analysis. The colours represent the calibrated driftwood ages B.P, separated into 500 year intervals for visual clarity, calibrated with the IntCal13 calibration curve using the program OxCal v4.2 (Bronk Ramsey, 2009). The resulting age range represents the 95% confidence interval ± 2 sigma, and the median value was used for the purpose of the map. Square bracketed figures denote the number of samples from within each interval. For list of data and sources see Supporting Information table A1.

proxy for sea ice reconstruction due to not being within the pan-Arctic watershed (R. M. Holmes et al., 2013). The greatest driftwood abundance occurs in the most recent ~1000 year across much of the Arctic, whereas in some localities, such as Svalbard, there is substantial driftwood occurrence throughout the Holocene (Figure 3.3) making the cause of this trend unlikely a result of preservation issues; this was also concluded in other studies due to the lack of this bias in many other Arctic raised beach sites and driftwood studies (Nixon et al., 2016). An important factor of this database in its current state is the large proportion of driftwood

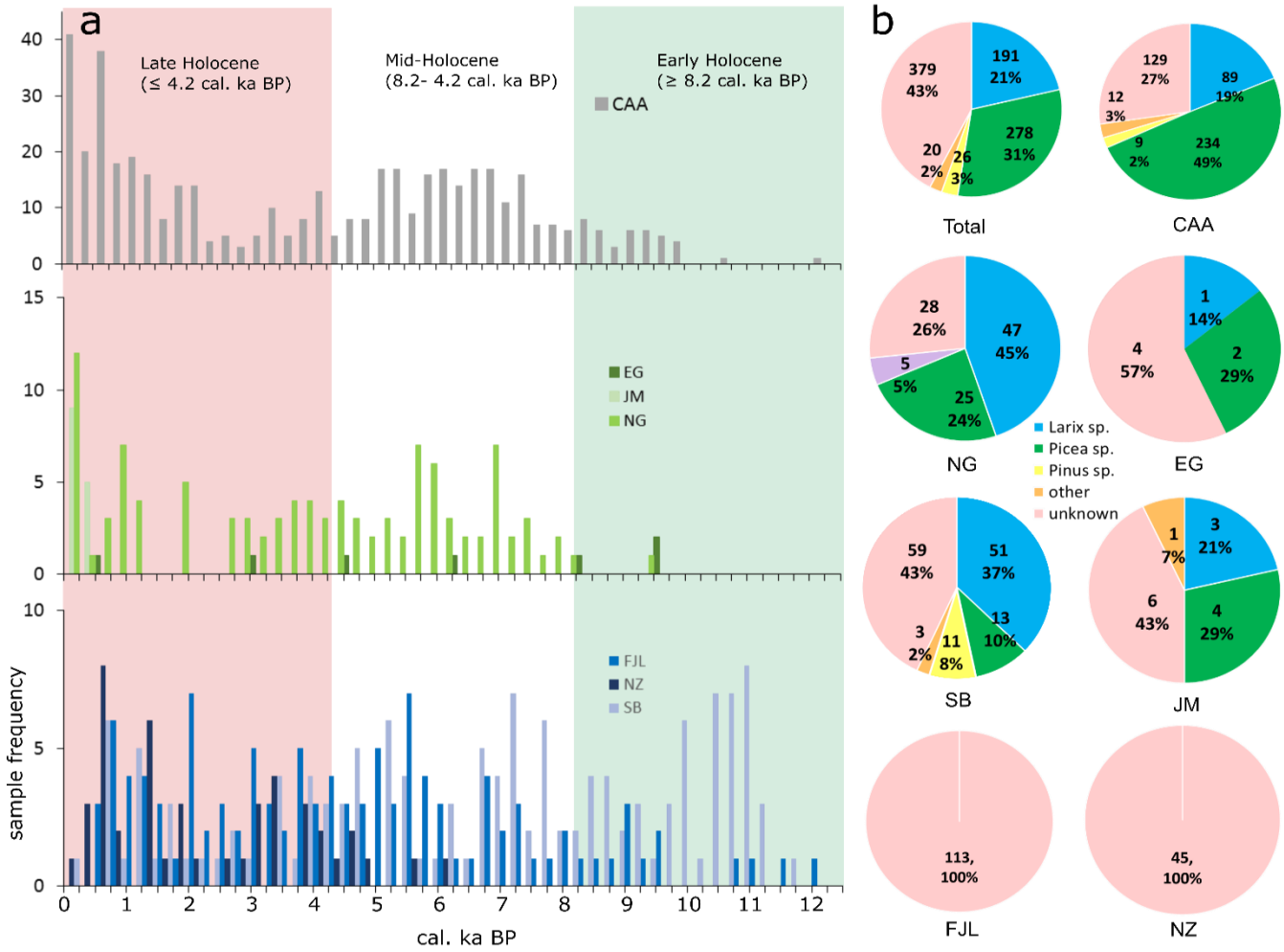

Figure 3.3. a) Frequency distribution of median calibrated radiocarbon dates for Arctic driftwood, 12ka BP to present in 250 year intervals, by region. CAA = Canadian Arctic Archipelago. EG = East Greenland. JM = Jan Mayen. NG = North Greenland. FJL = Franz Josef Land. NZ = Novaya Zemlya. SB = Svalbard. Divisions into late, mid, and early Holocene shown by red, white and green shaded regions; intervals follow Walker et al.(2012)). b) Abundance and genus of driftwood throughout the Holocene for each region where driftwood data has been collated.

samples not yet taxonomically classified, with unknown genera contributing 43% of the total dataset (comprising 100% of the datasets from Franz Josef Land and Novaya Zemlya, Figure 3.3). This is due to the fact that the original studies collecting this material used it for dating purposes and sea level reconstruction and did not require such information, and limits any determination of provenance for these regions, though whole abundance variations can still be utilised where there is sufficient data abundance. For example, in Jan Mayen there are currently 14 samples in the database from one previous study (Johansen, 1998). All are from <1.4 ka BP, making interpretations of abundance variations in this location limited without further data.

In the CAA and Northern Greenland (NG), low driftwood abundances throughout the region at ~12-9ka BP give way to an increase throughout the Holocene Thermal Maximum

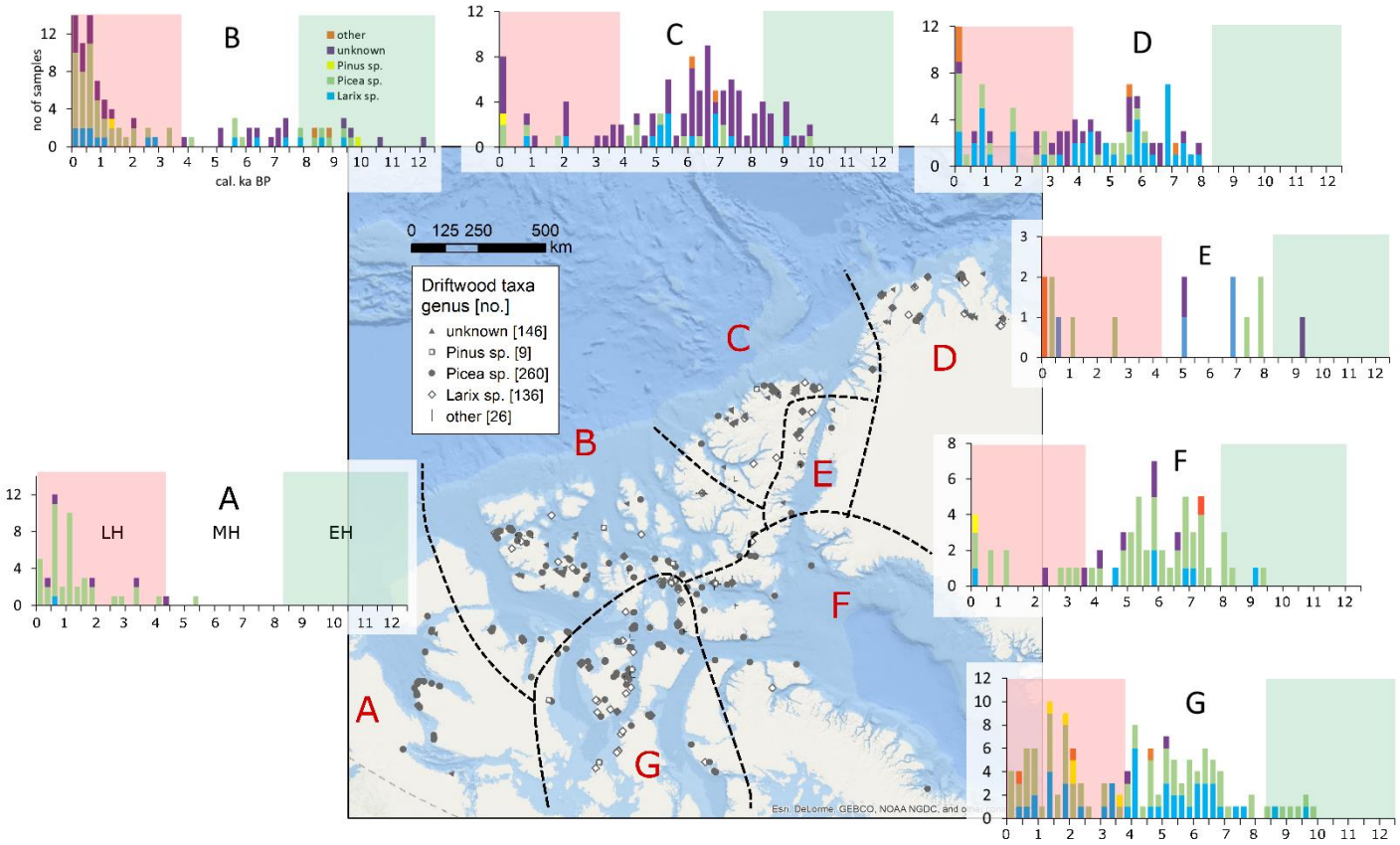

Figure 3.4. Map and frequency distributions of median calibrated driftwood radiocarbon dates from 12.5 cal. ka BP to present, for driftwood across the regions of the CAA (divisions into channel-based intraregional distributions A-G adapted from Dyke et al. (1997)). As in Figure 3.3, distribution divided into LH = Late Holocene, MH = mid Holocene, EH = early Holocene.

(HTM) ~8.6-4.9 cal. ka BP (Kaufman et al., 2004). There remains variability in abundance between different channels and inlets, with higher abundances in the northern central channels (vertex of B, F, G boundary; Figure 4), than inlets further south. The increasing driftwood abundance throughout the early HTM ~8-6.5ka BP across the CAA and NG is matched in Svalbard (SB) and Franz Josef Land (FJL) until ~7ka BP, when a decrease in these eastern regions coincides with increases on Ellesmere Island (England et al., 2008) and NG.

Picea is more abundant on the shores of the CAA throughout the Holocene, which is expected due to its proximity to the BG and the *Picea*-rich North American boreal forest. In Svalbard, driftwood occurs in the greatest numbers in the early Holocene, with a lack of more

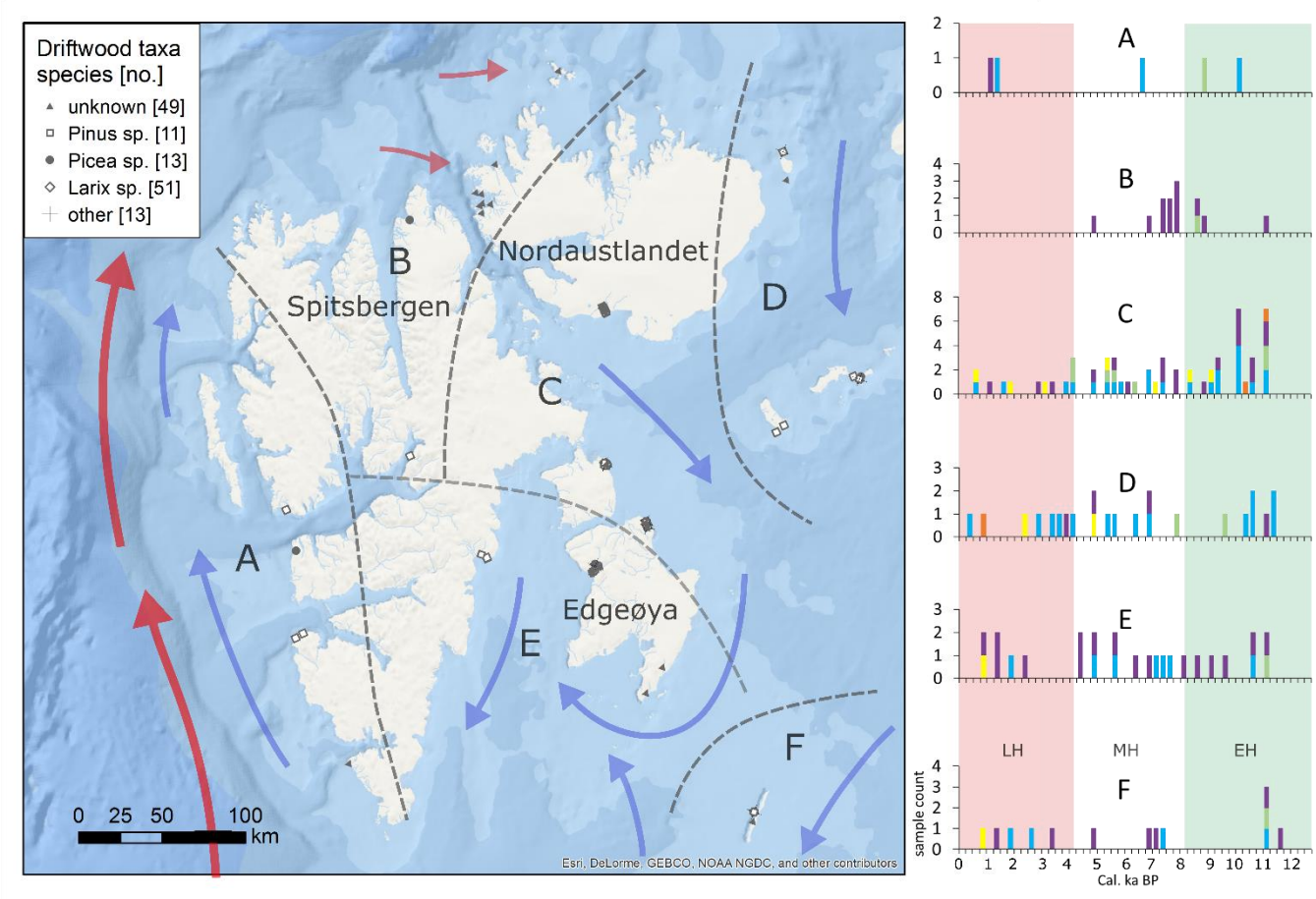

Figure 3.5. Modern ocean currents and frequency distributions of median calibrated radiocarbon dates for driftwood across Svalbard 12.5 cal. ka BP to present, divided as in Figure 3.4 into intraregional distributions A-F based on regions of dominant channel flow direction to highlight regional signals. Ocean currents from (Stiansen et al., 2009); red and blue arrows: Atlantic and Arctic water currents respectively. As in Figure 3.3, distribution divided into LH = Late Holocene, MH = mid Holocene, EH = early Holocene.

recent driftwood in the North and West (Figure 3.5). The greatest proportion of driftwood on Svalbard is of unknown genera, while the *Larix*/*Picea* ratio of 3.92 suggests the likely overall dominance of Siberian driftwood being delivered to the Svalbard coastline. In the Russian Arctic, driftwood has been delivered to the shores of Franz Josef Land throughout the Holocene, with data available from studied raised-beach sequences in the southern half of the archipelago; particularly Hooker, Hayes and Alexandra island (Forman et al., 2004). Driftwood was incurred in low abundances until ~6ka BP, correlating with the initiation of driftwood incursion onto northern Novaya Zemlya coasts. The location of Jan Mayen in the focal point of the Fram Strait outlet means that it is in a prime location for receiving driftwood. However, the distance from the central Arctic Ocean and Jan Mayen's small size diminishes the amount of driftwood likely to reach its coastlines, and here the record is limited: all the samples in the current dataset collected there date to the past 500 years, and so have limited scope in providing insights into the Holocene context.

3.5 Discussion

3.5.1 Early Holocene (≥ 8.2 cal. ka BP – subdivision intervals follow Walker et al. (2012))

The earliest regions to receive driftwood are Svalbard and the northern islands of the CAA (regions B & C in Figure 3.4), with a paucity in NG, FJL and NZ. The processes of deglaciation and consequent glacioisostatic rebound affect much of the western Arctic, leading to raised beach sequences that preserve stranded driftwood, but also precluding driftwood in the early Holocene in areas influenced by the remnants of the ice sheets, local glaciers and perennial landfast sea ice of the LGM (Last Glacial Maximum) which peaked ~21ka BP (Clark et al., 2009). There is evidence of this in NG (Funder et al., 2011), with coasts blocked from wood

delivery by landfast ice and glaciers. The Innuitian ice sheet was retreating from the peak extent in the LGM, when it covered the Queen Elizabeth Islands in the northern CAA (England et al., 2006). A lack of driftwood in the southerly and most westerly inlets of the CAA during this period occurs in a region covered by remnants of the Laurentide ice sheet that peaked in the LGM (Dyke, 2004; England et al., 2009). As the Innuitian Ice Sheet and outflowing ice streams receded, abundant meltwater and local/regional currents likely also prevented driftwood deposition (Dyke, 1998). This north-westward deglacial outflow then reversed to form the modern circulation of south-eastward flow towards Baffin Bay, with evidence of this from inward driftwood influx in the western CAA from ~11 cal. ka BP (Nixon et al., 2016) and the eastern and southern CAA 9.7-9.3 cal. ka BP (Dyke et al., 1997). The relatively high proportion of *Larix* being delivered to the CAA ~9.7-8.5ka BP (Figures 3.4 & 3.6) also suggests an expanded TPD and associated positive AO conditions. The spatiotemporal variability in deglacial ice retreat (England et al., 2006) led to the opening of channels in the north-central CAA (region B; Figure 3.4) earlier than elsewhere in the region, possibly enabling driftwood deposition within these channels while neighbouring coastlines were blocked (such as NG and most westerly margins of the CAA). Such local dynamics however would not necessarily result in an increased influx of *Larix* (if of Russian origin); its frequent occurrence suggests a larger scale thermodynamic regime change and positive AO conditions. Strongly positive AO conditions are also proposed by Nixon *et al.* (2016) due to driftwood occurrence in Svalbard and the western channels of the CAA and local preclusion by outflow in the central CAA and icebergs in northern Greenland respectively. A strongly positive AO aligns with ice core evidence of peak Holocene temperatures for the early Holocene in the CAA (Lecavalier et al., 2017), and diminished sea ice cover (Mayewski et al., 1997; Fisher et al., 1998) during this period. The anomalous nature of regionally variable Arctic conditions and concurrent positive AO conditions and enduring glaciation at this time may also have been impacted by the opening

of the Bering Strait ~11ka BP (Bartlein et al., 2015). The 2015 study highlighted the influence of the transgression of Beringia on circulation dynamics, sea levels, and regional climatic changes, with inevitable influences on driftwood incursion to the region and impacts on the greater Arctic climatic regime The low sample density in the early Holocene (Figure 3.3), and the assumption of the likely Russian origin for the *Larix* occurrence, means that a more

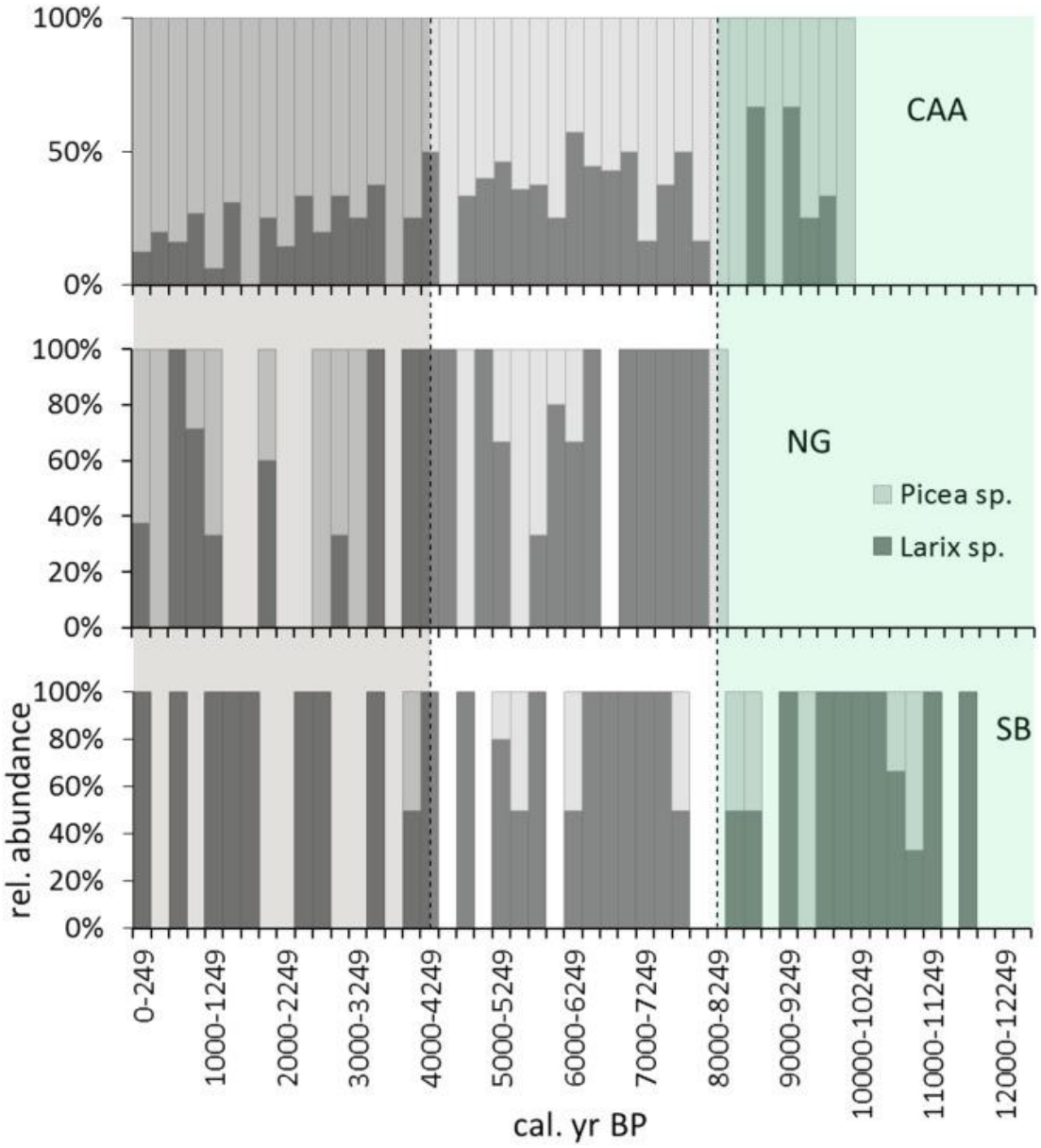

Figure 3.6. Relative abundance of *Larix sp.* and *Picea sp.* driftwood ~12 ka B.P. to present in 250-year intervals for (a) CAA = Canadian Arctic Archipelago, (b) NG = North Greenland, and (c) SB = Svalbard. As in Figure 3.3, distribution divided into LH = late Holocene, MH = mid-Holocene, and EH = early Holocene.

definitive provenance of these samples would better delineate the contribution of thermal and local dynamic forcing driving the driftwood pattern at this time.

In Svalbard, the highest abundances of driftwood occur in the early Holocene and throughout in the south-east of the archipelago. In addition to the off-shore sea ice conditions, such trends are expected to be influenced by the deglaciation of the late-Weichselian ice sheets, composed of the Svalbard–Barents–Kara (SBKIS), the Scandinavian (SIS), and the British-Irish Ice Sheets (BIIS) (A. L. C. Hughes et al., 2016), with the northern margin of SBKIS covering the archipelago. Deglaciation commenced on western and northern Spitsbergen ~13–12 ka ^{14}C BP (Forman et al., 2004) leading to raised beaches up to 65m above the present mean high tide mark (m aht) (Forman, 1990; Forman et al., 1997a). In eastern Svalbard and more distal sites on Franz Josef Land and Novaya Zemlya, deglaciation commenced at ~10.5 ka ^{14}C BP, with marine limit shorelines between 60 to 130 m aht. In the south and east (regions D-F in Figure 3.5), this later deglaciation and GIA may have combined with the presence of ice-carrying Arctic currents to favour driftwood influx and colder local conditions, whereas lower abundances and early-Holocene peak in the north and west (Figure 3.5; regions A & B) correlate with modern regions of northward flowing warm Atlantic currents. The western coast was also an area of low ice-rafted debris (IRD) concentrations 10-7.6ka BP, suggesting a period of Atlantic surface water inflow, and northward retreat of the Polar Front (Jessen et al., 2010).

3.5.2 Mid-Holocene (8.2- 4.2 cal. ka BP)

Driftwood incursion rates increase across the majority of the Arctic at ~7ka BP (Figure 3.3), along with an increase in *Larix* in NG in all but the most western regions of the CAA (Figure 3.4). This suggests the westward shift and expansion of the TPD, probably associated with a reduced BG and to positive AO conditions, increased temperatures, and reduced landfast

ice. This is evidence from glacial IRD of Russian provenance in cores proximal to the Alaskan coast (Darby & Bischof, 2004) indicating inflow of Russian waters and possible weakened westward BG flow. Sparse driftwood in NG at this time was described by Funder et al. (2011), but in the context of this larger dataset, which incorporates additional data from the region (Bennike & Weidick, 2001), such a decrease in driftwood deposition in NG is not observed, while it is also not matched by the driftwood record of the CAA (Nixon et al., 2016). This peak in driftwood and *Larix* abundance occurs earlier in Greenland and the easterly regions of the CAA (Figure 3.4), indicating a gradual shift in the orientation of the TPD and an intermediate phase of a previously discussed split TPD (Dyke et al., 1997). In the Eurasian Arctic, an initial increase in wood incursion in Svalbard and Franz Josef Land at 7 cal. ka BP – which occurred even earlier than in North America – was followed by a decrease from ~6ka BP. This decrease, along with IRD evidence of increased iceberg release and sea ice southwest of Svalbard and the Barents Sea (Jessen et al., 2010) and coeval colder surface conditions (Rasmussen et al., 2007) indicates colder conditions and increased glacial activity at the coastlines. The driftwood record also includes *Picea* in this period (Figures 3.3, 3.5) which under such conditions is more likely to result from a more local, Eurasian source, though a better determination of the driftwood provenance would be required to constrain the source. Reduction in driftwood delivery also occurs ~6 cal. ka BP in the eastern CAA and Greenland in North America (Figure 3.4), where there is coeval evidence of sea ice shelf formation at the north of Ellesmere Island ~5.5 cal. ka BP (England et al., 2008) and severe sea ice conditions in Parry Channel (central CAA) from ~6.5-3.0 cal. ka BP (St-Hilaire-gravel et al., 2010).

3.5.3 Late Holocene (≤ 4.2 cal. ka BP)

Evidence of cold conditions across both the CAA and Arctic continues into the late Holocene; when ice cap inception and growth across many parts of the CAA (Koerner & Paterson, 1974; Koerner, 2005) coincides with a decrease in driftwood occurrence and *Larix* ~5-3 ka BP (Figure 3.4) and southerly expansion of sea ice in the European Arctic (Ślubowska-Woldengen et al., 2007; Andrews et al., 2009). In Svalbard, the hiatus of driftwood incursion is again offset from that observed in the western Arctic, with reduced driftwood quantities occurring after the trends initiated in North America at ~3.2-1.8ka (Figure 3.3). This coincides with evidence of gradual cooling initiating ~4 ^{14}C ka BP, indicated by IRD, δ^{18}O and plankton records to the southwest of Svalbard that indicate an advance of the polar front and decrease in Atlantic water inflow, along with increased iceberg supply (Rasmussen et al., 2007). This agrees with suggested increased sea ice and driftwood incursion further south on Hopen island (Figure 3.5; region F) (Häggblom, 1982), as well as increased landfast sea ice in the Isfjorden region in west Svalbard (Forwick & Vorren, 2009). Thus, the hiatus of driftwood indicates colder conditions and driftwood incursion restricted to more southerly shorelines nearer the polar front margin and highlights the importance of consideration of additional proxy data when interpreting the driftwood record. This gradual, low-frequency alternation in driftwood incursion favouring eastern and western Arctic coasts may suggest fluctuations in AO mode in this period on the scale of 1-2 millennia.

3.5.4 Recent Holocene to present (~2.5 cal. ka BP – present)

Decreased driftwood incursion in NG 2.5-1ka BP (Figure 3.3), along with evidence of a lack of beach ridge morphology in multiple periods during this time (Funder et al., 2011) indicates continued cold conditions and perennial land-fast ice. Sporadic driftwood incursion

in FJL and NZ ~2.5-2ka BP correlate with hiatuses in the western Arctic, suggesting continued shorter-lived centennial fluctuations in the AO polarity and ocean circulation patterns, closer to observed in the modern Arctic sub-decadal fluctuations (Darby & Bischof, 2004). Additionally, peaks in driftwood delivery across Svalbard and FJL ~1.25-1ka BP are followed shortly by driftwood peaks ~1-0.75ka BP in the west – NG and the CAA, again showing the trend of offset between both regions in occurrence, indicating a much faster pace in the TPD orientation transition from east to west than in earlier periods of the Holocene. Evidence of a shifting TPD and AO mode also correlate with the transition from the Medieval Climate Anomaly (950-1250 AD) to the subsequent Little Ice Age (1400 and 1700 AD) (Mann et al., 2009). Such a mechanism would also fit with the temporal and regional heterogeneity of these periods across the Arctic and beyond (Jones & Mann, 2004), given the sea ice–ocean feedbacks that amplified these climatic transitions (Lehner et al., 2013). In the CAA, there is an increase in driftwood occurrence ~2ka BP onwards, reaching high frequencies of occurrence every twenty years from 1ka BP to present (Nixon et al., 2016). Nixon *et al.* highlight the potential biases in this most-recent section of the driftwood record possibly resulting from a) greater preservation of wood, though this is countered by great abundance of much older wood in other sampled regions, and b) influence from the development of Siberian logging activities ~70 cal. yr BP. *Pinus Sylvestris* from the Yenisei is the dominant logged species in Siberia in this time (Hellmann et al., 2015) and the CAA driftwood record includes only 2 incidences of *Pinus* ≤1ka BP. This may be an underestimate due to 22 samples from this period being of unknown species, and so without further insight into the provenance of these samples it cannot be definitively said if this increase is due to human influence and preservation factors or indicative of greater supply and incursion from favourable climatic conditions and AO mode.

3.6 Future considerations

In order to achieve a finer definition of the role of atmospheric and oceanic circulation in sea ice and climatic changes throughout the Holocene, a pan-Arctic focus incorporating a more definitive determination of driftwood provenance fluctuations is needed. This would strengthen its use as a proxy for sea ice reconstruction by enabling the dynamics of the BG and TPD to be better determined at key climatic points of the past 12,000 years. Isotopic analysis of the driftwood tissue is one future avenue, with the Strontium radiogenic isotope system previously explored for provenance studies in the form of $^{87}Sr/^{86}Sr$ ratios. Lithologies can be characterised by a defined $^{87}Sr/^{86}Sr$ ratio (English et al., 2001; Reynolds et al., 2005), which is not significantly fractionated by biological processes such as incorporation into wood tissue (English et al., 2001; Dijkstra et al., 2003). These features enable a spatial link between the wood and its growth site, providing that a framework of potential source Strontium signatures is established. A further provenance tool is that of ancient DNA (aDNA) analysis or palaeogenetics. As wood is a commonly occurring archaeological remain (Gugerli et al., 2005), a variety of studies have already shown the application of aDNA analysis for archaeological/preserved wood for uses such as wood traceability and monitoring species evolution (Speirs et al., 2009). Small aDNA fragments from plants and animals from up to 30,000 years ago have been successfully amplified and sequenced (Pääbo et al., 2004) and the possibilities of aDNA are likely to increase as technologies develop further.

3.7 Conclusion

The control of driftwood transport and deposition by sea ice and surface current dynamics enables insight into the variable climatic and environmental conditions that have impacted the Arctic throughout the past 12,000 years. Shifts in Arctic Oscillation's polarity result in variable Arctic circulation dynamics (Rigor et al., 2002). The collation of 913 driftwood samples from

across the Arctic coastline provides a dataset of higher spatial and temporal resolution than other sea ice proxy-based methods in the Arctic, with preservation of driftwood in substantial volumes from the early Holocene indicating a low likelihood of preservation issues in the interpreting distribution patterns. This enables the detection of the pattern of change at different frequencies through the Holocene. These include the following:

1) Early Holocene deglaciation preceding positive AO conditions coeval with extensive remnant glaciation over the CAA and NG.

2) Mid Holocene warming and sea ice reduction, with millennial scale east-west shifts in the TPD and associated BG weakening. This high-resolution record also offers a different view of mid-Holocene conditions to that proposed by Funder et al., (2011) with more coherence between NG and the CAA of an expansion of the TPD, increased temperatures, and reduced landfast ice.

3) Late Holocene millennial scale west-east TPD shift and strengthened BG and sea ice preservation.

4) Recent Holocene, high variability and higher frequency shifts in the TPD and BG strength and associated fluctuating climate conditions such as the MCA and LIA.

To further constrain a spatiotemporal reconstruction of variations in Holocene ocean current and sea ice dynamics, a more definitive determination of the provenance of driftwood samples would allow greater insights from the wealth of data available from the driftwood record of the Arctic.

3.8 Acknowledgements

This work was supported by the UK Natural Environmental Research Council (NERC IRF grant NE/L011859/1). G. M. Hole is funded by NERC (grant 1514291) and part of the Environmental Research Doctoral Training Program at the University of Oxford. The authors thank the contribution of driftwood sample data from researchers from multiple institutions that have contributed to the pan-Arctic driftwood database that formed the basis of this study (see Supporting Information Table A1 and references therein which contains all of the data used in this study). The authors also thank the anonymous reviewers for the helpful comments and suggestions received.

Chapter 4 Linking Statement

Chapter 4 continues the exploration and development of driftwood as a tool for proxy-based Arctic sea ice reconstructions by addressing the second of the three main aims of the Specific Aims and Hypotheses: the development and evaluation of the novel use of dendro-provenancing at a pan-Arctic scale to increase the spatio-temporal resolution of driftwood-based sea ice reconstructions. Through the analysis of newly collected material, the research paper presents a 500-year history of driftwood incursion to northern Svalbard, directly reflecting regional sea ice conditions and Arctic Ocean circulation. The study uses dendro-provenancing as a method to increase the spatio-temporal grain of Arctic driftwood provenancing, and considers alternate mathematical approaches to selecting probable origin sites by weighting scores via reference chronology span and visualising results through spatiotemporal density plots, as opposed to existing ranking systems. These methods aim to overcome potential biases in dendro-provenancing that stem from the uneven spatiotemporal availability of reference chronologies throughout the boreal forest. The resulting record indicates centennial- and decadal-scale shifts in source regions for driftwood incursion to Svalbard, aligning with Late Holocene high variability and high frequency shifts in the Transpolar Drift and Beaufort Gyre strengths and associated fluctuating climate conditions, as well as a clear decrease in sea ice at the beginning of the 20th century and in the recent decades. The new methodological approach successfully employs driftwood as a proxy for Arctic Ocean surface current and sea ice dynamics.

4 A driftwood-based record of Arctic sea ice during the last 500 years from northern Svalbard reveals sea ice dynamics in the Arctic Ocean and Arctic peripheral seas[2]

Georgia M. Hole[1], Thomas Rawson[2], Wesley R. Farnsworth[3,4], Anders Schomacker[5], Ólafur Ingólfsson[4,6], Marc Macias-Fauria[1]

[1]Biogeosciences Research Group, School of Geography and the Environment, University of Oxford, Oxford, OX1 3QY, UK.
[2]Mathematical Ecology Research Group, Department of Zoology, University of Oxford, Oxford, OX1 3SZ, UK.
[3]Nordic Volcanological Center, University of Iceland, Sturlugata 7, IS-102 Reykjavík, Iceland
[4]Department of Arctic Geology, The University Centre in Svalbard (UNIS), NO-9171, Longyearbyen Norway
[5]Department of Geosciences, UiT The Arctic University of Norway, Postboks 6050 Langnes, NO-9037 Tromsø, Norway
[6]Faculty of Earth Sciences, University of Iceland, Sturlugata 7, IS-102 Reykjavík, Iceland

Key Points

- We present a novel approach to utilizing naturally felled driftwood as a proxy for Arctic Ocean surface circulation and sea ice dynamics.
- A 500-year record of driftwood incursion to northern Svalbard reflects centennial to decadal variability in surface circulation and sea ice extent.
- A distinct decrease in driftwood from all provenances in the last 30 years matches the observed decline in pan-Arctic sea ice extent.

[2] Published as: Hole, G. M., Rawson, T., Farnsworth, W. R., Schomacker, A., Ingólfsson, Ó., & Macias-Fauria, M. (2021). A driftwood-based record of Arctic sea ice during the last 500 years from northern Svalbard reveals sea ice dynamics in the Arctic Ocean and Arctic peripheral seas. *Journal of Geophysical Research: Oceans*, e2021JC017563. https://doi.org/10.1029/2021JC017563.

4.1 Abstract

We present a 500-year history of naturally felled driftwood incursion to northern Svalbard, directly reflecting regional sea ice conditions and Arctic Ocean circulation. Provenance and age determinations by dendrochronology and wood anatomy provide insights into Arctic Ocean currents and climatic conditions at a fine spatial resolution, as crossdating with reference chronologies from the circum-Arctic boreal forests enables determination of the watershed the driftwood originated from. Sample crossdating may result in a wide range of matches across the pan-boreal region, which may be biased towards regions covered by the reference chronologies. Our study considers alternate approaches to selecting probable origin sites, by weighting scores via reference chronology span and visualising results through spatiotemporal density plots, as opposed to more basic ranking systems. As our samples come from naturally felled trees (not logged), the relative proportions of different provenances are used to infer past ocean current dominance. Our record indicates centennial- to decadal-scale shifts in source regions for driftwood incursion to Svalbard, aligning with Late Holocene high variability and high frequency shifts in the Transpolar Drift and Beaufort Gyre strengths and associated fluctuating climate conditions. Driftwood occurrence and provenance also track the northward ice formation shift in peripheral Arctic seas in the past century. A distinct decrease in driftwood incursion during the last 30 years matches the observed decline in pan-Arctic sea ice extent in recent decades. Our new approach successfully employs driftwood as a proxy for Arctic Ocean surface circulation and sea ice dynamics.

4.2 Introduction

The Arctic is vulnerable to climatic changes on a range of temporal and spatial scales from geological to inter-annual, and a hotspot of warming under modern climate change due

to the Arctic Amplification (Serreze & Francis, 2006) – a term for the feedbacks and interactions from the region's sea ice and snow cover resulting in enhanced and accelerated greenhouse gas-induced warming in the Arctic. Recent anthropogenic trends are well documented by a rapid decline in the extent and thickness of sea ice (Polyak et al., 2010; Maslowski et al., 2012). The continuing decline in sea ice cover is expected to result in wide-ranging consequences impacting the Arctic and beyond. These include impacts on terrestrial and marine productivity, changes to global atmospheric and ocean circulation patterns, increased temperatures and rainfall, terrestrial fauna and flora population fragmentation and habitat reduction, increased marine species interaction and connectivity, and northward expansion of lower-latitude species (Overland & Wang, 2010; Screen & Simmonds, 2010, 2014; Francis & Vavrus, 2012; Post & Høye, 2013; Overland et al., 2016; Vavrus et al., 2017; Bintanja & Andry, 2017; Macias-Fauria & Post, 2018; Bjorkman et al., 2020). The Arctic Oscillation (AO) or Northern Annular Mode/Northern Hemisphere Annular Mode (NAM), is defined as the principal component of extra-tropical Northern Hemisphere sea-level pressure and regarded as the most influential mode of atmospheric circulation and climate variability in the Arctic (Thompson & Wallace, 1998; Comiso & Hall, 2014). Dynamic processes affecting the Arctic Ocean such as the AO are being increasingly examined for their impact on ocean circulation and sea ice dynamics (e.g. Barnes & Screen, 2015; Comiso & Hall, 2014; Ding et al., 2017; Hole & Macias-Fauria, 2017; Rigor et al., 2002). Data on past conditions are needed to understand the region's abiotic and biotic responses to various climatic processes and forcings and their resulting impacts on a global scale (Dieckmann & Hellmer, 2010; Armand et al., 2016). Uncertainties remain on the spatiotemporal dynamics of Arctic sea ice throughout the Holocene, with discontinuous data on sea ice extent, discussed below, prior to the generation of spatially explicit sea ice extent information by satellite observations in the late 1970s (Post & Høye, 2013). The observational record has been extended back in time to the

late 19th century by compiling various observational data sources including ship reports, airplane surveys, compilations by naval oceanographers and analyses by national ice services (Walsh et al., 2017). Reconstructions of sea ice preceding observations commonly utilise ocean sedimentary core data. Such records are, however, limited in spatiotemporal resolution due to low sedimentation rates in the central Arctic Ocean (Backman et al., 2004; Polyak et al., 2010), limiting their insight into sea ice fluctuations at the sub-millennial scale. Moreover, they generally do not provide direct information on sea ice dynamics. Further knowledge of past sea ice dynamics is therefore needed to understand the context of recent change and gain insight into possible future sea ice trajectories under conditions of increasing global average temperatures.

4.2.1 The Arctic Ocean and sea ice

The extent, area, thickness and dynamics of Arctic sea ice are driven by both thermal and physical dynamics of the Arctic Ocean system, including spatiotemporally variable atmospheric and oceanic heat fluxes, prevailing winds, and ocean currents (Haas & Thomas, 2017). The position of Arctic Ocean circulation patterns is driven by prevailing winds, most notably the upper-ocean anticyclonic Beaufort Gyre (BG) (Timmermans et al., 2018). Together with the Transpolar Drift (TPD), BG and TPD are the primary circulation systems in the modern Arctic Ocean (Figure 4.1). Such physical dynamics also influence heat and salinity transport and storage in the Arctic, impacting climate both locally and beyond the Arctic (Carmack et al., 2016).The two systems initiated during the Early Holocene after the closure of the Bering-Chukchi land bridge and opening of the Bering Strait *c.* 11 ka BP (Bartlein et al., 2015). The BG displays a mean annual clockwise motion in the western Arctic Ocean (Polyak et al., 2010), recirculating and enhancing survival of sea ice within the Arctic basin. The mean residence time for ice in the BG is c. 5 yr (Rigor et al., 2002), aiding the formation and

preservation of multi-year ice that can reach up to 5 m thickness (Mahoney et al., 2019). The TPD is a surface ocean current running roughly parallel to the Siberian coast and transporting Arctic ice and waters southwards to the North Atlantic through the Fram Strait, favouring the loss of ice. Holocene fluctuations in the extent and orientation of the TPD have been proposed to vary between three overall states (Dyke et al., 1997). These involve lateral shifts from a) an eastward route toward Fram Strait, with sea ice (and any driftwood entrained in it) advection to the European Arctic; b) a westward route toward Greenland with sea ice advection to the Canadian Arctic Archipelago (CAA); and c) a split route with sea ice transport divided between the east and west. A driftwood-based reconstruction of the dynamics of Holocene sea ice extent and dynamics shows that there has been a progression from millennial to centennial shifts in the relative position of the TPD and BG throughout the Holocene, with indications of alignment with concurrent dynamics of the AO (Hole & Macias-Fauria, 2017). The AO Index is characterised as the variable atmospheric mass exchange between the Arctic Ocean and temperate latitudes (Rigor et al., 2002), with positive or negative polarity determined by anomalies in Sea Level Pressures (SLPs) over the polar regions and mid-latitudes (*c.* 55°–60°N; Kwok et al., 2013). The AO is a key physical driver of the position of the TPD and the balance between the strength of the BG and TPD circulation patterns (Rigor et al., 2002). The influence and variation in the AO over the Holocene is outlined in greater detail by Hole & Macias-Fauria (2017), including evidence of late Holocene centennial fluctuations in AO index polarity and ocean circulation patterns.

4.2.2 Sea ice observations

Sea ice observations provide information to varying degrees of accuracy, and the observational record encompasses – partially until the advent of remote sensing data – the past ~1,000 years. Since Iceland's settlement in c. 870 CE, records were kept of sea ice incidence

by Icelandic fisheries (Polyak et al., 2010), enabling a regional sea ice index for the period 1600 – 1850 CE to be developed (Ogilvie & Jónsdóttir, 2000). In Svalbard, sea ice information since 1800 has been collected from sealers, ships and trappers wintering on the archipelago by the Norwegian Polar Institute (Vinje, 2001). April sea ice extent from 1850–1998 has been generated from ship data, aircraft reconnaissance flights and satellite observation data (Vinje, 2001). In the Barents Sea, April sea ice was recorded by Norwegian ice charts by sealing and hunting expeditions from 1850-1949 and 1966-2001, and intervening years measured by Soviet reconnaissance aircraft (Shapiro et al., 2003). Sea ice draft and thickness were also measured through upwards sonar data by submarine cruises throughout the Arctic from 1958 onwards (Rothrock et al., 2008). These include comparison of drift data from two summer polar cruises in 1958 and 1970 (A. S. McLaren, 1989), before more extensive draft data collection as part of the Scientific Ice Expeditions (SCICEX) program (Gossett, 1996). Since the 1970s, spatially explicit sea ice extent information has been available by the development of satellite observations (Post & Høye, 2013). Using these records, Walsh et al. (2017) produced a spatially-explicit pan-Arctic sea ice dataset since the late 19th century at fine spatiotemporal resolution, enabling a comparison between historic data sets and proxy-based reconstructions (Post & Høye, 2013).

4.2.3 Using driftwood to infer past sea ice conditions

The geological record and proxy data provide information on environmental and climatic conditions preceding the observational record. Arctic biogenic and inorganic information on sea ice conditions can be gleaned from a variety of data. Inorganic data include the use of ice-rafted debris (IRD) and radiogenic isotopes for tracking ice drift and provenance (e.g. Fagel et al., 2014; Hillaire-Marcel et al., 2013; Stickley et al., 2009). Biogenic data are collected from ocean sediment cores and include dinoflagellate cysts, ostracods, diatom, and

benthic foraminifera assemblages (Cronin et al., 2013; De Vernal et al., 2013; Seidenkrantz, 2013). Highly branched isoprenoid (HBI) lipids produced by diatoms, notably IP_{25} (the ice proxy with 25 carbons; Belt et al., 2007), have also been used for sea ice reconstructions by assessing the relative proportion of sea ice to phytoplankton biomarkers, termed PIP_{25} (brassicasterol, dinosterol or HBI trienes; e.g. Müller et al., 2011; Belt, 2018).

Raised beaches that occur in north-western Eurasia are a clear sign of GIA related to the melting of past ice-sheets and glacier loads. Their current elevations result from the balance between eustatic sea level change and GIA following the latest deglaciation of northern Eurasian ice sheets (Forman et al., 2004). Such raised beaches in Svalbard often lack vegetation due to their low temperatures, aridity, high alkalinity and low nutrient availability (Dyke et al., 1997; Forman et al., 2004). Such harsh conditions preserve datable driftwood, whalebones and pumice as decomposition is limited (Feyling-Hanssen & Olsson, 1959; Blake Jr, 1961a; Bondevik et al., 1995; Schomacker et al., 2019; Farnsworth et al., 2020b). Driftwood is the preferred target for analysis in this study due to its terrestrial origin (and therefore radiocarbon dating suitability) and delivery to within 1-2 m above sea level by storm or ice pressure, although it can later migrate shoreward by slope processes (Funder et al., 2011). Driftwood can also be used as a proxy for sea ice extent and dynamics.

Deposits of driftwood on Arctic shorelines reveal the transport by sea ice within large-scale Arctic Ocean circulations, which enables the reconstruction of past surface-current dynamics and sea ice conditions in the Arctic (Häggblom, 1982; Dyke et al., 1997; Funder et al., 2011; Hole & Macias-Fauria, 2017). Up to now, driftwood-inferred sea ice conditions have not been directly compared with the observational record. Reconstructions of past sea ice conditions employing this proxy have been based on an understanding of the conditions required for felled wood in the boreal forest to reach high arctic shorelines. The delivery of driftwood to the shores of Svalbard requires initial entrainment in seasonal sea ice before

joining multi-year sea ice for long-distance transport due to its limited buoyancy once waterlogged (Häggblom, 1982). Seasonal sea ice around Svalbard, and therefore seasonally open waters, enable wave action to deliver the driftage to the shoreline (Farnsworth et al., 2020a). The incurred driftwood derives from the major rivers that drain the boreal forest regions of North America and Eurasia. The inflow from river runoff at ~3,300 $km^3\ yr^{-1}$ (Alkire et al., 2017), together with precipitation, constitutes the greatest proportion of annual freshwater influx into the Arctic Basin (Serreze et al., 2006). This is followed by the substantial inflow of Pacific water through Bering Strait, which contributes 2,300–3,500 $km^3\ yr^{-1}$ (Woodgate, 2018). In the boreal forest zone, tree-growth is limited by climate, leading to coherent (not individually highly variable) tree-ring growth patterns within broad climatic region/watersheds (O. Eggertsson, 1993). This coherency, or similarity in individual tree growth patterns, enables regional chronologies of mean tree-ring growth patterns to be created across the boreal forest zone (Schweingruber, 2012) and utilised for dendrochronological matching to driftwood derived from possible boreal source regions. Although the Arctic-draining rivers have been surrounded by boreal forest throughout the Holocene (Hopkins et al., 1981), the Eurasian boreal tree limit in the Early to Middle Holocene of c. 9.5-6 ka BP lay up to 200 km northwards at the circumpolar coastlines (MacDonald et al., 2000).

The geographical distribution of dominant and abundant tree species across the boreal forest (see MacDonald et al., 2008; Hellmann et al., 2013), has been used to infer a genus-based division of driftwood sources to indicate wood provenance. *Larix* (larch) is a markedly common genus of conifers throughout Asian boreal forests and is assumed to indicate a Siberian origin. *Picea (*spruce) is another boreal forest genus of coniferous species very common in North America, and is assumed to signify a North American origin (e.g. Dyke et al., 1997; Eggertsson, 1993; Funder et al., 2011; Häggblom, 1982; Hellmann et al., 2013; Nixon et al., 2016). In North America, *Picea* was present between 10 and 7 ka north of the Mackenzie

Delta, up to 70 km north of the modern treeline (Ritchie & Hare, 1971). This resulted from increased summer insolation and temperatures compared to modern conditions (MacDonald et al., 2008), which then migrated to the modern limit at 60-70°N (Sokolov et al., 1977; Bigelow et al., 2003). The boreal forest reached its current composition by *c.* 6 ka BP in Canada (Tremblay et al., 1997), and by 3-4 ka BP in Eurasia (MacDonald et al., 2000), with increased *Larix* occurrence during 10-3.5 ka BP.

For more spatially precise provenance determination, dendrochronology and tree ring width (TRW) analysis has proved a vital tool in dendroarchaeological efforts (R. E. Taylor & Aitken, 1997) and Arctic climatic and environmental reconstructions (Koch, 2009; Owczarek, 2010). Past driftwood dendrochronological studies have considered only reference chronologies associated with a particular drainage basin (Eggertsson, 1993; Eggertsson & Laeyendecker, 1995) based upon consideration of Arctic surface currents. However, recent studies have highlighted that such assumptions can be incorrect, and a far wider extent of circumpolar sites must be considered during such processes, to accurately capture the potential history of samples (Hellmann et al., 2013b). A recent combined assessment of radiocarbon and dendrochronological age estimates of Arctic driftwood samples found that radiocarbon dates from buried driftwood were in agreement with dendrochronological dating of modern beach ridge systems in coastal eastern Siberia (Sander et al., 2021), thus supporting the validity of age indications obtained from driftwood found on Holocene beaches.

The aim of this paper is to utilise Arctic driftwood collected from modern shorelines to create a proxy-based reconstruction of regional sea ice conditions and Arctic Ocean circulation dynamics at a decadal resolution, and to evaluate inferences made from naturally felled driftwood material against the observational record. In this study we provide a 500-year record of driftwood incursion onto northern Svalbard modern active shorelines. TRW series and genus information are determined for the samples where possible, before crossdating with reference

chronologies from the circum-Arctic boreal forest zone to determine the climatic regions/watersheds the driftwood originated from. As sample cross-dating may result in a wide range of possible matches across the pan-boreal region and possible bias towards the regions covered by reference chronologies, our study includes a new approach to select most probable origin sites from multiple crossdating matches and visualising these results through spatiotemporal density plots. The resulting spatiotemporal distribution of best matches for all samples provides a 500-year time series of driftwood delivery to northern Svalbard, enabling a proxy-based reconstruction of Arctic Ocean surface current and sea ice dynamics over this period. Our study tests for the first time the validity of Arctic driftwood as a proxy for sea ice dynamics at higher spatial and temporal resolutions than possible by other Arctic sea ice proxy data, by directly comparing driftwood-inferred sea ice information against other reconstructions and the observational record.

4.3 Methods

4.3.1 Sampling sites

The raised beaches on the Svalbard archipelago are ideal for preserving stranded driftwood. Svalbard is located at the proposed north-western part of the Late Weichselian Svalbard-Barents Sea Ice Sheet (SBSIS), with abundant preserved raised beach sequences reflecting the pattern and rate of relative sea level changes on Svalbard in response to the deglaciation of the SBSIS (Forman et al. 2004; Ingólfsson & Landvik, 2013). Samples were collected in August 2016 and July 2018 from three localities from the northern coastline of the Svalbard Archipelago. In 2016, driftwood was collected from the three largest islands of Sjuøyane (Martensøya, Phippsøya and Parryøya), and Ringhorndalen in Wijdefjorden, Spitsbergen. During a 2018 field campaign to Vassfarbukta in Wijdefjorden, Spitsbergen, a

total of 30 driftwood samples were collected between the active beach face and the storm berm up to c. 4 m above mean sea level along a 200 m stretch of coast. All sampling locations were expected to capture driftwood from the same large-scale ocean currents (Figure 4.1). On

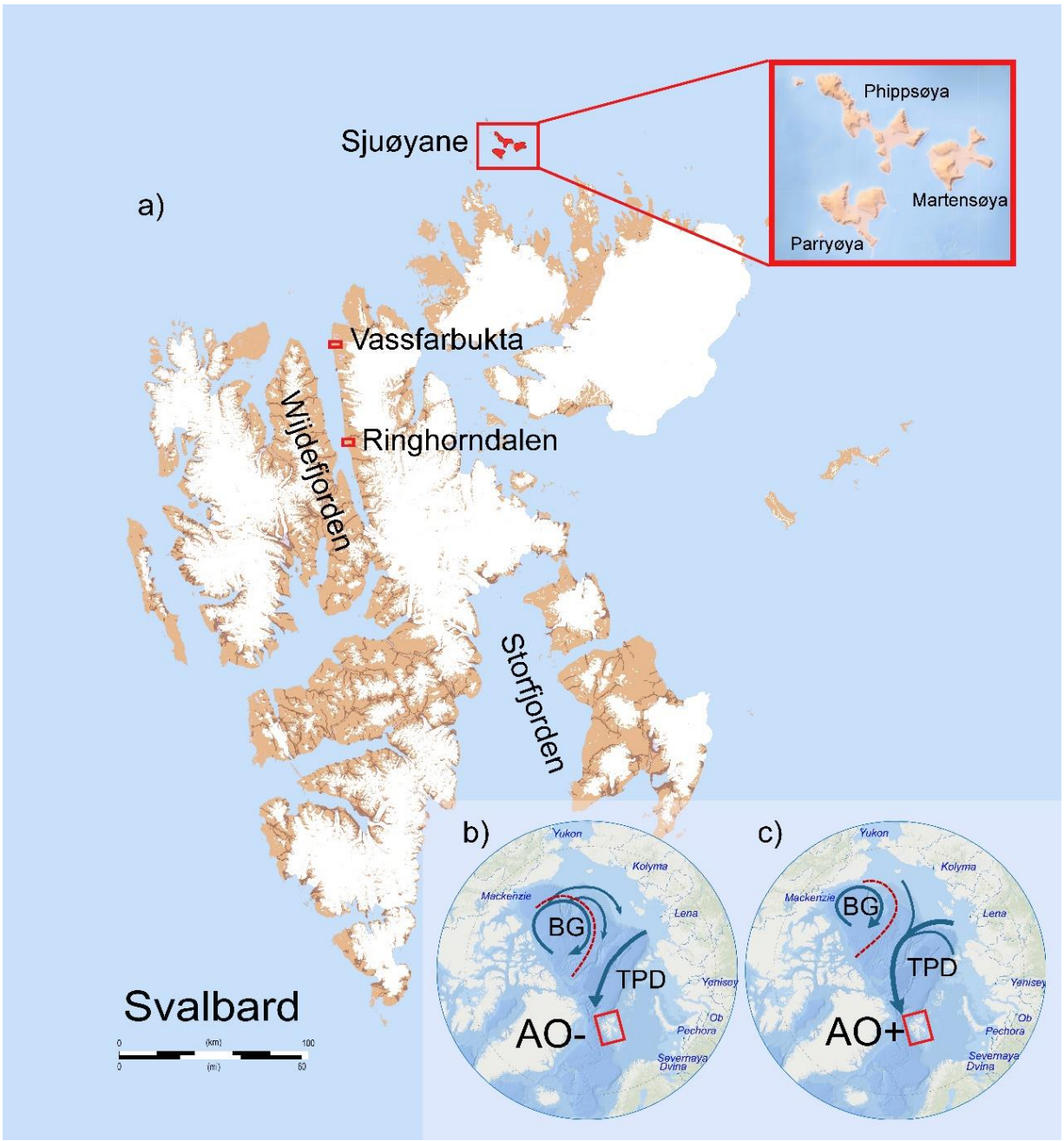

Figure 4.1. a) Driftwood sampling locations of Sjuøyane, Ringhorndalen (sampled 2016), and Vassfarbukta (sampled 2018). Insert panel: Two modes of the Arctic Oscillation Index (AO), showing wintertime surface circulation patterns of Beaufort Gyre (BG) and Transpolar Drift (TPD). Map figure modified from Norwegian Polar Institute (2014). (b) Low index, negative AO polarity with a strengthened Beaufort Gyre and recirculation of sea ice. (c) High index, positive AO polarity with a weakened BG. The red dashed lines encircle the region of ice recirculation in the BG by the mean sea ice motion field (circulations compiled and modified from Rigor et al. (2002)).

Sjuøyane, the lowlands above the marine limit are covered by glacial drift of angular to subangular cobbles and boulders, within a silty/clayey matrix. In this matrix there are abundant shell fragments, likely incorporated by glaciers originating from Nordaustlandet that also supplied erratics of granites and quartzites (Forman & Ingólfsson, 2000). Holocene arrival and incursion of driftwood onto Sjuøyane and Wijdefjorden is influenced not only by broader ocean circulation dynamics and sea ice conditions, but also by local deglaciation patterns and geomorphology. Dating of driftage deposits and preserved regressional strandlines indicate that deglaciation of Phippsøya occurred before *c*. 9.4 ka ago (Forman & Ingólfsson, 2000). The relative sea level fell to less than current sea level *c*. 9-7 ka BP, before a transgression rising sea level to above present levels at *c*. 6.2 ka BP indicated by cross-cutting beach ridges, and observed in other marginal foreland records around Svalbard such as a whalebone dated to *c*. 6 ka BP found at 5 metres above high tide (m a.h.t.), behind the modern storm beach of Kongsfjorden (Forman et al., 2004). Similar scales of isostatic readjustment and relative sea level changes patterns occur in northern Wijdefjorden (Schytt et al., 1968; Forman et al., 2004; Farnsworth et al., 2020a). The impact of such dynamics on driftwood incursion is minimal for this study, due to our aim to target samples from the modern shoreline for reconstruction of sea ice conditions over recent centuries, and for the comparison of modern sample spatiotemporal distribution with observed circulation patterns and sea ice dynamics in the Arctic Ocean during the last 120 years.

4.3.2 Field sampling methods

A total of 95 driftwood samples were collected from Sjuøyane, Vassfarbukta and Ringhorndalen shorelines and raised beach terraces where samples were deemed in-situ. A random sampling strategy was employed to minimise sampling bias on shorelines with high volumes of driftwood, and with all naturally-felled driftwood on shorelines with little driftwood. The datum for raised beach elevation measurements is the present mean high tide mark, m a.h.t., seen at the coastline as a swash limit (Forman et al., 2004). The storm beach elevation can reach over 4 metres on bays exposed to direct storm fetch (Forman, 1990; Zeeberg et al., 2001) and this can carry washed up material substantially above the sea level of the time, giving uncertainties to dating by local geomorphology for raised-beach samples. At

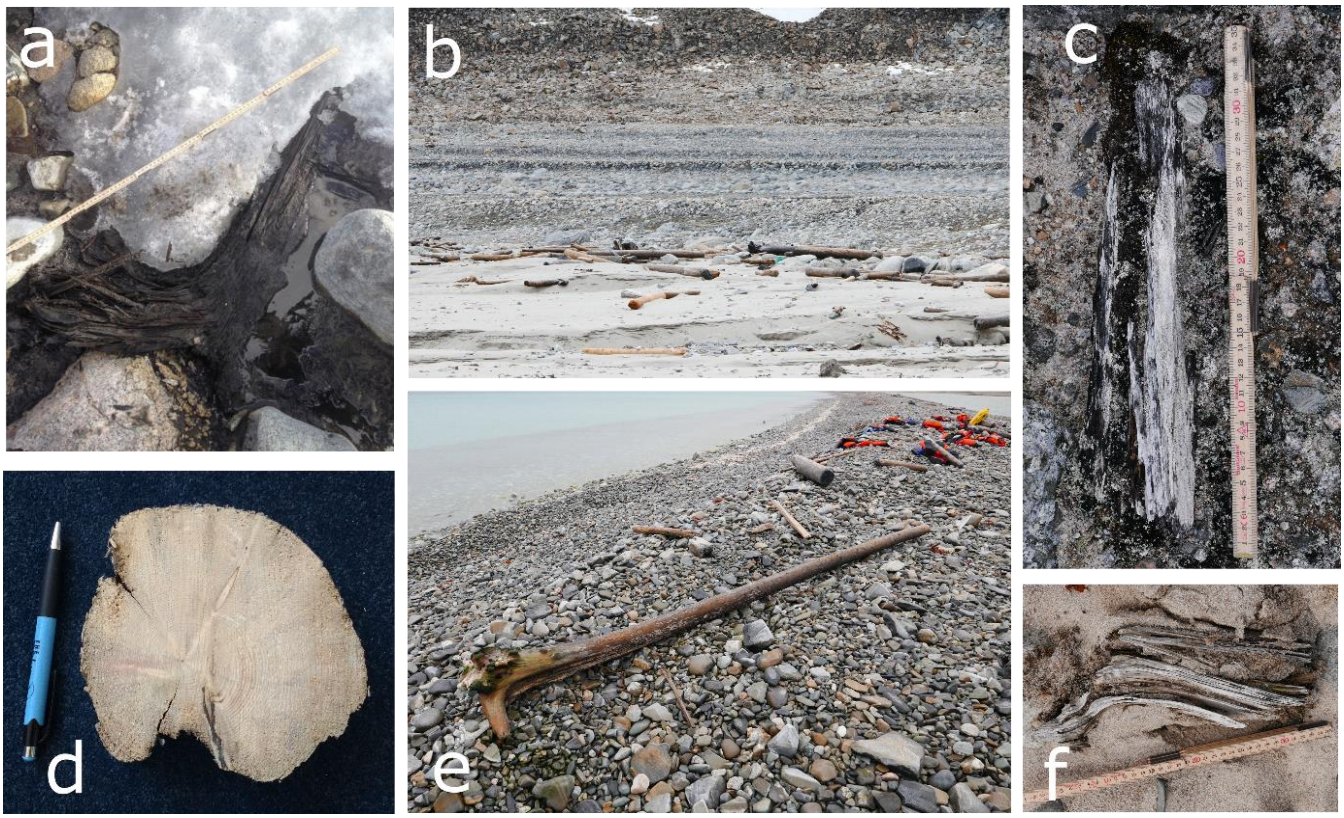

Figure 4.2. Range of preservation level of driftwood samples on Sjuøyane. Ruler placed for scale in a, c, f, and pen placed for scale in dry driftwood disc in d. Samples along the modern shoreline have the highest levels of preservation, with intact trunks and visible tree-ring series allowing dendrochronological analysis. Only samples that had sufficient preservation of tree rings and that preserved their root structure – and thus were likely naturally felled – were used to create our sample dataset (such as 2b, d, e). More degraded samples such as in 2a, c, f did not have sufficiently preserved rings to be included in the dataset.

all sites, naturally felled driftwood at the modern shoreline was targeted by the sampling of logs exhibiting intact root stock. These driftwood logs were sub-sampled at peak thickness with a saw, where sub-sampled slices exhibited the maximum amount of intact tree-rings (Figure 4.2). For elevation calculations, handheld GPS devices were used with occasional DGPS or altimeter data. Older driftwood was sparse, with most found ≤ 7 m a.h.t., and the majority of the samples are from the modern shoreline. The driftwood sampled varied in condition; more recently deposited driftwood samples (e.g., Figure 4.2d) had intact tree rings that were suitable for analysis.

4.3.3 Laboratory processing

Driftwood samples were assessed for viable tree ring series, with 59 of the 95 samples suitable for measurement and analysis. Of the 59 driftwood subsamples from northern Svalbard, 27% (16) were from Sjuøyane, while 73% were from Wijdefjorden (n=28 and n=15 from Ringhorndalen and Vassfarbukta respectively). These were then sanded using drill-mounted sanding bands, and annual ring widths of each sample were measured to 1/1000 mm accuracy using LINTAB tree-ring measurement table and TSAP-Win Professional version 0.89 (Rinn, 2011). Where possible, the genus of the driftwood samples was identified by microscopy through examination of stained radial, tangential and longitudinal sections.

In the majority of dendrochronological studies, reference chronologies are limited to a specific temporal and geographical range based upon the context of the samples taken, be it by pre-existing knowledge of logging activity (Drake, 2018), or sapwood estimation (M. K. Hughes et al., 1981; Daly, 2007). Once a reference subgroup is determined, the “best match" is then identified as that with the highest t-value, a statistical measure of a sample’s similarity to a period in the reference chronology. Identifying such reference subgroups is a more difficult

process when investigating naturally felled driftwood origins. The measured tree-ring series were cross-dated both visually by comparison of ring-width marker ring lists and by use of the chronology-building statistics of TSAP-Win software. Tree ring series were amassed and standardised to remove non-climatic trends such as ontogenetic growth and competition effects using a two-part trend elimination (Cook & Peters, 1997). Firstly, a negative exponential curve was fitted, before taking the residuals. Secondly, to completely remove multi-year variance, a 5-year moving average was applied, with the resulting residuals then taken. This was undertaken to remove autocorrelation (year-to-year variance) to facilitate the computation of correlation coefficients. At least two radii per driftwood disc were measured and combined through a bi-weight robust estimate of the mean to form one chronology per sample.

4.3.3.1 Chronology building – driftwood floating chronologies

The 59 samples with sufficient measured time series were cross-dated using TSAP-Win using a variety of statistical parameters, discussed below. Multiple scoring metrics have been utilised in assessing between-TRW time series similarity. A t-statistic is commonly employed to compare a sample set against a reference chronology. TRW data are standardised by converting to a percentage of the mean of the five ring widths of which it is the centre value, which ensures the data have bi-variate normal distribution. The resulting values are then normalised by taking the natural log of percentage figures (Baillie & Pilcher, 1973). This de-trended value is referred to as TVBP (T-value Baillie-Pilcher), however the measure lacks descriptive power in the absence of extreme ring-differences between chronologies. For cases with less extreme ring-differences, the Gleichläufigkeit (Glk) parameter (or concordance coefficient) is also employed, which instead assesses similarity of sample slope intervals (Eckstein & Bauch, 1969; Schweingruber, 2012). To capture the strengths of both metrics, we

considered the Cross-Date Index (CDI) within our study, provided by the TSAP-Win package (Rinn, 2011). CDI gives the quality of agreement between sample series by combining the Glk measure of overall accordance of two series with the t-value measure of the correlation significance:

$$CDI = \frac{\left(Glk - 50 + \left(50 \times \sqrt{\frac{overlap}{\max overlap}}\right)\right) \times t - value}{10}$$

With the inclusion of both Glk and t-value in the above equation, CDI captures the magnitude of both measures. Therefore, the CDI gives a date index of possible series matches (Rinn, 2011). Significant correlation was set to Glk >60%, TBP>3.0 and a CDI≥10 (Rinn, 2011). The cross-dating of series within the chronologies was examined using the COFECHA-style Cross-Date Check feature of TSAP-Win (R. L. Holmes, 1983). Any series or segments of series that did not surpass sufficient cross-date parameters were removed. Successfully cross-dated individual series were combined to floating chronologies.

4.3.3.2 Reference chronologies from the boreal forest

Reference chronologies from the circum-Arctic boreal forest zone were sourced from the *International Tree Ring Data Bank* (ITRDB, http://www.ncdc.noaa.gov/data-access/paleoclimatology-data/datasets/tree-ring) (Grissino-Mayer & Fritts, 1997). Individual, dated TRW measurement series used to form locality reference chronologies were downloaded before undergoing the same detrending process as driftwood samples. These dated series were then formed into chronologies via the TSAP-Win™ chronology building tool. The

spatiotemporal spread of these reference chronologies (Figure 4.3) provided possible age and source data for crossdating with each driftwood sample.

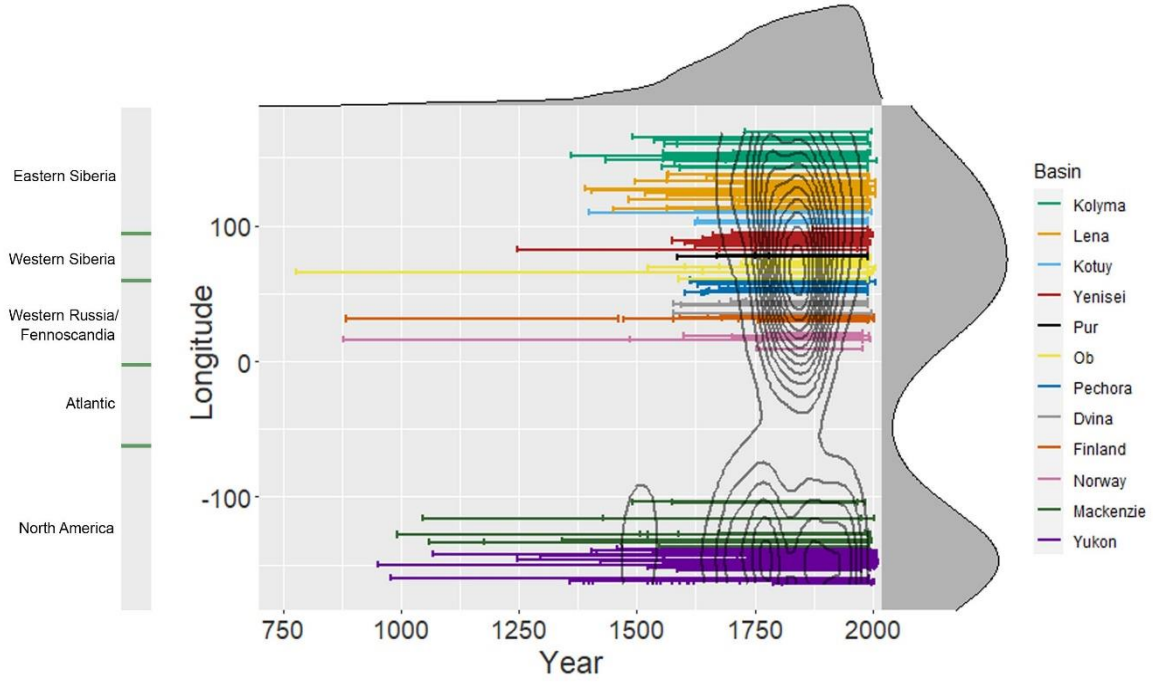

Figure 4.3. Spatiotemporal distribution of 222 reference chronologies from across the Eurasian and North American circum-Arctic boreal forest zone, sourced from the International Tree Ring Data Bank (ITRDB, http://www.ncdc.noaa.gov/data-access/paleoclimatology-data/datasets/tree-ring) (Grissino-Mayer & Fritts, 1997). Each line represents a single chronology, depicting the longitude and timespan covered, with line colours depicting the river basin/longitude of each chronology. The longitudinal density plot is directly calculated from the plotted longitudes, and the top density plot captures the number of chronologies that include the respective year. The overlaid contour plot is mapped using the longitudinal and time range midpoint data for each chronology.

4.3.4 Data Analysis

Floating driftwood chronologies were compared with all available boreal forest reference chronologies in order to determine their most probable origin. In a first approach, all matches considered viable by TSAP-Win (CDI≥10) were plotted to display and investigate the spatiotemporal trend of matches, providing the density plots of the longitude and felling dates of all potential matches. However, since we consider a pan-boreal reference chronology, there

is a risk of over-representing the geographic regions and time-periods that are better constrained by our reference chronology. That is, a sample may be more likely to match to a period/region for which there are more reference chronologies available. Each chronology within our reference chronology dataset was examined by the longitude and timespan covered (Figure 4.3). The grey-shaded y-axis density plot displays the geographic distribution represented, while the x-axis density plot depicts the abundance of chronologies associated with each individual year. The geographic distribution is approximately represented evenly between the two key landmasses of the northern hemisphere (North America and Eurasia). More recent years are better represented by our reference chronology due to the reliance of the database on the collection of reference chronology data, which is more abundant in recent centuries. Information from several centuries ago is restricted to a few individual chronologies, with a marked dearth of data from ~1000-1500 CE in eastern Siberia.

Other dendrochronological studies that have considered a wider potential source region have demonstrated a wide range of t-value matches, which would all have been considered a sign of good-fit by more restrictive references (Daly, 2007; Daly & Nymoen, 2008). Such studies will still routinely use the highest t-value as a measure of the most probable origin, however such approaches risk bias towards regions with better developed reference chronologies. Based upon this, we computed a new metric (Weighted Score) to help determine the most likely match within our results for each sample. This was achieved through weighting the CDI scores by the inverse of the density plots in Figure 4.3. As such, matches that were considered more “unlikely” by appearing in less-reported regions and time periods of the reference chronologies were rewarded. A new reference score was constructed for each potential match representing the initial CDI scores, corrected by the overall reference chronology spans, and increased by the number of identical temporal matches for the sample, i.e.:

$$Weighted\ Score = CDI\ \times \frac{(Total\ number\ of\ matches\ with\ the\ same\ timespan)}{Reference\ chronology\ densities\ for\ the\ match}$$

A match was considered better if it had a higher CDI. Additionally, matches to a poorly represented region in the reference chronology were weighted positively. We constructed linear interpolations of the reference chronology densities (Figure 4.3) via the *approxfun* function within R. This produced two functions, $f_{time}(x)$, $f_{long}(y)$, which provide the relative densities for a given year x, and longitude y. We then calculated the new score for each match as:

$$Weighted\ Score = \frac{CDI\ \times n}{f_{time}(x) \times\ f_{long}(y) \times \sum^{matches} CDI}$$

where x and y are the start-date and longitude of the match in question, respectively, and $matches$ is the total number of matches for the sample with the same start/end dates. n is the total of all match CDIs for the sample. In order to determine the 'best match' for each sample, the CDI values and Weighted Score values were examined, with high CDI values showing high Weighted Score values considered a sign of a good match. A decision workflow was employed when assessing the matching parameters (Figure 4.4). With all data available, the match values of CDI and Weighted Score were chosen. If there was a cross-date match with sufficiently high CDI and/or Weighted Score, a match was chosen, with a preference to the Weighted Score in case of doubt. Additional information was employed to assess the uncertainty in the choice of the best match. Chronology density plot surfaces, the presence of multiple matches for a common date and region, and genus agreement between sample and reference chronology, as well as visual comparison between floating and reference TRW chronologies, were considered for match choice. Additional information was not used to determine a match but could be used to gain confidence on the chosen match or to decide that either the existing match had high uncertainty or that there was not enough information to determine a match (Figure 4.4). CDI scores, Weighted Scores and match choices are available in Supplementary Materials –

Appendix B2. All match distribution plots for samples can be seen in the Supplementary Materials Dataset – Appendix B3. All data processing, visualisation and score calculations were performed in *R* utilising the *tidyverse* suite of packages. All data and code used is made freely available at https://osf.io/z4t3a/.

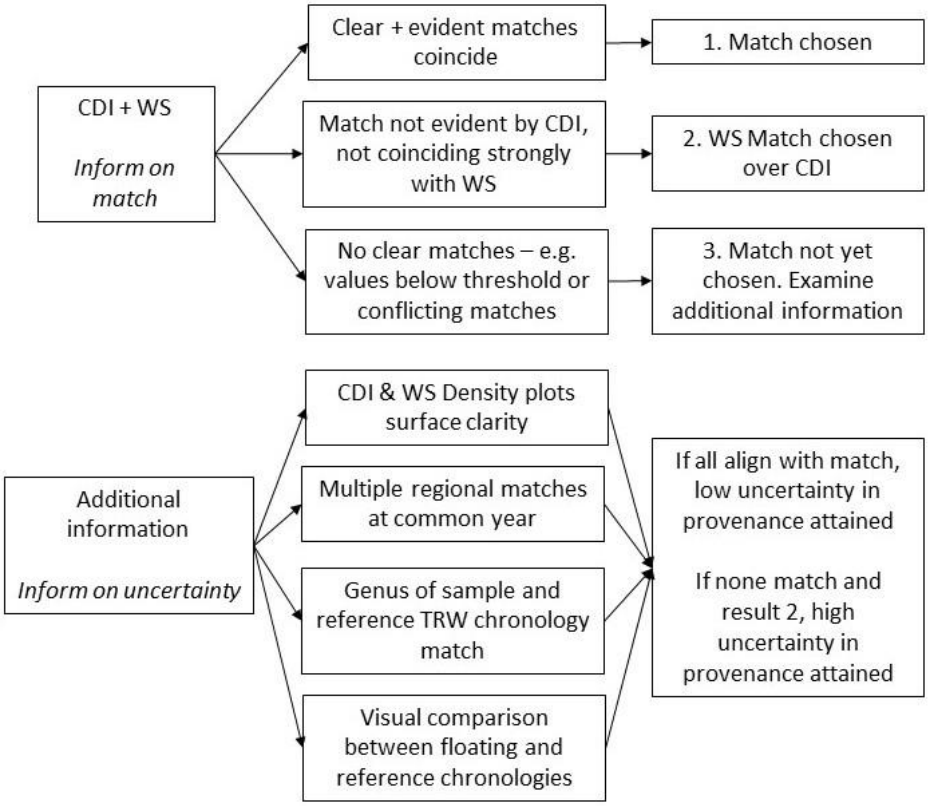

Figure 4.4. Decision workflow for the determination of cross-dating matches between samples and reference chronologies from the ITRDB. WS = Weighted Score.

4.4 Results

Match plots are available for all samples in Supplementary Materials – Appendix B3. Plots for two contrasting samples (RIN24 and RIN28) are provided as an example in Figure 4.5. RIN24 exemplifies a low uncertainty provenance case, whereas RIN28 exemplifies a sample with higher uncertainty where a match is obtained by Weighted Score supported by multiple regional matches. Each point on the plot represents a potential match, where the colour

of the point shows its associated drainage basin, and the size of the point represents the CDI value of the match. The density plots provided were constructed based upon the respective x and y value of each point and are weighted by the CDI value. RIN24 (segment length = 58 years) correlated very clearly with reference chronologies from the Yukon basin, and its most recent year was determined as 1831 CE, showing the highest similarity with a reference TRW chronology named 'Frost Valley'. In contrast, RIN28 (segment length = 78 years) had a higher number of possible matches. Taken individually, the highest t-value (or CDI value) suggested

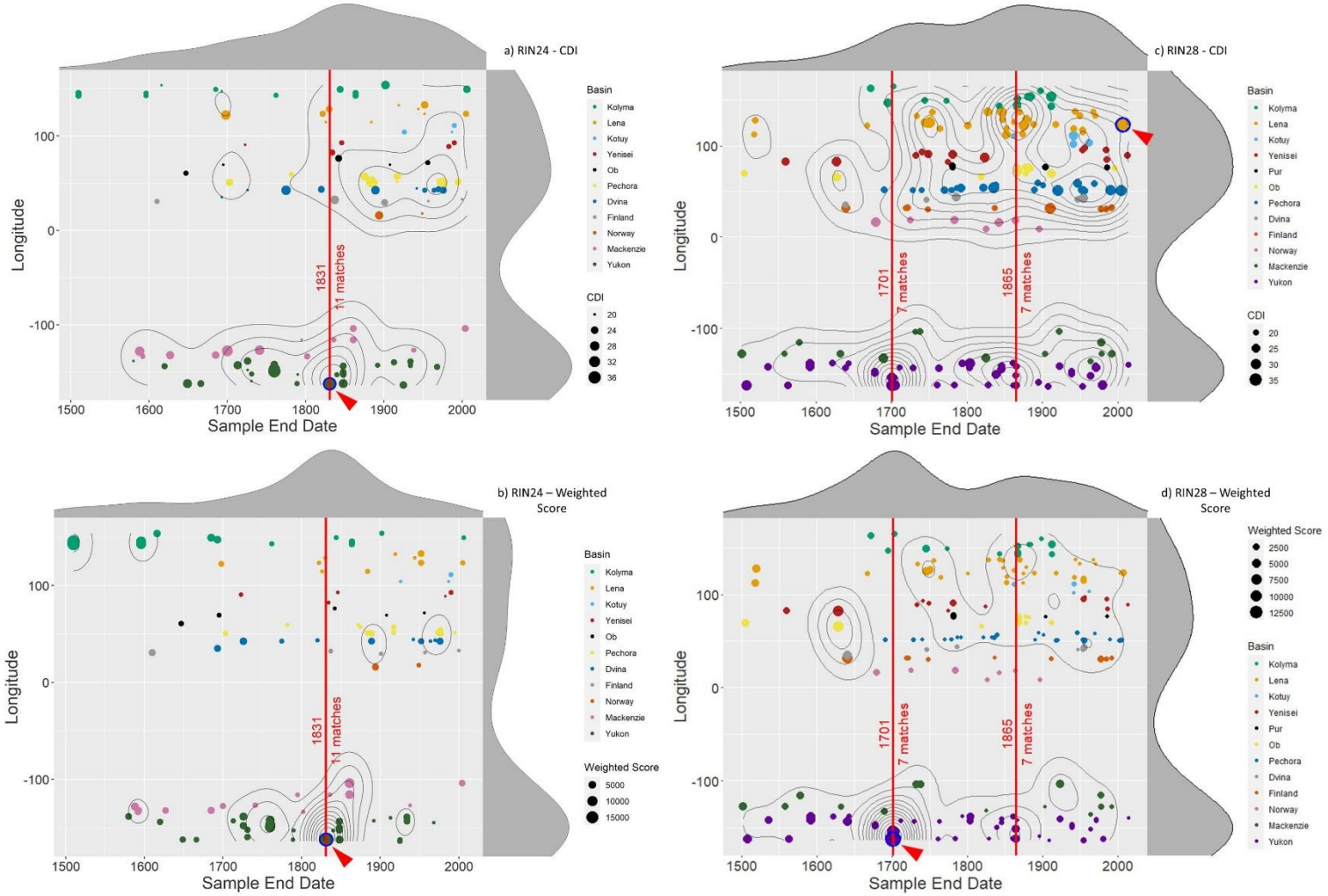

Figure 4.5. All potential matches for samples RIN24(a,b) and RIN289c,d) using the scores CDI and Weighted Score, demonstrating two examples of the employment of the decision workflow. Each point represents a match to a chronology with the chosen best match denoted by blue circle and red arrow. The colour of the point displays the associated drainage basin, and the size of the point represents the CDI of the match in the upper plot and the Weighted Score in the lower plot. The density plots and contours depict the densities of the associated time and longitude axes, weighted by the scores of the matches.

the best match depicts a fell date of 2007 from the Lena River region (blue-outlined circle and arrow; Figure 5a), longitude 123.36, with a CDI of 36. However, this match is isolated: sample RIN28 showed a high CDI value with one reference chronology only, despite the abundance of chronologies that encompass the year 2007 in the reference dataset, including several in the Lena River drainage basin. This suggests that such value might be due to chance. The year with the most concordance of common date matches is plotted in red, in this case 1701 and 1865 with 7 matches for each date (Figure 4.5c). The contour plot surfaces computed using unweighted CDI values (Figure 4.5a) suggested the best match would be in the late 1800s from the Ob region. By utilising the Weighted Score metric, factors were judged together to assess the most probable match in the face of all available data, which was determined to be a match to an end date of 1701 from the Yukon region, via the `Bye Rosanne/ak061' reference chronology in Alaska (highlighted with a blue-outlined circle and arrow in Figure 5b). All best matches and weighted scores, with rationale behind match choices via this method, are available in Supplementary Materials – Appendix B2.

The spatiotemporal distribution of best matches for all samples collected were assessed for distribution trends (Figure 4.6). Multiple matches were included when a sample resulted in more than one possible matching chronology (this was only required for one sample, which indicated 2 possible best matches – RIN40). The CDIs for each match were utilised for assessment of the distribution trends, due to the inter-sample comparability, whereas the Weighted Scores values consisted of a more variable magnitude making comparison between samples less useful than comparison of scores per sample. Best matches divided by sampling locality (Sjuøyane, Ringhorndalen and Vassfarbukta; Supplementary Materials – Appendix B1) showed a consistent trend across the three localities, with no distinct variation of driftwood age, provenance, or species. Segment lengths of series ranged from a minimum of 34 to a maximum of 281 years (Figure B1.1 in Supplementary Materials - Appendix B1). Samples

with greater segment length had more likelihood of cross-dating success with reference chronologies, and thus only a proportion of the samples were expected to be successfully cross-

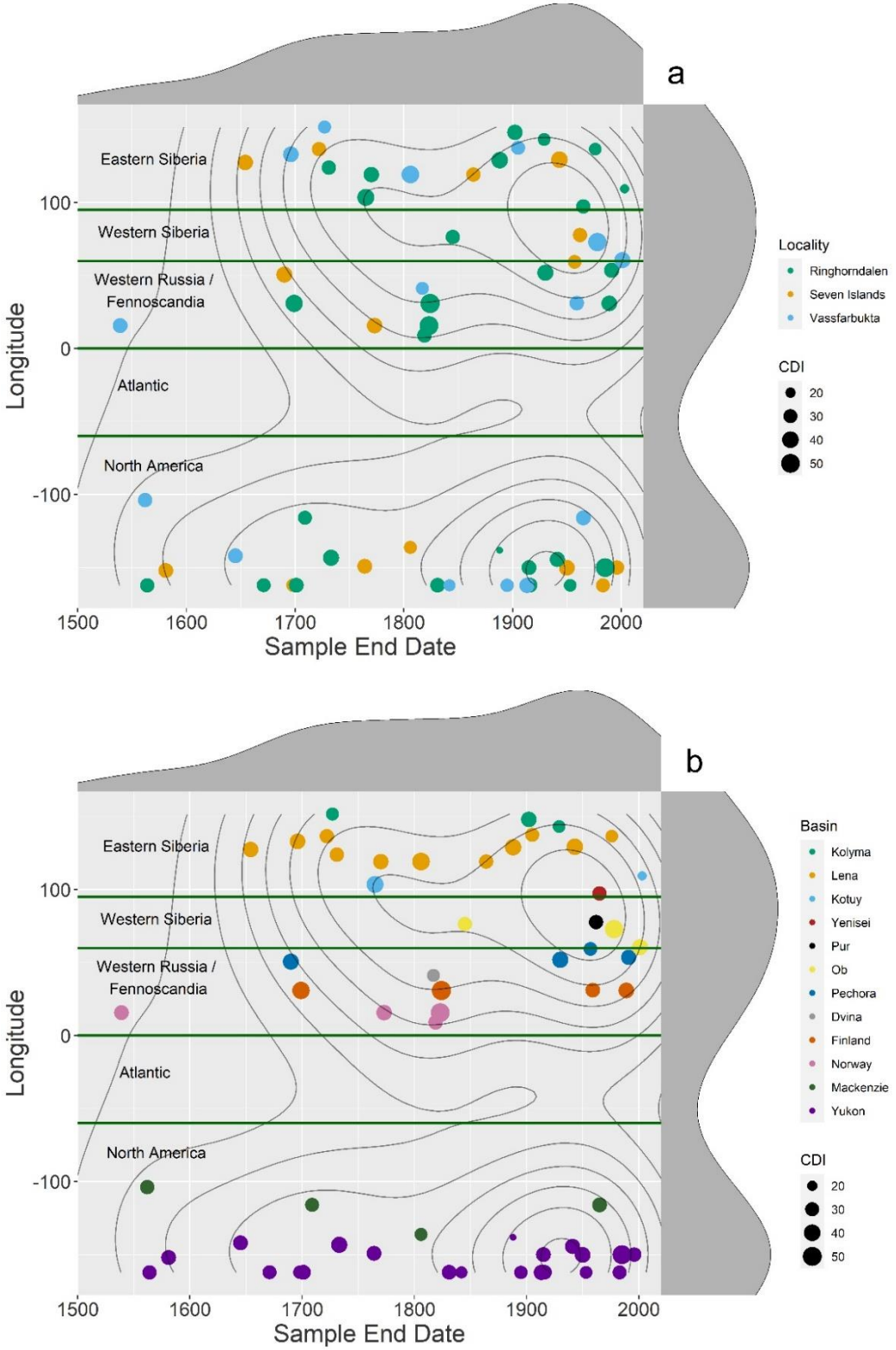

Figure 4.6. Plot of best matches for all samples. Each point represents a sample's best match to a chronology, with both matches included when a sample shows two possible matching chronologies (1 case – RIN40). a) The colour of each data point corresponds to the sampling site and the size of the point represents the CDI of the match. b) The colour of each data point displays the associated drainage basin, and the size of the point represents the CDI of the match. The density plots depict the densities of the associated time and longitude axes, weighted by the CDI of the matches. Contours depict the unweighted densities of the spatiotemporal spread of the matches.

dated and therefore have a provenance determined. Regional density plots depicted the distribution of driftwood provenance through densities of the associated time and longitude axes, weighted by the CDI of the matches (Figure 4.7), which were consistent with the regional divisions (Figure 4.6). Examination of the spatiotemporal distribution of these samples reveals centennial-scale shifts in the contributing sources of Arctic Driftwood to northern Svalbard. Shifting patterns in the regional density plots indicate increases from Western Siberia over the last two centuries, with smaller centennial variability in North American driftwood delivery. There was a peak in overall driftwood delivery centred around the 19th century, an early drop in driftwood delivery from the Barents Sea starting in mid-19th century, increased driftwood delivery in the Siberian shelf during mid-20th century, and a synchronous decrease in driftwood delivery to northern Svalbard in the recent decades (Figure 4.7). The main sea ice features inferred from driftwood incursion to Northern Svalbard in this study are summarised in Table 1 and will be discussed in the following section.

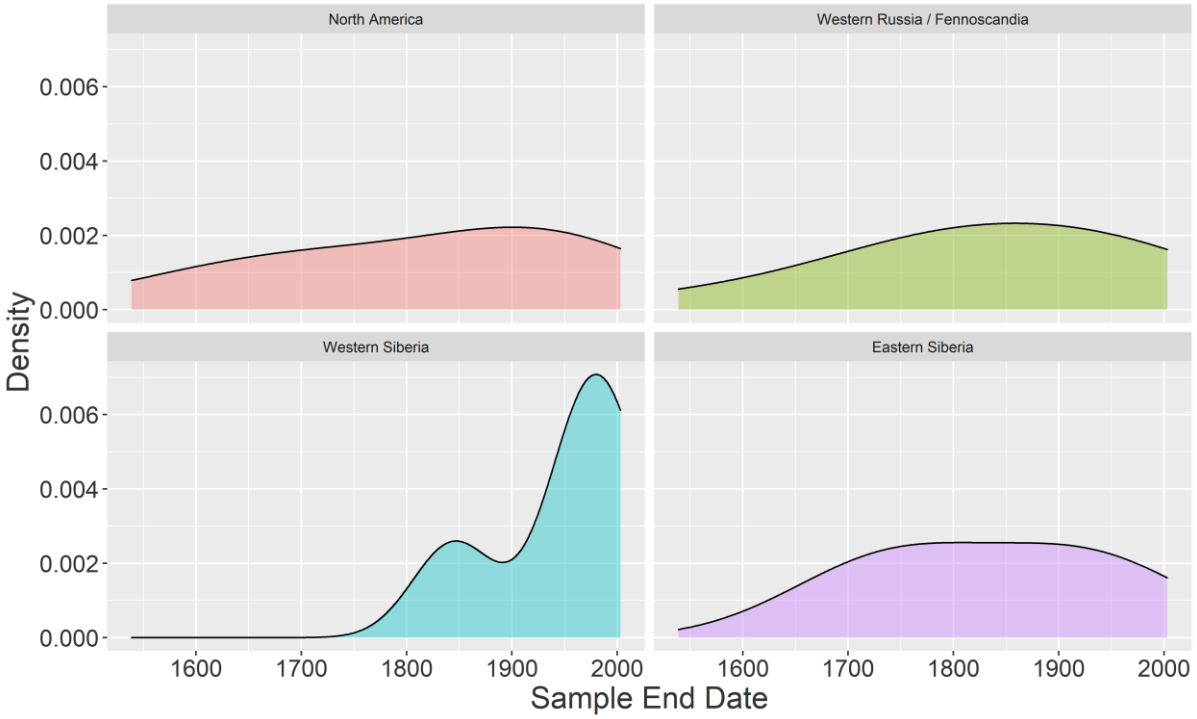

Figure 4.7. Plot of best match density plots for the four regions a) North America, b) Western Siberia, c) Western Russia/Fennoscandia, and d) Eastern Siberia, matching regions shown in Figure 4.6. The density plots depict the densities of the associated time and longitude axes, weighted by the CDI of the matches.

4.5 Discussion

The best matches and regional density plots from our model show that the proportion of Siberian driftwood arriving in Svalbard was greater than that from North American regions as a whole (Figures 4.6 & 4.7; Table 4.1), as expected due to a greater number of boreal zone-draining rivers. These findings agree with both observations of felled and logged driftwood transport (Hellmann et al., 2017) and modelling of driftwood transport based on sea ice velocity, concentration and the sea surface current velocity (Dalaiden et al., 2018). Within North American samples, Yukon River basin dominates over Mackenzie River basin origin. This is expected given the overall direction of the eastward-flowing coastal current at the Mackenzie River mouth, that will tend to divert driftwood towards the Canadian Arctic Archipelago (Dyke & Savelle, 2000): this result gives confidence in the dendro-provenancing methodology employed in this study. A lack of samples of Siberian origin arriving before 1650 CE correlates to the period of low Arctic sea ice cover that spanned the 16th and early 17th centuries (T2 in the multiproxy reconstruction by Kinnard et al., 2011, that did not employ driftwood; Table 4.1). A lack of driftwood arriving from Western Siberia before the 20th century may indicate a lack of sufficient ice in the Kara Sea, although there is no evidence of this in other palaeo-records (Table 4.1). Another possibility is the Kara Sea acting as a closed system not delivering driftwood to the TPD, which aligns with observed strong closed summer anticyclonic circulation in the Kara Sea, associated with river runoff (Panteleev et al., 2007). Driftwood delivery (and thus inferred sea ice extent) increased markedly in the subsequent ~150 years (again, in line with Kinnard et al., 2011), with a mixed arrival of both Eurasian and North American driftwood between 1700 and 1850 CE, suggesting a well-developed BG able to deliver North-American wood to Svalbard entrained in the TPD. This indicator of cold conditions and multi-year sea ice aligns with inferred late Holocene sea ice increases via a

proxy-based sea ice reconstruction including sediment core IP_{25} data from northern Wijdefjorden, Svalbard (Allaart et al., 2020). In that reconstruction, continuous increase in IP_{25} concentrations after *c*. 0.5 cal. ka BP, in combination with decreased water temperatures and the increased ice-rafted debris, were inferred to indicate increase in sea ice and cold conditions correlating with the onset of the Little Ice Age (LIA). That record aligns with this study's inferred sea ice increase and well-developed BG after 1650 CE. Cooling in the Barents Sea at c. 1650 CE is also recorded by a cooling period between c. 1650 and 1850 CE based on oxygen isotope analysis and benthic foraminiferal assemblages (Wilson et al., 2011). Cool temperatures are also indicated ~1705 to 1824 CE based on southern Barents Sea $\delta^{18}O$ shell-temperature reconstruction (Mette et al., 2021). A reconstruction of annual sea ice persistence from the southern Barents Sea from dinoflagellate cyst assemblages indicates longer sea ice season after 1650 CE (Voronina et al., 2001). A combination of that reconstruction with other proxy-based reconstructions of Barents Sea air-ice-ocean variability also indicates cool conditions during the last ~300 years (Smedsrud et al., 2013).

There is a notable halt of Western Russian/Fennoscandian driftwood delivery after 1850 CE (Figure 4.6; Table 4.1). For this material to arrive on the northern shores of Svalbard, sea ice is required in the Barents Sea which will carry it north / north-eastwards towards the Arctic Ocean before joining the TPD. Driftwood from north-eastern Europe returns in the mid-20th century, whereas driftwood originating from Norway is constrained to the period 1650-1850 CE, indicating sea ice in the southern Barents Sea at this time and a lack thereafter. This aligns with analysis of a continuous observational record of April ice edge in the Barents Sea, which indicates a retreat in the winter mean ice edge position since 1850 CE (Shapiro et al., 2003). This also correlates with a reduction in sea ice occurrence and north-easterly retreat of the ice edge during this time (Divine & Dick, 2006; Vare et al., 2010). There is a lack of driftwood originating from the most eastern Siberian sources such as the Kolyma basin between 1750 and

1900 CE. This may be indicative of the trajectory of such distal driftwood sources. Given the mean residence time of ice from North America and far-eastern Russia region is *c.* 5 years (Rigor et al., 2002), there is the possibility of entrainment into the Beaufort Gyre disrupting travel to northern Svalbard, or sea ice formation focused in the Barents Sea region, favouring driftwood delivery from this region before 1850 CE.

Further information from direct observations of sea ice dynamics is available since mid-19th century and can be compared to the driftwood record to assess the accuracy of driftwood temporal distribution reflecting the known conditions of the time (Table 4.1). A composite historical record of Arctic sea ice margins from 1870-2003 CE shows a trend of northward and eastward retreat in seasonal ice from 1900 CE onwards, with acceleration of seasonal and annual ice retreat during the last five decades with spatially-variable sea ice distribution changes across the Arctic (Kinnard et al., 2008). There is further evidence of such conditions favouring reduced ice, with atmospheric warming driven by enhanced atmospheric and ocean heat transport from the North Atlantic into the region from 1900 to 1940 CE (Vinje, 2001; Bengtsson et al., 2004). The decline in driftwood arriving to northern Svalbard from Western Russian/Fennoscandian sources after the 1850s may be an indication of a reduction of sea ice in the Barents Sea in this period, as indicated by a sustained reduction in March and September ice extent from 1850 - 2013 CE (Walsh et al., 2017). The increase in September sea ice during the late mid-20th century is seen in a peak in Western Siberian driftwood delivery in the latter half of the 20th century, in contrast to decreases for other regions (Figure 4.7b). A relative maximum is reached by the 1970s within a framework of strong decadal and multidecadal variability on a regional basis, indicating the favouring of proximal sources of driftwood from Eurasian coasts in this period. The steady – even centennial – increase in the delivery of North American driftwood until the last several decades (Figure 4.7a) likely reflects a more stable (i.e., less variable) source of driftwood in recent centuries. This observation is in agreement

with a higher occurrence of sea ice variability in the Eurasian peripheral Arctic seas (most notably the Barents Sea) compared to the Beaufort and Chukchi Seas until late 20th century (Walsh et al., 2017). As a consequence, increases in the overall frequency of North American wood delivery in Svalbard can signal, depending on the context, lack of sea ice in the Eurasian peripheral seas.

Finally, there is a distinct decrease in driftwood incursions during the last 30 years from each region of our study (Figure 4.7; Table 4.1), suggesting a lack of sufficient multi-year sea ice throughout the Arctic to raft driftwood to Svalbard shorelines, matching the record of systematic decrease in pan-Arctic sea ice extent since the 1970s (Walsh et al., 2017). For the period 1990-2003 CE, synthesised historical sources and satellite data show the trend continues with an Arctic-wide retreat of the summer (i.e. multi-year/permanent) sea ice cover resulting in a net increase in the extent, and a northward migration of seasonal sea ice from the peripheral seas, with earlier sea ice retreat in the Barents Sea and a later onset in the Beaufort and Chukchi Seas (Walsh et al., 2017; Kinnard et al., 2008). This spatial shift is matched with multi-year ice loss and replacement with first-year ice, with resulting reduction in driftwood-carrying potential expected to affect the most recent driftwood incursion rates. The most recent driftwood samples, comprised of three samples matched to dates from 1991-1996 (Supplementary Materials - Appendix B2), originated from eastern Eurasia and the Yukon drainage basins. Based on the average travel time of up to 7 years for Arctic driftwood (Häggblom, 1982), these recent driftwood samples suggest a reduction in the influx of driftwood during this period. However, there are not enough data points to robustly support this conclusion within the context of the observational record. The lack of naturally felled driftwood arriving to our study site more recently than 1996 CE is remarkable, especially given the ample availability of reference dendro-chronologies since the 1990s in this study.

These centennial- to decadal-scale shifts in source regions for driftwood incursion to Svalbard align with the high variability and high frequency shifts in the TPD and BG strength throughout the late Holocene and associated fluctuating climate conditions, as found in a previous driftwood-based reconstruction of Holocene Arctic Ocean surface current and sea ice dynamics (Hole & Macias-Fauria, 2017). A recent study of 380 driftwood samples collected on eastern and south-western Svalbard (Linderholm et al., 2021) found a dominance (87%) in driftwood originating from northern Russia, with samples dated to the nineteenth and twentieth centuries which were periods of high logging activity in Russia. The study incorporates logged wood which is subject to anthropogenic influence on trends that reflect the logging activity at the time of their harvesting (Sidorova et al., 2016). Therefore a direct comparison is not applicable to our spatiotemporal record, which targets naturally felled wood only. Other proxy-based reconstructions of sea ice, such as those derived from the IP_{25} biomarker, also suggest variability in sea ice cover during the Late Holocene associated with intermittent warm sea surface temperatures (Sarnthein et al., 2003; Müller et al., 2012; Jernas et al., 2013; Allaart et al., 2020; Pawłowska et al., 2020). Records of brine formation can be interpreted as a proxy for sea ice cover above basins, with a varied Late Holocene record from Storfjorden (Figure 4.1) suggesting episodic fluctuations between intense and reduced brine formation and concurrent sea ice cover variability (Rasmussen & Thomsen, 2014). A reconstruction of maximum sea ice extent in the Western Nordic Seas based upon tree ring chronologies and ice core oxygen isotopes (Macias-Fauria et al., 2010) again shows such variability, including the sea ice maxima during the Little Ice Age (LIA), and of record strong overall 20^{th} century decline.

.

Table 4.1. Summary of comparison of main sea ice inferences resulting from this study with existing proxy-based reconstructions and observational data.

Sea Ice Inference from driftwood	Corresponding reference	
Pre 1650 CE *Observation*: general lack of driftwood from Siberia. *Inference*: low sea ice in Siberian seas.	T2 in Kinnard et al., 2011.	**Proxy-based data**
1700-1850 CE *Observation*: marked increase in driftwood delivery from all sources. *Inference*: more sea ice generally.	Kinnard et al., 2011; Allaart et al., 2020.	
1650-1850 CE *Observation*: abundant driftwood delivery from the Barents Sea. *Inference*: more sea ice in Barents Sea.	Voronina et al., 2001. Cool T in Southern Barents: Mette et al., 2021. Figure 19 in Smedsrud et al., 2013. Cooling in Western Barents in LIA: Wilson et al., 2011.	
1750-1900 CE *Observation*: lack of driftwood from E-Siberia. *Inference*: either very strong BG OR more sea ice in Barents region dominating transport.	More Barents sea ice: Mörner et al., 2020, Zhang et al., 2018. Cool T in Southern Barents: Mette et al., 2021.	
After 1850 CE *Observation*: reduced driftwood delivery from the Barents Sea. *Inference*: less sea ice in Barents Sea, resumed in mid-20th century, but not noticeable close to Norway (western Barents Sea).	Walsh et al., 2017; Shapiro et al., 2003; Divine & Dick, 2006; Vare et al., 2010.	**Observational data**
Pre 1900 CE *Observation*: lack of driftwood from W-Siberia – the dip in the 20th century (Figure 4.6) is due to 1 sample only in ~1850 CE. *Inference*: closed Kara Sea system not delivering much to the TPD OR lack of sufficient sea ice in the Kara Sea.	Kara sea has variable circulation driven by wind more than thermohaline: Pavlov & Pfirman, 1995. Strong closed anticyclonic circulation associated with river runoff - a prominent feature of the Kara Sea dynamics in summer: Panteleev et al., 2007. No evidence of low sea ice in the Kara Sea during this period – discarded.	

~1940-1980 CE *Observation*: abundant driftwood delivery from Eurasia *Inference*: abundant multiyear sea ice circulation from Eurasia in mid-20th century: abundant thick ice with a circulation that fed to the TDP.	Sea ice extent: Walsh et al., 2017. Lack of reference observations for driftwood-based inference on sea ice circulation.	
~1900-2000 CE *Observation*: more driftwood variability from Eurasian than from North American sources. *Inference*: overall more variability of sea ice in the Siberian Seas, with more changes regarding multiyear sea ice in these regions during much of the 20th century (except the last decades of the 20th century – see below).	Figure 11 in Walsh et al., 2017.	
~1980-2012 CE *Observation*: drop in driftwood delivery from all sources *Inference*: sea ice decline overall pan-arctic in the last decades.	Figure 11 in Walsh et al., 2017.	

4.5.1 Sources of Uncertainty

The utilisation of the Weighed Score aids in reducing the bias of varied spatiotemporal coverage of the reference chronology, but sources of uncertainty do remain when interpreting the record. Late Holocene transgression may influence the preservation of older samples (Forman et al., 2004; Farnsworth et al., 2020a). Degraded samples not included in the tree ring width dataset (Figure 4.2) may have implications for observed Arctic driftwood densities, although these were predominantly observed at higher elevations than our target sampling sites at the modern day shoreline, suggesting older ages, and were often found from melting snowbanks and hence very moist. Given these more heavily degraded samples cannot be cross-referenced to our reference chronology, the ages of these ~30 samples are unknown. Therefore,

when interpreting the contrasting regional trends in the earlier years of our dataset (Figure 4.7), we assume that driftwood degradation is a risk equally applicable to all samples irrespective of their origin. Local sea ice conditions must also be considered when intrepreting the driftwood record from these Svalbard collection sites, as persistent or semi-permanent land-fast ice resulting from localised cold conditions would minimize the transport of and catchment for driftwood accumulation (Funder et al., 2011), especially when considering that our sample sites are in the northernmost part of the archipelago which may also be subject to impacts from Atlantic currents.

Another feature to consider when utilising and interpreting driftwood as a proxy for sea ice dynamics is the impact that circumpolar rivers flow regimes responsible for transporting driftwood from boreal forest zones to the Arctic basin may have played. Wohl et al. (2019) summarised these processes, whereby characteristics of flow are the first-order controls on wood transport, while spatial and temporal variation in channel and floodplain geometry, sediment inputs and mobility, wood piece size, and wood storage (e.g., dispersed pieces versus jams) all influence wood transport. Variation in outflow and its impacts on sea ice also have an impact on driftwood transport (Park et al., 2020). Therefore, the survival and time delay between a boreal forest tree falling into a cirumpolar river and entering the Arctic Ocean will be impacted by conditions affecting wood entrainment into channel margins and downstream transport such as channel size (Gregory et al., 2003), local flow regime and flow width and depth (Kramer & Wohl, 2017) and channel–floodplain connectivity (Wohl et al., 2018). Temporal factors such as spring melt, storms and flooding impacts these features and so also impacts downstream flow and ocean entry. Given the centennial spatiotemporal scope of the dataset, and lack of sufficient available data on these variety of factors for the pan-Arctic across the past 500 years, these impacts are assumed not to have had a substantial impact on the trends observed.

4.6 Conclusions

We present a 500-year history of driftwood incursion to Northern Svalbard reflecting associated sea ice and Arctic Ocean circulation and provide for the first time a direct evaluation of sea ice dynamics inferred from naturally felled driftwood against the observational record. By crossdating samples against a circumpolar reference chronology across North American and Eurasian boreal forest zone drainage basins, a wide range of statistically significant matches can occur across the region, which would be considered a sign of good- fit by more restrictive references. To minimise the risk of bias towards regions covered by more reference chronologies, our study employs a novel approach to selecting probable origin sites, by weighting matches via reference chronology span and visualising results through spatiotemporal density plots.

Our spatiotemporal record of driftwood incursion to northern Svalbard indicates centennial- to deacadal-scale shifts in driftwood source regions, aligning with Late Holocene high variability and high frequency shifts in the TPD and BG strength and associated fluctuating climate conditions, and northward seasonal ice formation shift and migration of seasonal sea ice to the peripheral Arctic seas in the past century. In particular, we find that the increased spatio-temporal grain of the provenance of driftwood material informs not only about the relative contributions of the TPD and the Beaufort Gyre (as in Funder et al., 2011), but also about the presence – or lack thereof – of sea ice in Arctic peripheral seas key to the global circulation (e.g., the Barents Sea), and of the overall sea ice conditions in the Arctic peripheral seas in general. A distinct decrease in driftwood incursion during the last 30 years matches the observed decline in pan-Arctic sea ice extent in recent decades, further highlighting the sensitivity of this unique sea ice proxy.

Overall, the inferred sea ice dynamics align well with other observations and proxy-based reconstruction across key points in the record (summarised in Table 1). With driftwood transport and deposition determined by sea ice and surface current dynamics, driftwood deposits on Arctic shorelines form a unique and currently under-utilised resource for the reconstruction of sea ice transport within large-scale Arctic Ocean circulations throughout the Holocene. Past driftwood dendrochronological studies have primarily been limited to geographically constrained settings or limited in the precision of provenance determination. This study is a step forward towards testing the validity of driftwood as a sea ice proxy, with driftwood-inferred sea ice conditions directly compared with the observational record for the first time. The study strengthens the use of dendro-provenancing as a method for increasing the spatiotemporal resolution of Arctic driftwood provenancing. Reconstructions of past sea ice conditions employing this proxy have scope for further development in the continued refinement of provenance and age determinations. With abundant driftwood deposits across the Arctic, this may enable a finer scale study of the role of atmospheric and oceanic circulation in sea ice and climatic changes throughout the Holocene.

4.7 Author Contributions

GMH and MMF conceived this work. GMH authored the paper with contributions from all co-authors. All authors contributed with literature compilation, data interpretation and the discussion of results. This study is based on data collected in collaboration with the University Centre in Svalbard (UNIS), with the field campaign to Sjuøyane, training and logistics provided and funded by UNIS. The 2016 fieldwork was completed with sample collection by GMH and MMF across Sjuøyane in collaboration with the field course cohort. The samples from Ringhorndalen, Wijdefjorden were collected in 2016 by MMF and WRF, and from Vassfarbukta in 2018 by WRF and S. Brynjolfsson.

4.8 Acknowledgments

GMH is funded by the Natural Environment Research Council (NERC grant: 1514291) and part of the Environmental Research Doctoral Training Program at the University of Oxford. Support and funding were also provided by MMF and grant funds from NERC (NERC IRF grant: NE/L011859/1). TR is supported through an Engineering and Physical Sciences Research Council (EPSRC) (https://epsrc.ukri.org/) Systems Biology studentship award (EP/G03706X/1). Thanks to S. Brynjolfsson for assistance in sample collection during 2016 and 2018 at Wijdefjorden locations and to L. Allaart for leading funding of the 2018 field campaign to Vassfarbukta. The Wijdefjorden field campaigns in 2016 and 2018 were funded by grant numbers 16/35 (to WRF) and 17/01132-3 (to LA) from the Svalbard Environmental Protection Fund respectively, Arctic Field grant no. 282643 awarded to LA by Svalbard Science Forum/Research Council of Norway, and the Arctic Research and Studies Program of the Ministries for Foreign Affairs of Norway and Iceland (grant agreement No. 2017-ARS-79772 to AS). The authors also thank the anonymous reviewers for the helpful comments and suggestions received.

4.9 Data Availability Statement

All data used in this study are available at https://osf.io/z4t3a/.

Chapter 5 Linking Statement

Chapter 5 builds on the exploration and development of driftwood as a tool for proxy-based Arctic sea ice reconstructions by addressing the third of the three main aims of the Specific Aims and Hypotheses: the development and evaluation of novel techniques to refine the provenance of driftwood. Provenance by genus is limited by spatially coarse resolution, while provenance by dendrochronology is reliant on existing boreal forest reference chronologies. The use of geochemical techniques addresses the limitations of these current methods, and with development may enable a finer scale study of the role of atmospheric and oceanic circulation in sea ice and climatic changes throughout the Holocene. This chapter presents the development of the technique to refine the provenance of driftwood through radiogenic isotopic analysis ($^{87}Sr/^{86}Sr$). Methods for the extraction, isolation and purification of strontium from driftwood through microwave digestion, extraction chromatography and MC-ICP-MS analysis were successfully developed. The utilisation of $^{87}Sr/^{86}Sr$ ratios to establish provenance for Arctic driftwood was determined to hold potential, with confounding factors in the potential overprinting of the source signature by biological and physicochemical processes from interaction with river and ocean water, and in the scale and heterogeneity and temporal variations of pan-Arctic source regions. Increased sample populations and source samples for calibration to enable validation are recommended for this work to be built upon in combination with previously developed provenance tools and reconstructions. The chapter provides a first step the use of geochemical techniques for provenance in Arctic driftwood.

5 Dropped in the Ocean – $^{87}Sr/^{86}Sr$ as a provenance tool for ice-rafted Arctic driftwood[3]

Georgia M. Hole[1], Danielle Sinclair[2] & Marc Macias-Fauria[1]
[1]Biogeosciences Research Group, School of Geography and the Environment, University of Oxford, Oxford, OX1 3QY, UK.
[2]Department of Zoology, 11a Mansfield Rd, Oxford OX1 3SZ, UK.

Corresponding author: Georgia M. Hole (georgia.hole@ouce.ox.ac.uk)

Keywords: palaeoenvironments, proxy-based reconstruction, $^{87}Sr/^{86}Sr$, geochemical provenance, Arctic driftwood, sea ice.

Key Points

- Driftwood is a novel tool for insights into Holocene Arctic sea ice dynamics.
- Fine spatial and temporal resolution of driftwood provenance is needed.
- Geochemical $^{87}Sr/^{86}Sr$ fingerprinting of Arctic driftwood is explored in this study.
- $^{87}Sr/^{86}Sr$ shows some promise, with limitations in reference data and sample signals.
- We conclude that a combined approach to driftwood provenance shows the most promise.

5.1 Abstract

Provenance and age determinations of driftwood provide insights into Holocene Arctic Ocean surface currents and sea ice dynamics, with detailed reconstructions requiring a provenance methodology with fine temporal and spatial resolution. Provenance by genus is limited by spatially coarse resolution, while provenance by dendrochronological crossdating is reliant on available boreal forest reference chronologies which are most abundant for recent centuries. We present the development of novel techniques to refine the provenance of driftwood through

[3] In review as: Hole, G.M., Sinclair, D., Macias-Fauria, M. (2021). Dropped in the Ocean – $^{87}Sr/^{86}Sr$ as a provenance tool for ice-rafted Arctic driftwood. *Palaeogeography, Palaeoclimatology, Palaeoecology.*

radiogenic isotopic analysis ($^{87}Sr/^{86}Sr$). The use of geochemical techniques addresses limitations of current methods and opens the possibility of defining the role of atmospheric and oceanic circulation in sea ice and climatic changes throughout the Holocene at a finer spatial resolution than currently possible. This study investigates and develops geochemical $^{87}Sr/^{86}Sr$ fingerprinting of Arctic driftwood. To this end, it analyses driftwood samples from northern Svalbard and compares this technique with provenance regions obtained through dendrochronology, and with modelled and measured global $^{87}Sr/^{86}Sr$ reference databases. We conclude that the utilisation of $^{87}Sr/^{86}Sr$ ratios to establish provenance for Arctic driftwood has some potential, but identify important limitations in the method, concerning both the signal in samples and reference values required for provenance. Increased sample populations and source samples for calibration, as well as methodological improvements that address the likely overprinting linked to driftwood transport, are recommended to build upon this work. We conclude that at present dendro-provenancing continues to be the most powerful method to study sea ice dynamics from Arctic driftwood and suggest that given the high spatial granularity of $^{87}Sr/^{86}Sr$ across the boreal forest, this technique might only be usable in combination with previously developed provenance tools and reconstructions. This study provides a first step in the use of radiogenic isotopic analysis in a multi-proxy reconstruction of Holocene driftwood incursion onto high Arctic shorelines.

5.2 Introduction

The state of the Arctic is an influential factor in the wider climatic picture. This is due to the enhanced and accelerated greenhouse-induced warming occurring in the region due to feedbacks and interactions of sea ice and snow cover – termed the Arctic Amplification (Serreze & Francis, 2006). Recent anthropogenic trends are well documented by a rapid decline in the extent and thickness of sea ice (Polyak et al., 2010; Maslowski et al., 2012). The

continuing decline in sea-ice cover is expected to have a diverse range of consequences, impacting on terrestrial and marine productivity, global atmospheric and ocean circulation patterns and terrestrial fauna and flora population fragmentation and habitat reduction, amongst others (Overland & Wang, 2010; Screen & Simmonds, 2010, 2014; Francis & Vavrus, 2012; Post & Høye, 2013; Overland et al., 2016; Vavrus et al., 2017; Bintanja & Andry, 2017; Macias-Fauria & Post, 2018; Bjorkman et al., 2020). Data on past conditions are needed to understand the region's climatic and biotic responses to various climatic processes and forcings and their resulting impacts on a global scale.

Arctic sea ice extent, distribution, dynamics and thickness are driven by both thermal and physical dynamics of the Arctic Ocean system, including spatiotemporally variable atmospheric and oceanic heat fluxes, prevailing winds, and ocean currents (Haas & Thomas, 2017). Uncertainties remain on the spatiotemporal dynamics of Arctic sea ice throughout the Holocene, with limited, discontinuous data on sea-ice extent prior to the generation of spatially explicit sea-ice extent information by satellite observations in the late 1970s (Post & Høye, 2013). The observational record has been extended back in time to the late 19th century by compiling various observational data sources including ship reports, airplane surveys, compilations by naval oceanographers and analyses by national ice services (Walsh et al., 2017). Further knowledge of past sea ice dynamics is therefore needed to understand the context of recent change and gain insight into possible future sea ice trajectories under conditions of increasing global average temperatures.

5.2.1 Driftwood as a proxy for Arctic sea ice extent and dynamics

Deposits of driftwood lining Arctic shorelines reveal the large-scale Arctic Ocean circulations and the incursion of driftwood-carrying sea ice onto circum-Arctic beaches. This

rafting of Arctic driftwood by sea-ice enables the reconstruction of surface-current dynamics and sea-ice conditions in the Arctic (Häggblom, 1982; Dyke et al., 1997; Funder et al., 2011; Hole & Macias-Fauria, 2017; Hole et al., 2021). The delivery of driftwood to the shores of Svalbard requires multi-year sea ice for long-distance transport due to driftwood's limited buoyancy once waterlogged (Häggblom, 1982), and seasonally open waters to enable wave action to deliver the driftage to the shoreline. The incurred driftwood derives from the major rivers that drain the boreal forest regions of North America and Eurasia, which together with precipitation, constitutes the greatest proportion of annual freshwater influx into the Arctic Basin (Serreze et al., 2006). The geographical distribution of tree taxa across the boreal forest (see MacDonald et al., 2008; Hellmann et al., 2013) has traditionally been used to establish a genus-based division of driftwood sources to indicate wood provfenance, although this provides only a spatially coarse resolution in provenancing of driftwood: this rule of thumb distinguishes Eurasian from North-American provenances based on relative differential abundances of key genera (larch – *Larix* – and spruce – *Picea*) between both landmasses, despite these genera existing throughout the pan-boreal forest.

Dendrochronology based on tree ring width (TRW) analysis allows for more spatially – and temporally – precise provenance determination, and is already a valued tool in dendroarchaeological research (R. E. Taylor & Aitken, 1997) and Arctic climatic and environmental reconstructions (e.g. Hellmann et al., 2013; Hole et al., 2021; Koch, 2009; Owczarek, 2010). By employing modern wood samples and dendrochronological provenance with reference chronologies, Arctic driftwood can serve a proxy for sea ice dynamics through the use of high spatial and temporal resolutions. However, dendro-provenancing is reliant on the spatial and temporal coverage of reference chronologies, while a matching reference chronology provides a spatial approximation of the target material for matching due to the riparian nature of trees that become driftwood, which are not the target for reference

chronology measures. Thus, while the potential for temporal accuracy is large, the spatial resolution is always going to be offset from the reference chronology to a proximal riverbank. This spatial offset would be minimised given enough spatio-temporal coverage of reference dendro-chronologies. However, for most of the Holocene and regions/basins along the pan-boreal forest, availability of reference dendro-chronologies is largely limited. Moreover, uncertainties exist in the determination of provenance, such as confidence in the matching metrics, and the preservation level of the driftwood determining the ability to analyse the tree ring width and anatomy (e.g. Hole et al., 2021). Therefore, to achieve a more definitive determination of driftwood provenance, exploration of other provenancing tools is warranted.

5.2.2 Strontium as a provenance tool for Arctic driftwood

Whereas radiocarbon dating of driftwood provides a good temporal resolution and is thus a valid alternative to dendrochronological cross-dating of Holocene material (e.g. Funder et al., 2011), at present the alternative to dendro-provenancing is the genus rule of thumb explained above, which can only approximate provenance to the two major landmasses surrounding the Arctic Ocean. The isotopic analysis of driftwood tissue is a possible avenue for the development of new provenance tools. The strontium radiogenic isotope system has been widely employed for provenance studies in the form of $^{87}Sr/^{86}Sr$ ratios for over 30 years, in environmental, archaeological and in regulatory uses such as food product provenance authentication (e.g. Aberg, 1995; Durante et al., 2013; Gosz & Moore, 1989; Graustein & Armstrong, 1983; Voerkelius et al., 2010). The element strontium is present within all rocks (English et al., 2001), with relative abundance of the radiogenic isotope (expressed as $^{87}Sr/^{86}Sr$) specific to certain rock types (Guinn, 1978). Therefore, lithologies can be characterized by a defined $^{87}Sr/^{86}Sr$ ratio (English et al., 2001; Reynolds et al., 2005). Strontium is not as prone to geological or biological fractionation as lighter elements, meaning that soils and the plants

growing on them will uptake bedrock values without fractionation (Capo et al., 1998; English et al., 2001; Dijkstra et al., 2003; Bentley, 2006). Yet, the Sr signature of surface waters above bedrock does not directly reflect bedrock's $^{87}Sr/^{86}Sr$ signature, due to uneven weathering of certain lithologies and minerals, upstream inputs, and additions from other exogenous sources of strontium (Blum et al., 1998; Blum & Erel, 2003; Bataille et al., 2014).

The bioavailable Sr signatures of soils are often dominated by weathering processes, with alluvial soils containing a mixture of sediment and their Sr signatures from upstream inputs. A study on groundwater strontium in southeast Australia has highlighted the likely importance of rainfall $^{87}Sr/^{86}Sr$ ratios (Raiber et al., 2009), while studies demonstrated that in regions proximal to the coast, plant ratios were closely coupled to the signatures found in sea-induced rainfall and sea-spray (Kennedy et al., 1998; Vitousek et al., 1999; Whipkey et al., 2000; J. A. Evans et al., 2009). In Scotland, precipitation $^{87}Sr/^{86}Sr$ values were found to be consistent across sites ~300km apart and closely matched ocean water $^{87}Sr/^{86}Sr$ values (Bain & Bacon, 1994). The Sr signature of trees is dependent on rooting depth and the residence time of the soil water (Reynolds et al., 2005), with rainfall also a significant influencer on $^{87}Sr/^{86}Sr$ ratios (Raiber et al., 2009). The Sr signature of soil water originates not only from soil-forming weathering processes but also atmospheric dust (Graustein & Armstrong, 1983), as well as rainfall and groundwater (Poszwa et al., 2004); that can all lead to varied Sr signatures. Moreover, variation has been found between European coastal (<100 km) and non-coastal (>100 km) surface soil $^{87}Sr/^{86}Sr$ values, with the variance correlated with sodium concentrations, suggesting a significant contribution from sea spray in regions proximal to coastlines (Hoogewerff et al., 2019). Similarly, in regions proximal to the coast, plant strontium ratios were also closely coupled to the signatures found in sea-induced rainfall and sea-spray (Kennedy et al., 1998; Vitousek et al., 1999; Whipkey et al., 2000; J. A. Evans et al., 2009).

Even in regions hundreds of kilometres from coastlines, precipitation compositions can reflect sea-salt aerosols (Bain & Bacon, 1994).

For riparian trees flanking Arctic Ocean-draining rivers that become driftwood and are expected to constitute the majority of naturally-felled driftwood material, the Sr signature of the tree while living is likely to be dominated by the river water Sr signature. The main contributions of Sr in river systems are weathering of the local bedrock and rainfall and runoff water: therefore, the Sr isotopic composition of rivers varies geographically (depending on the bedrock inputs and precipitation of the river watershed). The species of tree also influences the bioavailability of Sr and therefore the ratio that results: different species growing in the same region can have differing $^{87}Sr/^{86}Sr$ ratios, such as spruce and pine, where spruce trees recycle Sr from leaf litter up to 12 times as much as pine (Poszwa et al., 2004). However it has been reasoned that the differences in Sr cycling likely derive from the specific differences in the root-surrounding soils for each tree, not from biological species differences (Dijkstra et al., 2003). The motility of isotopes within the wood after uptake also affects the resulting signals, as radial transport between the pith and bark may lead to isotopic re-equilibration between older and younger rings (Stille et al., 2012). In a study of beech trees limed in the 20th century, the alteration in tree-ring $^{87}Sr/^{86}Sr$ ratios was evident in rings that preceded the date of the liming of the trees by half a century, due to the radial redistribution of isotopes after the event (Drouet et al., 2005). In a study of Cypriot cedars (Rich et al., 2012), local bedrock, early heartwood of the innermost pith ring and the late heartwood $^{87}Sr/^{86}Sr$ signature were compared to enable a physiological comparison between samples. The bedrock $^{87}Sr/^{86}Sr$ ratios were substantially lower than the sampled wood, but very consistent between the two sites. A more uniform Sr signature in the cedar's early heartwood was found, but with an overall lack of

differentiation between the early and late heartwood of the measured samples, suggesting that either part could be utilised for Sr isotope provenance studies.

Consideration must also be given to possible contamination once the tree has fallen, entered the river, and eventually reached the ocean, potentially overprinting the source signature by biological and physicochemical processes from interaction with river water, ocean water, and sea salt aerosols (Hajj et al., 2017). Investigations into the isotopic impact of waterlogging found that waterlogging significantly contributes to the overall Sr content in wood and hence there is a large proportion of exogenous Sr in waterlogged-wood (Steelandt et al., 2016; Hajj et al., 2017).

5.2.3 Mapping strontium baselines

With these complexities in mind, the local geological and sediment isotopic signature of target materials such as driftwood can be linked to the source region providing that a framework of potential source strontium signatures can be established (Brennan et al., 2014). Either the framework is established through extensive sampling of potential sources such as bedrock and water sources (e.g. Frei & Frei, 2011; Maurer et al., 2012; Rich et al., 2012), or the baseline can be described through developing a model (e.g. Bataille et al., 2012, 2020; Beard & Johnson, 2000; Brennan et al., 2014). For baseline establishment, the method of geochemical map-building requires reference databases of $^{87}Sr/^{86}Sr$ that can be assembled through several methods. Measured bedrock $^{87}Sr/^{86}Sr$ extracted from potential source localities can be used, or, if a region has been covered by geological mapping, then an extrapolated map of assumed $^{87}Sr/^{86}Sr$ values can be derived from the lithologies and ages (Laffoon et al., 2012). Bio-available strontium is not necessarily primarily driven by the local lithology, while achieving sufficient coverage for sampling is costly and inevitably incapable of covering the

entire target region (Brennan et al., 2014), particularly for a global (or pan-Arctic) scope. For high-latitude rivers, there is also temporal variation on Sr signatures on an intra-annual scale (Douglas et al., 2013; Keller et al., 2010), due to permafrost causing a seasonal variation in the contributing sources of strontium to groundwater. An example is the Chena River basin in Alaska (Douglas et al., 2013), which samples an area underlain by discontinuous permafrost. In winter, with soil profiles frozen and a shallow active layer, the river $^{87}Sr/^{86}Sr$ values reflect the low $^{87}Sr/^{86}Sr$ signature of subsurface carbonate rocks. In spring the thawed active layer is sampled by the groundwater, increasing the $^{87}Sr/^{86}Sr$ signature due to the carbonate-depleted soils. Such seasonal variations in groundwater interaction paths are also seen in Siberian rivers, with strong $^{87}Sr/^{86}Sr$ fluctuations from seasonal change in vegetation, ice cover etc, resulting in variable contribution of rock units within a catchment (Douglas et al., 2013; Voss et al., 2014). A significant hurdle when determining a viable circum-Arctic map of $^{87}Sr/^{86}Sr$ for provenance (or indeed for any location), as revealed in these studies, is that the local variations in $^{87}Sr/^{86}Sr$ can exceed the variation in major regional lithological trends. Hoogewerff et al. (2019) note that locally there is often a significant statistical correlation between bedrock and soil and/or plant $^{87}Sr/^{86}Sr$, but that the slope of such correlation is often <1 in a plot of $^{87}Sr/^{86}Sr$ bedrock on the X-axis versus $^{87}Sr/^{86}Sr$ soil or plant (Baroni et al., 2011; Goitom Asfaha et al., 2011). This indicates an influence of contamination on the lithological signal, such as surface deposits, sea spray, airborne dust, and land use.

In summary, as highlighted in a recent comprehensive review of mapping $^{87}Sr/^{86}Sr$ (Holt et al., 2021), it is not straightforward to interpret the results of strontium analyses against an isoscape to determine provenance. The range of values within distinct locations can be exceeded by intra-sample and inter-sample range, with overlap found in such wide-ranging spatial scope preventing distinct regions being definable by $^{87}Sr/^{86}Sr$ signatures. Strontium therefore is seen as most effective if it can be combined with other proxies (Madgwick et al.,

2019). To address some of these limitations, increasing the collection of sampled bioavailable datasets, improving data management and metadata collection for bioavailable $^{87}Sr/^{86}Sr$ data, and advancing in remote sensing and geological mapping techniques to improve mapped geological datasets are recommended (Bataille et al., 2020).

The aim of this study is to investigate and develop geochemical $^{87}Sr/^{86}Sr$ fingerprinting of Arctic driftwood for the creation of a proxy-based reconstruction of regional sea-ice conditions and Arctic Ocean circulation dynamics. In combination with provenance tools and reconstruction developed in a previous study (Hole et al., 2021), this provides a first step in a multi-proxy reconstruction of Holocene driftwood incursion onto northern Svalbard shorelines. In a previous study, tree-ring-width (TRW) series and genus information were determined for the samples where possible, before cross-dating with reference chronologies from the circum-Arctic boreal forest zone to determine the region/watershed the driftwood originated from. In this study, the resulting provenance locations for each of the samples in Hole et al. (2021) are compared to the $^{87}Sr/^{86}Sr$ signature measured, to investigate possible alignment between driftwood $^{87}Sr/^{86}Sr$ signatures and available bioavailable/river values for the determined provenance regions.

5.3 Methods

5.3.1 Sample Collection

The Svalbard archipelago is located at the proposed north-western part of the Late Weichselian Svalbard-Barents Sea Ice Sheet (SBSIS), with abundant preserved raised beach sequences – many of those with stranded driftwood – reflecting the pattern and rate of relative sea level changes on Svalbard in response to the deglaciation of the SBSIS (Forman et al. 2004;

Ingólfsson & Landvik, 2013). A total of 95 samples were collected from three localities in northern Svalbard: Sjuøyane, an archipelago north of Nordaustlandet and the northernmost land in Svalbard, and two localities within Wijdefjorden, northern Spitsbergen: Vassfarbukta and Ringhorndalen. At all sites, naturally-felled driftwood at the modern shoreline was targeted by the sampling of logs exhibiting intact root stock. These driftwood logs were sub-sampled at peak thickness with a saw, where sub-sampled slices exhibited the maximum number of intact tree-rings.

Figure 5.1. Driftwood sampling locations of Sjuøyane, Ringhorndalen, and Vassfarbukta. Map figure modified from Norwegian Polar Institute (2014).

5.3.2 Geochemical analysis

A randomly determined initial subset of 20 of the Svalbard samples was prepared for isotopic analysis. An initial trial run of methods was initially undertaken on test samples of driftwood with further detail available in Supplementary Materials (Appendix C1). Sample preparation was carried out in the laboratory of the Oxford Long Term Ecology Lab, Department of Plant Science, University of Oxford, before microwave digestion and chemistry were carried out in the Department of Earth Sciences, Oxford.

Figure 5.2. Example of range of condition and morphology of sampled driftwood from northern Svalbard modern beaches included in this study, with ruler for scale.

5.3.3 Preparation of samples

Samples of bulk wood tissue weighing ~50mg were taken using a planning chisel, Dremel 3000 and 3mm drill bit, as this mass would provide sufficient Sr for analysis estimated from typical wood concentrations. The top few millimetres were removed by chisel shaving to reduce post-sampling contamination. Chiselled wood shavings and drill-powdered wood were trialled, with both found to dissolve completely during later digestion stages. Two samples per driftwood slice were taken; outer samples were within 1cm of the outer edge of the wood and inner samples were taken at a central point furthest from any cracks or other possible contact with seawater (see sample MAR11, Figure 5.2).

5.3.3.1 Pre-treatments

In addition to bulk wood extraction, both alpha-cellulose extraction and lignin extraction were trialled in order to test the possibility of these pre-treatment methods for the removal of contamination with exogenous strontium, but neither method retained enough strontium to continue to analysis.

5.3.3.2 Digestion and chemistry

The drilled wood powder and shavings were collected and weighed in foil and transferred into clean microwave vessels for the addition of 4.5ml of distilled concentrated nitric acid (HNO_3), followed by 3ml of hydrogen peroxide (H_2O_2) to digest overnight at room temperature. Samples were then digested using a microwave reaction system (CEM Mars 5, manufactured by CEM Corp., USA) in CEM Omni XP1500 vessels for the dissolution into liquid of strontium that is bound within the wood sample matrix via raised temperature and pressure by microwave irradiation. The resulting digests were dried in a Class 100 laminar flow

exhaust hood in Teflon beakers at 85°C overnight. Any samples with yellow or brown colour were treated 50µl of 30% H_2O_2 at 150°C; this was repeated until no more fizzing was observed. 50µl of HNO_3 was added and then the digests again dried. If the sample still appeared to not be fully digested, these steps were repeated.

All wet chemistry was undertaken under a Class 100 laminar flow exhaust hood. The acids and reagents used were prepared through sub-boiling distillation. Water used was high purity deionised MilliQ-element water with a resistivity of 18.2 MΩ cm^{-1}. Further details of labware, reagents and procedures are outlined in Supplementary Materials (Appendix C1).

Test samples of driftwood underwent manual extraction chromatography with Teflon elution columns and Triskem Sr resin. The Svalbard samples included in this study then underwent automated chromatographic purification of Sr using the prepFAST-MC™ system (Elemental Scientific (ESI), Omaha, NE, USA), on an ESI Sr/Ca-1000 column (ESI part no. CF-MC-SrCa-1000). The methodology used follows that by Romaniello et al. (2015), with a longer wash of 4ml between each sample. The eluted Sr was then dried down on hotplate ready to be redissolved for analysis by MC-ICP-MS.

For each batch of samples, a blank and standard were prepared using the same digestion procedures to validate the reproducibility and accuracy of the lab methods. The standard used was the NIST 1515 apple leaf reference material.

5.3.3.3 Mass spectrometry

Strontium concentration for test samples was measured via Thermo Element 2 ICP-MS (Table C1 in Appendix C1). Radiogenic Sr can be measured either by thermal ionisation mass spectrometry (TIMS) or multiple-collector inductively coupled plasma mass spectrometry

(MC-ICPMS). Radiogenic Sr measurements can be made using a constant normalisation $^{88}Sr/^{86}Sr$ ratio to correct for instrumental mass-dependent fractionation. The NIST SRM 987 was used as the instrumental standard during MC-ICP-MS analysis with samples and standards were run using standard - sample bracketing and measured in 3 blocks of 50 measurements. Final values are the mean of the 3 blocks (Figure 5.2). The internationally agreed value for $^{88}Sr/^{86}Sr$ ratio (0.1194) was used as a normalization ratio to correct for instrumental mass-dependent fractionation and after analysis sample $^{87}Sr/^{86}Sr$ values were normalised to a value of 0.710248 for the bracketing SRM987 standards, following Lewis et al. (2017).

The reproducibility of the Sr isotopic analysis was evaluated via the international standard for $^{87}Sr/^{86}Sr$, SRM 987, with $^{87}Sr/^{86}Sr$ ratios measured as 0.710249±0.000025 (2SD, n=36). The procedural blank values were below detectable levels. The dataset and further details of the methodology used is available in Supplementary Materials (Appendix C1).

Table 5.1. Driftwood samples included in this study, with collection locality information and provenance determined by TRW crossdating.

Sample	Collection locality	segment length (yrs)	Crossdating provenance (Hole et al., 2021)				
			matching genus	date begin	date end	latitude	longitude
MAR01inner	Sjuøyane	88	*Pinus sylvestris*	1686	1773	68.8	15.73
MAR01outer	Sjuøyane	88	*Pinus sylvestris*	1686	1773	68.8	15.73
MAR02inner	Sjuøyane	59	*Picea glauca*	1925	1983	65.07	-162.23
MAR02outer	Sjuøyane	59	*Picea glauca*	1925	1983	65.07	-162.23
MAR05inner	Sjuøyane	64	*Picea glauca*	1701	1764	64.73	-149.18
MAR05outer	Sjuøyane	64	*Picea glauca*	1701	1764	64.73	-149.18
MAR09inner	Sjuøyane	166	*Picea abies/Larix russica*	1797	1962	66.08	77.68
MAR09outer	Sjuøyane	166	*Picea abies/Larix russica*	1797	1962	66.08	77.68
MAR11inner	Sjuøyane	112	*Picea glauca*	1695	1806	66.72	-136.28
MAR11outer	Sjuøyane	112	*Picea glauca*	1695	1806	66.72	-136.28
MAR12inner	Sjuøyane	32	*Larix gmelinii*	1623	1654	71.22	127.43
MAR12outer	Sjuøyane	32	*Larix gmelinii*	1623	1654	71.22	127.43
PAR03inner	Sjuøyane	60	*Picea glauca*	1937	1996	63.1	-150
PAR04inner	Sjuøyane	85	*Picea glauca*	1497	1581	67	-152
PAR04outer	Sjuøyane	85	*Picea glauca*	1497	1581	67	-152
PHI02inner	Sjuøyane	110	*Larix gmelinii*	1755	1864	69.78	119.12
PHI02outer	Sjuøyane	110	*Larix gmelinii*	1755	1864	69.78	119.12
RIN01inner	Ringhorndalen	138	*Picea glauca*	1816	1953	65.07	-162.23
RIN01outer	Ringhorndalen	138	*Picea glauca*	1816	1953	65.07	-162.23
RIN05inner	Ringhorndalen	153	*Larix dahurica*	1618	1770	69.78	119.12
RIN05outer	Ringhorndalen	153	*Larix dahurica*	1618	1770	69.78	119.12
RIN06inner	Ringhorndalen	71	*Pinus sylvestris*	1749	1819	61.42	8.98
RIN06outer	Ringhorndalen	71	*Pinus sylvestris*	1749	1819	61.42	8.98
RIN20inner	Ringhorndalen	166	*Picea abies/Larix russica*	1826	1991	64.25	53.57
RIN20outer	Ringhorndalen	166	*Picea abies/Larix russica*	1826	1991	64.25	53.57
RIN24inner	Ringhorndalen	58	*Picea glauca*	1774	1831	65.08	-162.15
RIN24outer	Ringhorndalen	58	*Picea glauca*	1774	1831	65.08	-162.15
RIN25inner	Ringhorndalen	65	*Picea glauca*	1921	1985	63.1	-150
RIN25outer	Ringhorndalen	65	*Picea glauca*	1921	1985	63.1	-150
RIN28inner	Ringhorndalen	78	*Picea glauca*	1624	1701	65.08	-162.18
RIN28outer	Ringhorndalen	78	*Picea glauca*	1624	1701	65.08	-162.18
RIN38inner	Ringhorndalen	73	*Picea obovata*	1858	1930	66.88	51.95
RIN38outer	Ringhorndalen	73	*Picea obovata*	1858	1930	66.88	51.95
RIN42inner	Ringhorndalen	230	*Larix gmelinii*	1747	1976	61.15	136.57
RIN42outer	Ringhorndalen	230	*Larix gmelinii*	1747	1976	61.15	136.57
VFB28inner	Vassfarbukta	60	*Larix sibirica*	1919	1978	65.38	72.87
VFB28outer	Vassfarbukta	60	*Larix sibirica*	1919	1978	65.38	72.87

5.3.4 Data Analysis

5.3.4.1 Comparison with TRW provenance and $^{87}Sr/^{86}Sr$ isoscapes

Provenance regions for driftwood samples provided by TRW cross-dating (Hole et al., 2021) (Figure 5.3; Dataset Cds01 in Supplementary Materials – Appendix C2) can be used to examine the $^{87}Sr/^{86}Sr$ results in comparison with existing continental and global isoscapes in order to assess the validity of the obtained $^{87}Sr/^{86}Sr$ ratios from this study's samples. A recent compilation of ~17,000 published and newly generated global bioavailable $^{87}Sr/^{86}Sr$ (Bataille et al., 2020) forming a high-resolution $^{87}Sr/^{86}Sr$ isoscape at the global scale enables

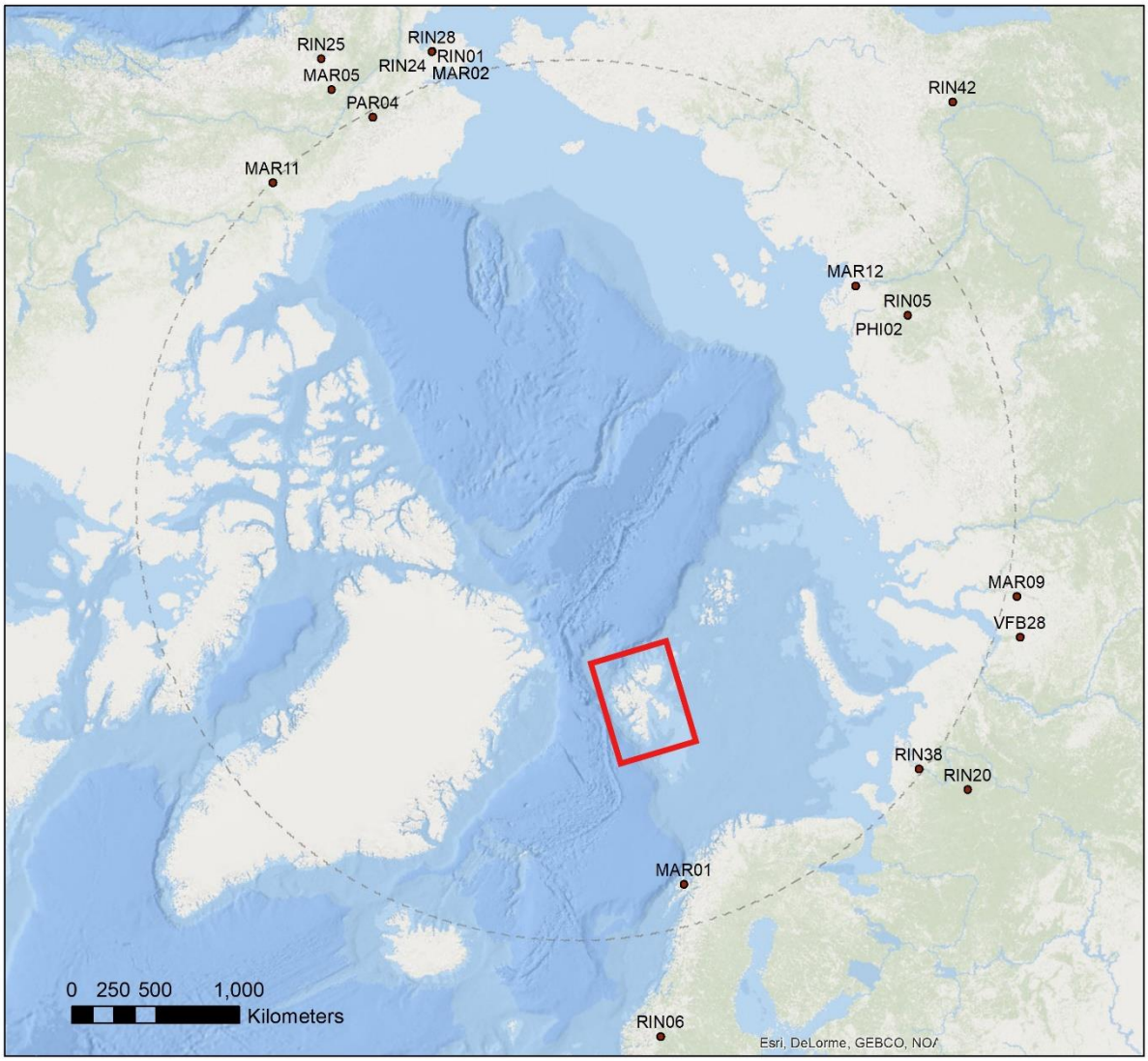

Figure 5.3. Locations of sample originating regions as determined from dendrochronological TRW crossdating (Hole et al., 2021). Location of driftwood sampling location of Svalbard is highlighted in red.

comparison to the samples in this study. Additionally, multiple country and continent-scale isoscapes have also been developed in recent years, providing high resolution isoscapes for certain regions (e.g. Funck et al., 2021).

The localities in Figure 5.3 determined by TRW cross-dating for each sample indicates not a point provenance location, but the locality of the cross-date match, and therefore a possible watershed/climatic region that the sample likely originated from. A buffer zone around the reference chronology match points provided by TRW crossdating can then be used to denote a viable source area for the sample. This buffer zone can then be used to investigate strontium values coverage for these regions, as covered by the global bioavailable Sr isoscape by Bataille et al. (2020). The isoscape model was queried by obtaining the average $^{87}Sr/^{86}Sr$ value for the buffer zone surrounding each sample, employing buffer zones with radii of 5km, 20km, 100km, 200km, and 500km (Dataset Cds02 in Supplementary Materials C2). The correlation between average $^{87}Sr/^{86}Sr$ values per sample with these isoscape buffer averages was then calculated (Table 5.3).

5.3.4.2 Inter- and intra-sample $^{87}Sr/^{86}Sr$

The internal strucuture of the readings of $^{87}Sr/^{86}Sr$ within and between the driftwood samples was investigated through Unweighted pair-group average (UPGMA) cluster analysis, which creates groups of similar valued data by minimising the joined averaged Euclidean distances between all members in any two groups. A separate cluster analysis was done for inner, outer, and averaged $^{87}Sr/^{86}Sr$ readings. Consistency between clusters (intra-sample consistency) and between the cluster and their TRW-inferred provenances were analysed. Cluster analysis was performed using Past 4.04 (Hammer et al., 2001).

5.4 Results

Of the 20 driftwood samples from northern Svalbard, 45% (9) are from the Seven Islands, while 55% are from Wijdefjorden (n=10 and n=1 from Ringhorndalen and Vassfarbukta respectively). One sample of the analysed subset, RIN18, lacks TRW data but was included in the dataset for the stage of investigation of intra-sample variation in $^{87}Sr/^{86}Sr$. Only an inner subsample for sample PAR03 was analysed. Isotopic $^{87}Sr/^{86}Sr$ ratios for driftwood subsamples (including subsamples of inner and outer wood regions of each sample) are presented in Table 5.2. Sr concentrations as determined on test samples ranged from 1-12 ppm (further details in Supplementary Materials Table – Appendix C1), aligning with the order of magnitude and range found in other studies (e.g. Bataille et al., 2014; Miller et al., 1993; Poszwa et al., 2004) and sufficient for $^{87}Sr/^{86}Sr$ extraction and analysis.

$^{87}Sr/^{86}Sr$ values reflected those expected for wood material, ranging from 0.707251 to 0.711212, with a mean value of $^{87}Sr/^{86}Sr = 0.709396 \pm 0.000065$ (2σ, $n = 39$) and an interquartile range of 0.0006965. Results show a variation in $^{87}Sr/^{86}Sr$ within the samples. In some samples, this variation in $^{87}Sr/^{86}Sr$ within a single sample exceeds the variation between samples and the variance from seawater $^{87}Sr/^{86}Sr$. Waterlogging has been found to significantly contribute to the $^{87}Sr/^{86}Sr$ signature within wood (Hajj et al., 2017), with outer parts of wood found to have $^{87}Sr/^{86}Sr$ signatures closer to seawater and internal parts more divergent from seawater values. In our samples, there was not as clear a trend towards seawater nearer outer sections (8 samples showed greater difference from seawater in outer areas, while 11 showed greater difference from seawater in inner areas of the sample; Table 5.2). This may be a result of the varied geometry of each sample, with the most 'inner' region hard to determine, as well as cracks and other features that may cause irregular intra-sample variation in seawater infiltration or other forms of contamination.

Table 5.2. $^{87}Sr/^{86}Sr$ for samples included in this study, with range in value between inner and outer wood sections subsampled and the difference for measured values to seawater $^{87}Sr/^{86}Sr$.

Sample	$^{87}Sr/^{86}Sr$	±2σ	intra-tree $^{87}Sr/^{86}Sr$ range	variation from seawater
MAR01inner	0.709029	0.000005	0.000246	-0.000141
MAR01outer	0.709275	0.000065		0.000105
MAR02inner	0.709755	0.00002	0.000112	0.000585
MAR02outer	0.709643	0.000023		0.000473
MAR05inner	0.708955	0.000028	0.001704	-0.000215
MAR05outer	0.707251	0.000012		-0.001919
MAR09inner	0.709234	0.000019	0.000070	0.000064
MAR09outer	0.709164	0.00002		-0.000006
MAR11inner	0.709387	0.000028	0.000048	0.000217
MAR11outer	0.709435	0.000005		0.000265
MAR12inner	0.708982	0.000005	0.001534	-0.000188
MAR12outer	0.710516	0.000024		0.001346
PAR03inner	0.710400	0.000031		0.00123
PAR04inner	0.707971	0.000009	0.000579	-0.001199
PAR04outer	0.708550	0.000011		-0.00062
PHI02inner	0.709524	0.000032	0.000227	0.000354
PHI02outer	0.709297	0.000039		0.000127
RIN01inner	0.709039	0.000018	0.000174	-0.000131
RIN01outer	0.709213	0.000027		0.000043
RIN05inner	0.709271	0.000012	0.000152	0.000101
RIN05outer	0.709423	0.000018		0.000253
RIN06inner	0.709758	0.000018	0.000345	0.000588
RIN06outer	0.709413	0.000023		0.000243
RIN18inner	0.710375	0.000025	0.001173	0.001205
RIN18outer	0.709202	0.000017		0.000032
RIN20inner	0.709324	0.000013	0.000294	0.000154
RIN20outer	0.709618	0.000018		0.000448
RIN24inner	0.709360	0.000015	0.000055	0.00019
RIN24outer	0.709415	0.000035		0.000245
RIN25inner	0.708965	0.00002	0.001432	-0.000205
RIN25outer	0.710397	0.000014		0.001227
RIN28inner	0.711212	0.000007	0.001078	0.002042
RIN28outer	0.710134	0.00003		0.000964
RIN38inner	0.709988	0.00001	0.000282	0.000818
RIN38outer	0.709706	0.000008		0.000536
RIN42inner	0.710097	0.000011	0.000618	0.000927
RIN42outer	0.709479	0.000011		0.000309
VFB28inner	0.708171	0.000015	0.000540	-0.000999
VFB28outer	0.708711	0.000041		-0.000459

Driftwood sample $^{87}Sr/^{86}Sr$ values measured in this study were compared to existing collated sampled water $^{87}Sr/^{86}Sr$ and a global modelled isoscape (Bataille et al., 2020) (Figures C3.1-C3.6 in Supplementary Materials – Appendix C3). To illustrate the general issues found with interpreting the values for provenance, the example of sample PAR04 (inner-wood $^{87}Sr/^{86}Sr$=0.707974, outer-wood $^{87}Sr/^{86}Sr$=0.70855) is presented in Figure 5.4. PAR04 has a provenance region determined by TRW cross-dating in central Alaska, north of the Koyukuk River. Examining a bioavailable $^{87}Sr/^{86}Sr$ isoscape of the region by Funck et al. (2021), this sample is placed in an area of diverse range of $^{87}Sr/^{86}Sr$, with the surrounding range of 0.705201-0.715232 with multiple areas within each $^{87}Sr/^{86}Sr$ range. Examining river $^{87}Sr/^{86}Sr$ proximal to PAR04 from the Yukon, Koyukuk and its tributaries as collated by Bataille et al.

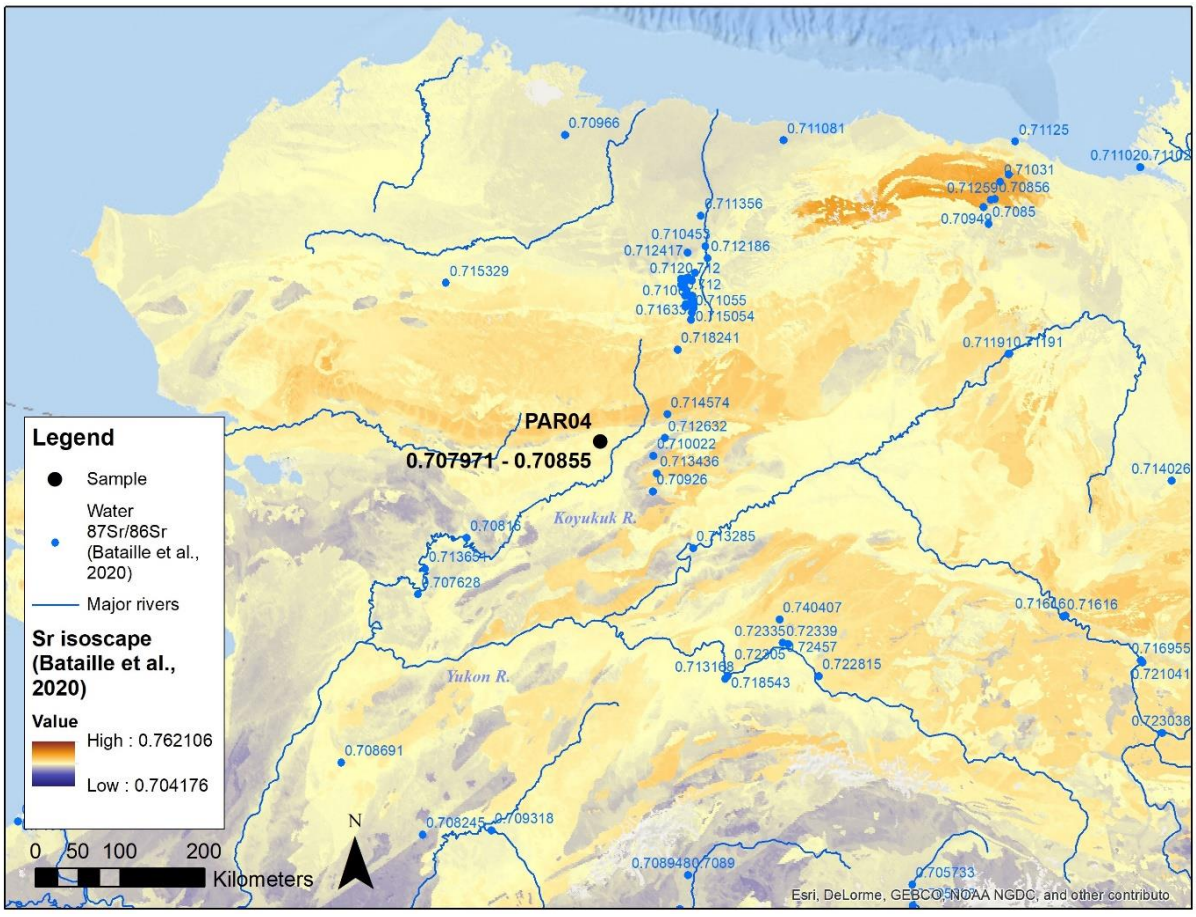

Figure 5.4. Map showing sample PAR04 crossdate match location determined by TRW crossdating by Hole et al. (2021), with measured $^{87}Sr/^{87}Sr$ value range displayed in black, with compiled river $^{87}Sr/^{86}Sr$ data by Bataille et al. (2020) in blue.

(2020), river values show a higher range of 0.70926-0.714574, out of the value obtained with sample PAR04. Downstream, ~200km south-west, river values reach more agreement with PAR04, in the range 0.70768-0.70816. This may indicate provenance of the driftwood to trees bordering the river Koyukuk in this area, though with the caveats discussed of intra-sample variability of $^{87}Sr/^{86}Sr$. Overall, when considering all samples, there is variable, patchy coverage of $^{87}Sr/^{86}Sr$ sampling data to compare to measured sample $^{87}Sr/^{86}Sr$ values for the provenance regions (Supplementary Materials – Appendix C2).

Comparison of values with the predicted bioavailable Sr provided by the isoscape by Bataille et al. (2020) shows that sample values obtained in this study tend to be below predicted bioavailable values. Moreover, no relationship was found between averaged bioavailable $^{87}Sr/^{86}Sr$ values (modelled by Bataille et al., 2020) across buffer zones surrounding dendro-provenance-based matching reference chronology localities (Table 5.3; Dataset Cds02 in Supplementary Materials – Appendix C2). The size of the buffer zones, of radii 5km, 20km, 100km, 200km, and 500km had no impact on correlation. Hence, $^{87}Sr/^{86}Sr$ alone are currently not sufficient to establish the likely provenance of Arctic driftwood at the pan-Arctic scale.

Table 5.3. Correlation calculations between 19 driftwood strontium values and averaged bioavailable strontium values as modelled in Bataille et al. (2020), averaged within buffer zones of variable radius from the location of the best-matching reference TRW chronology.

Correlation	5km buffer	20km buffer	100km buffer	200km buffer	500km buffer
Inner	0.00	0.01	-0.03	-0.05	-0.12
Outer	0.09	0.05	-0.12	-0.06	0.01
Average	0.02	0.00	-0.11	-0.08	-0.08

UPGMA cluster analysis confirmed that $^{87}Sr/^{86}Sr$ values did not cluster according to their TRW-inferred regional provenance (Figure 5.5). The structure of the clusters was

relatively preserved between the clusters, with relative outlier values (RIN28 for 'inner' and MAR05 for 'outer' affecting the cluster structure (Figures C4.1, C4.2 in Supplementary Materials – Appendix C4).

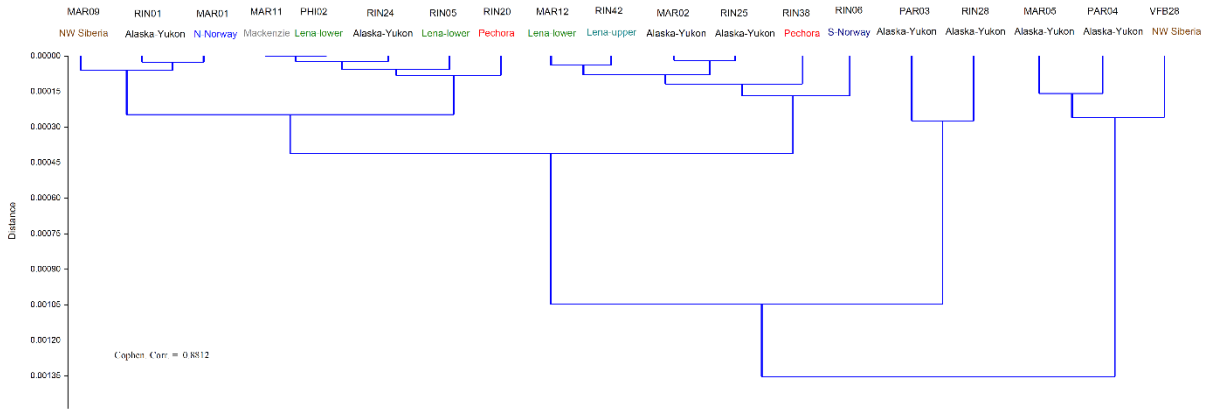

Figure 5.5. Unweighted pair-group average (UPGMA) cluster analysis on averaged $^{87}Sr/^{86}Sr$ readings for 19 driftwood samples. Cluster analysis was performed using PAST 4.04 (Hammer et al., 2001)

5.5 Discussion

The range of $^{87}Sr/^{86}Sr$ values obtained in this study are well within the range of expected values for wood samples, aligning with values in other studies (e.g. English et al., 2001; Rich et al., 2012; Aguzzoni et al., 2019; Britton et al., 2020), and thus we can consider that overall, the extraction protocol was successful. Nevertheless, the variation in $^{87}Sr/^{86}Sr$ within driftwood samples may be due to the range in condition, shape and other exogenous strontium sources that may impact the signature. The contributions of strontium from other sources, such as sea salt aerosols, the variable $^{87}Sr/^{86}Sr$ signature taken up by the tree during growth at boreal riverbanks, or access of sea water to the inner parts of the samples due to cracks in the driftwood are also possible causes of such variation within the wood tissue. The $^{87}Sr/^{86}Sr$ values retrieved from the 'inner' wood subsamples may also not necessarily be the most sheltered from alteration by sea water, rainwater and weathering, due to effects such as individual disc shape variations, cracks and shipworm (*Teredinidae navalis*) boreholes. As yet, investigated pre-treatment and cleaning regimes that aim to remove seawater waterlogging contamination have

been unsuccessful in retrieving the endogenous $^{87}Sr/^{86}Sr$ signature (Van Ham-Meert et al., 2020; Snoeck et al., 2021). Various studies' methods of multiple Milli-Q washes, MQ and Hydrofluoric acid (HF), alpha-cellulose extraction, and acid-leaching with hydrochloric acid and acetic acid were all unable to retrieve the original signature. Therefore, the methodology used in this study requires caution when interpreting the measured values given the likely remaining contributions of exogenous $^{87}Sr/^{86}Sr$ to the retrieved values.

Given the pan-Arctic scale of possible source regions for Arctic driftwood, the range of possible strontium signatures on such a scale extensively overlap, meaning that it is not possible to fingerprint individual samples to an originating source region with a distinctive $^{87}Sr/^{86}Sr$ source ratio alone. Therefore, when comparing these locations to surrounding available $^{87}Sr/^{86}Sr$ isoscapes, the heterogeneity in the values within the underlying regions of the localities for each sample can complicate interpretation, given that they fall within the same watershed. The developed global isoscapes for the examined regions, such as discussed for sample PAR04, are also formed on the basis of lower density of reference $^{87}Sr/^{86}Sr$ measurement data. The variability in values and spatial coverage provides caveats to the interpretation and indicates the need for increased data coverage of many pan-Arctic regions. The global $^{87}Sr/^{86}Sr$ isoscape by Bataille et al. (2020) was created via random forest regression, with extraction of values of covariates using site location and the closest underlying 1 km^2 pixel. For plants, soils and local animals this is fitting, as such substrates integrate Sr sources over local spatial scales. River water however, particularly for the large Arctic-draining rivers that are the target sources for this study, frequently integrate Sr sources over much larger spatial scales and from groundwater sources that are not represented in geological maps. Large rivers therefore also have a broader distribution of $^{87}Sr/^{86}Sr$ due to the input of groundwaters sampling large varieties of surrounding geologies. Given the riparian nature of the boreal tree growth preceding becoming driftwood, developing the existing terrestrial global $^{87}Sr/^{86}Sr$

isoscapes into global river water $^{87}Sr/^{86}Sr$ isoscapes could also further refine the isoscape used for driftwood provenance and is an avenue for future development.

The cluster analysis on the sampled values reinforces our interpretation that $^{87}Sr/^{86}Sr$ values obtained in this study do not provide a regional provenance signal, as seen in the fact that the resulting clusters of highly similar values are composed of driftwood material from a variety of provenances (Figure 5.5, Supplementary Figures C4.1, C4.2 in Appendix C3). Such results agree with the large overlap of $^{87}Sr/^{86}Sr$ across the pan-Arctic, and the probably very large influence of local factors and transport processes in determining the $^{87}Sr/^{86}Sr$ values in Arctic driftwood. The large spatial scale of the regional clustering also incorporates multiple watersheds and lithological diversity, increasing the likelihood of a high level of heterogeneity of $^{87}Sr/^{86}Sr$ signatures within the regional provenance subgroups employed to examine clustering. Finally, the analysis allowed the clear visualisation of outlier values that affect the overall structure of the data. Samples RIN28 and MAR05 exhibit outlier $^{87}Sr/^{86}Sr$ values (inner and outer subsamples, respectively), with values varying to a magnitude exceeding the variance within the remainder of the dataset. Such outlier values then impact clustering of their averaged $^{87}Sr/^{86}Sr$ values and the TRW-based provenance region group (Alaska-Yukon) used for the cluster analysis.

Placing driftwood within proxy-based mixing model using $^{87}Sr/^{86}Sr$ ratios measured in modern local vegetation, water and soil samples is also complicated by the diversity of environments and conditions driftwood encounters in the formation and transport to Arctic shorelines. Additionally, there are limits to current mixing models based on environmental proxies for predicting locally bioavailable strontium (Toncala et al., 2020), which currently underestimate $^{87}Sr/^{86}Sr$ ratios due to the limited sample size of modern environmental specimens and gaps in models of complex geobiological processes.

The varying spatial temporal scales of $^{87}Sr/^{86}Sr$, such as across watersheds, or localised for plants, complicate the comparisons between source and target strontium signatures (Erban Kochergina et al., 2021). For driftwood, this indicates a need for reference material that better reflects the spatial and temporal scale of riparian trees, such as watershed-scale strontium values, or coarser resolutions of provenance by other means followed by the utilisation of $^{87}Sr/^{86}Sr$ signatures at finer scales (e.g., dendro-provenancing). Further avenues for development may include measured $^{87}Sr/^{86}Sr$ targeting riparian wood along major rivers across the boreal forest region, although as with current sampling, such data is limited to modern $^{87}Sr/^{86}Sr$ characteristics which may not reflect the signatures across past millennia given potential temporal variation in weathering processes, river course paths hence underlying geology, and possible anthropogenic impacts on bioavailable Sr in recent centuries. An alternative is to invest in the development of millennial dendro-chronologies in the boreal forest to enable a more spatially constrained location for comparison with $^{87}Sr/^{86}Sr$ signatures.

As discussed as a remaining limitation to the use of isoscapes in provenance studies, interpreting the results of strontium analyses against an isoscape to determine provenance is currently subject to multiple confounding factors. Regarding this study, the isoscape by Bataille et al. (2020) shows predicted $^{87}Sr/^{86}Sr$ values consistently higher than those found in driftwood samples. This may be due to exogenous sources of Sr impacting the driftwood sample $^{87}Sr/^{86}Sr$, or it may be indicative of limitations in globally modelled $^{87}Sr/^{86}Sr$ to fully explain denote bioavailable $^{87}Sr/^{86}Sr$ at more localised scales within such heterogenous environments, climates and biota.

In order to further constrain provenance determinations for Arctic driftwood, exploration of further molecular techniques to refine the provenance of driftwood is a possibility. Genetic analysis through the extraction of ancient DNA or long-lived molecules

provide possible avenues to refine the wood's taxonomic identification, which could therefore aid determination of provenance by comparison to tree species distribution across the pan-Arctic forests. Determination of species of driftwood samples via ancient DNA extraction (if possible, down to the haplotype level) could enable a fine spatial resolution of provenance via comparison to the modern geographical distribution of chloroplast haplotypes across the pan-Arctic boreal forests. A further future avenue that may warrant investigation is protein analyses, such as a genus-specific collagen peptides by mass spectrometry (Buckley et al., 2009), which has been found productive even in cases when DNA cannot be retrieved.

5.6 Conclusions

Deposits of driftwood lining Arctic shorelines reveal the large-scale Arctic Ocean circulations and the incursion of driftwood-carrying sea ice onto circum-Arctic beaches. This rafting of Arctic driftwood by sea-ice enables the reconstruction of surface-current dynamics and sea-ice conditions in the Arctic. Refining the tools used for the provenance and age analysis of driftwood can develop reconstruction of Arctic Ocean surface currents and sea ice dynamics at a finer spatial resolution than previously achieved. Tools such as cross-dating with reference dendro-chronologies from the circum-arctic boreal forest zone enable determination of the originating climatic region/watershed. However, as with many current methodologies, uncertainties exist in the determination of provenance, such as confidence in the matching metrics, the preservation level of the driftwood determining the ability to analyse the tree ring width and anatomy and, most importantly, spatiotemporal coverage of the reference data.

The isotopic analysis of driftwood tissue is a possible avenue for the development of new provenance tools. The use of geochemical provenance techniques can address some of the limitations of current methods, warranting further development. The results of this study show

the utilisation of $^{87}Sr/^{86}Sr$ ratios to establish provenance for Arctic driftwood has some potential, since obtained values fall within the range of previously observed wood $^{87}Sr/^{86}Sr$ ratios. However, confounding factors in isolating endogenous strontium within driftwood samples, as well as the scale and heterogeneity and temporal variations of pan-Arctic source regions, currently limit the application of such isotopic approach as a stand-alone Arctic driftwood provenance technique. These limitations also highlight the value of dendro-provenancing as the current best-available tool at present to improve spatiotemporal determination of this material and thus further define the role of atmospheric and oceanic circulation in sea ice and climatic changes throughout the late Holocene. Further development of millennial-scale pan-boreal dendro-chronologies is thus encouraged, as they hold potential not only to inform of past climate and ecological conditions in the Boreal biome, but to provide essential information on past Arctic sea ice dynamics for the late Holocene.

5.7 Acknowledgments

GMH is funded by the Natural Environment Research Council (NERC grant: 1514291) and part of the Environmental Research Doctoral Training Program at the University of Oxford. Support and funding were also provided by MMF and grant funds from NERC (NERC IRF grant: NE/L011859/1). Geochemical analysis was undertaken in the clean-suite labs in the Earth Sciences Department, University of Oxford, by GMH and DS. Jane Barling and Kathrin Schilling provided assistance and training with equipment and clean-suite lab protocols. Yu-Te Alan Hsieh and Philip Holdship provided training and assistance with MC-ICP-MS/ICP-MS analysis. All authors contributed with literature compilation, data interpretation and the discussion of results.

6 Thesis Discussion

This thesis began with the introduction of the state of the field and research gaps within Holocene Arctic sea ice research, identifying that driftwood forms an informative, abundant, and accessible resource able to address some of these gaps in knowledge. The spatiotemporal dynamics of Arctic sea ice throughout the Holocene are limited by sparse data preceding satellite observation. This is pertinent given that modern trends cannot be accurately assessed within centennial and millennial timescales without knowledge of such trends in the recent Earth history. Therefore, further knowledge of past sea ice dynamics remains an important area for progress for revealing the late Quaternary Arctic climatic state, and to investigate the Arctic system's climatic and biotic responses and feedbacks to increasing global average temperatures.

In this discussion, I draw together the most important lessons from each chapter and demonstrate how they form a cohesive contribution to the exploration and development of driftwood as a tool for proxy-based Arctic sea ice reconstructions. Such additional tools merit exploration due to the limited abundance, length and/or resolution of existing proxy-based records (Abram et al., 2013). The inherent link between Arctic driftwood and sea ice drift routes (Funder et al., 2011), and its abundance on many Arctic coasts, mean it can help to fill the gaps of current proxy-based tools to reveal sea ice transport within large-scale Arctic Ocean circulation at the centennial to decadal scale and enable reconstruction of past surface-current dynamics and sea ice conditions (Häggblom, 1982; Dyke et al., 1997; Funder et al., 2011).

Chapter 3 further improves the resolution of Holocene reconstructions of environmental and climatic conditions by addressing the first aim of this thesis. The aim was the first-time assembly of existing pan-Arctic driftwood data to investigate hypotheses on Arctic surface currents, large-scale modes of climatic variability and the possible interplay of surface currents

driven by atmospheric circulation vs. thermal forcing on the sea ice extent during the Holocene. These hypotheses, as outlined in Specific Aims and Hypotheses in Chapter 1, were tested through a driftwood-based reconstruction of Holocene surface current and sea ice dynamics for the Arctic Ocean. Although regionally bounded, past driftwood-based sea ice reconstruction studies suggested spatiotemporally complex past Arctic sea ice extent and movement. A large-scale compilation of Holocene Arctic driftwood had not previously been developed. Chapter 3 – research paper 1 of this thesis – provides new insights into the variable climatic and environmental conditions that have impacted the Arctic throughout the past 12,000 years. This has enabled the detection of the pattern of change at different temporal frequencies through the Holocene. The collation of 913 driftwood samples from across the Arctic coastline provides a dataset of higher spatial and temporal resolution than other sea ice proxy-based methods in the Arctic, with preservation of driftwood in substantial volumes from the early Holocene indicating a low likelihood of preservation issues in the interpreted distribution patterns. This enables the detection of the pattern of change at different frequencies through the Holocene. These include:

1) Early Holocene deglaciation preceding positive AO conditions coeval with extensive remnant glaciation over the Canadian Arctic Archipelago (CAA) and North Greenland (NG).

2) Mid Holocene warming and sea ice reduction, with millennial scale east-west shifts in the Transpolar Drift (TPD) and associated Beaufort Gyre (BG) weakening. This high-resolution record also offers a different view of mid Holocene conditions to that proposed by Funder et al., (2011), with more coherence between NG and the CAA, an expansion of the TPD, increased temperatures, and reduced landfast ice.

3) Late Holocene millennial-scale west-east TPD shift and strengthened BG and sea ice preservation.

4) Recent Holocene high variability and higher frequency shifts in the TPD and BG strength and associated fluctuating climate conditions such as the Medieval Climate Anomaly (MCA) and Little Ice Age (LIA).

This and previous studies exploring driftwood as a proxy for sea ice have used a genus-based division of driftwood to indicate wood provenance, with *Larix* and *Picea* signifying the Siberian and North American boreal forests, respectively (e.g. Dyke et al., 1997; Eggertsson, 1993; Funder et al., 2011; Häggblom, 1982; Hellmann et al., 2013; Nixon et al., 2016). The complexity of the boreal tree species and genera distributions (e.g. Hellmann et al., 2016), and the coarse spatial resolution of provenance possible via such methods – essentially Eurasian *vs.* North-American – highlights the need for a refinement of provenance determination. This would further constrain spatiotemporal reconstructions of variations in Holocene ocean current and sea ice dynamics. For more spatially precise provenance determination, dendrochronology has proved a vital tool, both in archaeological efforts (R. E. Taylor & Aitken, 1997) and Arctic climatic and environmental reconstructions (Koch, 2009; Owczarek, 2010). A recent combined assessment of radiocarbon and dendrochronological age estimates of Arctic driftwood samples found that radiocarbon dates from buried driftwood were in agreement with dendrochronological dating of modern beach ridge systems in coastal eastern Siberia (Sander et al., 2021). This supports the validity of age indications obtained from driftwood found on Holocene beaches. The majority of driftwood dendrochronological studies have considered only reference chronologies associated with a particular drainage basin (Eggertsson, 1993; Eggertsson & Laeyendecker, 1995), based upon consideration of Arctic surface currents. However, some recent studies have highlighted that such assumptions can be incorrect, and a far wider extent of circumpolar sites must be considered during such processes, to accurately capture the potential history of samples (Hellmann et al., 2013b). Moreover, such assumptions

are untenable in coastal regions receiving driftwood from multiple regions, such as northern Svalbard or northern Greenland.

Chapter 4 – research paper 2 in this thesis – builds upon this with the employment of tree ring width analysis on newly collected driftwood collected from northern Svalbard. This new data and novel methodological approach reveals a 500-year history of driftwood incursion to northern Svalbard, directly reflecting regional sea ice conditions and Arctic ocean circulation. As the samples come from naturally felled trees (as opposed to logged, or both), the relative proportions of different provenances can be used to infer past ocean current dominance. By crossdating samples against a circumpolar reference chronology database across North American and Eurasian boreal forest zone drainage basins, a wide range of matches can occur across the region, which would be considered a sign of good fit by some references. To minimise the risk of resulting bias towards regions and periods covered by more reference chronologies, Chapter 4 employs a novel approach to selecting probable origin sites, by weighting matches via reference chronology span and visualising results through spatiotemporal density plots. The resulting record indicates centennial- to decadal-scale variability in source regions for driftwood incursion to Svalbard, which was compared to information from existing reconstructions and direct observations of sea ice dynamics where available. This enabled the assessment of the accuracy of driftwood temporal distribution reflecting the known sea ice conditions of the time. The record was found to align with Late Holocene high variability and high frequency shifts in the Transpolar Drift and Beaufort Gyre strengths and associated fluctuating climate conditions. Notable variations in driftwood occurrence and provenance also track a northward shift of seasonal ice formation and spatiotemporal dynamics of seasonal sea ice in the peripheral Arctic seas in the past century, including an early sea ice reduction over the Barents Sea in mid-19th century and variability during the 20th century in the Siberian marginal seas. A distinct decrease in driftwood incursion

during the last 30 years matches the observed decline in pan-Arctic sea ice extent in recent decades. The chapter successfully employs driftwood as a proxy for Arctic Ocean surface current and sea ice dynamics, with alignment of the driftwood-based reconstruction with existing data on past sea ice and large-scale modes of climatic variability during the Holocene providing the up-to-date most robust validation of driftwood and the approach utilised.

The utilisation of the Weighed Score in Chapter 4 aids in reducing the bias of varied spatiotemporal coverage of the reference chronologies, but sources of uncertainty do remain when interpreting driftwood incursion records. These include Late Holocene sea level transgression, which may influence the preservation of older driftwood samples in some regions (Forman et al., 2004; Farnsworth et al., 2020a). Degraded samples may also have implications for observed Arctic driftwood densities, as heavily degraded samples cannot be cross-referenced to our reference chronology. However, these were predominantly observed at higher elevations than our target sampling sites at the modern-day shoreline, and on topographically wet areas such as melting snow beds. This suggests older ages and particular depositional environments, and so the impact of possible degraded samples is 1) likely more relevant for the earliest centuries of the dataset and 2) likely limited. Therefore, when interpreting the contrasting regional trends in the earlier years of our dataset, we assume that driftwood degradation is a risk equally applicable to all samples irrespective of their origin. Local sea ice conditions must also be considered when interpreting the driftwood record from these Svalbard collection sites, as persistent or semi-permanent land-fast ice resulting from localised cold conditions would minimize the transport of and catchment for driftwood accumulation (Funder et al., 2011), especially when considering that our sample sites are in the northernmost part of the archipelago. Another feature to consider is the impact of circumpolar rivers flow regimes that transport this wood from boreal forest zones on driftwood delivery to the Arctic basin. Given the centennial spatiotemporal scope of the dataset, and lack of sufficient

available data on these variety of factors for the pan-Arctic across the past 500 years, these impacts are assumed not to have had a substantial impact on the trends observed. Finally, in the interpretation of driftwood material, consideration of other sources of information – other proxies, geomorphological evidence etc. – is deemed to be essential (e.g., lack of driftwood can indicate land-fast ice or lack of multiyear ice).

Chapter 5 – research paper 3 in this thesis – progresses on the needs identified for the use of Arctic driftwood as a robust sea ice proxy for the Holocene, and addresses the third main aim of this thesis as specified in the Specific Aims and Hypotheses: to develop and validate novel techniques to refine the provenance of driftwood through radiogenic isotopic analysis ($^{87}Sr/^{86}Sr$). Provenance by genus is limited by spatially coarse resolution, while provenance by dendrochronology is reliant on the spatiotemporal coverage of existing boreal forest reference chronologies and levels of driftwood preservation enabling TRW analysis. Geochemical and genetic techniques hold the potential to address the limitations of these current methods and achieve a finer definition of the role of atmospheric and oceanic circulation in sea ice and climatic changes throughout the Holocene. Chapter 5 presents the development of geochemical techniques – specifically radiogenic isotopic analysis ($^{87}Sr/^{86}Sr$) of driftwood as a provenance tool. Methods for the extraction, isolation and purification of strontium from driftwood through microwave digestion, extraction chromatography and MC-ICP-MS analysis were successfully developed. The utilisation of $^{87}Sr/^{86}Sr$ ratios to establish provenance for Arctic driftwood was determined to hold potential, with confounding factors in the potential contamination of the material after the fall of the driftwood-to-be tree on the river and through its transport in fresh- and seawater, and the scale and heterogeneity and temporal variations of pan-Arctic source regions. Increased sample populations and source samples for calibration to enable validation are recommended for this work to be built upon, most probably in combination with previously developed provenance tools and reconstructions (e.g. dendro-provenancing). The observed

small-scale heterogeneity of $^{87}Sr/^{86}Sr$ ratios precludes its use as a pan-Arctic provenance stand-alone tool. The chapter provides a first step the use of geochemical techniques for provenance in Arctic Driftwood.

The development of novel analytical techniques was continued further via attempted ancient DNA extraction from driftwood, with details in Appendix D. Microanatomical analysis of driftwood can only glean taxonomy to genus level – in some rare occasions such as with some *Pinus*, to species; requiring further techniques to refine the wood's taxonomic identification and therefore enhance determination of provenance. As wood is a commonly occurring archaeological remain (Gugerli et al., 2005), a variety of studies have already shown the application of ancient DNA analysis for archaeological/preserved wood for uses such as wood traceability and monitoring species evolution (Speirs et al., 2009). The extraction of ancient DNA requires preservation of sufficiently long sequences of DNA, which is known to be problematic for fossil and subfossil wood due to the speed of DNA degradation leading to fragmentation and modification of the recoverable DNA (Lindahl, 1993; Pääbo et al., 2004). Specifically, in the case of Arctic driftwood, the long duration of exposure to ocean waters and in situ on shorelines means DNA-degrading temperature fluctuations of up to tens of degrees. However, the cold and dry conditions of the Arctic and alkaline soils act as preserving factors and limiting any microbial action on the wood (Dyke et al., 1997). A PCR protocol was chosen specifically for applicability to degraded DNA to determine what recoverable DNA may be present with test sub-Arctic driftwood samples from Nordkapp, Norway. The resulting amplicons were all too weak to be sufficient for sequencing, indicating that currently aDNA extraction for Arctic driftwood is unlikely to be viable, although there remain future avenues for developments in ancient DNA retrieval from Arctic driftwood, with continuing progress in aDNA retrieval from subfossil wood material as techniques and technologies develop. An

example is long-lived protein analyses such as genus-specific collagen peptides (Buckley et al., 2009), which has been found productive in cases when DNA cannot be retrieved.

Via the collation and analysis of existing driftwood data, new sample collection, methodological testing and development and validation of approaches and techniques, the chapter components of the thesis describe the potential and realised employment and development of driftwood as a proxy for Arctic Ocean surface current and sea ice dynamics. This has also brought new insights into Holocene Arctic sea ice and climate dynamics at a higher spatiotemporal resolution than previously possible, and enables future further integration with other observations, proxy-based reconstructions, and modelling of the Holocene Arctic.

7 Thesis Conclusions

With the successful utilisation of driftwood, future investigations and combination of the developed and explored techniques can further define the role of atmospheric and oceanic circulation in sea ice and climatic changes throughout the Holocene. Some key results from the project include:

- A first insight into pan-Arctic decadal to centennial trends in surface currents, climate variability and sea ice dynamics during the Holocene, via the collation and analysis of existing Arctic driftwood data.
- The provenance and age determination of newly collected driftwood samples via dendrochronological approaches was achieved with development and improvement upon older methods.
- New methodological approaches to provenance and age analysis of driftwood (Sr and aDNA) were tested and with promising but so far limited progress, with further development needed.
- Overall, the project confirms the utility of driftwood as a proxy tool for Holocene Arctic sea ice reconstructions, with the potential for even better results once the new techniques are fully deployed.

The reconstructed of Holocene sea ice dynamics then serve as the basis for future proxy-model comparison of climate and sea ice-conditions, as well as a framework for testing hypotheses on the coupling between sea ice and Arctic biota. Benefits beyond the thesis arise from this gathering of new and re-analysed pan-Arctic driftwood data, in contribution to efforts around the boreal region to construct long-term millennial tree-ring chronologies that serve as proxies for past climatic reconstructions. The driftwood-based sea ice chronology can also be

validated and combined with a suite of other sea ice proxies, such as deep ocean cores, other proxy measures of Arctic sea ice, and modelling, with some of these already underway and utilising the data produced from this thesis (Dalaiden et al., 2018; Farnsworth et al., 2020a; Linderholm et al., 2021; Sander et al., 2021). Dalaiden et al. (2018) proposed and tested a driftwood transport model for compatibility with reconstructions including Hole et al. (2017) / Chapter 3, and confirmed a strong influence of atmospheric circulation variability on spatial driftwood distribution. Farnsworth et al. (2020) incorporated the collated data of Hole et al. (2017) / Chapter 3 into a first compilation of Holocene geochronology for Svalbard and the surrounding waters in the SVALHOLA database, including over 1,800 radiocarbon, terrestrial cosmogenic nuclide and optically stimulated luminescence ages. The other studies build less directly on Arctic driftwood analysis and findings of Hole et al. (2017) / Chapter 3 with new driftwood provenance analyses (Linderholm et al., 2021), hydrogen, oxygen, and strontium isotope analysis (Pinta et al., 2021), and use of driftwood as coastal deposit chronological markers (Sander et al., 2021). These new studies cover a variety of geographical areas and timespans and so provide opportunities for comparison and integration of the data produced.

By increasing the understanding of the Arctic system and dynamics, the feedback links between biotic and abiotic processes in the light of current environmental change can be better addressed, therefore aiding to plan and manage this highly sensitive region. Given the increasing importance of Arctic climate change on a global scale, and the well documented recent rapid decline in Arctic sea ice extent, age and thickness, increasing the understanding of Arctic sea ice fluctuations is relevant to current and future UK and international climate research. This scientific field is constantly evolving and remains under active research, giving added benefit to the research outcomes and new datasets arisen from the work of this thesis.

8 Bibliography

Aberg, G. (1995). The Use of Natural Strontium Isotopes as Tracers in Environmental-Studies. *Water Air and Soil Pollution*, *79*(1–4), 309–322.

Abram, N. J., Wolff, E. W., & Curran, M. A. J. (2013). A review of sea ice proxy information from polar ice cores. *Quaternary Science Reviews*, *79*, 168–183. https://doi.org/10.1016/j.quascirev.2013.01.011

Agardh, I. G. (1869). Om den Spetsbergska Drif-vedens ursprung. In *Kungliga Svenska Vetenskaps Academiens Förhandlingar* (Vol. 26). éditeur non identifié.

Aguzzoni, A., Bassi, M., Robatscher, P., Scandellari, F., Tirler, W., & Tagliavini, M. (2019). Intra- and Intertree Variability of the 87Sr/86Sr Ratio in Apple Orchards and Its Correlation with the Soil 87Sr/86Sr Ratio. *Journal of Agricultural and Food Chemistry*, *67*(20), 5728–5735. https://doi.org/10.1021/acs.jafc.9b01082

Alix, C. (2005). Deciphering the impact of change on the driftwood cycle: Contribution to the study of human use of wood in the Arctic. *Global and Planetary Change*, *47*(2-4 SPEC. ISS.), 83–98. https://doi.org/10.1016/j.gloplacha.2004.10.004

Alkire, M. B., Morison, J., Schweiger, A., Zhang, J., Steele, M., Peralta-Ferriz, C., & Dickinson, S. (2017). A meteoric water budget for the Arctic Ocean. *Journal of Geophysical Research: Oceans*, *122*(12), 10020–10041.

Allaart, L., Müller, J., Schomacker, A., Rydningen, T. A., Håkansson, L., Kjellman, S. E., Mollenhauer, G., & Forwick, M. (2020). Late Quaternary glacier and sea-ice history of northern Wijdefjorden, Svalbard. *Boreas*, *49*(3), 417–437. https://doi.org/10.1111/bor.12435

Allard, M., & Tremblay, G. (1983). La dynamique littorale des îles Manitounuk durant l'Holocène in Coastal and inland periglacial processes. Canadian Arctic. *Zeitschrift Für Geomorphologie. Supplementband Stuttgart*, *47*, 61–95.

Allègre, C. J. (2008). Isotope Geology. In *Physics of the Earth and Planetary Interiors*. Cambridge University Press. http://www.cambridge.org/9780521862288

Andrews, J. T. (1970). *A geomorphological study of post-glacial uplift: with particular reference to Arctic Canada* (Issue 2). London: Institute of British Geographers.

Andrews, J. T., Darby, D., Eberle, D., Jennings, a. E., Moros, M., & Ogilvie, a. (2009). A robust, multisite Holocene history of drift ice off northern Iceland: implications for North Atlantic climate. *The Holocene*, *19*(1), 71–77. https://doi.org/10.1177/0959683608098953

Aré, F. E. (1988). Thermal abrasion of sea coasts (part I). *Polar Geography and Geology*, *12*(1), 1. https://doi.org/10.1080/10889378809377343

Armand, L., Ferry, A., & Leventer, A. (2016). Advances in palaeo sea ice estimation. In *Sea Ice: Third Edition* (pp. 600–629). John Wiley & Sons Ltd Chichester. https://doi.org/10.1002/9781118778371.ch26

Ashton, W. S., & Bredthauer, S. R. (1986). Riverbank erosion processes on the Yukon River

at Galena, Alaska. *Proceedings of the Symposium: Cold Regions Hydrology.*

Atkinson, N., & England, J. H. (2004). Postglacial emergence of Amund and Ellef Ringnes islands, Nunavut: implications for the northwest sector of the Innuitian Ice Sheet. *Canadian Journal of Earth Science*, *41*, 271–283. https://doi.org/10.1139/e03-095

Backman, J., Jakobsson, M., Løvlie, R., Polyak, L., & Febo, L. A. (2004). Is the central Arctic Ocean a sediment starved basin? *Quaternary Science Reviews*, *23*(11–13), 1435–1454. https://doi.org/10.1016/j.quascirev.2003.12.005

Bagard, M.-L., Schmitt, A.-D., Chabaux, F., Pokrovsky, O. S., Viers, J., Stille, P., Labolle, F., & Prokushkin, A. S. (2013). Biogeochemistry of stable Ca and radiogenic Sr isotopes in a larch-covered permafrost-dominated watershed of Central Siberia. *Geochimica et Cosmochimica Acta*, *114*, 169–187. https://doi.org/https://doi.org/10.1016/j.gca.2013.03.038

Baillie, M., & Pilcher, J. (1973). A simple crossdating program for tree-ring research. In *Tree ring Bulletin* (Vol. 33, pp. 7–14). https://doi.org/S

Bain, D. C., & Bacon, J. R. (1994). Strontium isotopes as indicators of mineral weathering in catchments. *Catena*, *22*(3), 201–214. https://doi.org/10.1016/0341-8162(94)90002-7

Bain, D. C., Midwood, a. J., & Miller, J. D. (1998). Strontium isotope ratios in streams and the effect of flow rate in relation to weathering in catchments. *Catena*, *32*(2), 143–151. https://doi.org/10.1016/S0341-8162(97)00055-6

Banner, J. L. (2004). Radiogenic isotopes: Systematics and applications to earth surface processes and chemical stratigraphy. *Earth-Science Reviews*, *65*(3–4), 141–194. https://doi.org/10.1016/S0012-8252(03)00086-2

Barnes, E. A., & Screen, J. A. (2015). The impact of Arctic warming on the midlatitude jet-stream: Can it? Has it? Will it? *Wiley Interdisciplinary Reviews: Climate Change*, *6*(3), 277–286. https://doi.org/10.1002/wcc.337

Baroni, M. V, Podio, N. S., Badini, R. G., Inga, M., Ostera, H. A., Cagnoni, M., Gallegos, E., Gautier, E., Peral-García, P., & Hoogewerff, J. (2011). How much do soil and water contribute to the composition of meat? A case study: Meat from three areas of Argentina. *Journal of Agricultural and Food Chemistry*, *59*(20), 11117–11128.

Bartlein, P. J., Edwards, M. E., Hostetler, S. W., Shafer, S. L., Anderson, P. M., Brubaker, L. B., & Lozhkin, A. V. (2015). Early-Holocene warming in Beringia and its mediation by sea-level and vegetation changes. *Climate of the Past*, *11*(9), 1197–1222. https://doi.org/10.5194/cp-11-1197-2015

Bataille, C. P., Brennan, S. R., Hartmann, J., Moosdorf, N., Wooller, M. J., & Bowen, G. J. (2014). A geostatistical framework for predicting variations in strontium concentrations and isotope ratios in Alaskan rivers. *Chemical Geology*, *389*, 1–15. https://doi.org/10.1016/j.chemgeo.2014.08.030

Bataille, C. P., Crowley, B. E., Wooller, M. J., & Bowen, G. J. (2020). Advances in global bioavailable strontium isoscapes. *Palaeogeography, Palaeoclimatology, Palaeoecology*, *555*, 109849. https://doi.org/https://doi.org/10.1016/j.palaeo.2020.109849

Bataille, C. P., Laffoon, J., & Bowen, G. J. (2012). Mapping multiple source effects on the strontium isotopic signatures of ecosystems from the circum-Caribbean region. *Ecosphere*, *3*(December), 1–24. https://doi.org/10.1890/ES12-00155.1

Beard, B. L., & Johnson, C. M. (2000). Strontium isotope composition of skeletal material can determine the birth place and geographic mobility of humans and animals. *Journal of Forensic Sciences*, *45*(5), 1049–1061.

Becagli, S., Castellano, E., Cerri, O., Curran, M., Frezzotti, M., Marino, F., Morganti, A., Proposito, M., Severi, M., Traversi, R., & Udisti, R. (2009). Methanesulphonic acid (MSA) stratigraphy from a Talos Dome ice core as a tool in depicting sea ice changes and southern atmospheric circulation over the previous 140 years. *Atmospheric Environment*, *43*(5), 1051–1058. https://doi.org/10.1016/j.atmosenv.2008.11.015

Bednarski, J. (1984). Glacier fluctuations and sea level history of Clements Markham Inlet, Northern Ellesmere Island. *Unpublished PhD Thesis, University of Alberta Libraries*, 232.

Bell, T. (1996). The last glaciation and sea level history of Fosheim Peninsula, Ellesmere Island, Canadian High Arctic. *Canadian Journal of Earth Sciences*, *33*(7), 1075–1086. https://doi.org/10.1139/e96-082

Belt, S. T. (2018). Source-specific biomarkers as proxies for Arctic and Antarctic sea ice. *Organic Geochemistry*, *125*, 277–298.

Belt, S. T., Massé, G., Rowland, S. J., Poulin, M., Michel, C., & LeBlanc, B. (2007). A novel chemical fossil of palaeo sea ice: IP25. *Organic Geochemistry*, *38*(1), 16–27. https://doi.org/https://doi.org/10.1016/j.orggeochem.2006.09.013

Belt, S. T., & Müller, J. (2013). The Arctic sea ice biomarker IP25: A review of current understanding, recommendations for future research and applications in palaeo sea ice reconstructions. *Quaternary Science Reviews*, *79*, 9–25. https://doi.org/10.1016/j.quascirev.2012.12.001

Bengtsson, L., Semenov, V. A., & Johannessen, O. M. (2004). The early twentieth-century warming in the Arctic—A possible mechanism. *Journal of Climate*, *17*(20), 4045–4057.

Bennike, O. (1987). Quaternary geology and biology of the Jorgen Bronlund Fjord area, North Greenland. In *Meddelelser om Gronland, Geoscience* (Vol. 18). Kommissionen for Videnskabelige Undersøgelser i Grønland.

Bennike, O. (2004). Holocene sea-ice variations in Greenland: onshore evidence. *The Holocene*, *14*(4), 607–613. https://doi.org/10.1191/0959683604hl722rr

Bennike, O., & Weidick, A. (2001). Late Quaternary history around Nioghalvfjerdsfjorden and Jøokelbugten, North-East Greenland. *Boreas*, *30*(3), 205–227. https://doi.org/10.1111/j.1502-3885.2001.tb01223.x

Bentley, R. A. (2006). Strontium isotopes from the earth to the archaeological skeleton: A review. *Journal of Archaeological Method and Theory*, *13*(3), 135–187. https://doi.org/10.1007/s10816-006-9009-x

Betcher, M. A., Fung, J. M., Han, A. W., O'Connor, R., Seronay, R., Concepcion, G. P., Distel, D. L., & Haygood, M. G. (2012). Microbial Distribution and Abundance in the Digestive System of Five Shipworm Species (Bivalvia: Teredinidae). *PLoS ONE*, *7*(9), 3–10. https://doi.org/10.1371/journal.pone.0045309

Bhatt, U. S., Walker, D. A., Walsh, J. E., Carmack, E. C., Frey, K. E., Meier, W. N., Moore, S. E., Parmentier, F. J. W., Post, E., Romanovsky, V. E., & Simpson, W. R. (2014). Implications of arctic sea ice decline for the earth system. *Annual Review of*

Environment and Resources, *39*(1), 57–89. https://doi.org/10.1146/annurev-environ-122012-094357

Bigelow, N. H., Brubaker, L. B., Edwards, M. E., Harrison, S. P., Prentice, I. C., Anderson, P. M., Andreev, A. A., Bartlein, P. J., Christensen, T. R., Cramer, W., Kaplan, J. O., Lozhkin, A. V., Matveyeva, N. V., Murray, D. F., McGuire, A. D., Razzhivin, V. Y., Ritchie, J. C., Smith, B., Walker, D. A., … Volkova, V. S. (2003). Climate change and Arctic ecosystems: 1. Vegetation changes north of 55°N between the last glacial maximum, mid-Holocene, and present. *Journal of Geophysical Research: Atmospheres*, *108*(19). https://doi.org/10.1029/2002jd002558

Bintanja, R., & Andry, O. (2017). Towards a rain-dominated Arctic. *Nature Clim. Change*, *7*(4), 263–267. http://dx.doi.org/10.1038/nclimate3240

Birkenmajer, K., & Olsson, I. U. (1969). Radiocarbon dating of raised marine terraces at Hornsund, Spitsbergen, and the problem of land uplift. *Norsk Polarinstitutt Årbok*, 17–43.

Björdal, C. G., Nilsson, T., & Daniel, G. (1999). Microbial decay of waterlogged archaeological wood found in Sweden. Applicable to archaeology and conservation. *International Biodeterioration and Biodegradation*, *43*(1–2), 63–73. https://doi.org/10.1016/S0964-8305(98)00070-5

Bjorkman, A. D., García Criado, M., Myers-Smith, I. H., Ravolainen, V., Jónsdóttir, I. S., Westergaard, K. B., Lawler, J. P., Aronsson, M., Bennett, B., Gardfjell, H., Heiðmarsson, S., Stewart, L., & Normand, S. (2020). Status and trends in Arctic vegetation: Evidence from experimental warming and long-term monitoring. *Ambio*, *49*(3), 678–692. https://doi.org/10.1007/s13280-019-01161-6

Blake Jr, W. (1961a). *Radiocarbon Dating of Raised Beaches in Nordaustlandet, Spitsbergen* (G. O. Raasch (ed.); pp. 133–146). University of Toronto Press. https://doi.org/doi:10.3138/9781487584979-010

Blake Jr, W. (1961b). Russian settlement and land rise in Nordaustlandet, Spitsbergen. *Arctic*, *14*(1), 101–111.

Blake Jr, W. (1970). Studies of glacial history in Arctic Canada. I. Pumice, radiocarbon dates, and differential postglacial uplift in the eastern Queen Elizabeth Islands. *Canadian Journal of Earth Sciences*, *7*(2), 634–664.

Blake Jr, W. (1972). Climatic implications of radiocarbon-dated driftwood in the Queen Elizabeth Islands, Arctic Canada. In *Climatic Changes in Arctic Areas During the Last Ten-Thousand Years: a symposium held at Oulanka and Kevo, 4-10 October.* Y. Vasari, H. Hyvairnen, and S. Hicks.

Blake Jr, W. (1974). Studies of glacial history in Arctic Canada. II. Interglacial peat deposits on Bathurst Island. *Canadian Journal of Earth Sciences*, *11*(8), 1025–1042.

Blake Jr, W. (1975). Radiocarbon Age Determinations and Postglacial Emergence at Cape Storm , Southern Ellesmere Island , Arctic Canada Author (s): Weston Blake , Jr . Published by : Wiley on behalf of the Swedish Society for Anthropology and Geography Stable URL : http://w. *Geografiska Annaler*, *57*(1).

Blake Jr, W. (1984). *Geological Survey of Canada: Radiocarbon Dates XXIII*. The Survey. https://books.google.co.uk/books?id=ObHKzQEACAAJ

Blake Jr, W. (1986). *Geological Survey of Canada radiocarbon dates XXV*. *7*. https://doi.org/https://doi.org/10.4095/120615

Blake Jr, W. (1987). *Geological Survey of Canada radiocarbon dates XXVI*.

Blake Jr, W. (1989). Application of 14C AMS dating to the chronology of Holocene glacier fluctuations in the High Arctic, with special reference to Leffert Glacier, Ellesmere Island, Canada. *Radiocarbon*, *31*(3), 570–578.

Blake Jr, W. (1993). Holocene emergence along the Ellesmere Island coasts of northernmost Baffin Bay. *Norsk Geologisk Tidsskrift*, *73*(3), 147–160.

Blanchette, R. a. (2000). A review of microbial deterioration found in archaeological wood from different environments. *International Biodeterioration and Biodegradation*, *46*(3), 189–204. https://doi.org/10.1016/S0964-8305(00)00077-9

Blanchette, R. A., Held, B. W., Hellmann, L., Millman, L., & Büntgen, U. (2016). Arctic driftwood reveals unexpectedly rich fungal diversity. *Fungal Ecology*, *23*, 58–65. https://doi.org/10.1016/j.funeco.2016.06.001

Blum, J. D., & Erel, Y. (2003). Radiogenic isotopes in weathering and hydrology. *Surface and Ground Water, Weathering, and Soils*, *5*, 365–392. https://doi.org/10.1016/B0-08-043751-6/05082-9

Blum, J. D., Gazis, C. a., Jacobson, A. D., & Chamberlain, C. P. (1998). Carbonate versus silicate weathering in the Raikhot watershed within the High Himalayan Crystalline Series. *Geology*, *26*(5), 411–414. https://doi.org/10.1130/0091-7613(1998)026<0411:CVSWIT>2.3.CO

Boettger, T., Hiller, A., & Kremenetski, K. (2003). Mid-Holocene warming in the northwest Kola Peninsula, Russia: northern pinelimit movement and stable isotope evidence. *The Holocene*, *13*(3), 403–410. https://doi.org/10.1191/0959683603hl633rp

Böhlke, J. K., & Horan, M. (2000). Strontium isotope geochemistry of groundwaters and streams affected by agriculture, Locust Grove, MD. *Applied Geochemistry*, *15*(5), 599–609. https://doi.org/10.1016/S0883-2927(99)00075-X

Bondevik, S., Mangerud, J., Ronnert, L., & Salvigsen, O. (1995). Postglacial sea-level history of Edgeøya and Barentsøya, eastern Svalbard. *Polar Research*, *14*(2), 153–180.

Borg, L. E., & Banner, J. L. (1996). Neodymium and strontium isotopic constraints on soil sources in Barbados, West Indies. *Geochimica et Cosmochimica Acta*, *60*(21), 4193–4206. https://doi.org/10.1016/S0016-7037(96)00252-9

Brackhage, C., Hagemeyer, J., Breckle, S. W., & Greszta, J. (1996). Radial distribution patterns of Cd and Zn in stems of Scots pine (Pinus sylvestris L.) trees analyzed 12 years after a contamination event. *Water, Air, and Soil Pollution*, *90*(3–4), 417–428.

Brandes, E., Kodama, N., Whittaker, K., Weston, C., Rennenberg, H., Keitel, C., Adams, M. a., & Gessler, A. (2006). Short-term variation in the isotopic composition of organic matter allocated from the leaves to the stem of Pinus sylvestris: Effects of photosynthetic and postphotosynthetic carbon isotope fractionation. *Global Change Biology*, *12*(10), 1922–1939. https://doi.org/10.1111/j.1365-2486.2006.01205.x

Brennan, S. R., Fernandez, D. P., Mackey, G., Cerling, T. E., Bataille, C. P., Bowen, G. J., & Wooller, M. J. (2014). Strontium isotope variation and carbonate versus silicate

weathering in rivers from across Alaska : Implications for provenance studies. *Chemical Geology*, *389*, 167–181. https://doi.org/10.1016/j.chemgeo.2014.08.018

Briner, J. P., McKay, N. P., Axford, Y., Bennike, O., Bradley, R. S., de Vernal, A., Fisher, D., Francus, P., Fréchette, B., Gajewski, K., Jennings, A., Kaufman, D. S., Miller, G., Rouston, C., & Wagner, B. (2016). Holocene climate change in Arctic Canada and Greenland. *Quaternary Science Reviews*, *147*, 340–364. https://doi.org/10.1016/j.quascirev.2016.02.010

Britton, K., Le Corre, M., Willmes, M., Moffat, I., Grün, R., Mannino, M. A., Woodward, S., & Jaouen, K. (2020). Sampling Plants and Malacofauna in 87Sr/86Sr Bioavailability Studies: Implications for Isoscape Mapping and Reconstructing of Past Mobility Patterns. In *Frontiers in Ecology and Evolution* (Vol. 8, p. 446). https://www.frontiersin.org/article/10.3389/fevo.2020.579473

Broecker, W. S., & Olson, E. A. (1959). Lamont Radiocarbon Measurements VI∗. *Radiocarbon*, *1*, 111–132.

Bronk Ramsey, C. (2009). Bayesian Analysis of Radiocarbon Dates. *Radiocarbon*, *51*(1), 337–360. https://doi.org/10.2458/azu_js_rc.v51i1.3494

Brown, T. a, Belt, S. T., Tatarek, A., & Mundy, C. J. (2014). Source identification of the Arctic sea ice proxy IP25. *Nature Communications*, *5*(May), 4197. https://doi.org/10.1038/ncomms5197

Buckley, M., Collins, M., Thomas-Oates, J., & Wilson, J. C. (2009). Species identification by analysis of bone collagen using matrix-assisted laser desorption/ionisation time-of-flight mass spectrometry. *Rapid Communications in Mass Spectrometry*, *23*(23), 3843–3854. https://doi.org/https://doi.org/10.1002/rcm.4316

Bullen, T. D., & Bailey, S. W. (2005). Identifying calcium sources at an acid deposition-impacted spruce forest: A strontium isotope, alkaline earth element multi-tracer approach. *Biogeochemistry*, *74*(1), 63–99. https://doi.org/10.1007/s10533-004-2619-z

Cabedo-Sanz, P., Belt, S. T., Jennings, A. E., Andrews, J. T., & Geirsd??ttir, ??slaug. (2016). Variability in drift ice export from the Arctic Ocean to the North Icelandic Shelf over the last 8000 years: A multi-proxy evaluation. *Quaternary Science Reviews*, *146*, 99–115. https://doi.org/10.1016/j.quascirev.2016.06.012

Capo, R. C., Stewart, B. W., & Chadwick, O. a. (1998). Strontium isotopes as tracers of ecosystem processes: Theory and methods. *Geoderma*, *82*(1–3), 197–225. https://doi.org/10.1016/S0016-7061(97)00102-X

Carmack, E. C., Yamamoto-Kawai, M., Haine, T. W. N., Bacon, S., Bluhm, B. A., Lique, C., Melling, H., Polyakov, I. V, Straneo, F., & Timmermans, M. (2016). Freshwater and its role in the Arctic Marine System: Sources, disposition, storage, export, and physical and biogeochemical consequences in the Arctic and global oceans. *Journal of Geophysical Research: Biogeosciences*, *121*(3), 675–717.

Clark, P. U., Dyke, A. S., Shakun, J. D., Carlson, A. E., Clark, J., Wohlfarth, B., Mitrovica, J. X., Hostetler, S. W., & McCabe, A. M. (2009). The Last Glacial Maximum. *Science*, *325*(5941), 710–714. https://doi.org/10.1126/science.1172873

Comiso, J. C., & Hall, D. K. (2014). Climate trends in the Arctic as observed from space. *Wiley Interdisciplinary Reviews: Climate Change*, *5*(3), 389–409.

https://doi.org/10.1002/wcc.277

Cook, E. R., Briffa, K. R., Meko, D. M., Graybill, D. A., & Funkhouser, G. (1995). The "segment length curse" in long tree-ring chronology development for palaeoclimatic studies. *The Holocene*, *5*(2), 229–237. https://doi.org/10.1177/095968369500500211

Cook, E. R., & Peters, K. (1997). Calculating unbiased tree-ring indices for the study of climatic and environmental change. *Holocene*, *7*(3), 361–370. https://doi.org/10.1177/095968369700700314

Costard, F., Dupeyrat, L., Gautier, E., & Carey-Gailhardis, E. (2003). Fluvial thermal erosion investigations along a rapidly eroding river bank: Application to the Lena River (Central Siberia). *Earth Surface Processes and Landforms*, *28*(12), 1349–1359. https://doi.org/10.1002/esp.592

Costard, F., Gautier, E., Brunstein, D., Hammadi, J., Fedorov, a., Yang, D., & Dupeyrat, L. (2007). Impact of the global warming on the fluvial thermal erosion over the Lena River in Central Siberia. *Geophysical Research Letters*, *34*(14), 1–4. https://doi.org/10.1029/2007GL030212

Crary, A. P. (1960). Arctic ice island and ice shelf studies: Part II. *Arctic*, *13*(1), 32–50.

Criscitiello, A. S., Das, S. B., Evans, M. J., Frey, K. E., Conway, H., Joughin, I., Medley, B., & Steig, E. J. (2013). Ice sheet record of recent sea-ice behavior and polynya variability in the Amundsen Sea, West Antarctica. *Journal of Geophysical Research: Oceans*, *118*(1), 118–130. https://doi.org/10.1029/2012JC008077

Cronin, T. M., Polyak, L., Reed, D., Kandiano, E. S., Marzen, R. E., & Council, E. a. (2013). A 600-ka Arctic sea-ice record from Mendeleev Ridge based on ostracodes. *Quaternary Science Reviews*, *79*, 157–167. https://doi.org/10.1016/j.quascirev.2012.12.010

Dabney, J., Knapp, M., Glocke, I., Gansauge, M.-T., Weihmann, A., Nickel, B., Valdiosera, C., García, N., Pääbo, S., & Arsuaga, J.-L. (2013). Complete mitochondrial genome sequence of a Middle Pleistocene cave bear reconstructed from ultrashort DNA fragments. *Proceedings of the National Academy of Sciences*, *110*(39), 15758–15763.

Dalaiden, Q., Goosse, H., Lecomte, O., & Docquier, D. (2018). A model to interpret driftwood transport in the Arctic. *Quaternary Science Reviews*, *191*, 89–100. https://doi.org/https://doi.org/10.1016/j.quascirev.2018.05.004

Daly, A. (2007). The Karschau ship, Schleswig-Holstein: Dendrochronological results and timber provenance. *International Journal of Nautical Archaeology*, *36*(1), 155–166.

Daly, A., & Nymoen, P. (2008). The Bøle ship, Skien, Norway—Research history, dendrochronology and provenance. *International Journal of Nautical Archaeology*, *37*(1), 153–170.

Darby, D. a., & Bischof, J. F. (2004). A Holocene record of changing Arctic Ocean ice drift analogous to the effects of the Arctic Oscillation. *Paleoceanography*, *19*(1), 1–9. https://doi.org/10.1029/2003PA000961

de Vernal, A., Gersonde, R., Goosse, H., Seidenkrantz, M.-S. S., & Wolff, E. W. (2013). Sea ice in the paleoclimate system: The challenge of reconstructing sea ice from proxies - an introduction. *Quaternary Science Reviews*, *79*, 1–8. https://doi.org/10.1016/j.quascirev.2013.08.009

De Vernal, A., Hillaire-Marcel, C., Rochon, A., Fréchette, B., Henry, M., Solignac, S., & Bonnet, S. (2013). Dinocyst-based reconstructions of sea ice cover concentration during the Holocene in the Arctic Ocean, the northern North Atlantic Ocean and its adjacent seas. *Quaternary Science Reviews*, *79*, 111–121. https://doi.org/10.1016/j.quascirev.2013.07.006

Deguilloux, M., Pemonge, M., & Petit, R. (2002). Novel perspectives in wood certification and forensics: dry wood as a source of DNA. *Proceedings of the Royal Society of London. Series B: Biological Sciences*, *269*(1495), 1039–1046.

Deser, C., & Teng, H. (2008). Evolution of Arctic sea ice concentration trends and the role of atmospheric circulation forcing, 1979-2007. *Geophysical Research Letters*, *35*(2), 1–5. https://doi.org/10.1029/2007GL032023

Dibner, V. D. (1965). The history of late Pleistocene and Holocene sedimentation in Franz Josef Land. *Transactions of the Scientific Research Institute of the Geology of the Arctic*, *143*, 300–318.

Dieckmann, G. S., & Hellmer, H. H. (2010). The Importance of Sea Ice: An Overview. *Sea Ice: Second Edition*, *2*, 1–22. https://doi.org/10.1002/9781444317145.ch1

Dijkstra, F. a, Breemen, N. Van, Jongmans, A. G., Davies, G. R., & Likens, G. E. (2003). Calcium Weathering in Forested Soils and the Effect of Different Tree Species Calcium weathering in forested soils and the effect of different tree species. *Biogeochemistry*, *62*(3), 253–275.

Ding, Q., Schweiger, A., Battisti, D. S., Johnson, N. C., Wrigglesworth, E. B., Zhang, Q., Harnos, K., Eastman, R., & Steig, E. J. (2017). *Influence of the recent high-latitude atmospheric circulation change on summertime Arctic sea ice*. *March*. https://doi.org/10.1038/NCLIMATE3241

Distel, D. L., Beaudoin, D. J., & Morrill, W. (2002a). Coexistence of multiple proteobacterial endosymbionts in the gills of the wood-boring bivalve Lyrodus pedicellatus (Bivalvia: Teredinidae). *Applied and Environmental Microbiology*, *68*(12), 6292–6299. https://doi.org/10.1128/AEM.68.12.6292-6299.2002

Distel, D. L., Morrill, W., MacLaren-Toussaint, N., Franks, D., & Waterbury, J. (2002b). Teredinibacter turnerae gen. nov., sp. nov., a dinitrogen-fixing, cellulolytic, endosymbiotic γ-proteobacterium isolated from the gills of wood-boring molluscs (Bivalvia: Teredinidae). *International Journal of Systematic and Evolutionary Microbiology*, *52*(6), 2261–2269. https://doi.org/10.1099/ijs.0.02184-0

Divine, D. V, & Dick, C. (2006). Historical variability of sea ice edge position in the Nordic Seas. *Journal of Geophysical Research: Oceans*, *111*(C1).

Douglas, T. a., Blum, J. D., Guo, L., Keller, K., & Gleason, J. D. (2013). Hydrogeochemistry of seasonal flow regimes in the Chena River, a subarctic watershed draining discontinuous permafrost in interior Alaska (USA). *Chemical Geology*, *335*, 48–62. https://doi.org/10.1016/j.chemgeo.2012.10.045

Drake, B. L. (2018). Source & Sourceability: Towards a probabilistic framework for dendroprovenance based on hypothesis testing and Bayesian inference. *Dendrochronologia*, *47*, 38–47.

Drouet, T., Herbauts, J., & Demaiffe, D. (2005). Long-term records of strontium isotopic

composition in tree rings suggest changes in forest calcium sources in the early 20th century. *Global Change Biology*, *11*(11), 1926–1940. https://doi.org/10.1111/j.1365-2486.2005.01034.x

Durante, C., Baschieri, C., Bertacchini, L., Cocchi, M., Sighinolfi, S., Silvestri, M., & Marchetti, A. (2013). Geographical traceability based on 87Sr/86Sr indicator: A first approach for PDO Lambrusco wines from Modena. *Food Chemistry*, *141*(3), 2779–2787. https://doi.org/10.1016/j.foodchem.2013.05.108

Dyke, A. S. (1979). Glacial and sea-level history of southwestern Cumberland Peninsula, Baffin Island, NWT, Canada. *Arctic and Alpine Research*, *11*(2), 179–202.

Dyke, A. S. (1984). *Quaternary geology of Boothia Peninsula and northern District of Keewatin, central Canadian arctic* (Vol. 407). Geological Survey of Canada.

Dyke, A. S. (1993). Glacial and sea level history of Lawther and Griffith islands, Northwest Territories: A hint of tectonics. *Geographie Physique et Quaternaire.*, *47*(2), 133+.

Dyke, A. S. (1998). Holocene delevelling of Devon Island, Arctic Canada: implications for ice sheet geometry and crustal response. *Canadian Journal of Earth Sciences*, *35*(8), 885–904. https://doi.org/10.1139/cjes-35-8-885

Dyke, A. S. (2004). An outline of North American deglaciation with emphasis on central and northern Canada. *Developments in Quaternary Science*, *2*(PART B), 373–424. https://doi.org/10.1016/S1571-0866(04)80209-4

Dyke, A. S., England, J., Reimnitz, E., & Jette, H. (1997). Changes in Driftwood Delivery to the Canadian Arctic Archipelago: The Hypothesis of Postglacial Oscillations of the Transpolar Drift. *Arctic*, *50*(1), 1–16. https://www.jstor.org/stable/40512037

Dyke, A. S., McNeely, R. N., & Hooper, J. (1996). Marine reservoir corrections for bowhead whale radiocarbon age determinations. *Canadian Journal of Earth Sciences*, *33*(12), 1628–1637.

Dyke, A. S., & Morris, T. F. (1990). *Post-Glacial History of the Bowhead Whale and of Driftwood Penetration: Implications for Paleo Climate, Central Canadian Arctic* (Vol. 89, Issue 24). Geological Survey of Canada.

Dyke, A. S., Norris, T. F., & Green, D. E. C. (1991). Postglacial tectonic and sea level history of the central Canadian Arctic. *Bull./Canada. Geol. Survey*.

Dyke, A. S., & Savelle, J. M. (2000). Holocene Driftwood Incursion to Southwestern Victoria Island, Canadian Arctic Archipelago, and Its Significance to Paleoceanography and Archaeology. *Quaternary Research*, *54*(1), 113–120. https://doi.org/10.1006/qres.2000.2141

Dyke, A. S., & Savelle, J. M. (2001). Holocene History of the Bering Sea Bowhead Whale (Balaena mysticetus) in Its Beaufort Sea Summer Grounds off Southwestern Victoria Island, Western Canadian Arctic. *Quaternary Research*, *55*(3), 371–379. https://doi.org/10.1006/qres.2001.2228

Dyke, A. S., & Savelle, J. M. (2003). Surficial Geology, Southern Prince Albert Sound, Victoria Island, Northwest Territories (NTS 87E/4, 87E/5). *Geol. Surv. Can. Open File*.

Dyke, A. S., Savelle, J. M., & Johnson, D. S. (2011). Paleoeskimo demography and holocene sea-level history, Gulf of Boothia, arctic Canada. *Arctic*, *64*(2), 151–168.

Dyke, A. S., Vincent, J. S., Andrews, J. T., Dredge, L. A., & Cowan, W. R. (1989). The Laurentide Ice Sheet and an introduction to the Quaternary geology of the Canadian Shield. In *Quaternary geology of Canada and Greenland* (Vol. 1, pp. 175–312). Geological Survey of Canada Ottawa, Ontario.

Eckstein, D., & Bauch, J. (1969). Beitrag zur Rationalisierung eines dendrochronologischen Verfahrens und zur Analyse seiner Aussagesicherheit. *Forstwissenschaftliches Centralblatt*, *88*(1), 230–250. https://doi.org/10.1007/BF02741777

Eggertsson, O. (1993). Origin of the driftwood on the coasts of Iceland; a dendrochronological study. *Jokull*, *43*, 15–32.

Eggertsson, Ó. (1994a). Driftwood as an indicator of relative changes in the influx of Arctic and Atlantic water into the coastal areas of Svalbard. *Polar Research*, *13*(2), 209–218.

Eggertsson, Ó. (1994b). Mackenzie River driftwood - A dendrochronological study. *Arctic*, *47*(2), 128–136.

Eggertsson, Ó., & Laeyendecker, D. (1995). A dendrochronological study of the origin of driftwood in Frobisher Bay, Baffin Island, NWT, Canada. *Arctic and Alpine Research*, *27*(2), 180–186.

England, J. H. (1976a). Late Quaternary glaciation of the eastern Queen Elizabeth Islands, NWT, Canada: alternative models. *Quaternary Research*, *6*(2), 185–202.

England, J. H. (1976b). Postglacial isobases and uplift curves from the Canadian and Greenland High Arctic. *Arctic and Alpine Research*, *8*(1), 61–78.

England, J. H. (1978). The glacial geology of northeastern Ellesmere Island, NWT, Canada. *Canadian Journal of Earth Sciences*, *15*(4), 603–617.

England, J. H. (1983). Isostatic adjustments in a full glacial sea. *Canadian Journal of Earth Sciences*, *20*(6), 895–917.

England, J. H. (1985). The late Quaternary history of Hall Land, northwest Greenland. *Canadian Journal of Earth Sciences*, *22*, 1394–1408.

England, J. H. (1990). The late Quaternary history of Greely Fiord and its tributaries, west-central Ellesmere Island. *Canadian Journal of Earth Sciences*, *27*(2), 255–270.

England, J. H., Atkinson, N., Bednarski, J., Dyke, A. S., Hodgson, D. A., & Ó Cofaigh, C. (2006). The Innuitian Ice Sheet: configuration, dynamics and chronology. *Quaternary Science Reviews*, *25*(7–8), 689–703. https://doi.org/10.1016/j.quascirev.2005.08.007

England, J. H., & Furze, M. F. A. (2008). New evidence from the western Canadian Arctic Archipelago for the resubmergence of Bering Strait. *Quaternary Research*, *70*(1), 60–67. https://doi.org/10.1016/j.yqres.2008.03.001

England, J. H., Furze, M. F. A., & Doupé, J. P. (2009). Revision of the NW Laurentide Ice Sheet: implications for paleoclimate, the northeast extremity of Beringia, and Arctic Ocean sedimentation. *Quaternary Science Reviews*, *28*(17–18), 1573–1596. https://doi.org/10.1016/j.quascirev.2009.04.006

England, J. H., Lakeman, T. R., Lemmen, D. S., Bednarski, J. M., Stewart, T. G., & Evans, D. J. a. (2008). A millennial-scale record of Arctic Ocean sea ice variability and the demise of the Ellesmere Island ice shelves. *Geophysical Research Letters*, *35*(19), 2–6.

https://doi.org/10.1029/2008GL034470

English, N. B., Betancourt, J. L., Dean, J. S., & Quade, J. (2001). Strontium isotopes reveal distant sources of architectural timber in Chaco Canyon, New Mexico. *Proceedings of the National Academy of Sciences of the United States of America*, *98*(21), 11891–11896. https://doi.org/10.1073/pnas.211305498

Erban Kochergina, Y. V, Novak, M., Erban, V., & Stepanova, M. (2021). 87Sr/86Sr isotope ratios in trees as an archaeological tracer: Limitations of linking plant-biomass and bedrock Sr isotope signatures. *Journal of Archaeological Science*, *133*, 105438. https://doi.org/https://doi.org/10.1016/j.jas.2021.105438

Eriksen, A. M., Gregory, D., & Shashoua, Y. (2015). Selective attack of waterlogged archaeological wood by the shipworm, Teredo navalis and its implications for in-situ preservation. *Journal of Archaeological Science*, *55*, 9–15. https://doi.org/10.1016/j.jas.2014.12.011

Esper, J., Cook, E. R., Krusic, P. J., Peters, K., & Schweingruber, F. H. (2003). Tests of the RCS method for preserving low-frequency variability in long tree-ring chronologies. *Tree-Ring Research*, *59*(2), 81–98.

Eurola, S. (1971). The driftwoods of the Arctic Ocean. *Rep. Kevo Subarctic Research Station*, *7*, 74–80.

Evans, D. J. A. (1988). Glacial geomorphology and Late Quaternary history of Phillips Inlet and the Wootton Peninsula, northwest Ellesmere Island, Canada, Ph.D. thesis, University of Alberta. In *unpublished PhD Thesis*.

Evans, D. J. A., & England, J. (1992). Geomorphological evidence of Holocene climatic change from northwest Ellesmere Island, Canadian high arctic. *The Holocene*, *2*(2), 148–158.

Evans, J. A., Montgomery, J., & Wildman, G. (2009). Isotope domain mapping of 87Sr/86Sr biosphere variation on the Isle of Skye, Scotland. *Journal of the Geological Society*, *166*(4), 617–631. https://doi.org/10.1144/0016-76492008-043

Fagel, N., Not, C., Gueibe, J., Mattielli, N., & Bazhenova, E. (2014). Late Quaternary evolution of sediment provenances in the Central Arctic Ocean: Mineral assemblage, trace element composition and Nd and Pb isotope fingerprints of detrital fraction from the Northern Mendeleev Ridge. *Quaternary Science Reviews*, *92*, 140–154. https://doi.org/10.1016/j.quascirev.2013.12.011

Farnsworth, W. R., Allaart, L., Ingólfsson, Ó., Alexanderson, H., Forwick, M., Noormets, R., Retelle, M., & Schomacker, A. (2020a). Holocene glacial history of Svalbard: Status, perspectives and challenges. *Earth-Science Reviews*, *208*(April), 103249. https://doi.org/10.1016/j.earscirev.2020.103249

Farnsworth, W. R., Blake Jr, W., Guðmundsdóttir, E. R., Ingólfsson, Ó., Kalliokoski, M. H., Larsen, G., Newton, A. J., Óladóttir, B. A., & Schomacker, A. (2020b). Ocean-rafted pumice constrains postglacial relative sea-level and supports Holocene ice cap survival. *Quaternary Science Reviews*, *250*, 106654. https://doi.org/https://doi.org/10.1016/j.quascirev.2020.106654

Fengel, D. (1991). Aging and fossilization of wood and its components. *Wood Science and Technology*, *25*(3), 153–177. https://doi.org/10.1007/BF00223468

Fermé, L. C., Avilés, E. I., & Borrero, L. a. (2015). Tracing Driftwood in Archaeological Contexts: Experimental Data and Anthracological Studies at the Orejas De Burro 1 Site (Patagonia, Argentina). *Archaeometry*, *57*(April), 175–193. https://doi.org/10.1111/arcm.12129

Feyling-Hanssen, R. W. (1955). Stratigraphy of the marine late-pleistocene of Billefjorden, Vestspitsbergen. *Norsk Polurinstitutt*, *107*.

Feyling-Hanssen, R. W., & Olsson, I. (1959). Five radiocarbon datings of Post Glacial shorelines in Central Spitsbergen. *Norsk Geografisk Tidsskrift*, *17*(1–4), 122–131. https://doi.org/10.1080/00291955908551761

Fisher, D. A., Koerner, R. M., Bourgeois, J. C., Zielinski, G., Wake, C. P., Hammer, C. U., Clausen, H. B., Gundestrup, N. S., Johnsen, S. J., Goto-Azuma, K., Hondoh, T., Blake, E., & Gerasimoff, M. (1998). Penny Ice Cap Cores, Baffin Island, Canada, and the Wisconsinan Foxe Dome Connection: Two States of Hudson Bay Ice Cover. *Science*, *279*(5351), 692–695. https://doi.org/10.1126/science.279.5351.692

Forman, S. L. (1990). Post-glacial relative sea-level history of northwestern Spitsbergen, Svalbard. *Geological Society of America Bulletin*, *102*(11), 1580–1590.

Forman, S. L., & Ingólfsson, Ó. (2000). Late Weichselian glacial history and postglacial emergence of Phippsøya, Sjuøyane, northern Svalbard: a comparison of modelled and empirical estimates of a glacial-rebound hinge line. *Boreas*, *29*(1), 16–25. https://doi.org/10.1111/j.1502-3885.2000.tb01197.x

Forman, S. L., Ingölfsson, Ö., Gataullin, V., Manley, W. F., & Lokrantz, H. (1999a). Late Quaternary stratigraphy of western Yamal Peninsula; Russia: New constraints on the configuration of the Eurasian ice sheet. *Geology*, *27*(9), 807–810. https://doi.org/10.1130/0091-7613(1999)027<0807:LQSOWY>2.3.CO;2

Forman, S. L., Lubinski, D. J., Ingólfsson, Ó., Zeeberg, J. J., Snyder, J. A., Siegert, M. J., & Matishov, G. G. (2004). A review of postglacial emergence on Svalbard, Franz Josef Land and Novaya Zemlya, northern Eurasia. *Quaternary Science Reviews*, *23*(11–13), 1391–1434. https://doi.org/10.1016/j.quascirev.2003.12.007

Forman, S. L., Lubinski, D. J., Miller, G. H., Matishov, G. G., Korsun, S., Snyder, J., Herlihy, F., Weihe, R., & Myslivets, V. (1996). Postglacial emergence of western Franz Josef Land, Russia, and retreat of the Barents Sea Ice Sheet. *Quaternary Science Reviews*, *15*(1), 77–90. https://doi.org/10.1016/0277-3791(95)00090-9

Forman, S. L., Lubinski, D. J., Zeeberg, J. J., Polyak, L., Miller, G. H., Matishov, G., & Tarasov, G. (1999b). Postglacial emergence and Late Quaternary glaciation on northern Novaya Zemlya, Arctic Russia. *Boreas*, *28*(1), 133–145. https://doi.org/10.1111/j.1502-3885.1999.tb00210.x

Forman, S. L., Weihe, R., Lubinski, D. J., Tarasov, G., Korsun, S., & Matishov, G. (1997a). Holocene relative sea-level history of Franz Josef Land, Russia. *Geological Society of America Bulletin*, *109*(9), 1116–1133.

Forman, S. L., Weihe, R., Lubinski, D. J., Tarasov, G., Korsun, S., & Matishov, G. (1997b). Holocene relative sea-level history of Franz Josef Land, Russia. *Bulletin of the Geological Society of America*, *109*(9), 1116–1133. https://doi.org/10.1130/0016-7606(1997)109<1116:HRSLHO>2.3.CO;2

Forwick, M., & Vorren, T. O. (2009). Late Weichselian and Holocene sedimentary environments and ice rafting in Isfjorden, Spitsbergen. *Palaeogeography, Palaeoclimatology, Palaeoecology*, *280*(1–2), 258–274. https://doi.org/10.1016/j.palaeo.2009.06.026

Francis, J. A., & Vavrus, S. J. (2012). Evidence linking Arctic amplification to extreme weather in mid-latitudes. *Geophysical Research Letters*, *39*(6), 1–6. https://doi.org/10.1029/2012GL051000

Frei, K. M., & Frei, R. (2011). The geographic distribution of strontium isotopes in Danish surface waters - A base for provenance studies in archaeology, hydrology and agriculture. *Applied Geochemistry*, *26*(3), 326–340. https://doi.org/10.1016/j.apgeochem.2010.12.006

Funck, J., Bataille, C., Rasic, J., & Wooller, M. (2021). A bio-available strontium isoscape for eastern Beringia: a tool for tracking landscape use of Pleistocene megafauna. *Journal of Quaternary Science*, *36*(1), 76–90. https://doi.org/https://doi.org/10.1002/jqs.3262

Funder, S., Goosse, H., Jepsen, H., Kaas, E., Kjær, K. H., Korsgaard, N. J., Larsen, N. K., Linderson, H., Lyså, A., Möller, P., Olsen, J., & Willerslev, E. (2011). A 10,000-year record of Arctic Ocean Sea-ice variability - View from the beach. *Science*, *333*(6043), 747–750. https://doi.org/10.1126/science.1202760

Gärtner, H., Lucchinetti, S., & Schweingruber, F. H. (2015). A new sledge microtome to combine wood anatomy and tree-ring ecology. *IAWA Journal*, *36*(4), 452–459.

Gautier, E., Brunstein, D., Costard, F., & Lodina, R. (2003). Fluvial dynamics in a deep permafrost zone – the case of the middle Lena river (Central Siberia). *Permafrost: Proceedings of the 8th International Conference on Permafrost*, 271–275.

Geer, G. De. (1919). On the Physiographical Evolution of Spitsbergen Explaining the Present Attitude of the Coal-Horizons. *Geografiska Annaler*, *1*, 161. https://doi.org/10.2307/519769

Gelbrich, J., Mai, C., & Militz, H. (2008). Chemical changes in wood degraded by bacteria. *International Biodeterioration and Biodegradation*, *61*(1), 24–32. https://doi.org/10.1016/j.ibiod.2007.06.007

Gersonde, R., & De Vernal, A. (2013). Reconstrution of past sea ice extent. *PAGES News*, *21*(1), 30–31.

Giddings, J. L. (1952). Driftwood and problems of Arctic sea currents. *Proceedings of the American Philosophical Society*, *96*(2), 129–142.

Glazovskiy, A., Näslund, J.-O., & Zale, R. (1992). Deglaciation and Shoreline Displacement on Alexandra Land, Franz Josef Land. *Geografiska Annaler. Series A, Physical Geography*, *74*(4), 283–293. https://doi.org/10.2307/521427

Goitom Asfaha, D., Quétel, C. R., Thomas, F., Horacek, M., Wimmer, B., Heiss, G., Dekant, C., Deters-Itzelsberger, P., Hoelzl, S., Rummel, S., Brach-Papa, C., Van Bocxstaele, M., Jamin, E., Baxter, M., Heinrich, K., Kelly, S., Bertoldi, D., Bontempo, L., Camin, F., … Ueckermann, H. (2011). Combining isotopic signatures of n(87Sr)/n(86Sr) and light stable elements (C, N, O, S) with multi-elemental profiling for the authentication of provenance of European cereal samples. *Journal of Cereal Science*, *53*(2), 170–177. https://doi.org/https://doi.org/10.1016/j.jcs.2010.11.004

Gossett, J. (1996). Arctic research using nuclear submarines. *Oceanographic Literature Review*, *43*(11), 1171.

Gosz, J. R., & Moore, D. I. (1989). Strontium isotope studies of atmospheric inputs to forested watersheds in New Mexico. *Biogeochemistry*, *8*(2), 115–134. https://doi.org/10.1007/BF00001316

Graustein, W. C., & Armstrong, R. L. (1983). The use of strontium-87/strontium-86 ratios to measure atmospheric transport into forested watersheds. *Science*, *219*(4582), 289–292. https://doi.org/10.1126/science.219.4582.289

Gregory, S., Boyer, K. L., & Gurnell, A. M. (2003). Ecology and management of wood in world rivers. *International Conference of Wood in World Rivers (2000: Corvallis, Or.)*.

Grissino-Mayer, H. D., & Fritts, H. C. (1997). The International Tree-Ring Data Bank: an enhanced global database serving the global scientific community. *The Holocene*, *7*(2), 235–238.

Grosswald, M. E. (1963). Raised beaches in Franz Josef Land and the Late–Quaternary history of its ice sheets. *Glatsiologischeskiye Issl*, *9*, 283–293.

Gugerli, F., Parducci, L., & Petit, R. J. (2005). Ancient plant DNA: Review and prospects. *New Phytologist*, *166*(2), 409–418. https://doi.org/10.1111/j.1469-8137.2005.01360.x

Guinn, V. P. (1978). Principles of Isotope Geology. *Nuclear Science and Engineering*, *67*(2), 271–271. https://doi.org/10.13182/nse78-a15446

Haas, C., & Thomas, D. N. (2017). Sea ice thickness distribution. In *Sea ice* (pp. 42–64). Wiley.

Häggblom, A. (1982). Driftwood in Svalbard as an Indicator of Sea Ice Conditions. *Geografiska Annaler. Series A, Physical Geography*, *64*(1/2), 81–94. https://doi.org/10.2307/520496

Hajj, F., Poszwa, A., Bouchez, J., & Guérold, F. (2017). Radiogenic and "stable" strontium isotopes in provenance studies: A review and first results on archaeological wood from shipwrecks. *Journal of Archaeological Science*, *86*, 24–49. https://doi.org/https://doi.org/10.1016/j.jas.2017.09.005

Hammer, Ø., Harper, D. A. T., & Ryan, P. D. (2001). Past: Paleontological statistics software package for education and data analysis. *Palaeontologia Electronica*, *4*(1), 9.

Hattersley-Smith, G., Fuzesy, A., & Evans, S. (1969). *Glacier depths in northern Ellesmere Island: airborne radio echo sounding in 1966*. Defence Research Board. Department of National Defence.

Hellmann, L., Agafonov, L., Churakova Sidorova, O., Düthorn, E., Eggertsson, Ó., Esper, J., Kirdyanov, A. V., Knorre, A. A., Moiseev, P., Myglan, V. S., Nikolaev, A. N., Reinig, F., Schweingruber, F., Solomina, O., Tegel, W., & Büntgen, U. (2016). Regional coherency of boreal forest growth defines Arctic driftwood provenancing. *Dendrochronologia*, *39*, 3–9. https://doi.org/10.1016/j.dendro.2015.12.010

Hellmann, L., Tegel, W., Eggertsson, Ó., Schweingruber, F. H., Blanchette, R. A., Kirdyanov, A. V, Gärtner, H., & Büntgen, U. (2013a). On the importance of anatomical classification in Arctic driftwood research. *Scientific Technical Report STR*, *11*, 160–165.

Hellmann, L., Tegel, W., Eggertsson, Ó., Schweingruber, F. H., Blanchette, R., Kirdyanov, A., Gärtner, H., & Büntgen, U. (2013b). Tracing the origin of Arctic driftwood. *Journal of Geophysical Research: Biogeosciences*, *118*(1), 68–76. https://doi.org/10.1002/jgrg.20022

Hellmann, L., Tegel, W., Geyer, J., Kirdyanov, A. V., Nikolaev, A. N., Eggertsson, Ó., Altman, J., Reinig, F., Morganti, S., Wacker, L., & Büntgen, U. (2017). Dendro-provenancing of Arctic driftwood. *Quaternary Science Reviews*, *162*, 1–11. https://doi.org/10.1016/j.quascirev.2017.02.025

Hellmann, L., Tegel, W., Kirdyanov, A. V., Eggertsson, O., Esper, J., Agafonov, L., Nikolaev, A. N., Knorre, A. A., Myglan, V. S., Sidorova, O. C., Schweingruber, F. H., Nievergelt, D., Verstege, A., & Buntgen, U. (2015). Timber Logging in Central Siberia is the Main Source for Recent Arctic Driftwood. *Arctic, Antarctic, and Alpine Research*, *47*(3), 449–460. https://doi.org/10.1657/AAAR0014-063

Henoch, W. E. S. (1964). Preliminary geomorphological study of a newly discovered Dorset culture site on Melville Island, NWT. *Arctic*, *17*(2), 119–125.

Hillaire-Marcel, C. (1976). La déglaciation et le relèvement isostatique sur la côte est de la baie d'Hudson. *Cahiers de Géographie Du Québec*, *20*(50), 185–220.

Hillaire-Marcel, C., Maccali, J., Not, C., & Poirier, A. (2013). Geochemical and isotopic tracers of Arctic sea ice sources and export with special attention to the Younger Dryas interval. *Quaternary Science Reviews*, *79*, 184–190. https://doi.org/10.1016/j.quascirev.2013.05.001

Hillis, W. E. (1971). Distribution, properties and formation of some wood extractives. *Wood Science and Technology*, *5*(4), 272–289.

Hilmer, M., & Jung, T. (2000). Evidence for a recent change in the link between the North Atlantic Oscillation and Arctic sea ice export. *Geophysical Research Letters*, *27*(7), 989–992.

Hjort, C. (1997). Glaciation, climate history, changing marine levels and the evolution of the Northeast Water Polynya. *Journal of Marine Systems*, *10*(1–4), 23–33.

Hodgson, D. A. (1992). *Quaternary geology of western Melville Island, Northwest Territories*. Geological Survey of Canada Paper 89-21.

Hodgson, D. A., St-Onge, D. A., & Edlund, S. A. (1991). Surficial materials of Hot Weather Creek basin, Ellesmere Island, Northwest Territories. *Current Research, Part E: Geological Survey of Canada, Paper*, *91*, 157–163.

Hole, G. M., & Macias-Fauria, M. (2017). Out of the woods: Driftwood insights into Holocene pan-Arctic sea ice dynamics. *Journal of Geophysical Research: Oceans*, *122*(9), 7612–7629. https://doi.org/10.1002/2017JC013126

Hole, G. M., Rawson, T., Farnsworth, W. R., Schomacker, A., Ingólfsson, Ó., & Macias-Fauria, M. (2021). A Driftwood-Based Record of Arctic Sea Ice During the Last 500 Years From Northern Svalbard Reveals Sea Ice Dynamics in the Arctic Ocean and Arctic Peripheral Seas. *Journal of Geophysical Research: Oceans*, *126*(10). https://doi.org/10.1029/2021jc017563

Holmes, R. L. (1983). *Computer-assisted quality control in tree-ring dating and measurement*.

Holmes, R. M., Coe, M. T., Fiske, G. J., Gurtovaya, T., McClelland, J. W., Shiklomanov, A. I., Spencer, R. G. M., Tank, S. E., & Zhulidov, A. V. (2013). Climate change impacts on the hydrology and biogeochemistry of Arctic rivers. *Climatic Change and Global Warming of Inland Waters*, 1–26.

Holt, E., Evans, J. A., & Madgwick, R. (2021). Strontium (87Sr/86Sr) mapping: A critical review of methods and approaches. *Earth-Science Reviews*, *216*, 103593. https://doi.org/10.1016/j.earscirev.2021.103593

Hoogewerff, J. A., Reimann, C., Ueckermann, H., Frei, R., Frei, K. M., van Aswegen, T., Stirling, C., Reid, M., Clayton, A., Ladenberger, A., Albanese, S., Andersson, M., Baritz, R., Batista, M. J., Bel-lan, A., Birke, M., Cicchella, D., Demetriades, A., De Vivo, B., … Zomeni, Z. (2019). Bioavailable 87Sr/86Sr in European soils: A baseline for provenancing studies. *Science of The Total Environment*, *672*, 1033–1044. https://doi.org/https://doi.org/10.1016/j.scitotenv.2019.03.387

Hopkins, D. M., Smith, P. A., & Matthews, J. V. (1981). Dated wood from Alaska and the Yukon: Implications for forest refugia in Beringia. *Quaternary Research*, *15*(3), 217–249. https://doi.org/http://dx.doi.org/10.1016/0033-5894(81)90028-4

Hoppe, G., Schytt, V., Anders Häggblom, & Osterholm, H. (1969). Studies of the Glacial History of Hopen (Hopen Island). *Geografiska Annaler.*, *51*(4), 185–192.

Hughes, A. L. C., Gyllencreutz, R., Lohne, Ø. S., Mangerud, J., & Svendsen, J. I. (2016). The last Eurasian ice sheets - a chronological database and time-slice reconstruction, DATED-1. *Boreas*, *45*(1), 1–45. https://doi.org/10.1111/bor.12142

Hughes, M. K., Milsom, S. J., & Leggett, P. A. (1981). Sapwood estimates in the interpretation of tree-ring dates. *Journal of Archaeological Science*, *8*(4), 381–390.

Hutchings, J. K., & Rigor, I. G. (2012). Role of ice dynamics in anomalous ice conditions in the Beaufort Sea during 2006 and 2007. *Journal of Geophysical Research: Oceans*, *117*(5), 1–14. https://doi.org/10.1029/2011JC007182

Ingólfsson, Ó., & Landvik, J. Y. (2013). The Svalbard–Barents Sea ice-sheet – Historical, current and future perspectives. *Quaternary Science Reviews*, *64*, 33–60. https://doi.org/https://doi.org/10.1016/j.quascirev.2012.11.034

Ives, P. C., Levin, B., Robinson, R. D., & Rubin, M. (1964). US Geological Survey radiocarbon dates VII. *Radiocarbon*, *6*, 37–76.

Jakobsson, M., Mayer, L., Coakley, B., Dowdeswell, J. A., Forbes, S., Fridman, B., Hodnesdal, H., Noormets, R., Pedersen, R., Rebesco, M., Schenke, H. W., Zarayskaya, Y., Accettella, D., Armstrong, A., Anderson, R. M., Bienhoff, P., Camerlenghi, A., Church, I., Edwards, M., … Weatherall, P. (2012). The International Bathymetric Chart of the Arctic Ocean (IBCAO) Version 3.0. *Geophysical Research Letters*, *39*(12), 1–6. https://doi.org/10.1029/2012GL052219

Jane, F. W. (2013). The structure of wood. *The Structure of Wood., 2nd ed.(rev.)*, 153–178. https://doi.org/10.1090/gsm/146/03

Jernas, P., Klitgaard Kristensen, D., Husum, K., Wilson, L., & Koç, N. (2013). Palaeoenvironmental changes of the last two millennia on the western and northern Svalbard shelf. *Boreas*, *42*(1), 236–255. https://doi.org/10.1111/j.1502-3885.2012.00293.x

Jessen, S. P., Rasmussen, T. L., Nielsen, T., & Solheim, A. (2010). A new Late Weichselian and Holocene marine chronology for the western Svalbard slope 30,000-0 cal years BP. *Quaternary Science Reviews*, *29*(9–10), 1301–1312. https://doi.org/10.1016/j.quascirev.2010.02.020

Jiang, Y. (2011). Strontium isotope geochemistry of groundwater affected by human activities in Nandong underground river system, China. *Applied Geochemistry*, *26*(3), 371–379. https://doi.org/10.1016/j.apgeochem.2010.12.010

Johansen, S. (1998). The origin and age of driftwood on Jan Mayen. *Polar Research*, *17*(2), 125–146. https://doi.org/10.3402/polar.v17i2.6614

Johansen, S. (1999). Origin of driftwood in north Norway and its relevance for transport routes of drift ice and pollution to the Barents Sea. *Science of the Total Environment*, *231*(2–3), 201–225. https://doi.org/10.1016/S0048-9697(99)00101-1

Johansen, S. (2001). A dendrochronological analysis of driftwood in the Northern Dvina delta and on northern Novaya Zemlya. *Journal of Geophysical Research*, *106*(C9), 19929. https://doi.org/10.1029/1999JC000023

Jones, P. D., & Mann, M. E. (2004). Climate over past millennia. *Reviews of Geophysics*, *42*(2), n/a-n/a. https://doi.org/10.1029/2003RG000143

Kamenov, G. D., Perfit, M. R., Lewis, J. F., Goss, A. R., Arévalo, R., & Shuster, R. D. (2011). Ancient lithospheric source for Quaternary lavas in Hispaniola. *Nature Geoscience*, *4*(8), 554–557. https://doi.org/10.1038/ngeo1203

Kaufman, D. S., Ager, T. A., Anderson, N. J., Anderson, P. M., Andrews, J. T., Bartlein, P. J., Brubaker, L. B., Coats, L. L., Cwynar, L. C., Duvall, M. L., Dyke, A. S., Edwards, M. E., Eisner, W. R., Gajewski, K., Geirsdóttir, A., Hu, F. S., Jennings, A. E., Kaplan, M. R., Kerwin, M. W., … Wolfe, B. B. (2004). Holocene thermal maximum in the western Arctic (0-180°W). *Quaternary Science Reviews*, *23*(5–6), 529–560. https://doi.org/10.1016/j.quascirev.2003.09.007

Keller, K., Blum, J. D., & Kling, G. W. (2010). Stream geochemistry as an indicator of increasing permafrost thaw depth in an arctic watershed. *Chemical Geology*, *273*(1–2), 76–81. https://doi.org/10.1016/j.chemgeo.2010.02.013

Kelly, M. R., & Bennike, O. (1992). The Quaternary geology of central North Greenland. *Rapport Grønlands Geologiske Undersøgelse*, *153*, 34.

Kennedy, M. J., Chadwick, O. a., Vitousek, P. M., Derry, L. a., & Hendricks, D. M. (1998). Changing sources of base cations during ecosystem development, Hawaiian Islands. *Geology*, *26*(11), 1015–1018. https://doi.org/10.1130/0091-7613(1998)026<1015:CSOBCD>2.3.CO

Kim, Y. S., & Singh, A. P. (2000). Micromorphological characteristics of wood biodegradation in wet environments: A review. *IAWA Journal*, *21*(2), 135–155. https://doi.org/10.1163/22941932-90000241

Kindle, E. M. (1921). Mackenzie River driftwood. *Geographical Review*, *11*(1), 50–53.

Kinnard, C., Zdanowicz, C. M., Fisher, D. a., Isaksson, E., de Vernal, A., & Thompson, L. G. (2011). Reconstructed changes in Arctic sea ice over the past 1,450 years. *Nature*, *479*(7374), 509–512. https://doi.org/10.1038/nature10581

Kinnard, C., Zdanowicz, C. M., Koerner, R. M., & Fisher, D. A. (2008). A changing Arctic seasonal ice zone: Observations from 1870–2003 and possible oceanographic consequences. *Geophysical Research Letters*, *35*(2).

Kircher, M. (2012). Analysis of high-throughput ancient DNA sequencing data. In *Ancient DNA* (pp. 197–228). Springer.

Knuth, E. (1967). *Archaeology of the Musk-ox Way* (Issue 5). École pratique des hautes études, Sorbonne.

Koch, J. (2009). Improving age estimates for late Holocene glacial landforms using dendrochronology–Some examples from Garibaldi Provincial Park, British Columbia. *Quaternary Geochronology*, *4*(2), 130–139.

Koerner, R. M. (2005). Mass balance of glaciers in the Queen Elizabeth Islands, Nunavut, Canada. *Annals of Glaciology*, *42*(1), 417–423.

Koerner, R. M., & Paterson, W. S. B. (1974). Analysis of a core through the Meighen Ice Cap, Arctic Canada, and its paleoclimatic implications. *Quaternary Research*, *4*(3), 253–263.

Kovaleva, G. A. (1974). Modern movement of Admirality Peninsula (northern island of Novaya Zemlya). *Glaciotectonc Conditions for the Search for Resources on the Shelf of the Arctic Ocean. NI. IGA, Leningrad*, 87–93.

Kramer, N., & Wohl, E. (2017). Rules of the road: A qualitative and quantitative synthesis of large wood transport through drainage networks. *Geomorphology*, *279*, 74–97.

Kwok, R., & Rothrock, D. A. (1999). Variability of Fram Strait ice flux and North Atlantic oscillation. *Journal of Geophysical Research: Oceans*, *104*(C3), 5177–5189.

Kwok, R., & Rothrock, D. A. (2009). Decline in Arctic sea ice thickness from submarine and ICESat records: 1958-2008. *Geophysical Research Letters*, *36*(15). https://doi.org/10.1029/2009GL039035

Kwok, R., Spreen, G., & Pang, S. (2013). Arctic sea ice circulation and drift speed: Decadal trends and ocean currents. *Journal of Geophysical Research: Oceans*, *118*(5), 2408–2425. https://doi.org/10.1002/jgrc.20191

Laffoon, J. E., Davies, G. R., Hoogland, M. L. P., & Hofman, C. L. (2012). Spatial variation of biologically available strontium isotopes (87Sr/86Sr) in an archipelagic setting: a case study from the Caribbean. *Journal of Archaeological Science*, *39*(7), 2371–2384. https://doi.org/10.1016/j.jas.2012.02.002

Landvik, J. Y., Bondevik, S., Elverhøi, A., Fjeldskaar, W., Mangerud, J. A. N., Salvigsen, O., Siegert, M. J., Svendsen, J. I., & Vorren, T. O. (1998). The last glacial maximum of Svalbard and the Barents Sea area: ice sheet extent and configuration. *Quaternary Science Reviews*, *17*(1), 43–75.

Landvik, J. Y., & Salvigsen, O. (1987). The Late Weichselian and Holocene shoreline displacement on the west???central coast of Svalbard. *Polar Research*, *5*(1), 29–44. https://doi.org/10.1111/j.1751-8369.1987.tb00353.x

Landvik, J. Y., Weidick, A., & Hansen, A. (2001). The glacial history of the Hans Tausen Iskappe and the last glaciation of Peary Land, North Greenland. *Meddelelser Om Grønland, Geoscience*, *39*(April), 27–44.

Lecavalier, B. S., Fisher, D. A., Milne, G. A., Vinther, B. M., Tarasov, L., Huybrechts, P., Lacelle, D., Main, B., Zheng, J., & Bourgeois, J. (2017). High Arctic Holocene temperature record from the Agassiz ice cap and Greenland ice sheet evolution. *Proceedings of the National Academy of Sciences*, 201616287.

Lehner, F., Born, A., Raible, C. C., & Stocker, T. F. (2013). Amplified Inception of European Little Ice Age by Sea Ice–Ocean–Atmosphere Feedbacks. *Journal of Climate*, *26*(19), 7586–7602. https://doi.org/10.1175/JCLI-D-12-00690.1

Lemmen, D. S. (1988). *The glacial history of Marvin Peninsula, northern Ellesmere Island, and Ward Hunt Island, High Arctic Canada*.

Lendvay, B., Hartmann, M., Brodbeck, S., Nievergelt, D., Reinig, F., Zoller, S., Parducci, L., Gugerli, F., Büntgen, U., & Sperisen, C. (2018). Improved recovery of ancient DNA from subfossil wood – application to the world's oldest Late Glacial pine forest. *New Phytologist*, *217*(4), 1737–1748. https://doi.org/10.1111/nph.14935

Lepp, N. W. (1975). The potential of tree-ring analysis for monitoring heavy metal pollution patterns. *Environmental Pollution (1970)*, *9*(1), 49–61. https://doi.org/10.1016/0013-9327(75)90055-5

Levine, J. G., Yang, X., Jones, A. E., & Wolff, E. W. (2014). Sea salt as an ice core proxy for past sea ice extent: A process-based model study. *Journal of Geophysical Research: Atmospheres*, *119*(9), 5737–5756. https://doi.org/10.1002/2013JD020925

Lewis, J., Pike, A. W. G., Coath, C. D., & Evershed, R. P. (2017). Strontium concentration, radiogenic (87Sr/86Sr) and stable (δ88Sr) strontium isotope systematics in a controlled feeding study. *Science and Technology of Archaeological Research*, *3*(1), 45–57. https://doi.org/10.1080/20548923.2017.1303124

Lindahl, T. (1993). Instability and decay of the primary structure of DNA. *Nature*, *362*(6422), 709–715. https://doi.org/10.1038/362709a0

Linderholm, H. W., Gunnarson, B. E., Fuentes, M., Büntgen, U., & Hormes, A. (2021). The origin of driftwood on eastern and south-western Svalbard. *Polar Science*, 100658. https://doi.org/https://doi.org/10.1016/j.polar.2021.100658

Liu, B., Yang, D., Ye, B., & Berezovskaya, S. (2005). Long-term open-water season stream temperature variations and changes over Lena River Basin in Siberia. *Global and Planetary Change*, *48*(1–3), 96–111.

Loader, N. J., Robertson, I., & McCarroll, D. (2003). Comparison of stable carbon isotope ratios in the whole wood, cellulose and lignin of oak tree-rings. *Palaeogeography, Palaeoclimatology, Palaeoecology*, *196*(3–4), 395–407. https://doi.org/10.1016/S0031-0182(03)00466-8

Lowdon, J. A., & Blake Jr, W. (1973). Geological Survey of Canada Radiocarbon Dates XIII. *Geological Survey of Canada*, 61.

Lowdon, J. A., & Blake Jr, W. (1978). Geological Survey of Canada radiocarbon dates XVIII. *Geological Survey of Canada*, *6*, 167–181. https://doi.org/10.1126/science.ns-6.149S.521-a

Lowdon, J. A., & Blake Jr, W. (1979). *Geological Survey of Canada radiocarbon dates XIX: Geological Survey of Canada Paper 79–7*. Ottawa.

Lubinski, D. J. (1998). *Latest Pleistocene and Holocene Paleoenvironments of the Franz Josef Land Region, Northern Barents Sea, Arctic Russia*. University of Colorado at Boulder.

Lubinski, D. J., Forman, S. L., & Miller, G. H. (1999). Holocene glacier and climate fluctuations on Franz Josef Land, Arctic Russia, 80°N. *Quaternary Science Reviews*, *18*(1), 85–108. https://doi.org/10.1016/S0277-3791(97)00105-4

Lukaszewskp, Z., Zembrzuskp, W., Siwecki, R., & OpydoJadwiga. (1988). The effect of industrial pollution on Zinc, Cadmium and Copper concentration in the xylem rings of Scot's pine (Pinus sylvestris L.) and in the soil. *Trees - Structure and Function*, *2*, 1–6.

MacDonald, G. M., Kremenetski, K. V, & Beilman, D. W. (2008). Climate change and the northern Russian treeline zone. *Philosophical Transactions of the Royal Society of London. Series B, Biological Sciences*, *363*(1501), 2285–2299. https://doi.org/10.1098/rstb.2007.2200

MacDonald, G. M., Velichko, A. A., Kremenetski, C. V., Borisova, O. K., Goleva, A. A., Andreev, A. A., Cwynar, L. C., Riding, R. T., Forman, S. L., Edwards, T. W. D. D., Aravena, R., Hammarlund, D., Szeicz, J. M., & Gattaulin, V. N. (2000). Holocene treeline history and climate change across northern Eurasia. *Quaternary Research*, *53*(3), 302–311. https://doi.org/https://doi.org/10.1006/qres.1999.2123

Macias-Fauria, M., Grinsted, A., Helama, S., Moore, J., Timonen, M., Martma, T., Isaksson, E., & Eronen, M. (2010). Unprecedented low twentieth century winter sea ice extent in the Western Nordic Seas since A.D. 1200. *Climate Dynamics*, *34*(6), 781–795. https://doi.org/10.1007/s00382-009-0610-z

Macias-Fauria, M., & Post, E. (2018). Effects of sea ice on Arctic biota. *Biology Letters*, *14*(5), 20170702. https://doi.org/10.1098/rsbl.2018.0265

Madgwick, R., Lamb, A. L., Sloane, H., Nederbragt, A. J., Albarella, U., Pearson, M. P., & Evans, J. A. (2019). Multi-isotope analysis reveals that feasts in the Stonehenge environs and across Wessex drew people and animals from throughout Britain. *Science Advances*, *5*(3), eaau6078.

Mahoney, A. R., Hutchings, J. K., Eicken, H., & Haas, C. (2019). Changes in the thickness and circulation of multiyear ice in the Beaufort Gyre determined from pseudo-Lagrangian methods from 2003–2015. *Journal of Geophysical Research: Oceans*, *124*(8), 5618–5633.

Mann, M. E., Zhang, Z., Rutherford, S., Bradley, R. S., Hughes, M. K., Shindell, D., Ammann, C., Faluvegi, G., & Ni, F. (2009). Global Signatures and Dynamical Origins of the Little Ice Age and Medieval Climate Anomaly. *Science*, *326*(5957), 1256 LP – 1260. http://science.sciencemag.org/content/326/5957/1256.abstract

Marthinussen, M. (1962). 14C-datings referring to shore lines, transgressions, and glacial substages in northern Norway. *Norsk Geologisk Undersøkelse*, *215*, 37–67.

Maslanik, J. A., Serreze, M. C., & Barry, R. G. (1996). Recent decreases in Arctic summer ice cover and linkages to atmospheric circulation anomalies. *Geophysical Research Letters*, *23*(13), 1677–1680. https://doi.org/10.1029/96GL01426

Maslowski, W., Clement Kinney, J., Higgins, M., & Roberts, A. (2012). The Future of Arctic Sea Ice. *Annual Review of Earth and Planetary Sciences*, *40*(1), 625–654.

https://doi.org/10.1146/annurev-earth-042711-105345

Mason, O. K., & Beget, J. E. (1991). Late Holocene flood history of the Tanana River, Alaska Quaternary. *Arctic and Alpine Research*, *23*(4), 392–403.

Maurer, A. F., Galer, S. J. G., Knipper, C., Beierlein, L., Nunn, E. V., Peters, D., Tütken, T., Alt, K. W., & Schöne, B. R. (2012). Bioavailable 87Sr/ 86Sr in different environmental samples - Effects of anthropogenic contamination and implications for isoscapes in past migration studies. *Science of the Total Environment*, *433*, 216–229. https://doi.org/10.1016/j.scitotenv.2012.06.046

Mauritsen, T. (2016). Arctic climate change: Greenhouse warming unleashed. *Nature Geosci*, *9*(4), 271–272. http://dx.doi.org/10.1038/ngeo2677

Mayewski, P. a, Meeker, L. D., Twickler, M. S., Lyons, W. B., & Prentice, M. (1997). Major features and forcing of high latitude northern hemisphere atmospheric circulation using a 110,000 year long glaciochemical series. *Journal of Geophysical Research*, *102*(C12), 26,345-26,366.

McLaren, A. S. (1989). The under-ice thickness distribution of the Arctic Basin as recorded in 1958 and 1970. *Journal of Geophysical Research: Oceans (1978–2012)*, *94*(C4), 4971–4983. https://doi.org/10.1029/JC094iC04p04971

McLaren, P., & Barnett, D. M. (1978). Holocene emergence of the south and east coasts of Melville Island, Queen Elizabeth Islands, Northwest Territories, Canada. *Arctic*, 415–427.

McNeely, R. N. (2005). Geological Survey of Canada radiocarbon dates XXXIV. *Geological Survey of Canada*, 113.

McNeely, R. N. (2006). Geological Survey of Canada radiocarbon dates XXXV. *Current Research*.

McNeely, R. N., & McCuaig, S. (1991). *Geological Survey of Canada radiocarbon dates XXIX*.

Mette, M. J., Wanamaker Jr, A. D., Retelle, M. J., Carroll, M. L., Andersson, C., & Ambrose Jr, W. G. (2021). Persistent multidecadal variability since the 15th century in the southern Barents Sea derived from annually resolved shell-based records. *Journal of Geophysical Research: Oceans*, e2020JC017074.

Mielke, J. E., & Long, A. (1969). Smithsonian Institution Radiocarbon Measurements V. *Radiocarbon*, *11*(01), 163–182.

Miller, E. K., Blum, J. D., & Friedland, A. J. (1993). Determination of soil exchangeable-cation loss and weathering rates using Sr isotopes. *Nature*, *362*(6419), 438–441. https://doi.org/10.1038/362438a0

Miller, O. L., Kip, D., Fernandez, D. P., Cerling, T. E., & Bowling, D. R. (2014). Applied Geochemistry Evaluating the use of strontium isotopes in tree rings to record the isotopic signal of dust deposited on the Wasatch Mountains. *Applied Geochemistry*, *50*, 53–65. https://doi.org/10.1016/j.apgeochem.2014.08.004

Montgomery, J., Evans, J. a., & Cooper, R. E. (2007). Resolving archaeological populations with Sr-isotope mixing models. *Applied Geochemistry*, *22*(7), 1502–1514. https://doi.org/10.1016/j.apgeochem.2007.02.009

Mooney, D. E. (2018). Does the 'Marine Signature' of Driftwood Persist in the Archaeological Record? An Experimental Case Study from Iceland. *Environmental Archaeology*, *23*(3), 217–227. https://doi.org/10.1080/14614103.2017.1377404

Moore, G., Tessler, M., Cunningham, S. W., Betancourt, J., & Harbert, R. (2020). Paleo-metagenomics of North American fossil packrat middens: Past biodiversity revealed by ancient DNA. *Ecology and Evolution*, *10*(5), 2530–2544.

Mörner, N.-A., Solheim, J.-E., Humlum, O., & Falk-Petersen, S. (2020). Changes in Barents Sea ice Edge Positions in the Last 440 years: A Review of Possible Driving Forces. *International Journal of Astronomy and Astrophysics*, *10*(02), 97.

Müller, J., Wagner, A., Fahl, K., Stein, R., Prange, M., & Lohmann, G. (2011). Towards quantitative sea ice reconstructions in the northern North Atlantic: A combined biomarker and numerical modelling approach. *Earth and Planetary Science Letters*, *306*(3–4), 137–148. https://doi.org/10.1016/j.epsl.2011.04.011

Müller, J., Werner, K., Stein, R. R., Fahl, K., Moros, M., & Jansen, E. (2012). Holocene cooling culminates in sea ice oscillations in Fram Strait. *Quaternary Science Reviews*, *47*, 1–14. https://doi.org/10.1016/j.quascirev.2012.04.024

Naiman, Z., Quade, J., & Patchett, P. J. (2000). Isotopic evidence for eolian recycling of pedogenic carbonate and variations in carbonate dust sources throughout the southwest United States. *Geochimica et Cosmochimica Acta*, *64*(18), 3099–3109. https://doi.org/10.1016/S0016-7037(00)00410-5

Näslund, J.-O., Zale, R., & Glazovskiy, A. (1994). The mid Holocene transgression on Alexandra Land, Franz Josef Land, Russia. *Geografiska Annaler: Series A, Physical Geography*, *76*(1–2), 97–101.

Négrel, P., Petelet-Giraud, E., & Widory, D. (2004). Strontium isotope geochemistry of alluvial groundwater: a tracer for groundwater resources characterisation. *Hydrology and Earth System Sciences*, *8*(5), 959–972. https://doi.org/10.5194/hess-8-959-2004

Nicholls, M., Wesche, G., Bring, A., Carmack, E., Holland, M., Instanes, A., Johansson, M., Mård, J., Prowse, T., Vihma, T., & Wrona, F. J. (2016). The Arctic freshwater system in a changing Climate. *CliC/AMAP/IASC Assessment Report*, 28 pp.

Nixon, F. C., England, J. H., Lajeunesse, P., & Hanson, M. A. (2014). Deciphering patterns of postglacial sea level at the junction of the Laurentide and Innuitian Ice Sheets, western Canadian High Arctic. *Quaternary Science Reviews*, *91*, 165–183. https://doi.org/10.1016/j.quascirev.2013.07.005

Nixon, F. C., England, J. H., Lajeunesse, P., & Hanson, M. A. (2016). An 11 000-year record of driftwood delivery to the western Queen Elizabeth Islands, Arctic Canada. *Boreas*, *45*(3), 494–507. https://doi.org/10.1111/bor.12165

Nordenskiöld, A. E. (1866). *Utkast till Spetsbergens geologi*.

Norwegian Polar Institute. (2014). Kartdata Svalbard 1:100 000 (S100 Kartdata) / Map Data [Data set]. *Norwegian Polar Institute*. https://doi.org/https://doi.org/10.21334/npolar.2014.645336c7

Nydal, R. (1960). Trondheim Natural Radiocarbon Measurements II. *Radiocarbon*, *2*, 82–96. https://doi.org/DOI: 10.1017/S1061592X00020627

Ó Cofaigh, C. (1999). Holocene emergence and shoreline delevelling, southern Eureka Sound, high Arctic Canada. *Géographie Physique et Quaternaire*, *53*(2), 235–247.

Ogilvie, A. E. J., & Jónsdóttir, I. (2000). Sea ice, climate, and Icelandic fisheries in the eighteenth and nineteenth centuries. *Arctic*, *53*(4), 383–394.

Olsson, M. T., & Melkerud, P.-A. (2000). Weathering in three podzolized pedons on glacial deposits in northern Sweden and central Finland. *Geoderma*, *94*(2), 149–161. https://doi.org/https://doi.org/10.1016/S0016-7061(99)00081-6

Orlando, L., Allaby, R., Skoglund, P., Der Sarkissian, C., Stockhammer, P. W., Ávila-Arcos, M. C., Fu, Q., Krause, J., Willerslev, E., & Stone, A. C. (2021). Ancient DNA analysis. *Nature Reviews Methods Primers*, *1*(1), 1–26.

Orlando, L., Gilbert, M. T. P., & Willerslev, E. (2015). Reconstructing ancient genomes and epigenomes. *Nature Reviews Genetics*, *16*(7), 395–408.

Orlando, L., Ginolhac, A., Zhang, G., Froese, D., Albrechtsen, A., Stiller, M., Schubert, M., Cappellini, E., Petersen, B., & Moltke, I. (2013). Recalibrating Equus evolution using the genome sequence of an early Middle Pleistocene horse. *Nature*, *499*(7456), 74–78.

Overland, J. E., Dethloff, K., Francis, J. A., Hall, R. J., Hanna, E., Kim, S.-J., Screen, J. A., Shepherd, T. G., & Vihma, T. (2016). Nonlinear response of mid-latitude weather to the changing Arctic. *Nature Clim. Change*, *6*(11), 992–999. http://dx.doi.org/10.1038/nclimate3121

Overland, J. E., & Wang, M. (2010). Large-scale atmospheric circulation changes are associated with the recent loss of Arctic sea ice. *Tellus, Series A: Dynamic Meteorology and Oceanography*, *62*(1), 1–9. https://doi.org/10.1111/j.1600-0870.2009.00421.x

Overland, J. E., Wang, M., Walsh, J. E., & Stroeve, J. C. (2013). Future Arctic climate changes : Adaptation and mitigation time scales. *Earth's Future*, *2*, 68–74. https://doi.org/10.1002/2013EF000162.Received

Overland, J. E., Wood, K. R., & Wang, M. (2011). Warm Arctic-cold continents: Climate impacts of the newly open arctic sea. *Polar Research*, *30*(SUPPL.1), 1–14. https://doi.org/10.3402/polar.v30i0.15787

Owczarek, P. (2010). Dendrochronological dating of geomorphic processes in the High Arctic. *Landform Analysis*, *14*, 45–56.

Pääbo, S., Poinar, H., Serre, D., Jaenicke-Despres, V., Hebler, J., Rohland, N., Kuch, M., Krause, J., Vigilant, L., & Hofreiter, M. (2004). Genetic analyses from ancient DNA. *Annual Review of Genetics*, *38*, 645–679. https://doi.org/10.1146/annurev.genet.37.110801.143214

Panteleev, G., Proshutinsky, A., Kulakov, M., Nechaev, D. A., & Maslowski, W. (2007). Investigation of the summer Kara Sea circulation employing a variational data assimilation technique. *Journal of Geophysical Research: Oceans*, *112*(C4).

Park, H., Watanabe, E., Kim, Y., Polyakov, I., Oshima, K., Zhang, X., Kimball, J. S., & Yang, D. (2020). Increasing riverine heat influx triggers Arctic sea ice decline and oceanic and atmospheric warming. *Science Advances*, *6*(45), eabc4699. https://doi.org/10.1126/sciadv.abc4699

Parkinson, C. L., & Comiso, J. C. (2013). On the 2012 record low Arctic sea ice cover:

Combined impact of preconditioning and an August storm. *Geophysical Research Letters*, *40*(7), 1356–1361. https://doi.org/10.1002/grl.50349

Patton, H., Hubbard, A., Andreassen, K., Auriac, A., Whitehouse, P. L., Stroeven, A. P., Shackleton, C., Winsborrow, M., Heyman, J., & Hall, A. M. (2017). Deglaciation of the Eurasian ice sheet complex. *Quaternary Science Reviews*, *169*, 148–172.

Pavlov, V. K., & Pfirman, S. L. (1995). Hydrographic structure and variability of the Kara Sea: Implications for pollutant distribution. *Deep-Sea Research Part II*, *42*(6), 1369–1390. https://doi.org/10.1016/0967-0645(95)00046-1

Pawłowska, J., Łącka, M., Kucharska, M., Pawlowski, J., & Zajączkowski, M. (2020). Multiproxy evidence of the Neoglacial expansion of Atlantic Water to eastern Svalbard. *Climate of the Past*, *16*(2).

Pinta, É., Pacheco-Forés, S. I., Wallace, E. P., & Knudson, K. J. (2021). Provenancing wood used in the Norse Greenlandic settlements: A biogeochemical study using hydrogen, oxygen, and strontium isotopes. *Journal of Archaeological Science*, *131*, 105407. https://doi.org/https://doi.org/10.1016/j.jas.2021.105407

Plomion, C., Leprovost, G., & Stokes, A. (2001). Wood formation in trees. *Plant Physiology*, *127*(4), 1513–1523.

Pokrovsky, O. S., Schott, J., Kudryavtzev, D. I., & Dupré, B. (2005). Basalt weathering in Central Siberia under permafrost conditions. *Geochimica et Cosmochimica Acta*, *69*(24), 5659–5680. https://doi.org/https://doi.org/10.1016/j.gca.2005.07.018

Polyak, L., Alley, R. B., Andrews, J. T., Brigham-Grette, J., Cronin, T. M., Darby, D. A., Dyke, A. S., Fitzpatrick, J. J., Funder, S., Holland, M., Jennings, A. E., Miller, G. H., O'Regan, M., Savelle, J., Serreze, M., St. John, K., White, J. W. C., & Wolff, E. (2010). History of sea ice in the Arctic. *Quaternary Science Reviews*, *29*(15–16), 1757–1778. https://doi.org/10.1016/j.quascirev.2010.02.010

Post, E., & Høye, T. T. (2013). Advancing the long view of ecological change in tundra systems. *Philosophical Transactions of the Royal Society of London. Series B, Biological Sciences*, *368*(1624), 20120477. https://doi.org/10.1098/rstb.2012.0477

Poszwa, A., Ferry, B., Dambrine, E., & Pollier, B. (2004). Variations of bioavailable Sr concentration and 87Sr/86Sr ratio in boreal forest ecosystems. *Biogeochemistry*, *67*, 1–20. http://link.springer.com/article/10.1023/B:BIOG.0000015162.12857.3e

Preston, R. S., Person, E., & Deevey, E. S. (1955). Yale natural radiocarbon measurements II. *Science*, *122*, 954–960.

Raiber, M., Webb, J. a., & Bennetts, D. a. (2009). Strontium isotopes as tracers to delineate aquifer interactions and the influence of rainfall in the basalt plains of southeastern Australia. *Journal of Hydrology*, *367*(3–4), 188–199. https://doi.org/10.1016/j.jhydrol.2008.12.020

Randriamazaoro, R., Dupeyrat, L., Costard, F., & Gailhardis, E. C. (2007). Fluvial thermal erosion: Heat balance integral method. *Earth Surface Processes and Landforms*, *32*(12), 1828–1840.

Rasmussen, T. L., & Thomsen, E. (2014). Brine formation in relation to climate changes and ice retreat during the last 15,000years in Storfjorden, Svalbard, 76-78N. *Paleoceanography*, *29*(10), 911–929. https://doi.org/10.1002/2014PA002643

Rasmussen, T. L., Thomsen, E., Ślubowska, M. A., Jessen, S., Solheim, A., & Koç, N. (2007). Paleoceanographic evolution of the SW Svalbard margin (76°N) since 20,000 14C yr BP. *Quaternary Research*, *67*(1), 100–114. https://doi.org/10.1016/j.yqres.2006.07.002

Reynolds, A. C., Betancourt, J. L., Quade, J., Patchett, P. J., Dean, J. S., & Stein, J. (2005). 87Sr/86Sr sourcing of ponderosa pine used in Anasazi great house construction at Chaco Canyon, New Mexico. *Journal of Archaeological Science*, *32*(7), 1061–1075. https://doi.org/10.1016/j.jas.2005.01.016

Rich, S., Manning, S. W., Degryse, P., Vanhaecke, F., & Van Lerberghe, K. (2012). Strontium isotopic and tree-ring signatures of Cedrus brevifolia in Cyprus. *Journal of Analytical Atomic Spectrometry*, *27*(5), 796. https://doi.org/10.1039/c2ja10345a

Rich, S., Manning, S. W., Degryse, P., Vanhaecke, F., & Van Lerberghe, K. (2015). Provenancing East Mediterranean cedar wood with the 87Sr/86Sr strontium isotope ratio. *Archaeological and Anthropological Sciences*. https://doi.org/10.1007/s12520-015-0242-7

Rigor, I. G., Wallace, J. M., & Colony, R. L. (2002). Response of sea ice to the Arctic Oscillation. *Journal of Climate*, *15*(18), 2648–2663. https://doi.org/10.1175/1520-0442(2002)015<2648:ROSITT>2.0.CO;2

Rinn, F. (2011). TSAP-Win. Time Series Analysis and Presentation for Dendrochronology and Related Applications. *User Reference*, 110.

Ritchie, J. C., & Hare, F. K. (1971). Late-quaternary vegetation and climate near the arctic tree line of northwestern North America. *Quaternary Research*, *1*(3), 331–342. https://doi.org/http://dx.doi.org/10.1016/0033-5894(71)90069-X

Romaniello, S. J., Field, M. P., Smith, H. B., Gordon, G. W., Kim, M. H., & Anbar, A. D. (2015). Fully automated chromatographic purification of Sr and Ca for isotopic analysis. *Journal of Analytical Atomic Spectrometry*, *30*(9), 1906–1912. https://doi.org/10.1039/c5ja00205b

Rothrock, D. A., Percival, D. B., & Wensnahan, M. (2008). The decline in arctic sea-ice thickness: Separating the spatial, annual, and interannual variability in a quarter century of submarine data. *Journal of Geophysical Research: Oceans*, *113*(5), 1–9. https://doi.org/10.1029/2007JC004252

Rothrock, D. A., & Zhang, J. (2005). Arctic Ocean sea ice volume: What explains its recent depletion? *Journal of Geophysical Research: Oceans*, *110*(1), 1–10. https://doi.org/10.1029/2004JC002282

Salvigsen, O. (1978). Holocene emergence and finds of pumice, whalebones, and driftwood at Svartknausflya, Nordaustlandet. *Norsk Polarinstitutt Arbok, 1977*, *1977*, 217–228.

Salvigsen, O. (1984). Occurrence of pumice on raised beaches and Holocene shoreline displacement in the inner Isfjorden area, Svalbard. *Polar Research*, *2*(1), 107–113. https://doi.org/10.1111/j.1751-8369.1984.tb00488.x

Salvigsen, O., Elgersma, A., & Landvik, J. Y. (1991). Radiocarbon dated raised beaches in the Northwestern {Wedel Jarlsberg Land}, {Spitsbergen}, {Svalbard}. *Polar Session. Arctic Environment Research*, 9–16.

Salvigsen, O., & Mangerud, J. (1991). Holocene shoreline displacement at Agardhbukta,

eastern Spitsbergen, Svalbard. *Polar Research*, *9*(1), 1–7. https://doi.org/10.1111/j.1751-8369.1991.tb00398.x

Salvigsen, O., & Nydal, R. (1981). The Weichselian glaciation in Svalbard before 15,000 BP. *Boreas*, *10*(4), 433–446.

Salvigsen, O., & Österholm, H. (1982). Radiocarbon dated raised beaches and glacial history of the northern coast of Spitsbergen, Svalbard. *Polar Research*, *1982*(1), 97–115. https://doi.org/10.1111/j.1751-8369.1982.tb00473.x

Sandak, A., Sandak, J., Babiński, L., Pauliny, D., & Riggio, M. (2014). Spectral analysis of changes to pine and oak wood natural polymers after short-term waterlogging. *Polymer Degradation and Stability*, *99*(1), 68–79. https://doi.org/10.1016/j.polymdegradstab.2013.11.018

Sander, L., Kirdyanov, A., Crivellaro, A., & Büntgen, U. (2021). Short communication: Driftwood provides reliable chronological markers in Arctic coastal deposits. *Geochronology*, *3*(1), 171–180. https://doi.org/10.5194/gchron-3-171-2021

Sarnthein, M., Van Kreveld, S., Erlenkeuser, H., Grootes, P. M., Kucera, M., Pflauman, U., & Schulz, M. (2003). Centennial-to-millennial-scale periodicities of Holocene climate and sediment injections off the western Barents shelf, 75°N. *Boreas*, *32*(3), 447–461. https://doi.org/10.1111/j.1502-3885.2003.tb01227.x

Savard, M. M., Bégin, C., Marion, J., Arseneault, D., & Bégin, Y. (2012). Evaluating the integrity of C and O isotopes in sub-fossil wood from boreal lakes. *Palaeogeography, Palaeoclimatology, Palaeoecology*, *348–349*, 21–31. https://doi.org/10.1016/j.palaeo.2012.06.003

Schledermann, P. (1978). Prehistoric Demographic Trends in the Canadian High Arctic. *Canadian Journal of Archaeology / Journal Canadien d'Archéologie*, *2*, 43–58. http://www.jstor.org/stable/23006522

Schoch, W., Heller, I., Schweingruber, F. H., & Kienast, F. (2004). *Wood anatomy of central European Species*.

Schomacker, A., Farnsworth, W. R., Ingólfsson, Ó., Allaart, L., Håkansson, L., Retelle, M., Siggaard-Andersen, M.-L., Korsgaard, N. J., Rouillard, A., & Kjellman, S. E. (2019). Postglacial relative sea level change and glacier activity in the early and late Holocene: Wahlenbergfjorden, Nordaustlandet, Svalbard. *Scientific Reports*, *9*(1), 6799. https://doi.org/10.1038/s41598-019-43342-z

Schweingruber, F. H. (2007). Preparation of Wood and Herb Samples for Microscopic Analysis. *Wood Structure and Environment*, 1–4. https://doi.org/10.1007/978-3-540-48548-3

Schweingruber, F. H. (2012). *Tree rings: basics and applications of dendrochronology*. Springer Science & Business Media.

Schytt, V., Hoppe, G., Blake Jr, W., & Grosswald, M. G. (1968). The extent of the Würm glaciation in the European Arctic. *Int. Assoc. Sci. Hydrol*, *79*, 207–216.

Screen, J. a, & Simmonds, I. (2010). The central role of diminishing sea ice in recent Arctic temperature amplification. *Nature*, *464*(7293), 1334–1337. https://doi.org/10.1038/nature09051

Screen, J. a, & Simmonds, I. (2014). Amplified mid-latitude planetary waves favour particular regional weather extremes. *Nature Climate Change*, *4*(August), 704–709. https://doi.org/10.1038/NCLIMATE2271

Seidenkrantz, M. S. (2013). Benthic foraminifera as palaeo sea-ice indicators in the subarctic realm - examples from the Labrador Sea-Baffin Bay region. *Quaternary Science Reviews*, *79*, 135–144. https://doi.org/10.1016/j.quascirev.2013.03.014

Serreze, M. C., Barrett, A. P., Slater, A. G., Woodgate, R. A., Aagaard, K., Lammers, R. B., Steele, M., Moritz, R., Meredith, M., & Lee, C. M. (2006). The large-scale freshwater cycle of the Arctic. *Journal of Geophysical Research: Oceans*, *111*(11), 1–19. https://doi.org/10.1029/2005JC003424

Serreze, M. C., & Francis, J. A. (2006). The Arctic Amplification Debate. *Climatic Change*, *76*(3), 241–264. https://doi.org/10.1007/s10584-005-9017-y

Serreze, M. C., Holland, M. M., & Stroeve, J. (2007). Perspectives on the Arctic's Shrinking Sea-Ice Cover. *Science* , *315*(5818), 1533–1536. https://doi.org/10.1126/science.1139426

Serreze, M. C., & Stroeve, J. (2015). Arctic sea ice trends, variability and implications for seasonal ice forecasting. *Philosophical Transactions. Series A, Mathematical, Physical, and Engineering Sciences*, *373*(2045), 20140159. https://doi.org/10.1098/rsta.2014.0159

Shapiro, I., Colony, R., & Vinje, T. (2003). April sea ice extent in the Barents Sea , 1850 – 2001. *Polar Research*, *22*(1), 5–10. https://doi.org/10.1111/j.1751-8369.2003.tb00089.x

Sharpe, D. R. (1992). Quaternary geology of Wollaston Peninsula, Victoria Island, Northwest Territories. In *Memoir - Geological Survey of Canada* (Vol. 434). Ottawa. https://doi.org/10.4095/134059

Sidorova, O. C., Hellmann, L., Agafonov, L., Ljungqvist, F. C., Düthorn, E., Esper, J., Hülsmann, L., Kirdyanov, A. V., Moiseev, P., Myglan, V. S., Nikolaev, A. N., Reinig, F., Schweingruber, F. H., Solomina, O., Tegel, W., & Büntgen, U. (2016). Diverse growth trends and climate responses across Eurasia's boreal forest. *Environmental Research Letters*, *11*(7), 74021. https://doi.org/10.1088/1748-9326/11/7/074021

Silkin, P. P., & Ekimova, N. V. (2012). Relationship of strontium and calcium concentrations with the parameters of cell structure in Siberian spruce and fir tree-rings. *Dendrochronologia*, *30*(2), 189–194. https://doi.org/10.1016/j.dendro.2011.06.003

Sillen, A., Hall, G., Richardson, S., & Armstrong, R. (1998). 87Sr/86Sr ratios in modern and fossil food-webs of the Sterkfontein Valley: Implications for early hominid habitat preference. *Geochimica et Cosmochimica Acta*, *62*(14), 2463–2473. https://doi.org/10.1016/S0016-7037(98)00182-3

Ślubowska-Woldengen, M., Rasmussen, T. L., Koç, N., Klitgaard-Kristensen, D., Nilsen, F., & Solheim, A. (2007). Advection of Atlantic Water to the western and northern Svalbard shelf since 17,500 cal yr BP. *Quaternary Science Reviews*, *26*(3–4), 463–478. https://doi.org/10.1016/j.quascirev.2006.09.009

Smedsrud, L. H., Esau, I., Ingvaldsen, R. B., Eldevik, T., Haugan, P. M., Li, C., Lien, V. S., Olsen, A., Omar, A. M., & Otterå, O. H. (2013). The role of the Barents Sea in the Arctic climate system. *Reviews of Geophysics*, *51*(3), 415–449.

Snoeck, C., Schulting, R. J., Brock, F., Rodler, A. S., Van Ham-Meert, A., Mattielli, N., &

Ostapkowicz, J. (2021). Testing Various Pre-treatments on Artificially Waterlogged and Pitch-Contaminated Wood for Strontium Isotope Analyses. In *Frontiers in Ecology and Evolution* (Vol. 8, p. 497). https://doi.org/10.3389/fevo.2020.589154

Sokolov, S. Y., Svyazeva, O. A., & Kubli, V. A. (1977). *Arealy Derev Ev I Kustarnikov SSSR [Ranges of Trees and Shrubs of the USSR], vol. 1*. Leningrad: Nauka.

Speirs, A. K., McConnachie, G., & Lowe, A. J. (2009). Chloroplast DNA from 16th century waterlogged oak in a marine environment: initial steps in sourcing the Mary Rose timbers. *Archaeological Science Under a Microscope: Studies in Residue and Ancient DNA Analysis in Honour of Thomas H. Loy*, *30*, 175–189. https://doi.org/10.22459/ta30.07.2009.13

Spolaor, A., Gabrieli, J., Martma, T., Kohler, J., Björkman, M. B., Isaksson, E., Varin, C., Vallelonga, P., Plane, J. M. C., & Barbante, C. (2013). Sea ice dynamics influence halogen deposition to Svalbard. *Cryosphere*, *7*(5), 1645–1658. https://doi.org/10.5194/tc-7-1645-2013

Spolaor, A., Opel, T., McConnell, J. R., Maselli, O. J., Spreen, G., Varin, C., Kirchgeorg, T., Fritzsche, D., Saiz-Lopez, A., & Vallelonga, P. (2016). Halogen-based reconstruction of Russian Arctic sea ice area from the Akademii Nauk ice core (Severnaya Zemlya). *Cryosphere*, *10*(1), 245–256. https://doi.org/10.5194/tc-10-245-2016

St-Hilaire-gravel, D., Bell, T. J., & Forbes, D. L. (2010). Raised gravel beaches as proxy indicators of past sea-ice and wave conditions, Lowther island, Canadian Arctic Archipelago. *Arctic*, *63*(2), 213–226. https://doi.org/10.14430/arctic976

St-Hilaire-Gravel, D., Forbes, D. L., & Bell, T. (2015). Evolution and morphodynamics of a prograded beach-ridge foreland, northern Baffin Island, Canadian Arctic Archipelago. *Geografiska Annaler: Series A, Physical Geography*, *97*(3), 615–631.

Steelandt, S., Pierson-Wickmann, A.-C., Bhiry, N., Marguerie, D., & Coz, M. B.-L. (2016). Chemical Differentiation between Immersed and Dry Wood Samples in Nunavik (Northern Quebec, Canada): Preliminary Results. *Arctic, Antarctic, and Alpine Research*, *48*(2), 315–325. https://doi.org/10.1657/aaar0014-082

Stewart, T. G., & England, J. H. (1983). Holocene Sea-Ice Variations and Paleoenvironmental Change, Northernmost Ellesmere Island, N.W.T., Canada. *Arctic and Alpine Research*, *15*(1), 1–17. https://doi.org/10.2307/1550979

Stiansen, J. E., Arneberg, P., Titov, O., & Filin, A. (2009). *Joint Norwegian-Russian environmental status report on the Barents Sea Ecosystem*. *3*.

Stickley, C. E., St. John, K., Koç, N., Jordan, R. W., Passchier, S., Pearce, R. B., & Kearns, L. E. (2009). Evidence for middle Eocene Arctic sea ice from diatoms and ice-rafted debris. *Nature*, *460*(7253), 376–379. https://doi.org/10.1038/nature08163

Stille, P., Schmitt, A. D., Labolle, F., Pierret, M. C., Gangloff, S., Cobert, F., Lucot, E., Guéguen, F., Brioschi, L., Steinmann, M., & Chabaux, F. (2012). The suitability of annual tree growth rings as environmental archives: Evidence from Sr, Nd, Pb and Ca isotopes in spruce growth rings from the Strengbach watershed. *Comptes Rendus - Geoscience*, *344*(5), 297–311. https://doi.org/10.1016/j.crte.2012.04.001

Taberlet, P., Coissac, E., Pompanon, F., Gielly, L., Miquel, C., Valentini, A., Vermat, T., Corthier, G., Brochmann, C., & Willerslev, E. (2007). Power and limitations of the

chloroplast trnL (UAA) intron for plant DNA barcoding. *Nucleic Acids Research*, *35*(3). https://doi.org/10.1093/nar/gkl938

Taylor, R. B. (1975). Coastal investigations of northern Somerset Island and Barrow Strait, District of Franklin. *Geological Survey of Canada*, *75*, 501–504.

Taylor, R. E., & Aitken, M. J. (1997). *Chronometric dating in archaeology* (Vol. 2). Springer Science & Business Media.

Thompson, D. W. J., & Wallace, J. M. (1998). The Arctic oscillation signature in the wintertime geopotential height and temperature fields. *Geophysical Research Letters*, *25*(9), 1297–1300. https://doi.org/10.1029/98GL00950

Timmermans, M.-L., Toole, J., & Krishfield, R. (2018). Warming of the interior Arctic Ocean linked to sea ice losses at the basin margins. *Science Advances*, *4*(8), eaat6773.

Tomlinson, G. H. (2003). Acidic deposition, nutrient leaching and forest growth. *Biogeochemistry*, *65*(1), 51–81. https://doi.org/10.1023/A:1026069927380

Toncala, A., Trautmann, B., Velte, M., Kropf, E., McGlynn, G., Peters, J., & Harbeck, M. (2020). On the premises of mixing models to define local bioavailable 87Sr/86Sr ranges in archaeological contexts. *Science of the Total Environment*, *745*, 140902. https://doi.org/10.1016/j.scitotenv.2020.140902

Trautman, M. A. (1963). Isotopes, Inc. radiocarbon measurements III. *Radiocarbon*, *5*, 62–79.

Tremblay, L. -B., Mysak, L. a., & Dyke, A. S. (1997). Evidence from driftwood records for century-to-millennial scale variations of the high latitude atmospheric circulation during the Holocene. *Geophysical Research Letters*, *24*(16), 2027. https://doi.org/10.1029/97GL02028

Tschudi, M. A., Stroeve, J. C., & Stewart, J. S. (2016). Relating the age of Arctic sea ice to its thickness, as measured during nasa's ICESat and IceBridge campaigns. *Remote Sensing*, *8*(6). https://doi.org/10.3390/rs8060457

Van Bergen, P. F., & Poole, I. (2002). Stable carbon isotopes of wood: A clue to palaeoclimate? *Palaeogeography, Palaeoclimatology, Palaeoecology*, *182*(1–2), 31–45. https://doi.org/10.1016/S0031-0182(01)00451-5

Van De Plassche, O. (1986). Sea-level research: a manual for the collection and evaluation of data. In *Sea-level research: a manual for the collection and evaluation of data.* Springer. https://doi.org/10.2307/1551353

Van Ham-Meert, A., Rodler, A. S., Waight, T. E., & Daly, A. (2020). Determining the Sr isotopic composition of waterlogged wood – Cleaning more is not always better. *Journal of Archaeological Science*, *124*, 105261. https://doi.org/10.1016/j.jas.2020.105261

Vare, L. L., Massé, G., & Belt, S. T. (2010). A biomarker-based reconstruction of sea ice conditions for the Barents Sea in recent centuries. *Holocene*, *20*(4), 637–643. https://doi.org/10.1177/0959683609355179

Vavrus, S. J., Wang, F., Martin, J. E., Francis, J. A., Peings, Y., & Cattiaux, J. (2017). Changes in North American Atmospheric Circulation and Extreme Weather: Influence of Arctic Amplification and Northern Hemisphere Snow Cover. *Journal of Climate*.

https://doi.org/10.1175/JCLI-D-16-0762.1

Viers, J., Prokushkin, A. S., Pokrovsky, O. S., Auda, Y., Kirdyanov, A. V., Beaulieu, E., Zouiten, C., Oliva, P., & Dupré, B. (2013). Seasonal and spatial variability of elemental concentrations in boreal forest larch foliage of Central Siberia on continuous permafrost. *Biogeochemistry*, *113*(1–3), 435–449. https://doi.org/10.1007/s10533-012-9770-8

Vinje, T. (2001). Anomalies and trends of sea-ice extent and atmospheric circulation in the Nordic Seas during the period 1864-1998. *Journal of Climate*, *14*(3), 255–267.

Vitousek, P. M., Kennedy, M. J., Derry, L. a., & Chadwick, O. a. (1999). Weathering versus atmospheric sources of strontium in ecosystems on young volcanic soils. *Oecologia*, *121*(2), 255–259. https://doi.org/10.1007/s004420050927

Voerkelius, S., Lorenz, G. D., Rummel, S., Quétel, C. R., Heiss, G., Baxter, M., Brach-Papa, C., Deters-Itzelsberger, P., Hoelzl, S., Hoogewerff, J., Ponzevera, E., Van Bocxstaele, M., & Ueckermann, H. (2010). Strontium isotopic signatures of natural mineral waters, the reference to a simple geological map and its potential for authentication of food. *Food Chemistry*, *118*(4), 933–940. https://doi.org/10.1016/j.foodchem.2009.04.125

Voronina, E., Polyak, L., Vernal, A. De, & Peyron, O. (2001). Holocene variations of sea-surface conditions in the southeastern Barents Sea, reconstructed from dinoflagellate cyst assemblages. *Journal of Quaternary Science*, *16*(7), 717–726.

Voss, B. M., Peucker-Ehrenbrink, B., Eglinton, T. I., Fiske, G., Wang, Z. A., Hoering, K. a., Montluçon, D. B., LeCroy, C., Pal, S., Marsh, S., Gillies, S. L., Janmaat, A., Bennett, M., Downey, B., Fanslau, J., Fraser, H., Macklam-Harron, G., Martinec, M., & Wiebe, B. (2014). Tracing river chemistry in space and time: Dissolved inorganic constituents of the Fraser River, Canada. *Geochimica et Cosmochimica Acta*, *124*, 283–308. https://doi.org/10.1016/j.gca.2013.09.006

Wagner, B., Bennike, O., Cremer, H., & Klug, M. (2010). Late Quaternary history of the Kap Mackenzie area, northeast Greenland. *Boreas*, *39*(3), 492–504. https://doi.org/10.1111/j.1502-3885.2010.00148.x

Wagner, S., Lagane, F., Seguin-Orlando, A., Schubert, M., Leroy, T., Guichoux, E., Chancerel, E., Bech-Hebelstrup, I., Bernard, V., Billard, C., Billaud, Y., Bolliger, M., Croutsch, C., Čufar, K., Eynaud, F., Heussner, K. U., Köninger, J., Langenegger, F., Leroy, F., … Orlando, L. (2018). High-Throughput DNA sequencing of ancient wood. *Molecular Ecology*, *27*(5), 1138–1154. https://doi.org/10.1111/mec.14514

Wales, N., Andersen, K., Cappellini, E., Ávila-Arcos, M. C., & Gilbert, M. T. P. (2014). Optimization of DNA recovery and amplification from non-carbonized archaeobotanical remains. *PLoS ONE*, *9*(1). https://doi.org/10.1371/journal.pone.0086827

Walker, H. J., & Hudson, P. F. (2003). Hydrologic and geomorphic processes in the Colville River delta, Alaska. *Geomorphology*, *56*(3–4), 291–303. https://doi.org/10.1016/S0169-555X(03)00157-0

Walker, M. J. C., Berkelhammer, M., Björck, S., Cwynar, L. C., Fisher, D. A., Long, A. J., Lowe, J. J., Newnham, R. M., Rasmussen, S. O., & Weiss, H. (2012). Formal subdivision of the Holocene Series/Epoch: A Discussion Paper by a Working Group of INTIMATE (Integration of ice-core, marine and terrestrial records) and the Subcommission on Quaternary Stratigraphy (International Commission on Stratigraphy). *Journal of Quaternary Science*, *27*(7), 649–659. https://doi.org/10.1002/jqs.2565

Walsh, J. E., Fetterer, F., Scott Stewart, J., & Chapman, W. L. (2017). A database for depicting Arctic sea ice variations back to 1850. *Geographical Review*, *107*(1), 89–107. https://doi.org/10.1111/j.1931-0846.2016.12195.x

Washburn, A. L. (1962). Radiocarbon-Dated Postglacial Delevelling in Northeast Greenland and Its Implications. *Arctic*, *15*(1), 66–73. http://www.jstor.org/stable/40506929

Webber, P. J., Richardson, J. W., & Andrews, J. T. (1970). Post-glacial uplift and substrate age at Cape Henrietta Maria, southeastern Hudson Bay, Canada. *Canadian Journal of Earth Sciences*, *7*(2), 317–325.

Weidick, A. (1972). Holocene shore-lines and glacial stages in Greenland - an attempt at correlation. *Rapport Grønlands Geologiske Undersøgelse*, *41*, 1–39. https://doi.org/10.34194/rapggu.v41.7281

Weidick, A. (1975). C14 dating of Survey material performed in 1974. *Rapport Grønlands Geologiske Undersøgelse*, *75*, 19–20. https://doi.org/10.34194/rapggu.v75.7436

Weidick, A. (1977). C14 dating of survey material carried out in 1976. *Rapport Grønlands Geologiske Undersøgelse*, *85*, 127–129.

Weihe, R. (1996). Late Quaternary glacial geology and relative sea level history of Franz Josef Land, Russia. In *unpublished MSci Thesis, Columbus, Ohio State University*.

Whipkey, C. E., Capo, R. C., Chadwick, O. a., & Stewart, B. W. (2000). The importance of sea spray to the cation budget of a coastal Hawaiian soil: A strontium isotope approach. *Chemical Geology*, *168*(1–2), 37–48. https://doi.org/10.1016/S0009-2541(00)00187-X

Wilson, L. J., Hald, M., & Godtliebsen, F. (2011). Foraminiferal faunal evidence of twentieth-century Barents Sea warming. *The Holocene*, *21*(4), 527–537.

Wohl, E., Cadol, D., Pfeiffer, A., Jackson, K., & Laurel, D. (2018). Distribution of large wood within river corridors in relation to flow regime in the semiarid western US. *Water Resources Research*, *54*(3), 1890–1904.

Wohl, E., Kramer, N., Ruiz-Villanueva, V., Scott, D. N., Comiti, F., Gurnell, A. M., Piegay, H., Lininger, K. B., Jaeger, K. L., Walters, D. M., & Fausch, K. D. (2019). The Natural Wood Regime in Rivers. *BioScience*, *69*(4), 259–273. https://doi.org/10.1093/biosci/biz013

Woodgate, R. A. (2018). Increases in the Pacific inflow to the Arctic from 1990 to 2015, and insights into seasonal trends and driving mechanisms from year-round Bering Strait mooring data. *Progress in Oceanography*, *160*, 124–154.

Yamada, H., Yamauchi, H., & Kurimoto, Y. (2014). Color analysis of combustion ashes of seawater-soaked wood: estimation of salt concentration. *Journal of Material Cycles and Waste Management*, *16*(3), 576–582. https://doi.org/10.1007/s10163-013-0212-z

Yang, D., Kane, D. L., Hinzman, L. D., Zhang, X., Zhang, T., & Ye, H. (2002). Siberian Lena River hydrologic regime and recent change. *Journal of Geophysical Research: Atmospheres*, *107*(D23), ACL-14.

Zale, R., & Brydsten, L. (1993). The pre-Holocene marine limit on Hopen, Svalbard. *Boreas*, *22*, 159–164.

Zayed, J., Loranger, S., & Kennedy, G. (1992). Variations of trace element concentrations in

red spruce tree rings. In *Water, Air, & Soil Pollution* (Vol. 65, Issues 3–4, pp. 281–291). https://doi.org/10.1007/BF00479892

Zeeberg, J., Lubinski, D. J., & Forman, S. L. (2001a). Holocene relative sea-level history of Novaya Zemlya, Russia, and implications for Late Weichselian ice-sheet loading. *Quaternary Research*, *56*(2), 218–230.

Zeeberg, J., Lubinski, D. J., & Forman, S. L. (2001b). Holocene Relative Sea-Level History of Novaya Zemlya, Russia, and Implications for Late Weichselian Ice-Sheet Loading. *Quaternary Research*, *56*(2), 218–230. https://doi.org/10.1006/qres.2001.2256

Zhang, Q., Xiao, C., Ding, M., & Dou, T. (2018). Reconstruction of autumn sea ice extent changes since AD1289 in the Barents-Kara Sea, Arctic. *Science China Earth Sciences*, *61*(9), 1279–1291.

Zhang, X., Sorteberg, A., Zhang, J., Gerdes, R., & Comiso, J. C. (2008). Recent radical shifts of atmospheric circulations and rapid changes in Arctic climate system. *Geophysical Research Letters*, *35*(22), 1–7. https://doi.org/10.1029/2008GL035607

Appendices

A. Supplementary material for chapter 3.

Supplementary Data File

Filename: Ads01.xlsx

Contents of the file:

Table A1 – Table uploaded separately as an Excel file. References within Chapter 3.

Description:

Data from 913 driftwood samples previously collected throughout the western Arctic coastline and covering the Holocene was collated to produce a spatiotemporal dataset of deposited driftwood identified at the genus level, where available. The ages are presented in median calibrated radiocarbon years before present (cal. yr BP), calibrated with the IntCal13 calibration curve using the program OxCal v4.2 (Bronk Ramsey, 2009) and directly comparable to calendar years BP for samples dated by other methods. The resulting age range represents the 95% confidence interval ± 2 sigma, with sample ages collated into 250yr intervals for analysis. The low errors associated with radiocarbon dating of wood material allow for the high temporal resolution of analysis compared to other proxy methods in the Arctic. The data was classified into the genera *Larix, Picea, Pinus, Populus, Salix* and *Tsuga.* Samples without taxonomic identification were classed as unknown.

Table A1. List of driftwood samples collated in the present study from a range of previous studies, as referenced. Median radiocarbon dated driftwood ages from calibrated radiocarbon age and ranges representing the 95% confidence interval (± 2 sigma) are displayed.

B. Supplementary material for chapter 4.

B1 Supplementary Data Plots

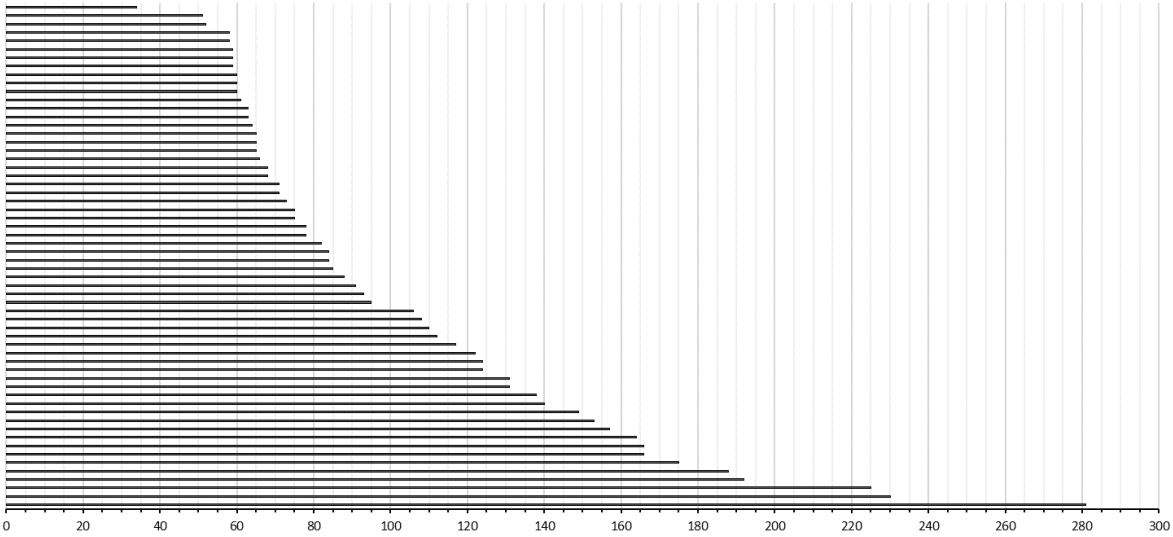

Figure B1.1. Distribution of segment lengths of 59 measured samples from northern Svallbard, ranging from a minimum of 34 years to a maximum of 281 years. Samples underwent annual ring width measurements to 1/1000 mm accuracy, using LINTAB tree-ring measurement table and TSAP-Win Professional version 0.89 (Rinn, 2011).

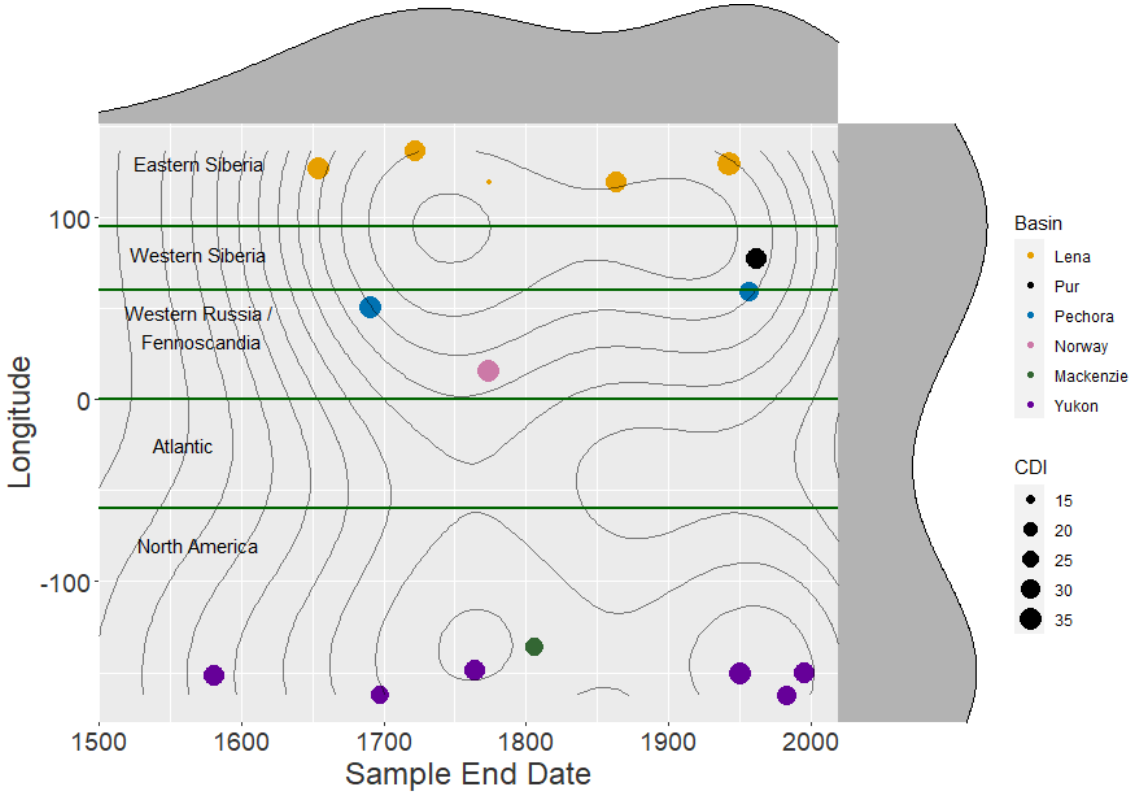

Figure B1.2. Plot of best matches for samples collected from Sjuøyane. Each point represents a sample's best match to a chronology. The colour of each data point displays the associated drainage basin, and the size of the point represents the CDI of the match. The density plots depict the densities of the associated time and longitude axes, weighted by the CDI of the matches.

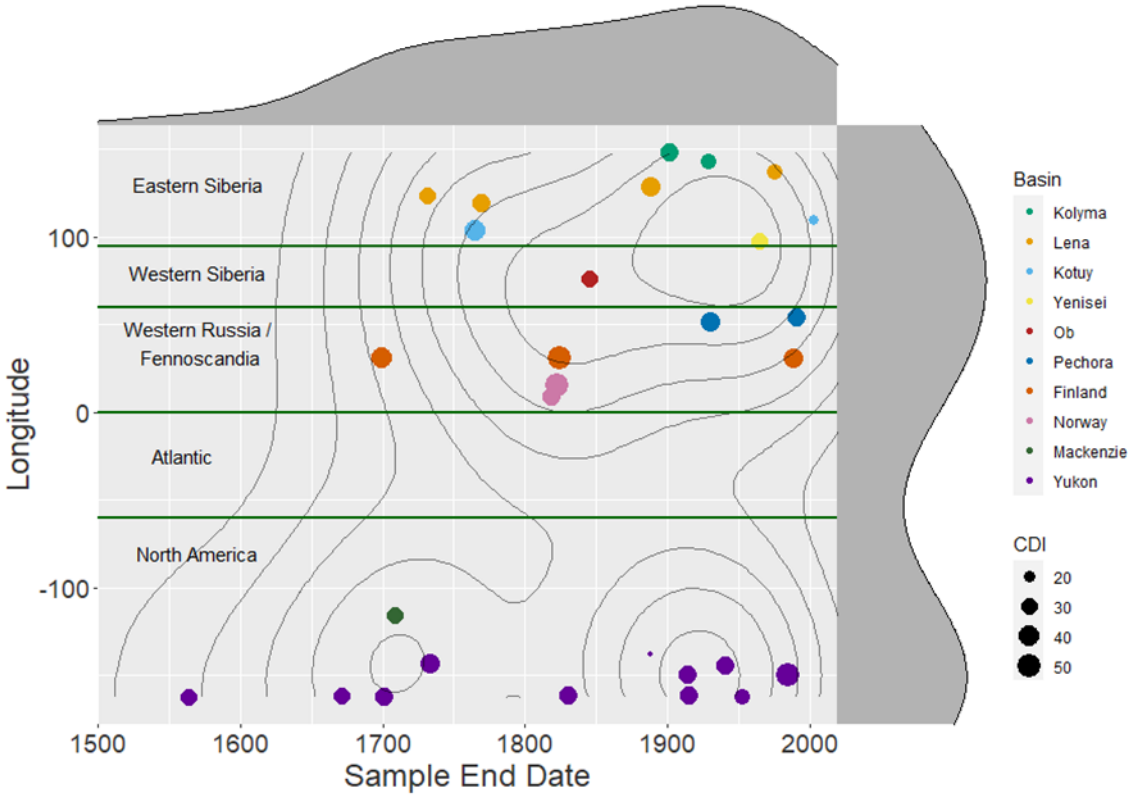

Figure B1.3. Plot of best matches for samples collected from Ringhorndalen. Each point represents a sample's best match to a chronology. The colour of each data point displays the associated drainage basin, and the size of the point represents the CDI of the match. The density plots depict the densities of the associated time and longitude axes, weighted by the CDI of the matches.

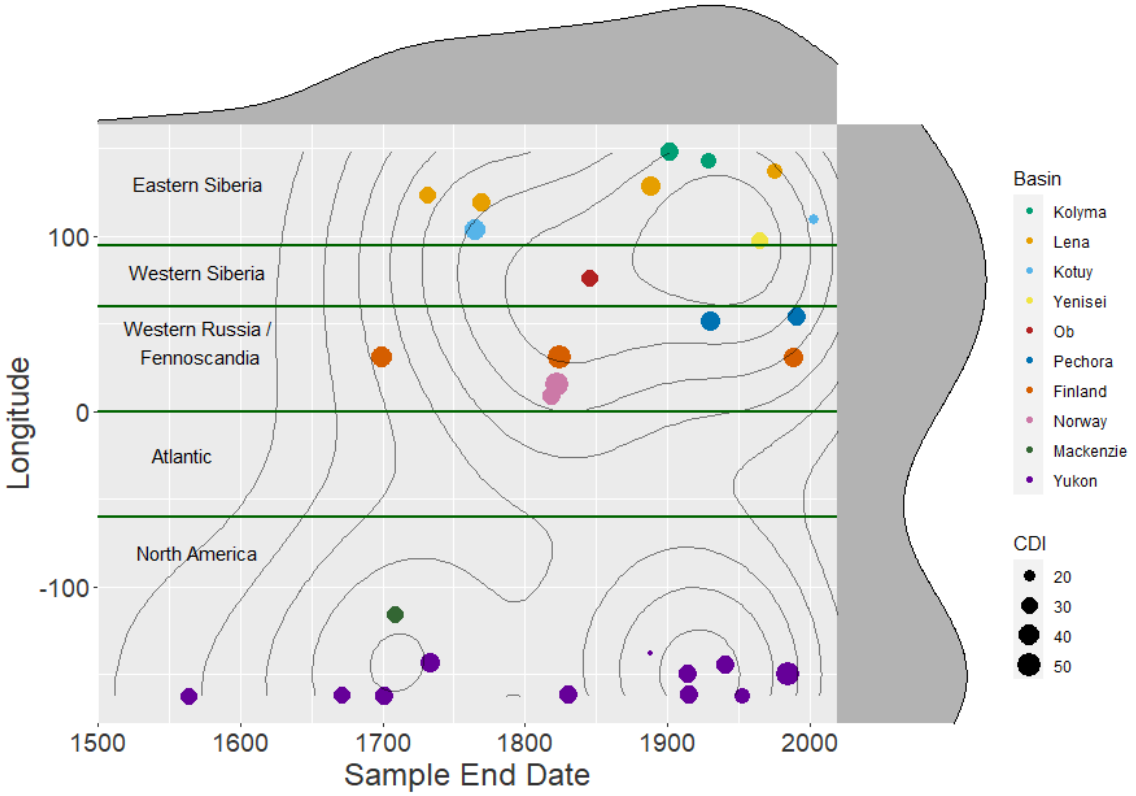

Figure B1.4. Plot of best matches for samples collected from Vassfarbukta. Each point represents a sample's best match to a chronology. The colour of each data point displays the associated drainage basin, and the size of the point represents the CDI of the match. The density plots depict the densities of the associated time and longitude axes, weighted by the CDI of the matches.

B2 Supplementary Dataset B2

Filename: Bds01.xlsx

Contents of the file: Sample information, CDI and Weighted scores, and best match choices for all samples. Uploaded separately as an xlsx file. References within Chapter 4.

B3 Supplementary Dataset B3

Filename: Folder Bds02

Contents of the file: CDI and Weighted score match distribution plots for all samples. Uploaded separately as a zip file. All potential matches are plotted for samples, with plots for

the both the CDI scores and Weighted Score. Each point represents a match to a chronology. The colour of the point displays the associated drainage basin, and the size of the point represents either the CDI of the match, or the Weighted Score of the match, respectively. The density plots depict the densities of the associated time and longitude axes, weighted by the scores of the matches. References within Chapter 4.

B4 Appendix B References

Rinn, F. (2003). TSAP-Win. Time series analysis and presentation for dendrochronology and 409 related applications. *User Reference*.

C. Supplementary material for chapter 5

C1 Further methodology details

C1.1 Sampling

Methods for the extraction, isolation and purification of strontium from driftwood through cleaning, microwave digestion, extraction chromatography and MC-ICP-MS (Multicollector-Inductively Coupled Plasma Mass Spectrometer) were developed in the clean-suite labs in the Earth Sciences Department, University of Oxford. Initially, method testing for strontium concentration and $^{87}Sr/^{86}Sr$ ratio analysis was conducted on 7 test samples of driftwood. Following the above method of manual column chemistry and testing, a subset of 20 Arctic driftwood samples collected from northern Svalbard then underwent the developed methodology. Further samples from the northern Svalbard collection were prepared for analysis, but disruption to the study workflow, including due to the COVID-19 pandemic, prevented MC-ICP-MS analysis of these samples and therefore limited the quantity of data for final analysis.

C1.2 Extraction Chromatography

Initial manual extraction chromatography on these test samples used Teflon elution columns and Triskem Sr resin. The stationary phase of Triskem Sr resin consists of a dicyclohexano 18-crown-6 derivative dissolved in octanol. The resin is selective of Sr over Ca which can be a major constituent in many samples. Pb is also strongly retained on the Sr Resin, allowing for a facile elution of Sr from the resin using dilute HNO3, leaving Pb retained. The eluted Sr was collected in Savillex® PFA vials and dried down on hotplates at 90°C. In addition to samples, a blank was prepared using the same digestion procedure, but without sample intake.

Following the above method of manual column chemistry and testing on test samples, a subset of the Arctic driftwood samples collected from northern Svalbard were analysed after utilising and refining these developed protocols. Sr extraction was undertaken via automated chromatographic purification using the prepFAST-MC^{TM} system (Elemental Scientific (ESI), Omaha, NE, USA), on an ESI Sr/Ca-1000 column (ESI part no. CF-MC-SrCa-1000) including supplied Sr-Ca ion exchange resin. including supplied Sr-Ca ion exchange resin. The methodology used was adapted from Romaniello et al. (2015), with a longer wash of 4ml between each sample. The $^{87}Sr/^{86}Sr$ analyses were performed on the Nu Plasma Multi-Collector Inductively Coupled Plasma Mass Spectrometer (MC-ICP-MS).

C1.3 Sr concentration Analysis

Following Sr extraction and purification, samples then underwent concentration and elemental analysis on the Thermo Element 2 Inductively Coupled Plasma Mass Spectrometer (ICP-MS), with concentrations of Sr (Table C1) consistent with values expected in wood material, and sufficient for further $^{87}Sr/^{86}Sr$ analysis.

Table C1. Sr concentrations for driftwood test samples. DL = Detectable Level.

sample	Concentration (ppm)	
	Sr86	Sr88
Microwave blank	below DL	below DL
JM1a1	7.731	7.805
JM1a2	6.553	6.502
JM1b1	11.903	11.717
JM1b2	9.651	9.419
NK01b	10.512	10.373
NK02a	6.029	5.979
NK02b	3.493	3.486
NK03a	4.684	4.665
NK03b	7.825	7.767
NK04a	4.439	4.301
NK04b	9.263	8.970
NK05a	7.852	7.768
NK05b	7.689	7.618
NK06a	3.118	3.050
NK06b	8.332	8.155

C1.4 Labware and Reagents

All labware underwent washing with analytical grade HCl and environmental grade HNO_3 to prevent contamination. Samples and Sr elutes were processed in Savillex® Teflon vials, with digestions, chromatography and cleaning undertaken in a Class 100 laminar flow exhaust hood. All acids used in this study were purified by sub-boiling distillation in-house from concentrated reagent grade acids. All acids and reagents used were stored within Parafilm-sealed Teflon or PTFE containers that had undergone cleaning. Ultra-pure water (≥ 18.2 MΩ cm) for cleaning and processing samples was prepared via a purification sequence with a Milli-Q® system (Millipore, USA).

C2 Datasets

C2.1 Dataset Cds01.xlsx contains the dataset produced and analysed in this study. Existing provenance data by tree-ring-width (TRW) cross-dating with reference chronologies from the circum-Arctic boreal forest zone Hole et al. (2021) are compared to the $^{87}Sr/^{86}Sr$ signature measured (in this study), to investigate possible alignment between driftwood $^{87}Sr/^{86}Sr$ signatures and available bioavailable/river values for the determined provenance regions.

C2.2 Dataset Cds02.xlsx contains correlation analysis between queried averaged $^{87}Sr/^{86}Sr$ values from modelled global bioavailable isoscape by Bataille et al. (2020) for buffer zones of 5km, 20km, 100km, 200km, and 500km radius around driftwood sample match points provided by TRW crossdating in Hole et al. (2021).

C3 Additional Sample crossdating plots

Description: Maps showing sample crossdate match locations determined by TRW crossdating by Hole et al. (2021), with this study's measured $^{87}Sr/^{86}Sr$ value ranges displayed in black, with existing river $^{87}Sr/^{86}Sr$ data (in blue), plant $^{87}Sr/^{86}Sr$ data (in green), soil $^{87}Sr/^{86}Sr$ data (in brown), compiled by Bataille (2020).

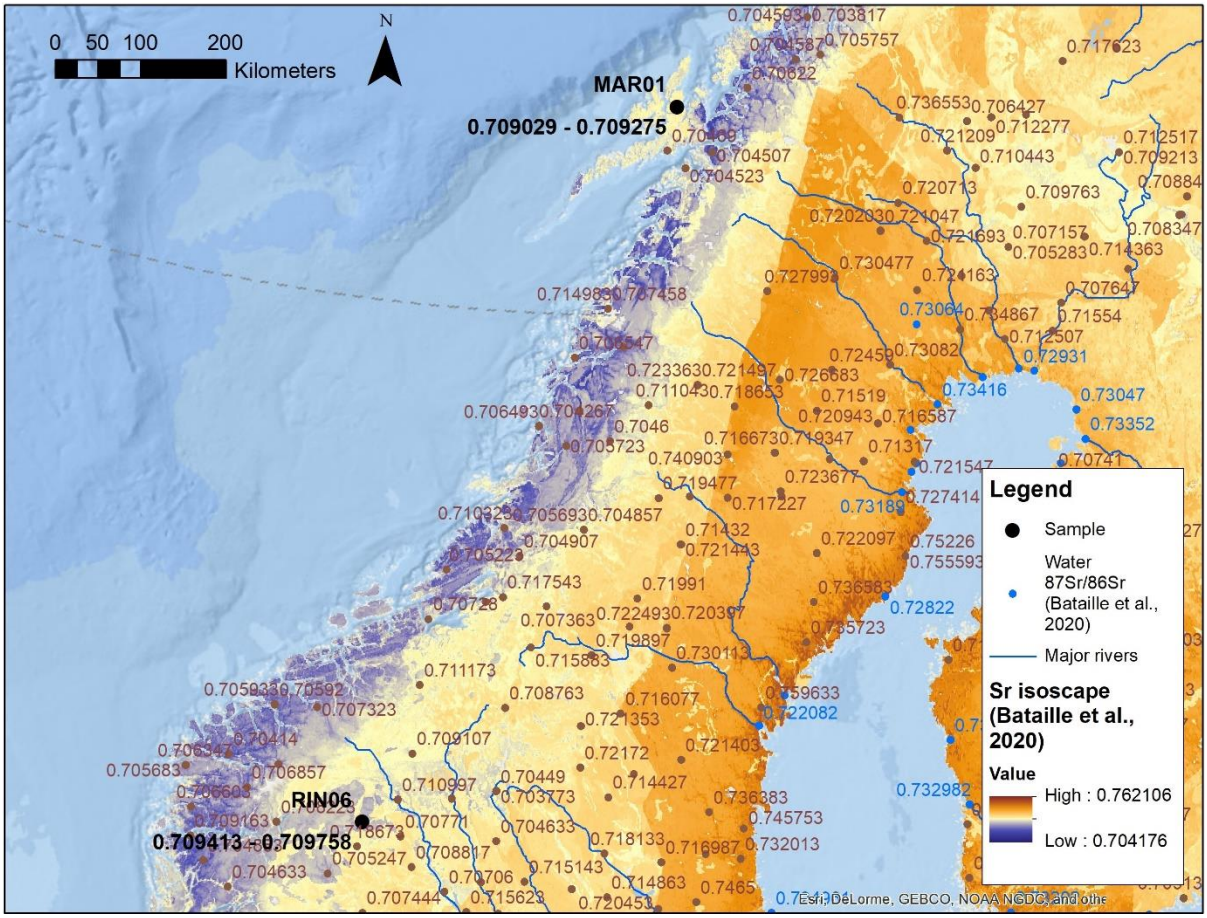

Figure C3.1. Samples **MAR01** and **RIN06** crossdate match locations determined by TRW crossdating by Hole et al. (2021), with measured $^{87}Sr/^{87}Sr$ value range displayed in black, compiled river $^{87}Sr/^{87}Sr$ data (blue) and soil $^{87}Sr/^{87}Sr$ data (brown) by Bataille (2020). There is no proximal river $^{87}Sr/^{87}Sr$ data available for assessing the measured $^{87}Sr/^{87}Sr$ values for this provenanced region. The available river $^{87}Sr/^{87}Sr$ surrounding the Eastern Norway coastline have higher $^{87}Sr/^{87}Sr$ values, while proximal soil $^{87}Sr/^{87}Sr$ have values that span the range of the measured sample $^{87}Sr/^{87}Sr$ values. High heterogeneity is seen in values and may also reflect different integration of Sr sources to those for riparian trees.

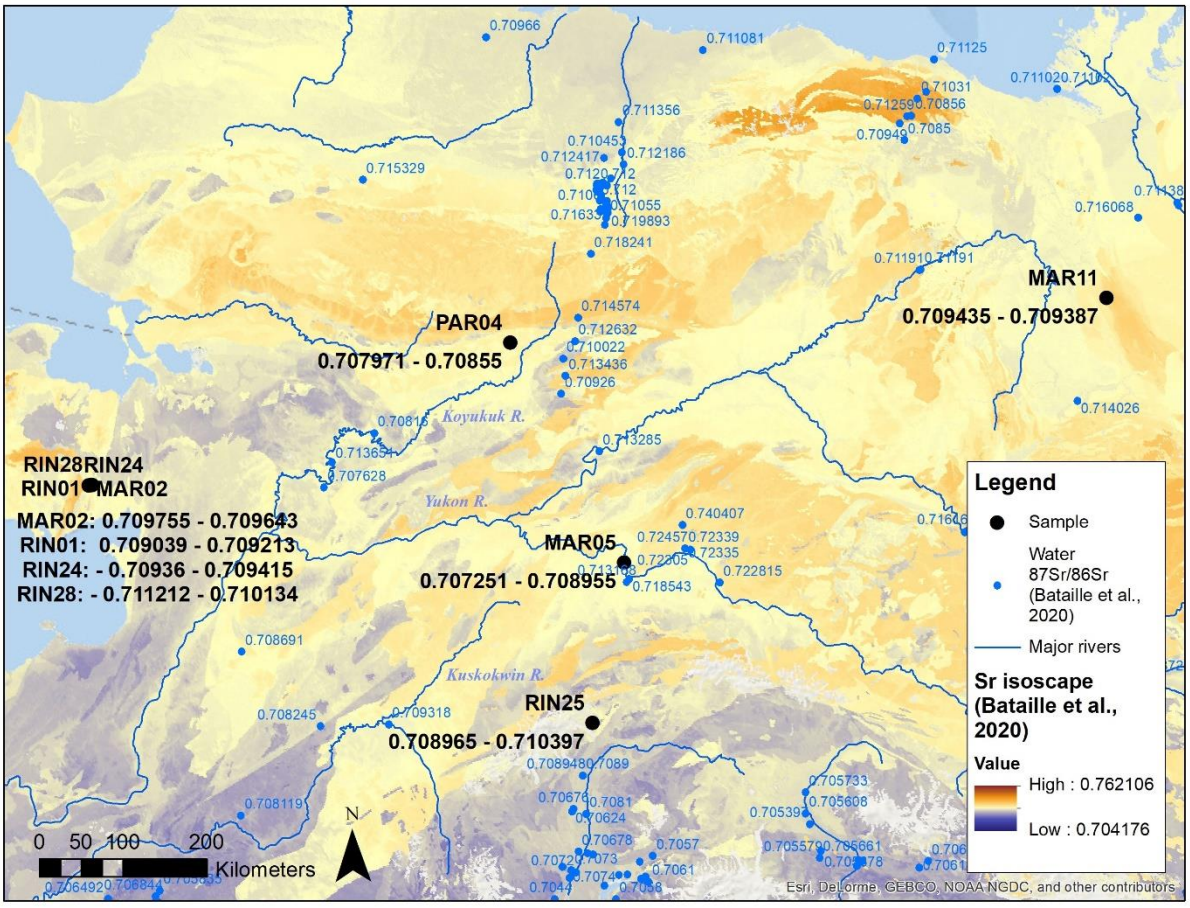

Figure C3.2. Sample MAR05 crossdate match locations in Alaska & Canada, determined by TRW crossdating by Hole et al. (2021), with measured $^{87}Sr/^{87}Sr$ value range displayed in black, compiled river $^{87}Sr/^{87}Sr$ data (blue) and soil $^{87}Sr/^{87}Sr$ data (brown) by Bataille (2020).

MAR02, RIN01, RIN24, RIN28: crossdate match locations in western Alaska, west of the Yukon and Koyukuk rivers, with measured $^{87}Sr/^{87}Sr$ value range displayed in black, and compiled river $^{87}Sr/^{87}Sr$ data by Bataille (2020) in blue. The closest river $^{87}Sr/^{87}Sr$ values show a range 0.707628-0.713651, which covers the sample measured range of all samples.

MAR05: crossdate match location in central Alaska along the Tanana River. A surrounding diverse range of $^{87}Sr/^{86}Sr$, with the surrounding range of 0.705201-0.715232 with multiple areas within each $^{87}Sr/^{86}Sr$ range. Examining river $^{87}Sr/^{86}Sr$ proximal to MAR05 from the Tanana river, as collated by Bataille et al. (2020), river values show a higher range of 0.713168-0.740407, out of the value obtained with sample MAR05. ~200km south-west, river values reach more agreement with MAR05, in the range 0.708245-0.709318.

MAR11: crossdate match location in northern Canada west of the Mackenzie River. The most proximal values show higher ranges or 0.71138-0.716068, although the lack of values close to the sample provenance region complicates interpretation.

PAR04: crossdate match location proximal to Koyukuk River. River values show a higher range of 0.70926-0.714574, out of the value obtained with sample PAR04. Downstream, ~200km south-west, river values reach more agreement with PAR04, in the range 0.70768-0.70816. Discussed further in main text.

RIN25: crossdate match location in southern Alaska, south of the Kuskokwim and Tanana rivers. The most proximal reference river 87Sr/87Sr values of 0.708948-0.7089 are close to the lower range of the sample.

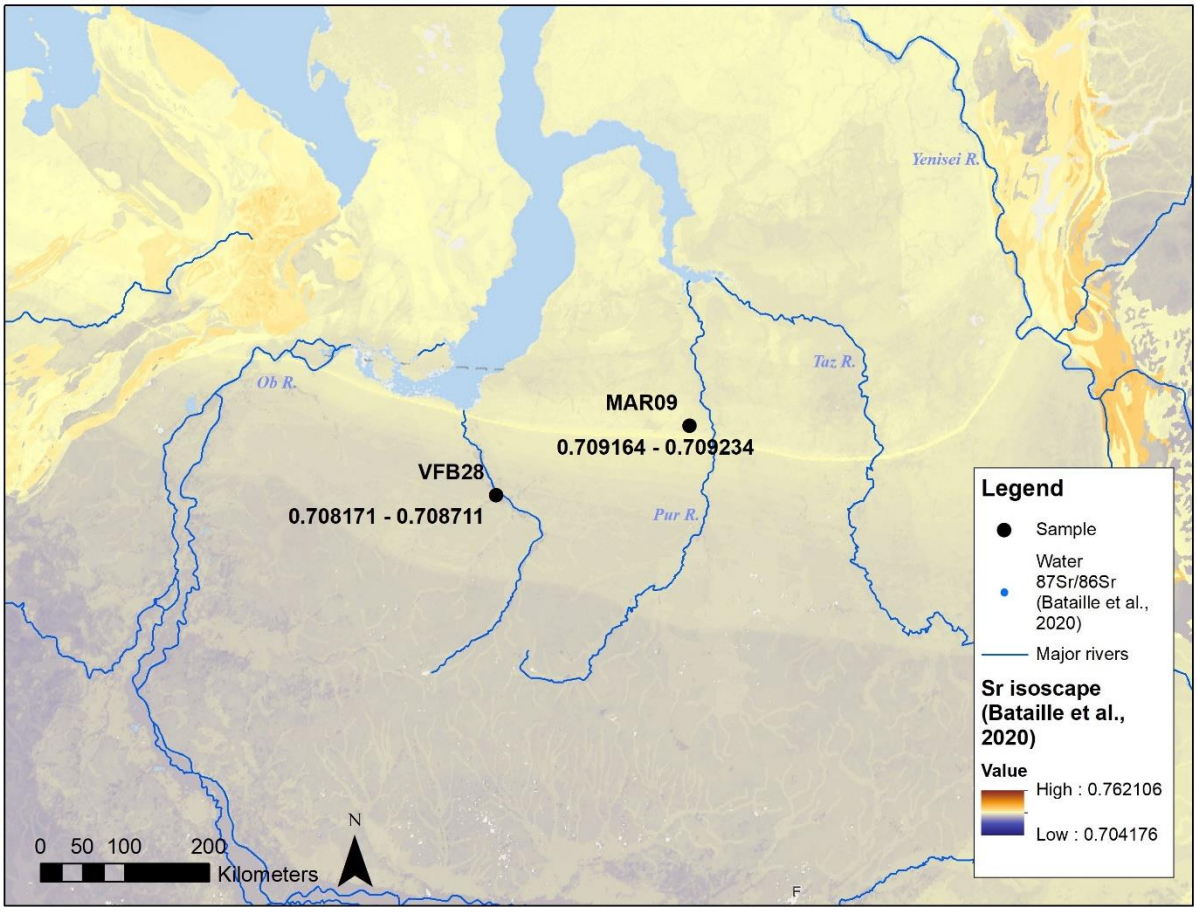

Figure C3.3. Sample MAR09 and VFB28 crossdate match locations in northern Russia east of the Ob river, determined by TRW crossdating by Hole et al. (2021). No available river $^{87}Sr/^{86}Sr$ in the region makes direct comparisons difficult, while the global isoscape of bioavailable $^{87}Sr/^{86}Sr$ by Bataille (2020) shows values of ~0.709 for the region, fitting with the samples.

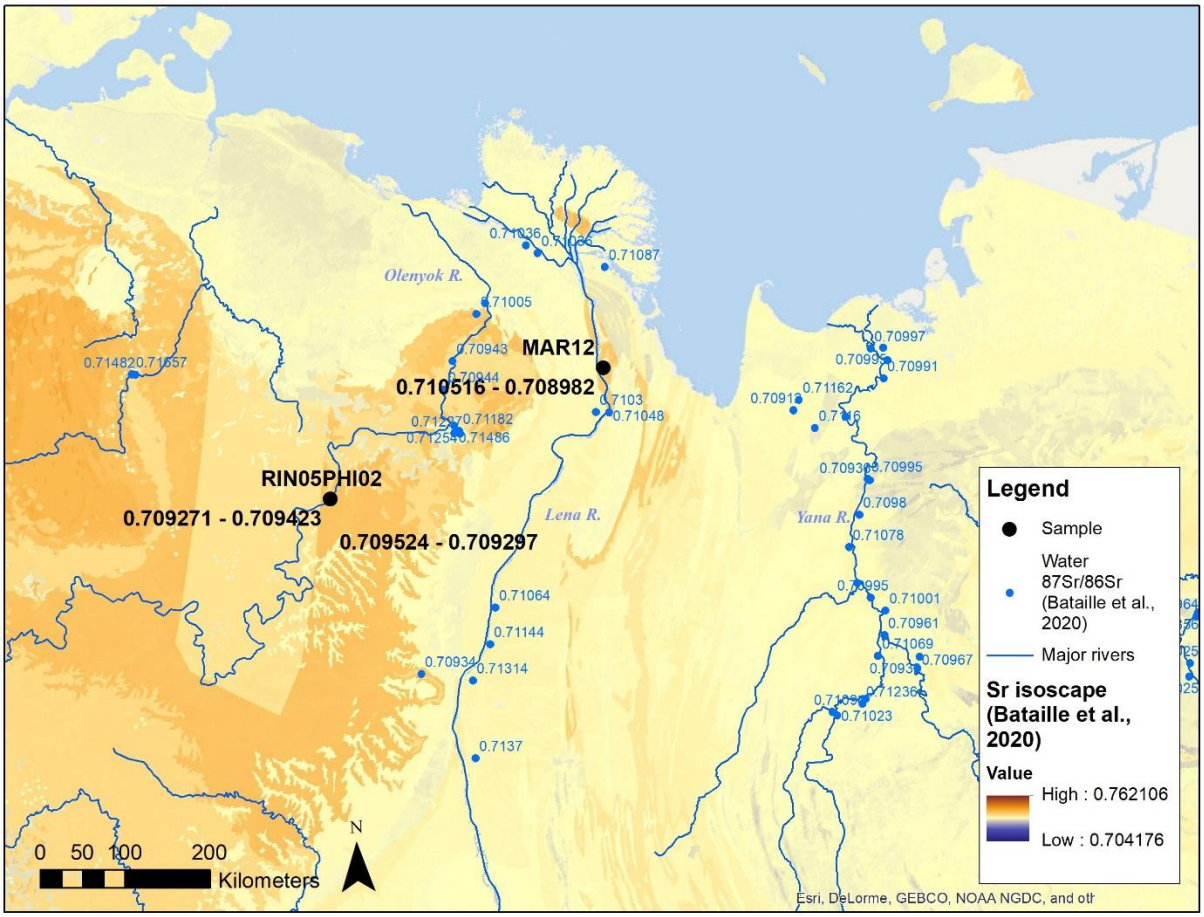

Figure C3.4. Sample crossdate match locations in eastern Siberia, determined by TRW crossdating by Hole et al. (2021), with measured $^{87}Sr/^{87}Sr$ value range displayed in black, with compiled river $^{87}Sr/^{87}Sr$ data by Bataille (2020) in blue.

MAR12: match location along the Lena River. The value range fits with the proximal river $^{87}Sr/^{87}Sr$ value range of 0.7103-0.7048.

PHI02: crossdate match location of eastern Siberia along the Olenyok River. There is a lack of measured river $^{87}Sr/^{87}Sr$ along the closest section of the Olenyok, although downstream the range 0.70943-0.71486 does overlap with the sample $^{87}Sr/^{87}Sr$ range, with river $^{87}Sr/^{87}Sr$ ~200km south-east near the Lena also showing aligning value of 0.70934.

RIN05: crossdate match location in eastern Siberia west of the Lena River. Similarly to sample PHI02, there is a lack of measured river $^{87}Sr/^{87}Sr$ along the closest section, with downstream the range 0.70943-0.71486 close to the upper end of the sample $^{87}Sr/^{87}Sr$ range, and river $^{87}Sr/^{87}Sr$ ~200km south-east near the Lena also showing aligning value of 0.70934.

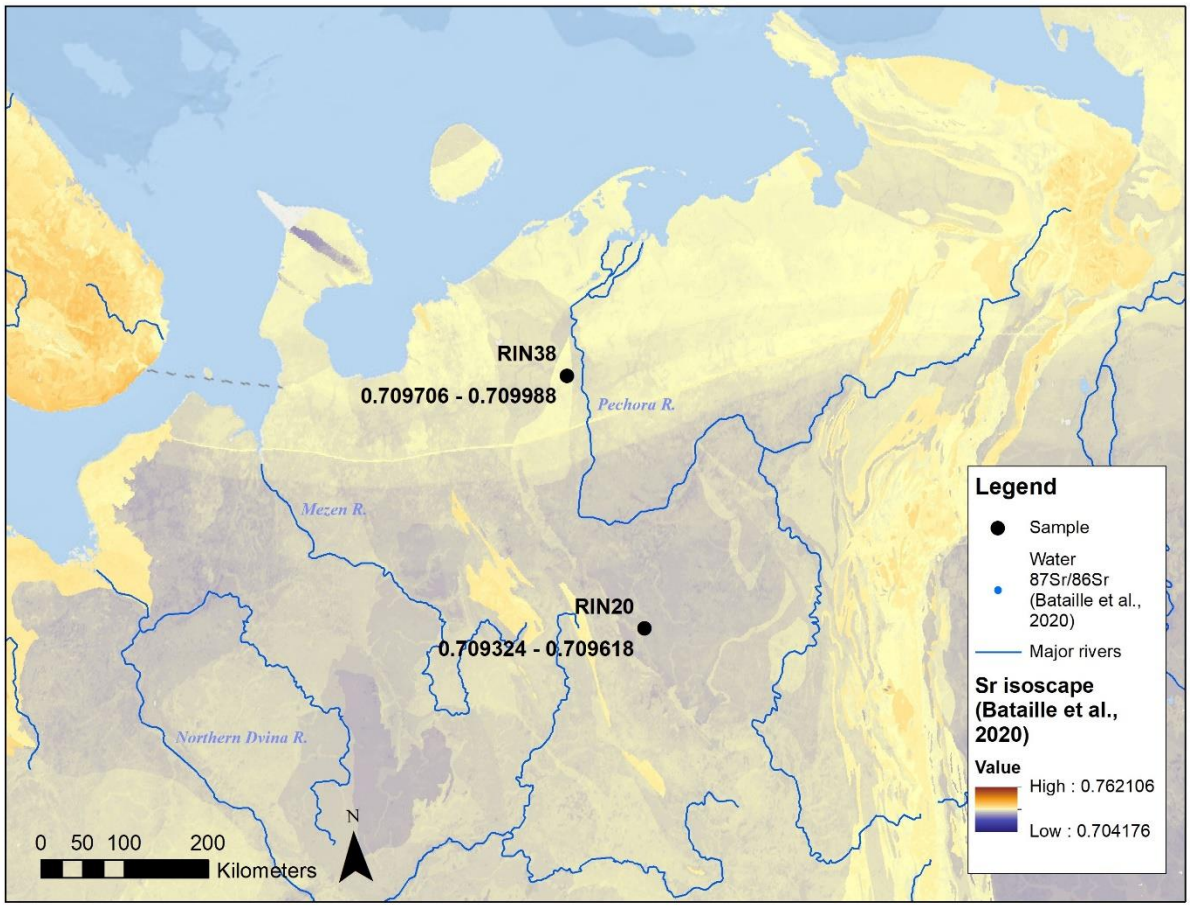

Figure C3.5. Sample crossdate match location in western Russia, determined by TRW crossdating by Hole et al. (2021), with measured $^{87}Sr/^{87}Sr$ value range displayed in black, and no available reference river $^{87}Sr/^{87}Sr$ data for comparison.

RIN20 & RIN38: match locations west of the Pechora River. The global bioavailable $^{87}Sr/^{87}Sr$ isoscape by Bataille (2020) shows the region with $^{87}Sr/^{87}Sr$ values ~0.709, fitting with the sample values.

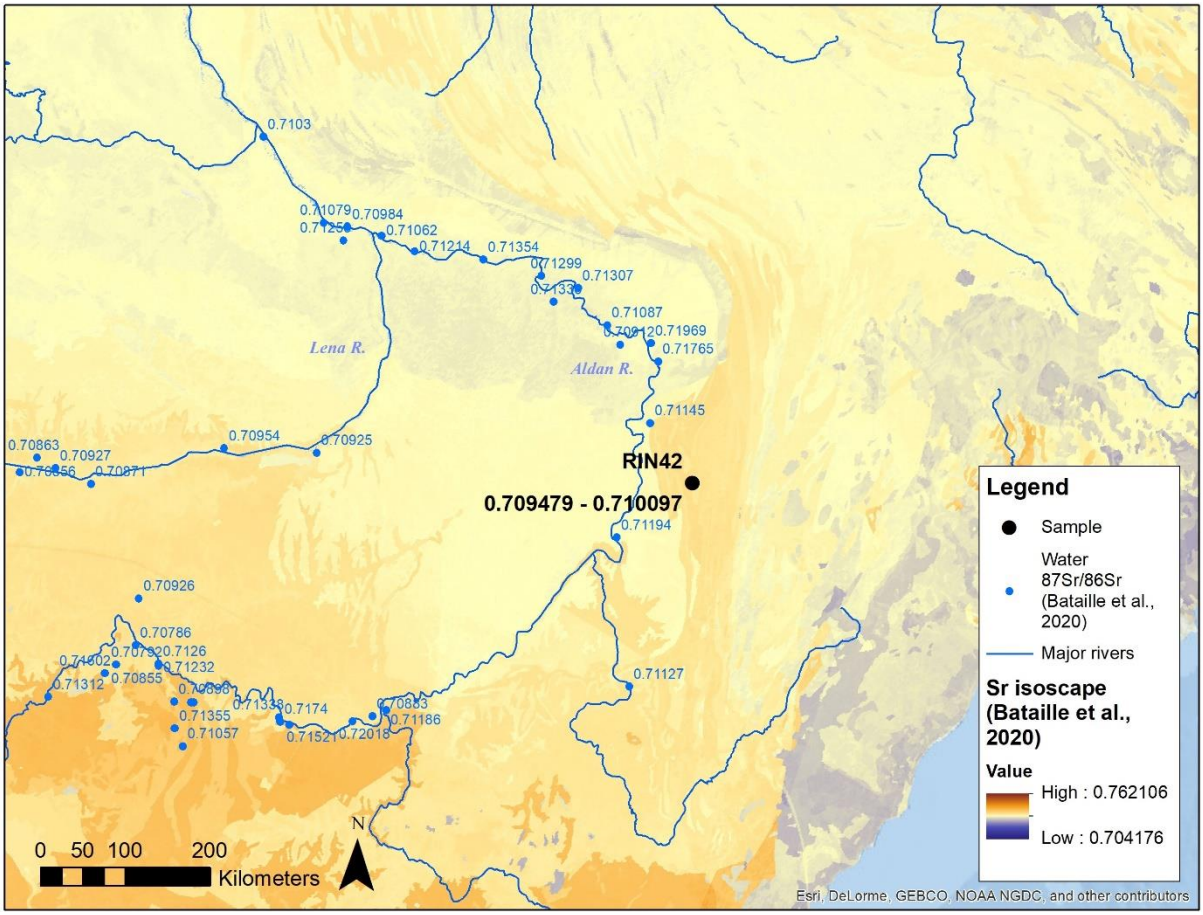

Figure C3.6. Sample RIN42 crossdate match location of eastern Siberia, east of the Aldan river, determined by TRW crossdating by Hole et al. (2021), with measured $^{87}Sr/^{87}Sr$ value range displayed in black, with compiled river $^{87}Sr/^{87}Sr$ data by Bataille (2020) in blue. The nearest river $^{87}Sr/^{87}Sr$ values of 0.70912-0.71765 cover the sample $^{87}Sr/^{87}Sr$ range.

C4 UPGMA analysis plots

Description: Unweighted pair-group average (UPGMA) cluster analysis was employed to create groups of similar valued data by minimising the joined averaged Euclidean distances between all members in any two groups. A separate cluster analysis was undetaken for inner, outer, and averaged $^{87}Sr/^{86}Sr$ readings (for averaged plot see Figure 5.5 within Chapter 5). Consistency between clusters (intra-sample consistency) and between the cluster and their TRW-inferred provenances were analysed. Cluster analysis was performed using Past 4.04 (Hammer et al., 2001).

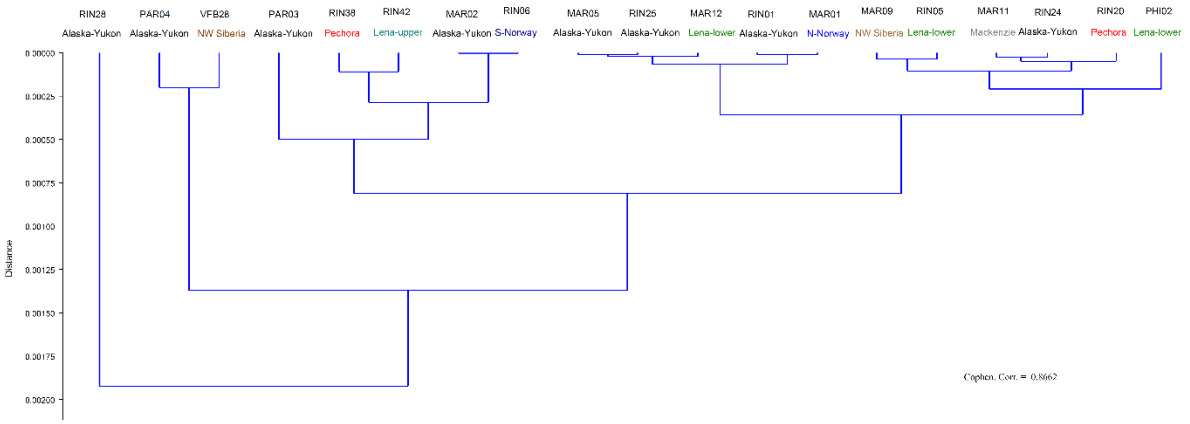

Figure C4.1. Unweighted pair-group average (UPGMA) cluster analysis on inner $^{87}Sr/^{86}Sr$ readings for 19 driftwood samples. Cluster analysis was performed using PAST 4.04 (Hammer et al., 2001).

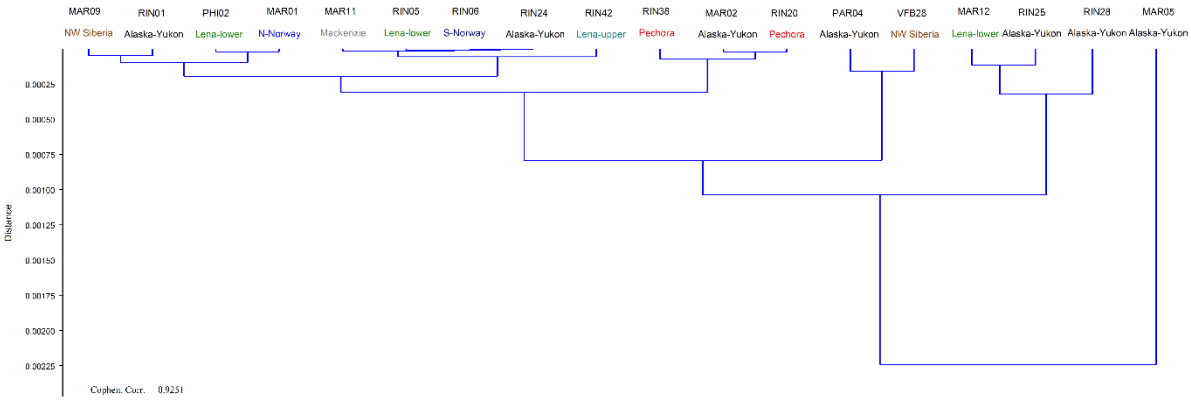

Figure C4.2. Unweighted pair-group average (UPGMA) cluster analysis on outer $^{87}Sr/^{86}Sr$ readings for 19 driftwood samples. Cluster analysis was performed using PAST 4.04 (Hammer et al., 2001).

C5 Appendix C references

Bataille, C. P., Crowley, B. E., Wooller, M. J., & Bowen, G. J. (2020). Advances in global bioavailable strontium isoscapes. *Palaeogeography, Palaeoclimatology, Palaeoecology*, *555*, 109849. https://doi.org/https://doi.org/10.1016/j.palaeo.2020.109849

Hammer, Ø., Harper, D. A. T., & Ryan, P. D. (2001). PAST: Paleontological statistics software package for education and data analysis. *Palaeontologia Electronica*, *4*(1), 9.

Hole, G. M., Rawson, T., Farnsworth, W. R., Schomacker, A., Ingolfsson, O., & Macias-Fauria, M. (2021). A driftwood-based record of Arctic sea ice during the last 500 years from northern Svalbard reveals sea ice dynamics in the Arctic Ocean and Arctic peripheral seas

[Preprint]. *Journal of Geophysical Research: Oceans*. https://doi.org/https://doi.org/10.1002/essoar.10507454.1

Romaniello, S. J., Field, M. P., Smith, H. B., Gordon, G. W., Kim, M. H., & Anbar, A. D. (2015). Fully automated chromatographic purification of Sr and Ca for isotopic analysis. *Journal of Analytical Atomic Spectrometry*, *30*(9), 1906–1912. https://doi.org/10.1039/c5ja00205b

D. Ancient DNA extraction from driftwood

D1 Linking Statement

Appendix D provides a final step further on the second of the two main aims of the Specific Aims and Hypotheses: the development and evaluation of novel techniques to refine the provenance of driftwood. The appendix chapter presents the exploration of techniques to refine the provenance of driftwood through palaeogenetics, with the aim to refine the provenance of driftwood via extraction of ancient DNA from test material - driftwood collected from the subarctic location of Nordkapp, northern Norway. Though not successful, there remain avenues for future investigation, as discussed below.

D2 Introduction

As explored in previous chapters, many of the existing methods utilised for driftwood analysis and utilisation as a proxy tool for sea ice reconstructions have limitations. Dendro-provenancing can only cover the regions and periods for which reference chronologies exist, while geochemical methods such as radiogenic strontium analysis have confounding factors in retrieving endogenous values, and in limited reference data for comparison. For provenance by genetic information, microanatomical analysis of driftwood can only glean taxonomy to genus level – with some small exceptions within the *Pinus* genus that allow for species identification, and therefore aDNA analysis provides the possibility to further refine the wood's taxonomic identification, and therefore aid determination of provenance by comparison to tree species – and potentially sub-species – distribution across the pan-Arctic forests. Therefore, to achieve a finer definition of the role of atmospheric and oceanic circulation in sea ice and climatic

changes throughout the Holocene, there remains scope to develop methods to more definitively determine driftwood provenance and spatiotemporal variations.

The extraction of ancient DNA from Arctic driftwood is one such method, as determination of species of samples including to the haplotype level could enable a fine spatial resolution of provenance via comparison to the modern geographical distribution of chloroplast haplotypes across the pan-Arctic boreal forests. The successful extraction of aDNA requires preservation of sufficiently unique sequences, which is known to be problematic for fossil and subfossil wood due to the speed of DNA degradation leading to fragmentation and modification of the recoverable DNA (Lindahl, 1993; Pääbo et al., 2004). However, with improvements in technology, sequencing of genomes of plant and animal tissue has been successfully employed on time scales exceed 0.5Ma (Orlando et al., 2021), with the oldest successful genome sequenced from horse bone tissue preserved in permafrost for 560,000–780,000 years (Orlando et al., 2013). It is therefore likely that the possibilities of aDNA are likely to increase as technologies develop further. There has been some success with aDNA analysis from archaeological/preserved wood, employed in studies such as wood traceability and monitoring species evolution (Speirs et al., 2009). In the study of the 16th century Mary Rose shipwreck, successful chloroplast DNA from waterlogged Mary Rose hull oak timber was extracted and amplified (Speirs et al., 2009).

PCR amplification of preselected DNA markers have been the most common method for DNA extraction, including for this Chapter. However, the molecular characteristics of ancient DNA, consisting of ultra-short fragments of degraded DNA molecules (Orlando et al., 2015) lessen the likelihood of success of such methods. For wood in particular, there are other confounding factors to consider due to its structure and varied molecular contents. Inner heartwood that is often targeted for reduced contamination contains predominantly dead cells (S. Wagner et al., 2018), limiting the possibility of sufficient DNA for extraction and

sequencing, while wood also contains many other compounds such as secondary metabolites that can hinder attempts to target and extract DNA (Plomion et al., 2001; Deguilloux et al., 2002). Specifically, in the case of Arctic driftwood, there is long duration of exposure to saline ocean waters, and once on shorelines, DNA-degrading temperature fluctuations of up to tens of degrees. However, conversely, the cold and dry conditions of the Arctic and alkaline soils act as preserving factors and limiting any microbial action on the wood (Dyke et al., 1997).

D3 Methods

Test material consisted of a disc of sub-Arctic driftwood collected from Nordkapp, northern Norway ~71.1075°N, 25.7910°E (Figure D1), with evidence of shipworm damage, fracturing and waterlogging. Ancient DNA extraction though PCR analysis was attempted on sub-Arctic driftwood samples from Nordkapp, northern Norway, in collaboration with Dr James Haile and the Palaeobarn research team, RLAHA, University of Oxford, led by Prof Greger Larson. The PCR recipe trialled was adapted from a protocol utilised by the Gilbert

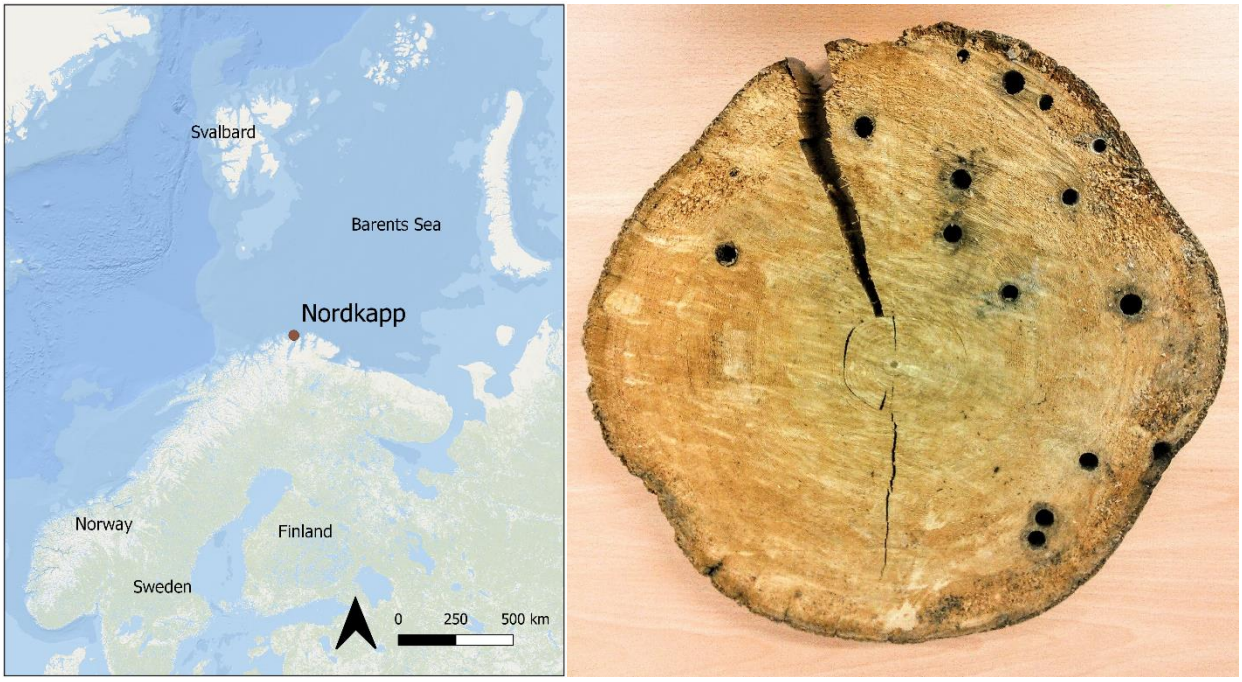

Figure D1. a) Location of sample collection from Nordkapp, northern Norway. b) subsampled driftwood disc collected and utilised as test material for DNA extraction.

group at the centre for GeoGenetics, Copenhagen for most of their plant tissue (e.g. Wales et al., 2014), optimized for maize cobs. A primer was chosen for primer pairs that amplify <200 base pairs; specifically trnL (g/h) primers (Taberlet et al., 2007) for its robust amplification and therefore applicability to degraded DNA. The primer's low resolution lessens the use for phytogeography and specific species of haplotype determination but would determine what recoverable DNA may be present within the tested samples.

D3.1 PCR Protocol

Digestion buffer

- 10 mM Tris (ph 8)
- 10 mM NaCl
- 2% w/v SDS
- 5mM CaCl2
- 2.5 mM EDTA (ph 8)
- 0.5 mg/mL pro K
- 4% w/v PVP

1. 24h digestion at 55ºC with gentle agitation in enough buffer to create a slurry.
2. Sample Spun at maximum in a benchtop centrifuge and liquid decanted to a new 2 mL tube.
3. Equal volume phenol added, rotated at room temperature for 5 minutes, spun fast 5 minutes, and upper aqueous layer then recovered to a new tube.
4. The phenol step was repeated 1 more time and the upper aqueous layer recovered(2x total).
5. The organic extraction with chloroform repeated 1 time with upper aqueous layer recovered.
6. From here methodology follows a modified MinElute® purification for short fragment retention, as in Dabney et al., (2013).
7. 13 volumes Buffer PB was added to the aqueous component from above, before binding to a Qiagen MinElute® column with a vacuum manifold and Qiagen® 25 mL extension reservoirs (Qiagen, Hilden, Germany). Then purified with a couple washes of PE buffer and a dry spin to remove trace ethanol.
8. To elute, 20-50 uL of normal TE buffer or TE with 0.05% tween was used, before incubation for 15 minutes at 37ºC. Finally, sample was spun at maximum to elute, and repeated for a total of 2x elutions.

D4 Results

Following the initial test with trnL (g/h) primers, the amplicons were all too weak to be sufficient for sequencing. Given that the samples failed at the combining samples stage, the sequencing stage was not reached. The tested sub-Arctic samples are likely to have experienced greater degradation than Arctic driftwood, meaning that there is a (albeit small) chance that future testing of Arctic samples might yield recoverable DNA.

D5 Discussion

There remain future avenues for developments in ancient DNA retrieval from Arctic driftwood, as there is continuing progress in aDNA retrieval from subfossil wood material, with method developments including shotgun high-throughput sequencing (HTS) (S. Wagner et al., 2018) and amplicon-sequencing on Illumina platforms (Lendvay et al., 2018), with additional cleaning method developments such as removal of exogenous DNA contamination via laser irradiation coupled with bleaching and surface removal. Shotgun HTS produces random reads from all of the available DNA molecules in a sample (Moore et al., 2020), whereas amplicon sequencing which short fragments of a specific gene that is then compared to a reference database. HTS has become established in analysis of the genome-scale variation present in ancient animals and pathogens (S. Wagner et al., 2018), and has dramatically changed the scope of ancient DNA (aDNA) research (Kircher, 2012), with gigabases of sequence data able to be produced within hours or days. By not targeting just one or a few genomic regions, shotgun HTS enables the characterisation of DNA preservation, contamination, and damage to an extent that had not been achieved previously (Kircher, 2012). Recent progress has been made through high throughput (HTS) DNA sequencing of archaeological and subfossil wood up to 9,800 years old (S. Wagner et al., 2018). The successful extraction supplies evidence in support of the feasibility of extraction of DNA from

marine waterlogged archaeological wood, and therefore indicates that the same may be possible for the extraction of driftwood aDNA for species and provenance analysis. Most recent studies have not yet explored the full potential of aDNA methods based on shotgun HTS (S. Wagner et al., 2018), making this a promising avenue for development in any future attempts at aDNA extraction from Holocene Arctic driftwood. A further future avenue might that may warrant investigation is protein analyses such as a genus-specific collagen peptides by mass spectrometry, by using solid-phase extraction (Buckley et al., 2009), which has been found productive in cases when DNA cannot be retrieved.

D6 Appendix D references

Buckley, M., Collins, M., Thomas-Oates, J., & Wilson, J. C. (2009). Species identification by analysis of bone collagen using matrix-assisted laser desorption/ionisation time-of-flight mass spectrometry. *Rapid Communications in Mass Spectrometry*, *23*(23), 3843–3854. https://doi.org/https://doi.org/10.1002/rcm.4316

Deguilloux, M., Pemonge, M., & Petit, R. (2002). Novel perspectives in wood certification and forensics: dry wood as a source of DNA. *Proceedings of the Royal Society of London. Series B: Biological Sciences*, *269*(1495), 1039–1046.

Dyke, A. S., England, J., Reimnitz, E., & Jette, H. (1997). Changes in Driftwood Delivery to the Canadian Arctic Archipelago: The Hypothesis of Postglacial Oscillations of the Transpolar Drift. *Arctic*, *50*(1), 1–16. https://www.jstor.org/stable/40512037

Kircher, M. (2012). Analysis of high-throughput ancient DNA sequencing data. In *Ancient DNA* (pp. 197–228). Springer.

Lendvay, B., Hartmann, M., Brodbeck, S., Nievergelt, D., Reinig, F., Zoller, S., Parducci, L., Gugerli, F., Büntgen, U., & Sperisen, C. (2018). Improved recovery of ancient DNA from subfossil wood–Application to the world's oldest Late Glacial pine forest. *New Phytologist*, *217*(4), 1737–1748.

Lindahl, T. (1993). Instability and decay of the primary structure of DNA. *Nature*, *362*(6422), 709–715. https://doi.org/10.1038/362709a0

Moore, G., Tessler, M., Cunningham, S. W., Betancourt, J., & Harbert, R. (2020). Paleo-metagenomics of North American fossil packrat middens: Past biodiversity revealed by ancient DNA. *Ecology and Evolution*, *10*(5), 2530–2544.

Orlando, L., Allaby, R., Skoglund, P., Der Sarkissian, C., Stockhammer, P. W., Ávila-Arcos, M. C., Fu, Q., Krause, J., Willerslev, E., & Stone, A. C. (2021). Ancient DNA analysis. *Nature Reviews Methods Primers*, *1*(1), 1–26.

Orlando, L., Gilbert, M. T. P., & Willerslev, E. (2015). Reconstructing ancient genomes and epigenomes. *Nature Reviews Genetics*, *16*(7), 395–408.

Orlando, L., Ginolhac, A., Zhang, G., Froese, D., Albrechtsen, A., Stiller, M., Schubert, M., Cappellini, E., Petersen, B., & Moltke, I. (2013). Recalibrating Equus evolution using the genome sequence of an early Middle Pleistocene horse. *Nature*, *499*(7456), 74–78.

Pääbo, S., Poinar, H., Serre, D., Jaenicke-Despres, V., Hebler, J., Rohland, N., Kuch, M., Krause, J., Vigilant, L., & Hofreiter, M. (2004). Genetic analyses from ancient DNA. *Annual Review of Genetics*, *38*, 645–679. https://doi.org/10.1146/annurev.genet.37.110801.143214
Plomion, C., Leprovost, G., & Stokes, A. (2001). Wood formation in trees. *Plant Physiology*, *127*(4), 1513–1523.

Speirs, A. K., McConnachie, G., & Lowe, A. (2009). Chloroplast DNA from 16th century waterlogged oak in a marine environment: initial steps in sourcing the Mary Rose timbers. *Archaeological Science under a Microscope: Studies in Residue and Ancient DNA Analysis in Honour of Thomas H. Loy. Terra Australis*, *30*, 175–189.

Taberlet, P., Coissac, E., Pompanon, F., Gielly, L., Miquel, C., Valentini, A., Vermat, T., Corthier, G., Brochmann, C., & Willerslev, E. (2007). Power and limitations of the chloroplast trnL (UAA) intron for plant DNA barcoding. *Nucleic Acids Research*, *35*(3). https://doi.org/10.1093/nar/gkl938

Wagner, S., Lagane, F., Seguin-Orlando, A., Schubert, M., Leroy, T., Guichoux, E., Chancerel, E., Bech-Hebelstrup, I., Bernard, V., Billard, C., Billaud, Y., Bolliger, M., Croutsch, C., Čufar, K., Eynaud, F., Heussner, K. U., Köninger, J., Langenegger, F., Leroy, F., … Orlando, L. (2018). High-Throughput DNA sequencing of ancient wood. *Molecular Ecology*, *27*(5), 1138–1154. https://doi.org/10.1111/mec.14514

Wales, N., Andersen, K., Cappellini, E., Ávila-Arcos, M. C., & Gilbert, M. T. P. (2014). Optimization of DNA recovery and amplification from non-carbonized archaeobotanical remains. *PLoS ONE*, *9*(1). https://doi.org/10.1371/journal.pone.0086827